

---

---

THE SYNTHESIS, CHARACTERIZATION AND  
ELECTROCATALYTIC BEHAVIOUR OF NOVEL  
COBALT(II) AND IRON(II)  
PHTHALOCYANINES BEARING  
BENZOPYRONE, BENZOXAZOLE,  
TETRAHYDROPYRAN AND FURAN MOIETIES

by

Sumayya Chohan

Submitted in the fulfillment of the requirements for the degree of

**Master of Science**

in the School of Chemistry and Physics at the

University of KwaZulu-Natal

November 2015

Supervisor: Dr. Irvin N. Booysen

Co-supervisor: Dr. Allen Mambanda

As the candidate's supervisor, I hereby approve this dissertation for submission:

Signed: \_\_\_\_\_ Date: \_\_\_\_\_

---

---

---

---

# TABLE OF CONTENTS

Abstract	I
Preface	IV
Declaration 1 - Plagiarism	V
Declaration 2 - Publications	VI
Acknowledgements	VII
Crystallographic Data	VIII

## CHAPTER 1

### Introduction

1.1	General Background	1
1.2	Aim and Motivation	3
1.3	Electronic Properties of Phthalocyanines	6
1.4	MPcs as Electrocatalysts	10
1.5	Methods of Electrode Modification	17
1.6	MPc-Based Electrochemical Sensors	22
1.7	References	27

---

---

## CHAPTER 2

### Materials and Instrumentation

2.1.	Materials	37
2.2.	Instrumentation	39
2.3.	References	41

## CHAPTER 3

### Synthesis, Characterization and Electrocatalytic Behaviour of Novel Cobalt and Iron Phthalocyanines Bearing Chromone and Coumarin Moieties

3.1.	Introduction	42
3.2.	Experimental	44
3.3.	Results and Discussion	50
3.4.	Conclusion	82
3.5.	References	84

## CHAPTER 4

### Cobalt $\beta$ -Tetra(3-oxyflavone/2-(2-oxyphenyl)benzoxazole)phthalocyanines and Their Carbon Nanotube Conjugates: Formation, Characterization and Dopamine Electrocatalysis

4.1.	Introduction	89
4.2.	Experimental	91
4.3.	Results and Discussion	96
4.4.	Conclusion	127
4.5.	References	128

---

---

## CHAPTER 5

### Formulation, Characterization and Electrochemical Properties of Novel Tetrasubstituted Cobalt Phthalocyanines Bearing Tetrahydropyran, Furan and Coumarin Moieties

5.1.	Introduction	131
5.2.	Experimental	133
5.3.	Results and Discussion	138
5.4.	Conclusion	171
5.5.	References	173

## CHAPTER 6

	Conclusion and Future work	178
	References	180

---

---

# ABSTRACT

The fabrication of metallophthalocyanine (MPc)-based modified electrodes has proven to be effective for the electrocatalysis of various bio-analytes and pollutants. The selectivity of these chemically modified electrodes can be fine-tuned by the attachment of biologically relevant substituents to MPcs which has shown to facilitate the detection of numerous analytes. Hence, this study focuses on the design of MPcs bearing chromone, coumarin, flavone, benzoxazole, tetrahydropyran and furan moieties. The formulated MPcs were characterized using UV-Vis and FT-IR spectroscopy, ESI-TOF mass spectrometry and elemental analysis. The redox properties of the complexes were investigated *via* voltammetry and the subsequent voltammetric assignments were corroborated by UV-Vis spectroelectrochemistry. Each metal complex displayed four redox processes of which the Pc ring oxidation is irreversible and the remaining redox couples are quasi-reversible.

Novel cobalt and iron phthalocyanines peripherally tetra-substituted with chromone (chr) or coumarin (cou) moieties were formulated and characterized in chapter three. The structural elucidations of the ligands, 4-(chromone-7-oxy)phthalonitrile (**1**) and 4-(4-(trifluoromethyl)-coumarin-7-oxy)phthalonitrile (**2**) were complemented by NMR spectroscopy and single crystal X-ray analysis (for **1**). Utilizing the respective MPcs, modified working electrodes were prepared by electropolymerization and their electrocatalytic activities towards nitrite oxidation were explored. All the metal complexes showed an increase in nitrite oxidation currents and a minor decrease in

oxidation potentials which is indicative of electrocatalysis. The trend of electrocatalytic activity was found to be as follows: CoPc-chr (**3**) > FePc-cou (**4**) > CoPc-cou (**5**).

Chapter four focuses on the synthesis and characterization of cobalt phthalocyanines (CoPcs) containing flavone (flav) and benzoxazole (bo) moieties. CoPc-flav (**3**), CoPc-bo (**4**), multi-walled carbon nanotubes (MWCNTs) and CoPc-MWCNT conjugates were used to prepare modified glassy carbon electrodes (GCEs) which were tested for dopamine electrocatalysis. Both CoPc modified electrodes (**3**-GCE and **4**-GCE) showed higher peak currents, slightly lower peak potentials and improved reversibility compared to the bare GCE. The respective CoPc-MWCNT conjugates were found to further enhance dopamine detection. **3**-MWCNT-GCE and **4**-MWCNT-GCE showed lower peak to peak separations than the respective CoPc modified electrodes indicating faster electron transfer kinetics. Chronoamperometry was employed to determine the catalytic rate constants of each electrode which were superior to previously reported values. **4**-MWCNT-GCE was noted to be the most effective electron mediator in the electrocatalysis of dopamine.

Chapter five reports on the synthesis of tetrahydropyran (thp) and furan (fur) substituted CoPcs. The electrocatalysis of *L*-cysteine was tested using CoPc-thp (**3**), CoPc-fur (**4**) and CoPc-cou (**5**) reported in chapter three. Modified electrodes were prepared using the drop-dry method. While the bare GCE and **4**-GCE showed no peaks for *L*-cysteine oxidation in the 0.0 - 0.70 V potential window; the modified

electrodes showed a well-defined peak at 0.40 V for **3**-GCE and a broad peak at 0.52 V for **5**-GCE. Kinetic parameters were determined using chronoamperometry, rotating disc electrode (RDE) studies and construction of Tafel plots. It was found that *L*-cysteine oxidation using **3**-GCE proceeded at a faster rate.

**Keywords:** Metallophthalocyanine, chromone, coumarin, flavone, benzoxazole, tetrahydropyran, furan, electrocatalysis, carbon nanotubes

---

---

# PREFACE

The experimental work described in this dissertation was carried out in the School of Chemistry and Physics at the University of KwaZulu-Natal, Pietermaritzburg, from January 2014 to November 2015, under the supervision of Dr. Irvin Noel Booysen and co-supervision of Dr. Allen Mambanda.

These studies represent original work by the author and have not otherwise been submitted in any form for any degree or diploma to any tertiary institution. Where use has been made of the work of others, it is duly acknowledged in the text.

---

---

# DECLARATION 1-PLAGIARISM

I, Sumayya Chohan, declare that:

1. The research reported in this dissertation, except where otherwise indicated, is my original research.
2. This dissertation has not been submitted for any degree or examination at any other university.
3. This dissertation does not contain any other persons' data, pictures, graphs or other information, unless specifically acknowledged as being sourced from other persons'.
4. This dissertation does not contain any other persons' writing, unless specifically acknowledged as being sourced from other researchers. Where other written sources have been quoted, then:
  - a. Their words have been re-written but the general information attributed to them has been referenced.
  - b. Where their exact words have been used, then their writing has been placed in italics and inside quotation marks, and referenced.
5. This dissertation does not contain text, graphics or tables copied and pasted from the internet, unless specifically acknowledged, and the source being detailed in the dissertation and in the References section.

Signed: \_\_\_\_\_

---

---

# DECLARATION 2-PUBLICATIONS

## *Manuscripts Published*

- [1] S. Chohan, I.N. Booyesen, A. Mambanda, M.P. Akerman, *J. Coord. Chem.*, 2015, **68**, 1829.
- [2] S. Chohan, I.N. Booyesen, A. Mambanda, *Polyhedron*, 2015, **102**, 284.

## *Submitted for Review*

- S. Chohan, I.N. Booyesen, A. Mambanda, M.P. Akerman, "Formulation, characterization and electrochemical properties of novel tetrasubstituted cobalt phthalocyanines bearing tetrahydropyran, furan and coumarin moieties." *S.A. J. Chem.*, 2015.

The compounds involved in all the aforementioned manuscripts have been synthesized, characterized and analysed by myself. Single crystal XRD was run and solved by Dr M.P. Akerman.

Signed: \_\_\_\_\_

*Sumayya Chohan*

Signed: \_\_\_\_\_

*Dr I.N. Booyesen*

Signed: \_\_\_\_\_

*Dr. A. Mambanda*

Signed: \_\_\_\_\_

*Dr M.P. Akerman*

---

---

# ACKNOWLEDGEMENTS

I would like to express sincere gratitude to my supervisor, Dr. I.N. Booysen, for the continuous support, patience, motivation and invaluable time that he has invested in my research.

Many thanks to Dr. A. Mambanda for his insightful comments, the technical staff for help with the characterization of my samples and my friends and fellow colleagues for their support and encouragement.

I am grateful to the National Research Foundation (NRF) for funding this project and the University of KwaZulu-Natal for providing laboratory facilities and a desk space to facilitate my research.

Most importantly, my studies would not be possible without the love and support of my grandfather, Mr. G.H. Chohan and my parents Asiah and Ahmed Chohan.

---

---

# CRYSTALLOGRAPHIC DATA

Supplementary data for all the crystal structures obtained during this study are stored on a compact disk that is attached to the inside back cover of this dissertation.

This data includes the following:

- Final coordinates and equivalent isotropic displacement parameters of the non-hydrogen atoms;
- Final crystal data and details of the structure determinations;
- Isotropic displacement parameters;
- Hydrogen atom positions;
- Contact distances;
- Torsion angles;
- Hydrogen-bonds.

---

---

# CHAPTER ONE

## Introduction

### 1.1 General Background

In 1928, the Grangemouth plant of Scottish Dyes Ltd. accidentally produced iron phthalocyanine (FePc) during the industrial preparation of phthalimide from phthalic anhydride [1, 2]. Upon investigation it was found that the glass lining of the reactor had cracked to expose the outer steel casing to the reaction which had resulted in the formation of a blue-green powder, FePc [3]. This discovery eventually led to the elucidation of H<sub>2</sub>Pc by Linstead in the 1930s [4].

Phthalocyanine, derived from the Greek words *naphtha* (rock oil) and *cyanine* (blue) [5], is an organic compound containing four isoindole units fused together by aza nitrogen atoms in a large ring. It possesses an inner N<sub>4</sub> structure that is common in naturally occurring molecules like chlorophyll, vitamin B<sub>12</sub> and haemoglobin [6]. The phthalocyanine macrocycle is highly conjugated and contains 18  $\pi$ -electrons in its core. More than 70 different metals are able to complex with its central cavity as derivatives of its conjugate base Pc<sup>2-</sup> [7]. Furthermore, in addition to axial substitution, various equatorial substitutions are possible on the metallophthalocyanine (MPc) ring both non-peripherally ( $\alpha$ -positions 1-9) and peripherally ( $\beta$ -positions 10-16), see **Fig. 1.1** [8, 9]. The electrochemical and physical

properties of these metal complexes can be modulated by meticulous selection of the metal centre as well as the substituents and their positions, making them highly versatile for application in numerous fields [10, 11].

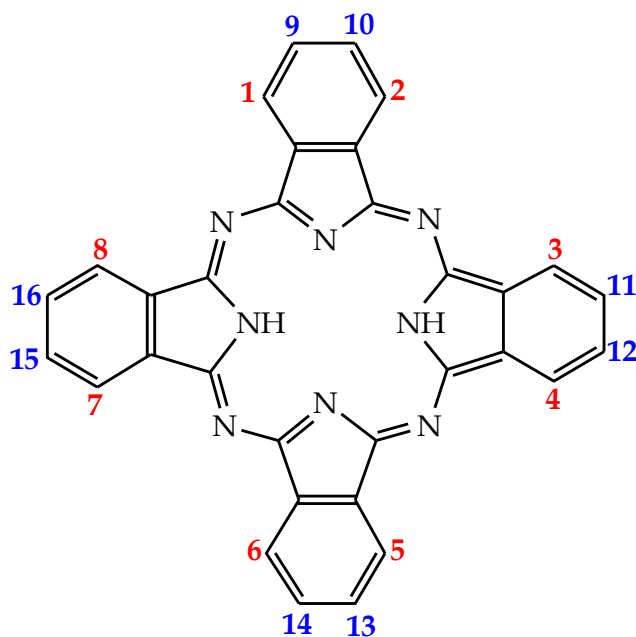


**Figure 1.1:** A structure of phthalocyanine depicting peripheral (blue) and non-peripheral (red) sites of substitution.

Phthalocyanines were originally used as dyes given their rich blue-green colour [12]. The optimal thermal and chemical properties of MPCs have over the years prompted research into various fields such as non-linear optics, molecular electronics, semiconductors, photovoltaic cells and photodynamic therapy (PDT) [13-16]. Of particular interest is their contemporary application in the preparation of biosensors [17].

## 1.2 Aim and Motivation

MPCs form nano films on electrode surfaces which facilitate electron mediation between an analyte and electrode, *i.e.* they act as electrocatalysts [18]. However, the detection capabilities of these chemically modified electrodes (CMEs) are diminished by a lack of linkage of biomolecules onto the chemical interface to enhance sensitivity and selectivity. Improvement in the efficiency of MPC-based chemical sensors thus depends on the inclusion of biologically relevant substituents on the macrocyclic ring [19, 20]. Therefore, this research study focuses on the design, synthesis and characterization of Fe(II) and Co(II) phthalocyanines bearing biologically relevant substituents including benzopyrone, benzoxazole, tetrahydropyran and furan moieties, respectively (see Fig. 1.2). In addition, probing the redox properties and investigating the electrocatalytic activities of the formulated MPCs are also focal aspects within this research study.

The flavonoids are a class of naturally occurring compounds found in plant pigments comprising predominantly benzo- $\gamma$ -pyrone derivatives [21]. These secondary metabolites include chromones, flavones and coumarins which are known to exhibit a wide range of pharmacological activities such as anti-viral, anti-inflammatory, anti-cancer, anti-allergic and anti-oxidant activities [22-25]. Coumarins in particular display blood anti-coagulant behaviour [26], *e.g.* warfarin sodium (see Fig. 1.3), a coumarin derivative, is a widely used drug for the treatment of thrombosis which is a life threatening condition resulting in an abnormal increase

in blood clotting factors like prothrombin [27]. Being a vitamin K antagonist, it inhibits the production of prothrombin thereby reducing blood clotting significantly.

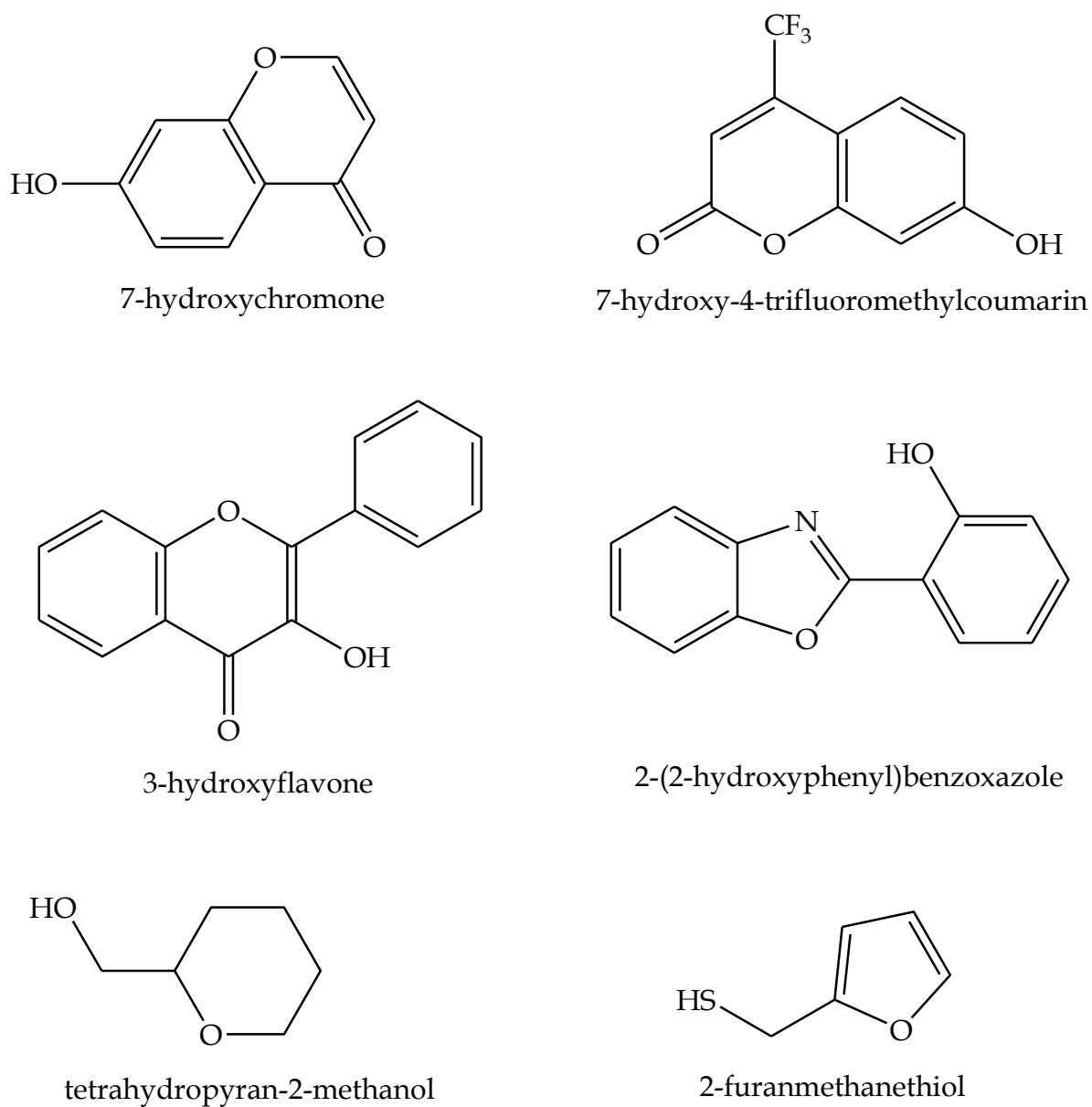


**Figure 1.2:** Structures of the biologically relevant molecules.

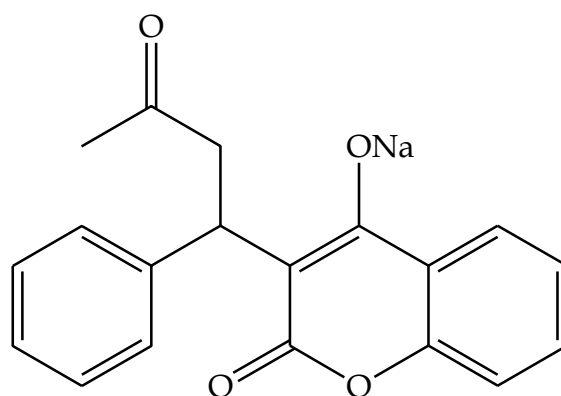


**Figure 1.3:** Structure of the anti-coagulant warfarin sodium.

Organic molecules containing benzoxazole, tetrahydropyran or furan moieties also possess diverse pharmacological activities including anti-bacterial, anti-fungal and anti-tumour activities [28-31]. Furans exhibit a wide range of biological activities as controlled by the nature of their substituents. They are useful in the treatment of ventricular and arterial fibrillation, hyperglycaemia and convulsions [32]. Tetrahydropyrans occur in a large number of natural products including the marine extract Halichondrin B [33, 34]. A structural analogue of this product, eribulin (see **Fig. 1.4**), is an FDA approved drug marketed as Halaven™ in the US for the treatment of metastatic breast cancer [35].

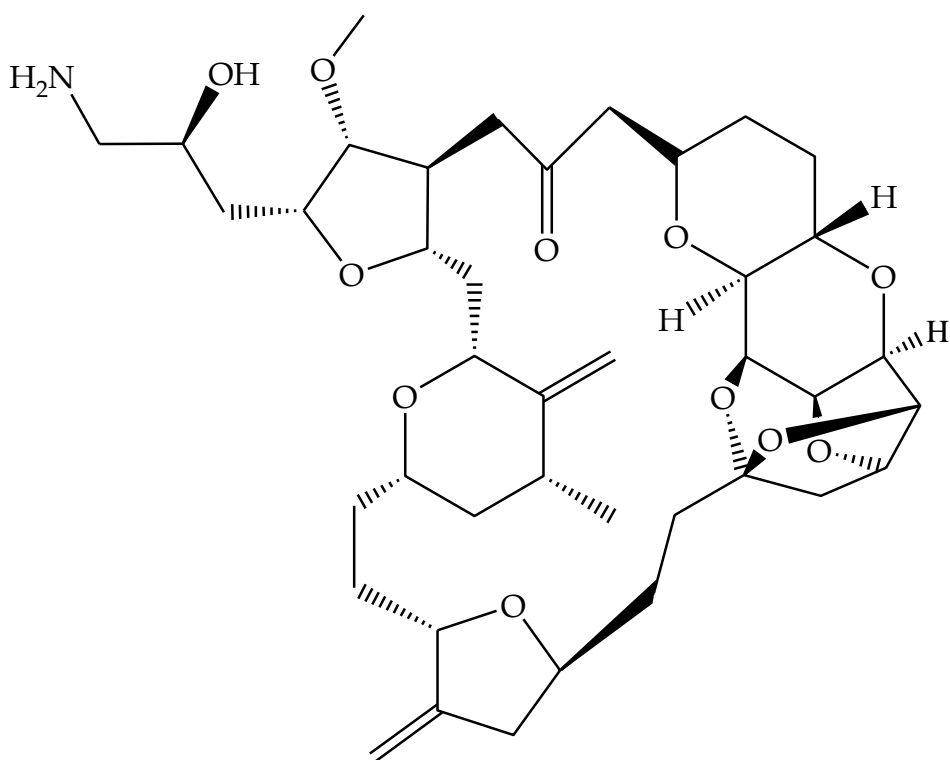


**Figure 1.4:** An intrinsic structure of the anti-cancer drug, eribulin.

### 1.3 Electronic Properties of Metallophthalocyanines

#### 1.3.1 Absorption Spectra

The absorption spectra of MPCs consists of a strong band near 670 nm referred to as the Q-band, and a typically weaker band near 340 nm called the B-(soret) band [36], both of which correspond to  $\pi \rightarrow \pi^*$  electronic transitions. Other electronic transitions (N, L and C) may be observed at higher energies [37]. Furthermore, the Q-band is associated with electronic transfer from the inner pyrrole rings to the outer benzene rings of the Pc skeleton while the B-band corresponds to electron transfer that involves a redistribution of electron density within the chelate [38]. **Fig. 1.5** illustrates the common electronic transitions that occur in MPCs.

Metallated Pcs have high  $D_{4h}$  symmetry since the metal centre maintains the planarity of the molecule while unmetallated Pcs have low  $D_{2h}$  symmetry. As a consequence, the degeneracy of the LUMO is lifted resulting in a split Q-band [39, 40]. Other factors like axial ligation, central metal, solvent, nature of substitution, aggregation and extended conjugation can affect the nature (broad or split) and position (red-shifted or blue-shifted) of the Q-band [41]. In MPcs with transition metal centres, the metal  $d$  orbitals may lie between the HOMO and LUMO of the Pc ligand resulting in charge transfer bands, *viz.* ligand-to-metal charge transfer (LMCT) or metal-to-ligand charge transfer (MLCT) [42]. These transitions occur between the Q- and B-bands near 500 nm [43].

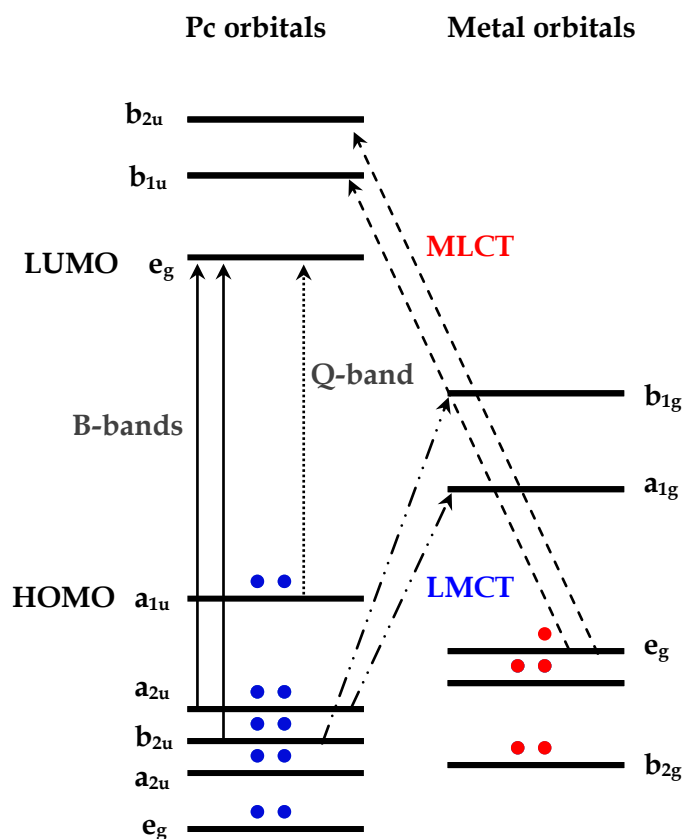


**Figure 1.5:** A Jablonski diagram depicting the common electronic transitions of MPcs.

### 1.3.2 Photodynamic Therapy (PDT)

Photodynamic therapy (PDT) is a technique involving the use of a photosensitizer (PS), light and oxygen for the treatment of diseases such as cancer [44]. The PDT of cancer is a minimally invasive technique in which malignant cancer cells are selectively targeted so as to reduce the likelihood of healthy cells being destroyed. In conventional cancer treatments such as chemotherapy, metal-based drugs like cisplatin are known to be acutely toxic to healthy cells and have a limited spectrum of activity since the tumor cells develop a resistance to the drug [45].

Photosensitizers are activated when they absorb light of a specific wavelength and undergo various photochemical pathways (see Fig. 1.6) to produce singlet oxygen ( $^1\text{O}_2$ ) which is toxic to malignant cells [44, 46]. The activated PS undergoes intersystem crossing to the longer-lived triplet state. Upon interaction with molecular oxygen ( $^3\text{O}_2$ ) in the triplet state, the PS exchanges its energy. As a result the PS relaxes and singlet oxygen ( $^1\text{O}_2$ ) is produced which in turn induces apoptosis of cancer cells.

MPcs are promising candidates as photosensitizers due to their favourable photochemical properties. They absorb in the near infrared region (600-850 nm) which provides ideal tissue penetration [47]. Wavelengths below this window result in photosensitization of the skin while higher wavelengths minimize energy transfer to oxygen due to absorption of radiation by water [48]. In addition, diamagnetic

MPcs like ZnPcs and AlPcs provide long triplet state life times, high efficiency in singlet oxygen generation, low dark toxicity and high photostability [49, 50]. The main concerns that arise with these MPcs involve low solubility, a high aggregation tendency and weak target specificity [48, 51]. These problems can be addressed by introducing anionic or cationic (e.g. sulfo, carboxy, ammonium) groups at the peripheral positions of the phthalocyanine ring to provide water soluble MPcs [52], using disaggregating agents like Cremophore® EL (macrogolglycerol ricinoleate) or adding bulky groups at the  $\alpha$ -positions to address aggregation concerns [48, 53], and conjugation with amino acids or peptides to provide enhanced target specificity [54].

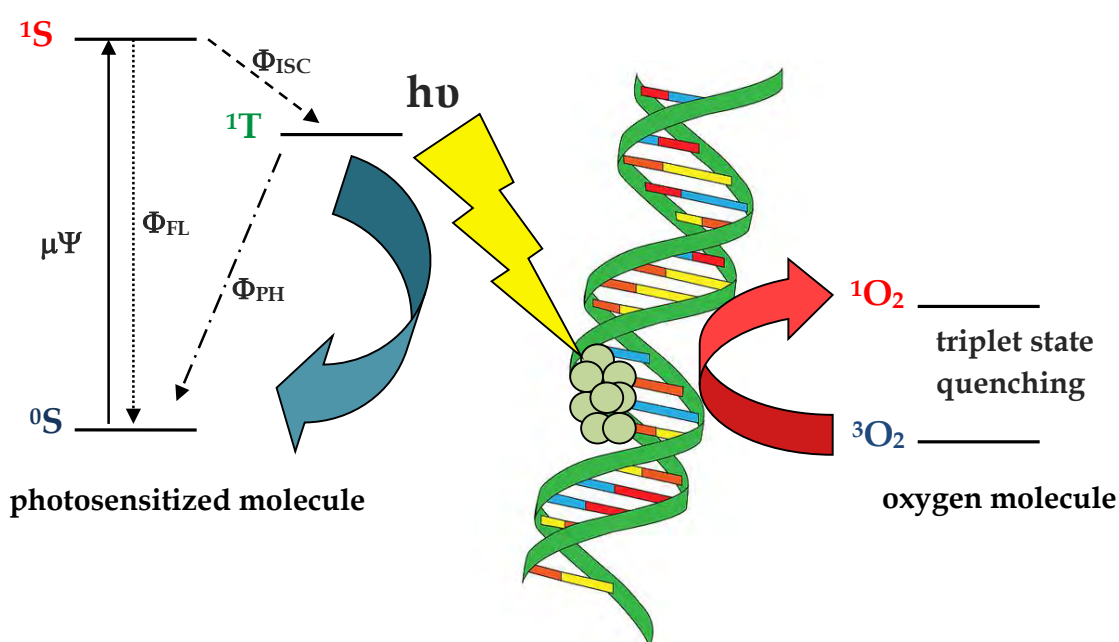


**Figure 1.6:** Energy diagram illustrating PDT (Photodynamic Therapy).

It is known that cationic MPcs are more efficient PDT agents with improved cell uptake and selective localization in the cell mitochondria [55]. They bind tightly to nucleic acids such as double and single stranded DNA [56, 57]. The singlet oxygen

produced upon illumination of the PS promotes DNA cleavage. Thus, in cancer therapy, MPcs are utilized to selectively target cancer cells and destroy them by oxidation of their DNA components [58].

## 1.4 MPcs as Electrocatalysts

### 1.4.1 Application in Fuel Cells

Polymer electrolyte membrane (PEM) fuel cells (**Fig. 1.7**) are considered promising candidates for stationary and mobile power generation [59]. They convert chemical energy into electrical energy by combining a fuel, usually hydrogen gas, with oxygen [60]. Despite the high energy conversion efficiency and minimal environmental impacts, the high cost of Pt-based catalysts which dominate the oxygen reduction reaction (ORR) in these cells is less than ideal [61]. Hence, a variety of non-precious materials like chalcogenides, nitrogen doped carbon nanotubes, transition metal oxides and metal N<sub>4</sub>-chelates have been explored as possible replacements for Pt-based electrocatalysts [62, 63].

In 1964, Jasinski discovered that a non-noble catalyst, cobalt phthalocyanine (CoPc), could enhance the rate of reduction of oxygen in fuel cells as an alternative to using conventional Pt-based catalysts [64]. Since then, research into using MPcs as electrocatalysts in fuel cells has been extensive and significant progress has been made, with FePcs being one of the leading candidates in this field [65]. The main drawback of using MPc-based electrocatalysts is their lack of stability under the

harsh operating conditions of PEM fuel cells resulting in demetallation [66]. Research has shown that the introduction of bulky electron donating protein substituents on the Pc ring can enhance electron transfer and reduce close-packing of the complexes thereby possibly enhancing their stability [67]. The cathodic component of the two electrochemical reactions occurring in a hydrogen PEM cell displays a higher overpotential than the anodic component, thus MPCs have been explored mainly as ORR catalysts [68]. The ORR is a complex process proceeding with a number of intermediates. The two half reactions can be simplified as:

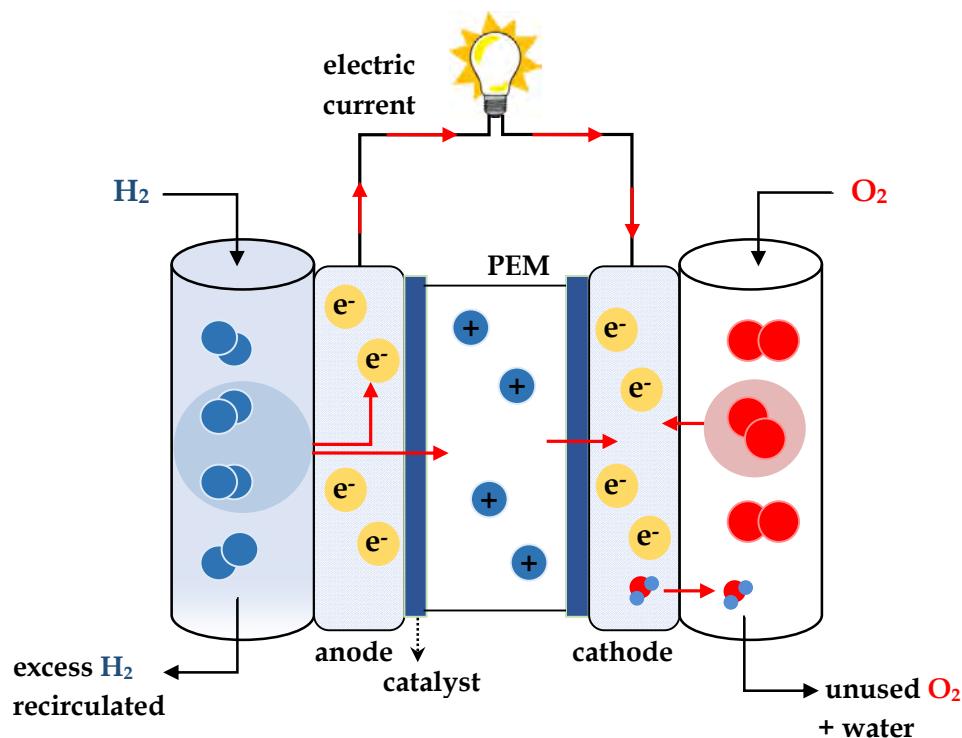
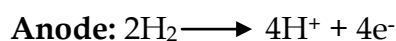
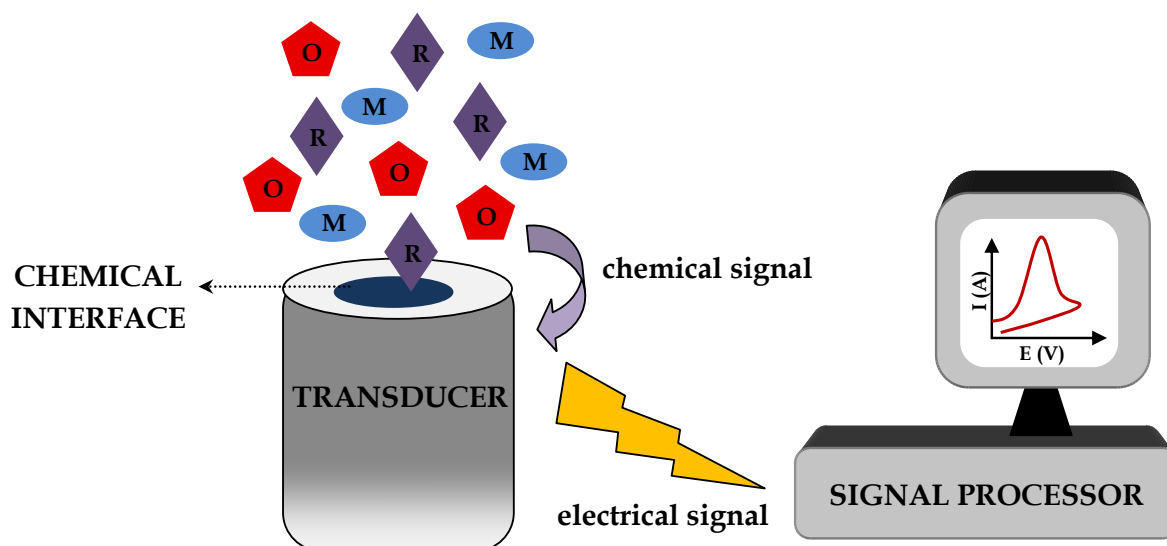


Figure 1.7: A PEM fuel cell setup.

### 1.4.2 Chemical Sensors

The optimal electrochemical properties of MPCs and their stability upon applied potential make them ideal for application in chemical sensors [69]. In general, a chemical sensor can be defined as a device that uses a chemical sensing element to quantitatively or qualitatively detect an analyte. Their compact design, simple operation, relatively low-costs and high efficiency have made them incredibly useful diagnostic tools in our everyday life. Chemical sensors can be used to detect allergens in food, toxins in water, blood glucose and electrolyte levels, certain diseases and the pregnancy hormone HCG (human chorionic gonadotropin) [70, 71].

A typical chemical sensor consists of a signal processor, a transducer and a chemical interface (CI) [72]. Different types of transducers exist which can for instance be electrochemical, optical, thermal or magnetic in nature [73]. Biosensors form a subset of chemical sensors wherein the CI comprises a natural biological sensing entity such as an enzyme, microorganism, tissue or antibody [73, 74]. Upon interaction with the analyte, the CI generates a chemical signal which is converted into an electrical signal (current, voltage, *etc*) by the transducer and made meaningful by a signal processor. The detected signal is proportional to the amount of biomolecule present in solution. **Fig. 1.8** depicts the typical setup of a chemical sensor where M is the matrix and R and O are the reduced and oxidized forms of the analyte, respectively.



**Figure 1.8:** Typical setup of an electrochemical sensor.

Different methods exist for operating electrochemical transducers which include voltammetric, amperometric, potentiometric and coulometric techniques [72, 75]. The traditional glucose meter is an example of an amperometric biosensor. Its design includes a Pt electrode consisting of the enzyme glucose oxidase (GOx) entrapped thereon *via* a dialysis membrane [76] (see Fig. 1.9). The co-factor flavin adenine dinucleotide (FAD) is required for GOx to operate as a catalyst [77]. GOx-FAD reacts with glucose at the cathode to form GOx-FADH<sub>2</sub> and gluconic acid [78]. The cofactor is regenerated by reacting with the surrounding oxygen to produce hydrogen peroxide which is then oxidized at the anode [79, 80]. The concentration of glucose can be determined by either measuring the consumption of oxygen, the production of H<sub>2</sub>O<sub>2</sub> or by the use of a mediator to transfer the electrons from GOx to the electrode [80].

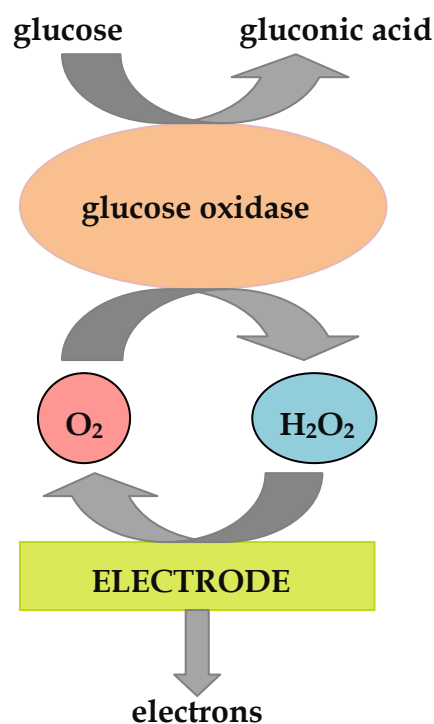


**Figure 1.9:** A biosensor mechanism for glucose oxidation.

#### 1.4.3 MPc Modified Electrodes

A good electrocatalyst is one that enhances the sensitivity and selectivity of an electrode, maintains its stability during electrocatalysis and lowers the redox potential of an analyte [81]. MPcs and similar metal macrocyclic complexes generally serve as suitable electrocatalysts due to their ability to occupy various oxidation states while retaining their stability and structure during electrocatalysis [81, 82]. Extensive research into preparing MPc modified electrodes has proven MPcs to be useful for the electrocatalysis of a number of different analytes like dopamine, L-cysteine, ascorbic acid, hydrazine, nitrite and glucose [82-86]. Certain factors like the metal centre and the nature and position of the substituents influence the

electrocatalytic behaviour of MPcs [87]. In turn, these factors can be carefully manipulated to optimize the electrocatalytic function of the formulated MPcs.

MPcs containing non-redox active metal centres like Zn and Cu do not change oxidation states very easily hence the redox properties of such complexes are dominated by their Pc rings [88]. These MPcs are therefore not usually suitable for electrocatalysis but are better suited for application in other areas such as photodynamic therapy. Metals like manganese, cobalt and iron can easily interchange oxidation states, thereby facilitating electron mediation [89]. Furthermore, the electrocatalytic potential of the analyte is commonly influenced by the metal redox couples [90]. Thus, the oxidation or reduction redox potentials of the central metal typically promote the electrocatalytic activity of the macrocyclic complex. For example, a typical mechanism for electrocatalytic reduction by an MPc complex can be expressed as shown in **Fig. 1.10**, where O and R are the oxidized and reduced species, respectively.

The oxidizing or reducing abilities of an MPc complex also depends on the type of substituents present. For instance, electron donating groups such as  $-NH_2$ ,  $Ar-S-$ ,  $RO-$ , *etc* increase the electron density on the Pc ring and the metal centre, making it easier to oxidize than reduce these complexes while the opposite holds for MPcs with electron withdrawing groups like  $-CF_3$ ,  $-F$ ,  $-Br$ ,  $-I$ ,  $-NO_2$ , *etc* [91]. Furthermore, the presence of biologically active moieties facilitates the detection of biological analytes by the MPc-modified electrode thereby promoting electrocatalysis.

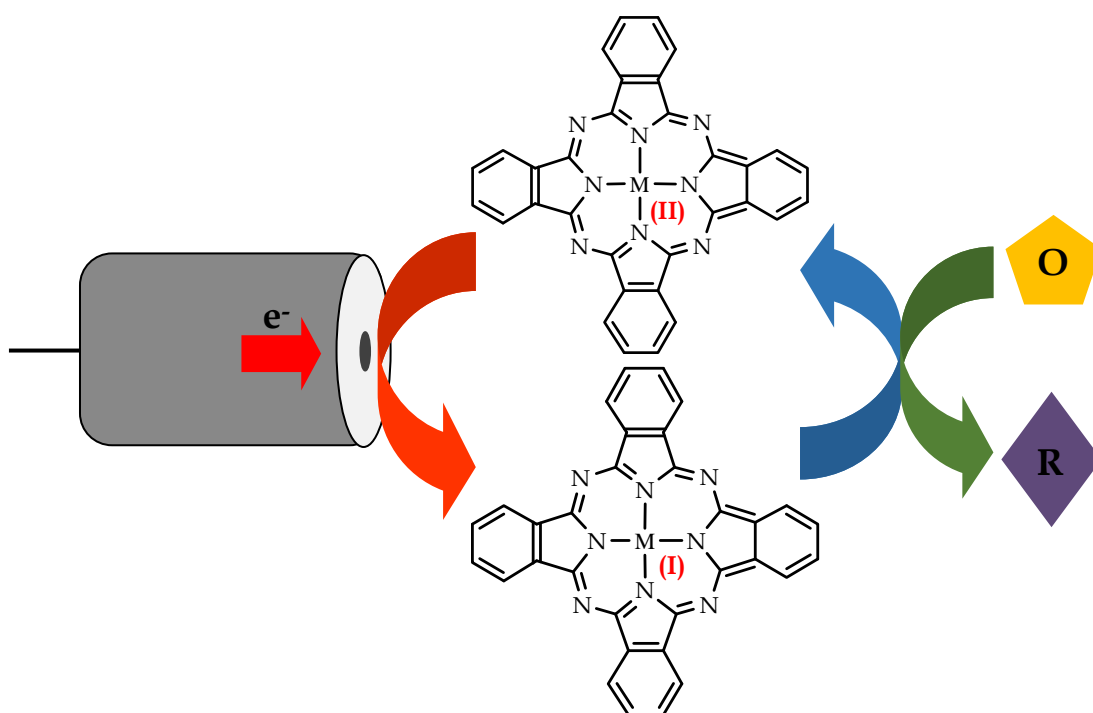


**Figure 1.10:** Mechanism of electrocatalytic reduction by a MPc modified electrode.

The physical properties of MPcs are also affected by the nature of the substituents. Due to the strong intermolecular interactions between macrocycles, unsubstituted MPcs as well as their unsubstituted metal-free Pc ligands are only slightly soluble or insoluble in aqueous and organic media consequently minimizing their application [92]. The solubility of these complexes can be enhanced by the addition of bulky or long chain substituents at the peripheral positions, and the use of donor solvents with the capability of coordinating to the axial position of the central metal atom [93, 94]. Furthermore, peripheral or non-peripheral substitution with alkoxy, alkyl, phenoxy and macrocyclic groups results in complexes that are soluble in organic solvents, while substitutions with sulfonyl, amino and carboxylic acid groups give rise to water soluble MPcs [92, 95, 96]. In addition to the size and nature of the

substituents, the symmetry of MPcs also affects their solubility. Octa-substituted MPcs with non-identical substituents along the periphery are more soluble than those containing identical ones [97].

## 1.5 Methods of Electrode Modification

The M-N<sub>4</sub> core monomers can readily adsorb onto the surfaces of various working electrodes to create electron-mediating thin or nano-sized films. Other electron mediating materials like carbon nanotubes (CNTs) can also be used in conjunction with MPcs to modify electrodes. Some of the numerous modification methods include adsorption, electrodeposition, electropolymerization, Langmuir-Blodgett films and self-assembled monolayer (SAM) formation [81, 98].

### 1.5.1 Adsorption

One method of adsorption involves the dip-dry technique whereby an electrode is immersed in a solution containing the monomer which results in the spontaneous formation of a nano layer on the electrode surface [99]. The other is the drop-dry method whereby a few drops of the monomer solution are cast onto the electrode surface and dried. Electrodes modified by adsorption are generally unstable, short-lived and vulnerable to passivation, rendering them unuseable for extended use [100].

### 1.5.2 *Electrodeposition*

Repetitive cyclic voltammetry scans applied to an electrode immersed in a solution of the complex results in deposition of the monomer onto the electrode. More monomer is electrodeposited with each repeated scan; as a result the peak current gradually increases. The number of scans controls the amount of MPc accumulated on the electrode surface [101].

### 1.5.3 *Electropolymerization*

This technique provides a simple but elegant method for the immobilization of electrocatalysts. Stable films are created by the electrochemical oxidation or reduction of a polymerizable group on the phthalocyanine ligand [69]. The growth of the polymer film is then facilitated by its electronic conductivity. Commonly used MPc substituents for this process include pyrrole, thiophene and aniline derivatives [102]. Electropolymerization like electrodeposition involves the application of repetitive cyclic voltammetry scans on an electrode immersed in a solution containing the complex. Upon polymerization, both an increase in the peak current and either a shift in peak potentials or the formation of new peaks occur.

#### 1.5.4 Langmuir-Blodgett Films

A well-defined monolayer, consisting of a regular planar array of molecules is formed by dissolving an amphiphile in a volatile organic solvent that is then spread across the water-air interface [103]. While the solvent is evaporating, the hydrophilic head of the amphiphile orientates itself toward the water while the hydrophobic tail directs itself in the opposite direction toward the air (see Fig. 1.11) [104]. In this manner, a film of highly orientated molecules is created which can then be transferred onto a solid substrate. The thickness of the films can be varied by controlling the number of Langmuir monolayers deposited. MPCs with long chain ester groups on the axial positions can act as amphiphiles [105]. The oxygen atoms act as hydrophilic heads while the carbon chains behave as hydrophobic tails.

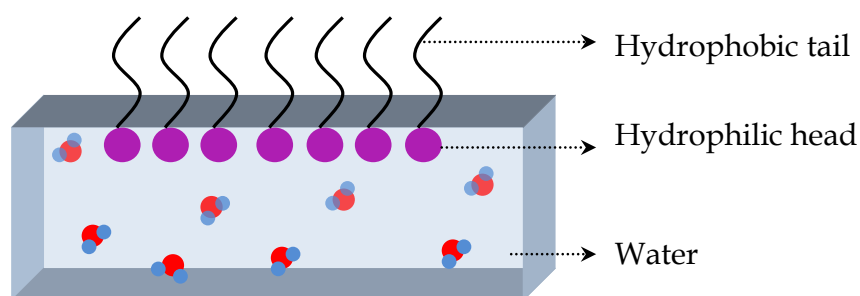


**Figure 1.11:** An illustration depicting the behaviour of an amphiphile at the water-air interface.

### 1.5.5 Self-Assembled Monolayers

A monolayer of highly orientated molecules is created by immersing a suitable solid substrate, usually a gold electrode into a solution containing the desired species with the appropriate functional group [106]. Sulfur containing substituents like thiols have a high affinity for gold electrodes. Specific arrangements of the adsorbent can be achieved by careful deposition of the appropriate functional groups onto the working electrode [69] (see Fig. 1.12). This technique forms reproducible and relatively stable films by spontaneous chemisorption.

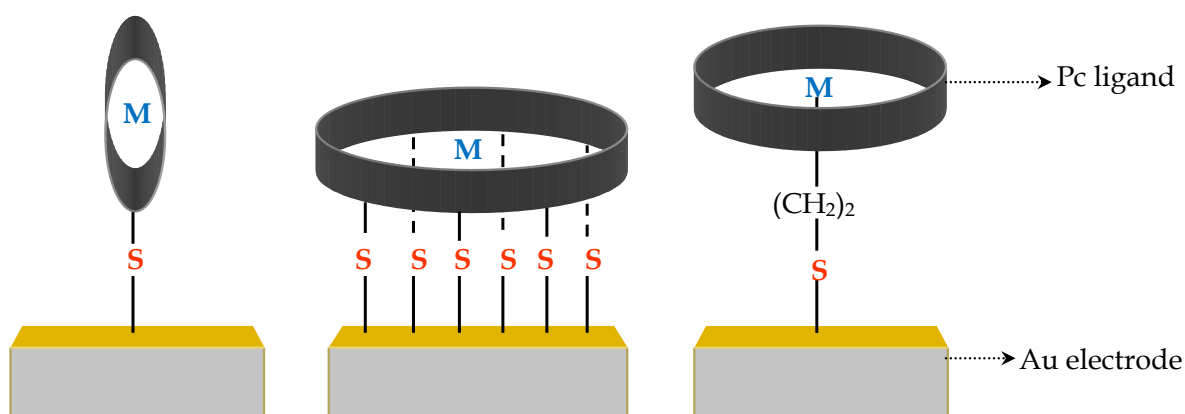


**Figure 1.12:** Different arrangements of immobilized sulfur derivatized MPcs on a gold electrode.

### 1.5.6 Carbon Nanotubes

CNTs are cylindrical graphite nanostructures which are categorized into single-walled CNTs (SWCNTs) and multi-walled CNTs (MWCNTs). While SWCNTs consist of a single graphite cylinder, MWCNTs consist of several concentric graphite

cylindrical shells [107]. Since the only exposed surface of CNTs is the unreactive graphite basal plane, they are considered to be chemically inert [108]. The ends of the cylindrical tubes and the presence of defects on the side walls; however, affect their reactivity [108, 109]. The end caps of CNTs are composed of fullerene-like hemispheres which are significantly more reactive than the side walls [110]. Defects on the side walls including Stone-Wales defects which are pentagon-heptagon pairs, vacancies in the CNT lattice and  $sp^3$ -hybridized defects, each provide unique alternatives for covalent modification of CNTs [111].

CNTs are known to promote electron transfer reactions due to their high electrical conductivity and enhanced mechanical properties [112, 113]. They can be used in conjunction with MPcs to modify electrodes either *via* adsorption or by chemical linking [114]. Amino-substituted MPcs can be covalently linked to CNTs *via* amide bond formations, while other substituted MPcs can be non-covalently adsorbed *via*  $\pi$ - $\pi$  stacking onto CNTs [113, 115, 116]. The latter possesses the electrocatalytic properties of MPcs while preserving the electronic structures and properties of CNTs [117].

Following dispersion in a suitable solvent, CNTs can be used to prepare conjugated MPc-CNT modified electrodes by casting a drop of the suspension on an electrode either prior to or following modification of the electrode with an MPc. However, CNTs tend to aggregate in solution due to the strong van der Waals interaction thereby diminishing the active surface area, mass transport and reproducibility

[118]. Enhanced dispersion can thus be achieved by first preparing the MPc-CNT conjugate, dispersing in an appropriate solvent and then casting the conjugate onto a bare electrode.

## 1.6 MPc-Based Chemical Sensors

### 1.6.1 A Graphene Oxide-Based Bioelectrochemical Sensor for L-cysteine

Graphene oxide (GO) is a two-dimensional monolayer consisting of  $sp^2$  hybridized carbon functionalized with hydroxyl, carboxyl, epoxy and ketone groups which facilitate covalent and non-covalent surface modification thereby allowing for optimized sensitivity. GO has potential application in electrochemistry due to its high chemical stability, electrical conductivity and tunable modification.

In a recent paper [119], a GO-CoPc hybrid was prepared to fabricate a biosensor for the electrooxidation of L-cysteine, an amino acid that plays a crucial role in biological systems for the functioning of various proteins [120].  $\beta$ -Tetra-4-(nitrophthalocyaninato)Co(II) functionalized by 3-(trimethoxysilyl)propane-1-thiol (CoPc-nthio) was heated with GO and triethylamine for 40 h to effect grafting. A suspension of the resulting conjugate (see **Fig. 1.13**) was obtained *via* ultrasonication in dimethyl formamide (DMF) and drop cast onto a glassy carbon electrode (GCE). CMEs using GO and CoPc-nthio were also prepared by the drop cast method.

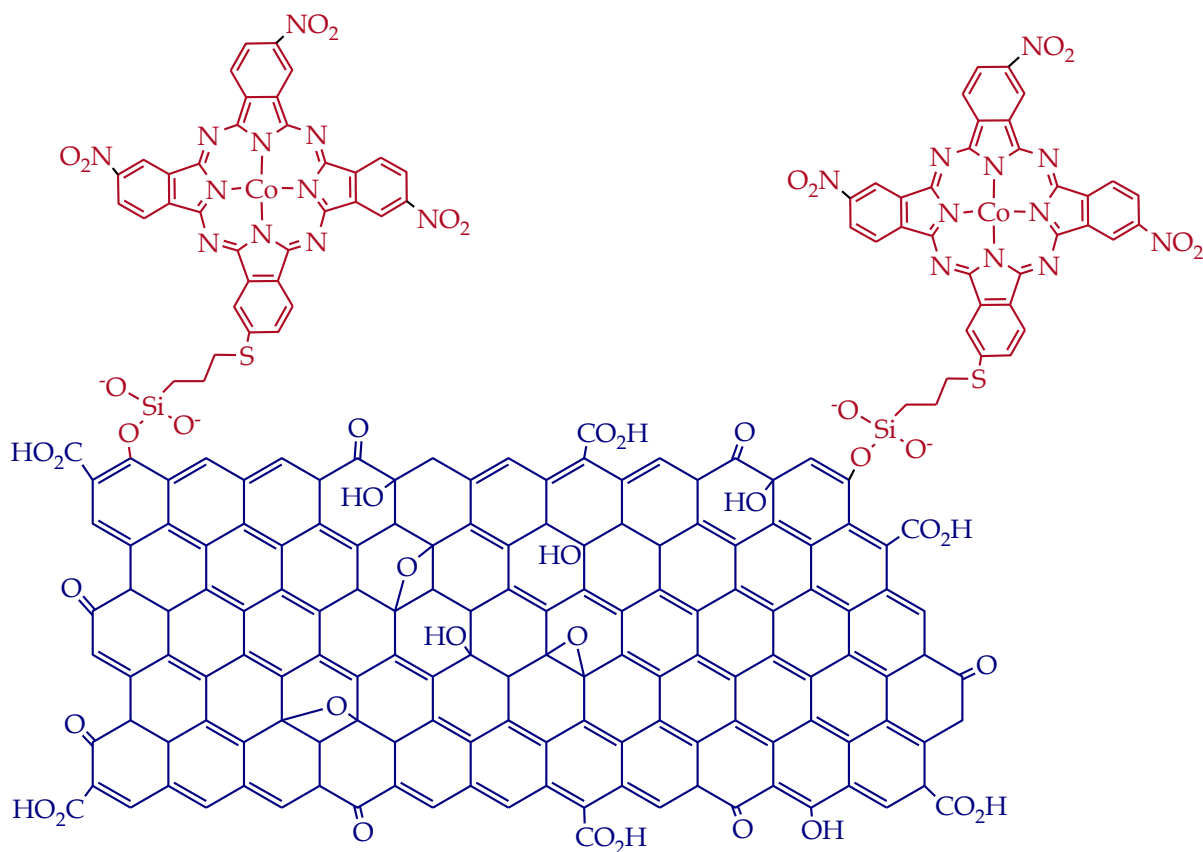


**Figure 1.13:** Illustration of the GO-CoPc hybrid.

Cyclic voltammograms were obtained for each CME for the electrooxidation of L-cysteine. Comparison of the electrocatalytic behaviour showed weak irreversible peaks for GO-GCE and CoPc-NO<sub>2</sub>-GCE at 0.73 and 0.64 V, respectively. The GO-CoPc-NO<sub>2</sub>-GCE however, showed a remarkable increase in the oxidation current as well as a decrease in the oxidation potential (0.52 V) indicative of good electrocatalytic behaviour.

### 1.6.2 *An Electronic Tongue for the Discrimination of Different Varieties of Grapes*

An electronic tongue (ET) is a multisensor tool comprising an array of low-selective sensors with cross sensitivity to different species in solution which is combined with a suitable method of pattern recognition and/or multivariate data analysis [121, 122]. This system is particularly useful for the analysis of complex mixtures like wines where the quality is determined by the amount of certain components in the mixture. Different varieties of grape musts for instance can be discriminated by their sugar and polyphenol content. A hybrid multisensory system consisting of an array of MPc-based sensors has been reported for this purpose [121].

Three different arrays consisting of five carbon paste electrode (CPE) sensors were prepared. The first array included a bare CPE, three MPc modified CPEs (CoPc-CPE, CuPc-CPE and ZnPc-CPE) and an MPc<sub>2</sub> modified CPE (LuPc<sub>2</sub>-CPE). The second array included the previous five sensors with immobilized tyrosinase (Tyr) cross-linked with glutaraldehyde (C-Tyr-CPE, CoPc-Tyr-CPE, CuPc-Tyr-CPE and ZnPc-Tyr-CPE and LuPc<sub>2</sub>-Tyr-CPE). The last array included the first five sensors with immobilized glucose oxidase (GOx) cross-linked with glutaraldehyde (C-GOx-CPE, CoPc-GOx-CPE, CuPc-GOx-CPE and ZnPc-GOx-CPE and LuPc<sub>2</sub>-GOx-CPE).

Model solutions of catechol and glucose were prepared to gauge the electrochemical responses of each array toward polyphenols and sugars, respectively. Following a comprehensive study wherein each modified electrode of the first array was tested

for its electrocatalytic responses to glucose and catechol, the second array towards catechol and the third array towards glucose; a second set of data was obtained for the responses of each modified electrode toward musts prepared from grapes of different varieties. Anodic peaks associated with catechol oxidation occurred in the 0.40–0.80 V region while the cathodic peak potentials for glucose occurred near -0.50 V. Each electrode exhibited a unique response to a given must sample and a certain degree of cross-selectivity was noted. Higher peak currents and lower peak potentials were observed for the sensors modified with CoPc and LuPc<sub>2</sub>.

Given that the obtained voltammograms convey information about the musts, principle component analysis (PCA) was used to discriminate the must samples using voltammetric data. A multisensory system consisting of the MPC-CPE, MPC-Tyr-CPE and MPC-GOx-CPE arrays was prepared and immersed in the different musts. A total of seven replicas were obtained for each must. The voltammetric data was subjected to PCA calculations using the kernel method to reduce the number of variables to ten. The PCA scores plot and loading plot revealed enhanced discrimination and depicted good separation of the musts. The multisensor thus provided a specific signature for each must thereby allowing discrimination of the samples based on the variety of grape. **Fig. 1.14** summarizes the approach used for discrimination of the grape samples.

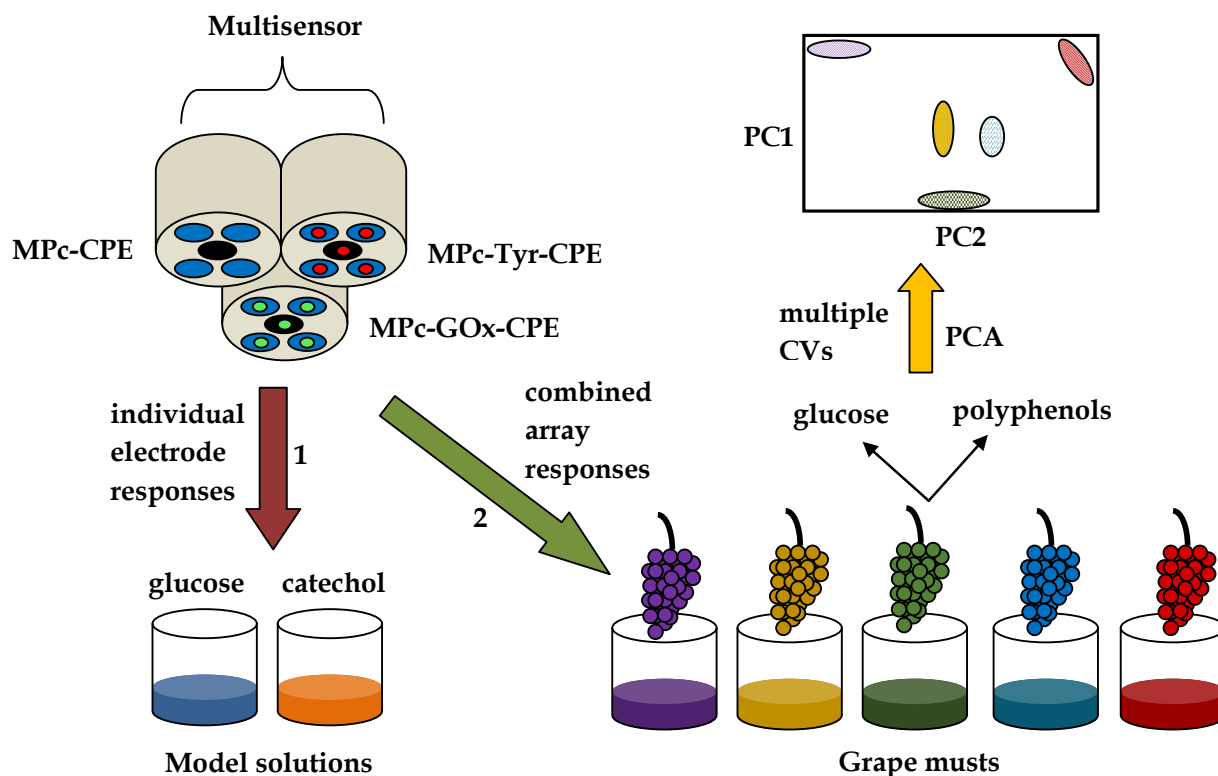


**Figure 1.14:** Illustration depicting the summarized analytical procedure for the detection of different grape musts.

### 1.6.3 A Bisphenol A Sensor

Gold electrodes modified with O-Ni-O bridged tetraamino (TA) substituted NiPc [Ni(OH)TAPc] films of varying thickness were tested for their electrocatalytic activities towards Bisphenol A (BPA) [123]. BPA used in polycarbonates and epoxy resins is a potent endocrine-disrupting compound [124, 125]. The NiTAPc modified gold electrode (*poly*-NiTAPc) was fabricated by electropolymerization of the complex over 20 consecutive CV cycles. Ni(OH)TAPc modified electrodes (*poly*-Ni(OH)TAPc) were prepared by running 30, 50, 70 or 90 repetitive CV cycles, respectively on NiTAPc electrodes immersed in NaOH to effect O-Ni-O bridge

formation and were represented as *poly-30-Ni(OH)TAPc*, *poly-50-Ni(OH)TAPc*, *poly-70-Ni(OH)TAPc* and *poly-90-Ni(OH)TAPc*.

Comparative analysis of the CVs obtained for each modified electrode in a solution of BPA revealed that each showed a peak for BPA oxidation at 0.45 V (vs. Ag | AgCl) whereas the bare gold electrode did not. Furthermore the largest peak current was obtained for *poly-70-Ni(OH)TAPc* showing that optimum electrocatalytic behaviour was obtained for 70 CV cycles. This electrode was used to obtain calibration curves for BPA detection at concentrations ranging from  $7 \times 10^{-4}$  to  $3 \times 10^{-2}$  mol/L. The limit of detection was found to be  $3.68 \times 10^{-9}$  mol/L which showed excellent sensitivity compared to previously reported MPc modified electrodes. The standard addition method was then employed to calculate the concentration of BPA in a plastic soda bottle and the microwave plastic covering of a meat package. The plastic covering had a larger BPA concentration ( $2.55 \mu\text{M}$ ) than the soft drink bottle ( $0.585 \mu\text{M}$ ).

## 1.7 References

- [1] N.B. McKeown, *Phthalocyanine Materials: Synthesis, Structure and Function*, Cambridge University Press, Cambridge, 1998, ch.1, pp. 1-10.
- [2] R.P. Linstead, *J. Chem. Soc.*, 1934, 1016.
- [3] R.M. Christie, *Colour Chemistry*, The Royal Society of Chemistry, Cambridge, 2<sup>nd</sup> edn., 2015, ch. 1, pp. 1-20.
- [4] K.D. Wael, P. Westbroek, E. Temmerman, *J. Electroanal. Chem.*, 2004, **567**, 167.

- [5] M. Evangelisti, *Encyclopaedia of Supramolecular Chemistry*, ed. J. L. Atwood, J. W. Steed, CRC Press, New York, 2004, vol.2, phthalocyanines, pp. 1069-1075.
- [6] I. Ponce, A.C. Aragoes, N. Darwish, P. Pla-Vilanova, R. Onate, M.C. Rezende, J.H. Zagal, F. Sanz, J. Pavez, I. Diez-Perez, *Electrochim. Acta*, 2015, <http://dx.doi.org/10.1016/j.electacta.2015.03.150>, in press.
- [7] H.T. Akcay, R. Bayrak, S. Karslioglu, E. Sahin, *J. Organomet. Chem.*, 2012, **713**, 1.
- [8] M. L'Her, A. Pondaven, *The Porphyrin Handbook: Phthalocyanines: Spectroscopic and Electrochemical Characterization*, ed. K.M. Kadish, K.M. Smith, R. Guilard, Academic Press, the Netherlands, ch. 104, pp. 118-164.
- [9] Z. Biyiklioglu, I. Acar, *Synth. Met.*, 2012, **162**, 1156.
- [10] K.R.V. Reddy, J. Keshavayya, B.E. Kumara Swamy, M.N.K. Harish, H.R. Mallikarjuna, B.S. Sherigara, *Dyes and Pigments*, 2009, **80**, 1.
- [11] A. Thimiopoulos, A. Vogiatzi, E.D. Simandiras, G.A. Mousdis, N. Psaroudakis, *Inorg. Chim. Acta*, 2010, **412**, 121.
- [12] D. Wöhrle, G. Schnurpfeil, S.G. Makarov, A. Kazarin, O.N. Suvorova, *Macroheterocycles*, 2012, **5**, 191.
- [13] M. Celebi, M.S. Agirtas, V. Okumus, S. Ozdemir, *Synth. Met.*, 2014, **195**, 154.
- [14] M. Camur, M. Durmus, M. Bulut, *J. Photochem. Photobiol., A*, 2011, **222**, 266.
- [15] M. Canlica, T. Nyokong, *Polyhedron*, 2011, **30**, 1975.
- [16] M. Kandaz, M.N.U. Yarasir, A. Koca, O. Bekaroglu, *Polyhedron*, 2002, **21**, 255.
- [17] L. Valli, *Adv. Colloid Interface Sci.*, 2005, **116**, 13.
- [18] A. Erdogmus, I.N. Booyesen, T. Nyokong, *Synth. Met.*, 2011, **161**, 241.

- [19] F. Bedioui, S. Griveau, T. Nyokong, A.J. Appleby, C.A. Caro, M. Gulppi, G. Ochoa, J.H. Zagal, *Phys. Chem. Chem. Phys.*, 2007, **9**, 3383.
- [20] J.C. Obirai, T. Nyokong, *J. Electroanal. Chem.*, 2007, **600**, 251.
- [21] H. Havsteen, *Pharmacol. Ther.*, 2002, **96**, 67.
- [22] M. Grazul, E. Budzis, *Coord. Chem. Rev.*, 2009, **253**, 2588.
- [23] V.Y. Sosnovskikh, A.V. Safrygin, V.A. Anufriev, O.S. Eltsov, V.O. Iaroshenko, *Tetrahedron Lett.*, 2011, **52**, 6271.
- [24] R.S. Keri, S. Budagumpi, R.K. Pai, R.G. Balakrishna, *Eur. J. Med. Chem.*, 2014, **78**, 340.
- [25] V.Y. Sosnovskikh, V.Y. Korotaev, A.Y. Barkov, A.A. Sokovnina, M.I. Kodess, *J. Fluorine Chem.*, 2012, **141**, 58.
- [26] M. Camur, M. Bulut, M. Kandaz, O. Guney, *Polyhedron*, 2009, **28**, 233.
- [27] M.M. Ghoneim, A. Tawfik, *Anal. Chim. Acta*, 2004, **511**, 63.
- [28] A. Bouchoucha, A. Terbouche, A. Bourouina, S. Djebbar, *Inorg. Chim. Acta*, 2014, **418**, 187.
- [29] K. Lee, *Springer Theses: Stereoselective Syntheses of Tetrahydropyrans*, Springer International Publishing, Switzerland, 2014.
- [30] J. Che, C.-J. Zheng, M.-X. Song, Y.-J. Bi, Y. Liu, Y.-J. Li, Y. Wu, L.-P. Sun, H.-R. Piao, *Med. Chem. Res.*, 2014, **23**, 426.
- [31] S.N. Aslam, P.C. Stevenson, T. Kokubun, D.R. Hall, *Microbiol. Res.*, 2009, **164**, 191.
- [32] A. Verma, S.N. Pandeya, S. Shweta, *Int. J. Res. Ayurveda Pharm.*, 2011, **2**, 1110.

- [33] R. Bai, T.L. Nguyen, J.C. Burnett, O. Atasoylu, M.H.G. Munro, G.R. Pettit, A.B. Smith III, R. Gussio, E. Hamel, *J. Chem. Inf. Model*, 2011, **51**, 1393.
- [34] M.J. Yu, Y. Kishi, B.A. Littlefield, *Anticancer Agents from Natural Products*, ed. G.M. Cragg, D.G.I. Kingston, D.J. Newman, CRC Press, USA, 2<sup>nd</sup> edn., 2011, ch. 13, pp. 317-340.
- [35] J.G. Napolitano, A.H. Daranas, M. Norte, J.J. Fernandez, *Advances in Anticancer Agents in Medicinal Chemistry*, ed. M. Prudhomme, Bentham Science Publishers, vol. 2, ch. 1, 2013, pp. 3-45.
- [36] A.T. Bilgicli, A. Gunzel, M. Kandaz, A. Altindal, H. Comert, *J. Organomet. Chem.*, 2015, **785**, 112.
- [37] M. Wojdyla, M. Rebarz, P. Dalasinski, W. Bala, Z. Lukasiak, B. Derkowska, B. Sahraoui, *Trends in Optical Materials*, ed. O.G. Gardens, Nova Science Publishers, New York, 2007, ch. 1, pp. 1-54.
- [38] D. Dini, M. Hanack, *The Porphyrin Handbook: Phthalocyanines: Properties and Materials*, ed. K.M. Kadish, K.M. Smith, R. Guilard, Academic Press, The Netherlands, 2003, vol. 17, ch. 107, pp. 1-32.
- [39] N. Kobayashi, C.C. Leznoff, *J. Porphyrins Phthalocyanines*, 2004, **8**, 1015.
- [40] V.N. Nemykin, E.A. Lukyanets, *Handbook of Porphyrin Science: with Applications to Chemistry, Physics, Material Science, Engineering, Biology and Medicine*, ed. K.M. Kadish, K.M. Smith, R. Guilard, World Scientific Publishing Co. Pte. Ltd., Singapore, 2010, vol. 3, ch. 11, pp. 1-324.
- [41] T. Nyokong, *Functional Phthalocyanine Molecular Materials*, ed. J. Jiang, D.M.P. Mingos, Springer, Berlin, 2010, pp. 45-88.

- [42] M.-S. Liao, S. Scheiner, *J. Chem. Phys.*, 2001, **114**, 9780.
- [43] F.R. Fan, L.R. Faulkner, *J. Am. Chem. Soc.*, 1979, **101**, 4779.
- [44] G.J. Chen, X. Qiao, P.Q. Qiao, G.J. Xu, J.Y. Xu, J.L. Tian, W. Gu, X. Liu, S.P. Yan, *J. Inorg. Biochem.*, 2011, **105**, 119.
- [45] M.S. Mathews, V. Vo, E.-C. Shih, G. Zamora, C.-H. Sun, S.J. Madsen, H. Hirschberg, *J. Environ. Pathol. Toxicol. Oncol.*, 2012, **31**, 49.
- [46] M. Rajendran, *Photodiagn. Photodyn. Ther.*, 2015, [doi:10.1016/j.pdpdt.2015.07.177](https://doi.org/10.1016/j.pdpdt.2015.07.177), in press.
- [47] T. Erdogan, M. Bulut, M. Camur, *J. Photochem. Photobiol., A*, 2015, **300**, 6.
- [48] N. Sekkat, H.V.D. Berg, T. Nyokong, N. Lange, *Molecules*, 2012, **17**, 98.
- [49] E. Guzel, A. Atsay, S. Nalbantoglu, N. Saki, A.L. Dogan, A. Gul, M.B. Kocak, *Dyes and Pigments*, 2013, **97**, 238.
- [50] K. Sakamoto, E. Ohno-Okumura, *Materials*, 2009, **2**, 1127.
- [51] J.-Y. Liu, J. Li, X. Yuan, W.-M. Wang, J.-P. Xue, *Photodiagn. Photodyn. Ther.*, 2015, [doi:10.1016/j.pdpdt.2015.07.003](https://doi.org/10.1016/j.pdpdt.2015.07.003), in press.
- [52] D. Cakir, V. Cakir, Z. Biyiklioglu, M. Durmus, H. Kantekin, *J. Organomet. Chem.*, 213, **745-746**, 423.
- [53] X.-S. Li, J. Guo, J.-J. Zhuang, B.-Y. Zheng, M.-R. Ke, J.-D. Huang, *Bioorg. Med. Chem. Lett.*, 2015, **25**, 2386.
- [54] A. Wang, Y. Li, L. Zhou, L. Yuan, S. Lu, Y. Lin, J. Zhou, S. Wei, *J. Photochem. Photobiol., B*, 2014, **141**, 10.
- [55] A. Erdogmus, T. Nyokong, *J. Mol. Struct.*, 2010, **977**, 26.

- [56] B.T. Yiltiz, T. Sezgin, Z.P. Cakar, C. Uslan, B.S. Sesalan, A. Gul, *Synth. Met.*, 2011, **161**, 1720.
- [57] K. Hirakawa, T. Hirano, Y. Nishimura, T. Arai, Y. Nosaka, *J. Phys. Chem. B*, 2012, **116**, 3037.
- [58] Y. Ishikawa, N. Yamakawa, T. Uno, *Bioorg. Med. Chem.*, 2002, **10**, 1953.
- [59] T. Zhou, R. Shao, S. Chen, X. He, J. Qiao, J. Zhang, *J. Power Sources*, 2015, **293**, 946.
- [60] R. Baker, D.P. Wilkinson, J. Zhang, *Electrochim. Acta*, 2008, **53**, 6906.
- [61] L. Zhang, J. Zhang, D.P. Wilkinson, H. Wang, *J. Power Sources*, 2006, **156**, 171.
- [62] H.-S. Oh, J.-G. Oh, B. Roh, I. Hwang, H. Kim, *Electrochem. Commun.*, 2011, **13**, 879.
- [63] R.A. Sidik, A.B. Anderson, N.P. Subramanian, S.P. Kumaraguru, B.N. Popov, *J. Phys. Chem., B*, 2006, **110**, 1787.
- [64] R. Jasinski, *Nature*, 1964, **201**, 1212.
- [65] C.W.B. Bezerra, L. Zhang, K. Lee, H. Liu, J. Zhang, Z. Shi, A.L.B. Marques, E.P. Marques, S. Wu, J. Zhang, *Electrochim. Acta*, 2008, **53**, 7703.
- [66] A.A. Tanaka, C. Fierro, D. Scherson, E.B. Yeager, *J. Phys. Chem.*, 1987, **91**, 3799.
- [67] W. Li, A. Yu, D.C. Higgins, B.G. Llanos, Z. Chen, *J. Am. Chem. Soc.*, 2010, **132**, 17056.
- [68] D.M. Bernardi, M.W. Verbrugge, *J. Electrochem. Soc.*, 1992, **139**, 2477.
- [69] J.H. Zagal, S. Griveau, J.F. Silva, T. Nyokong, F. Bedioui, *Coord. Chem. Rev.*, 2010, **254**, 2755.
- [70] D. Quesada-Gonzalez, A. Merkoci, *Biosens. Bioelectron.*, 2015, **73**, 47.

- [71] V. Scognamiglio, A. Antonacci, M.D. Lambreva, S.C. Litescu, G. Rea, *Biosens. Bioelectron.*, 2015, **74**, 1076.
- [72] J.R. Stetter, W.R. Penrose, S. Yao, *J. Electrochem. Soc.*, 2003, **150**, S11.
- [73] U.E. Spichiger-Keller, *Chemical Sensors and Biosensors for Medical and Biological Applications*, John Wiley and sons, Germany, 1998, ch. 1, 2, pp. 1-82.
- [74] E. Galindo, *Biotechnology*, ed. H.W. Doelle, J.S. Rokem, M. Berovic, *Encyclopedia of Life Support systems*, EOLSS publishers, France, ch. 2., [http://www.eolss.net].
- [75] S. Prasad, Y. Yadav, M. Bothara, V. Kunduru, S. Muthukumar, *Microfluidic Devices in Nanotechnology*, ed. C.S. Kumar, John Wiley and sons, Canada, 2010, ch. 2, pp. 47-90.
- [76] J. Wang, *Chem. Rev.*, 2008, **108**, 814.
- [77] A.M. Pisoschi, *Biochem. Anal. Biochem.*, **1**, 2012, <http://dx.doi.org/10.4172/2161-1009.1000e119>.
- [78] S.P. Mohanty, E. Koungianos, *IEEE Potentials*, 2006, **25**, 35.
- [79] A. Harper, M.R. Anderson, *Sensors*, 2010, **10**, 8248.
- [80] E.-H. Yoo, S.-Y. Lee, *Sensors*, 2010, **10**, 4558.
- [81] T. Nyokong, *N<sub>4</sub>-Macrocyclic Metal Complexes*, ed. J.H. Zagal, F. Bedioui, J.-P. Dodelet, Springer Science + Business Media, LLC, New York, 2006, ch. 7, pp. 315-361.
- [82] C. Barrera, I. Zhukov, E. Villagra, F. Bedioui, M.A. Paez, J. Costamagna, J.H. Zagal, *J. Electroanal. Chem.*, 2006, **589**, 212.
- [83] M. Sancy, J.F. Silva, J. Pavez, J.H. Zagal, *J. Chil. Chem. Soc.*, 2013, **58**, 2117.

- [84] J. Obirai, T. Nyokong, *Electrochim. Acta*, 2005, **50**, 5427.
- [85] M.H. Pournaghi-Azar, R. Sabzi, *J. Electroanal. Chem.*, 2003, **543**, 115.
- [86] I.N. Booysen, F. Matemadombo, M. Durmus, T. Nyokong, *Dyes and Pigments*, 2011, **89**, 111.
- [87] A. Aktas, I. Acar, A. Koca, Z. Biyiklioglu, H. Kantekin, *Dyes and Pigments*, 2013, **99**, 613.
- [88] M.B. Kılıçaslan, H. kantekin, A. Koca, *Dyes and Pigments*, 2014, **103**, 95.
- [89] M. Ozcesmeci, I. Nar, E. Hamuryudan, *Turk. J. Chem.*, 2014, **38**, 1064.
- [90] S. Maree, T. Nyokong, *J. Electroanal. Chem.*, 2000, **492**, 120.
- [91] S. Unlu, M.N. Yarasir, M. Kandaz, A. Koca, B. Salih, *Polyhedron*, 2008, **27**, 280.
- [92] E. Guzel, A. Atsay, S. Nalbantoglu, N. Saki, A.L. Dogan, A. Gul, M.B. Kocak, *Dyes and Pigments*, 2013, **97**, 238.
- [93] K.R.V. Reddy, J. Keshavayya, B.E. Kumara Swamy , M.N.K. Harish, H.R. Mallikarjuna, B.S. Sherigara, *Dyes and Pigments*, 2009, **80**, 1.
- [94] M. Arici, D. Arican, A.L. Ugur, A. Erdogmus, A. Koca, *Electrochim. Acta*, 2013, **87**, 554.
- [95] M. Camur, M. Bulut, *Dyes and Pigments*, 2008, **77**, 165.
- [96] A. Nas, H. Kantekin, A. Koca, *J. Organomet. Chem.*, 2014, **757**, 62.
- [97] H.R.P. Karaoglu, A. Koca, M.B. Kocak, *Dyes and Pigments*, 2012, **92**, 1005.
- [98] K.I. Ozoemena, T. Nyokong, *Microchem. J.*, 2003, **75**, 241.
- [99] C.M. Lieber, N.S. Lewis, *J. Am. Chem. Soc.*, 1984, **106**, 5033.
- [100] N. Sehlotho, T. Nyokong, J.H. Zagal, F. Bedioui, *Electrochim. Acta*, 2006, **51**, 5125.

- [101] P. Janda, J. Weber, L. Dunsch, A.B.P. Lever, *Anal. Chem.*, 1996, **68**, 960.
- [102] Deronzier, J.C. Moutet, *Acc. Chem. Res.*, 1989, **22**, 249.
- [103] R.H. Tredgold, *Rep. Prog. Phys.*, 1987, **50**, 1609.
- [104] O.N. Oliveira jnr., *Braz. J. Phys.*, 1992, **22**, 60.
- [105] Y. Fu, K. Jayaraj, A.B.P. Lever, *Langmuir*, 1994, **10**, 383.
- [106] G. Mbambisa, N. Nombona, T. Nyokong, *Microchem. J.*, 2009, **93**, 60.
- [107] F.C. Moraes, M.F. Cabral, S.A.S. Machado, L.H. Mascaro, *Electroanalysis*, 2008, **20**, 851.
- [108] Y.-Q. Dai, K.-K. Shiu, *Electroanalysis*, 2004, **16**, 20.
- [109] S.M. Lee, Y.H. Lee, Y.G. Hwang, J.R. Hahn, H. Kang, *Phys. Rev. Lett.*, 1999, **82**, 217.
- [110] S. Niyogi, M.A. Hamon, H. Hu, B. Zhao, P. Bhowmik, R. Sen, M.E. Itkis, R.C. Haddon, *Acc. Chem. Res.*, 2002, **35**, 1105.
- [111] H. Li, I. Kim, *Carbon Nanotubes-From Research to Applications*, ed. S. Bianco, InTech, 2011, ch. 13, pp. 211-228.
- [112] R.E. Sabzi, K. Rezapour, N. Samadi, *J. Serb. Chem. Soc.*, 2010, **75**, 537.
- [113] M.P. Siswana, K.I. Ozoemna, T. Nyokong, *Electrochim. Acta*, 2006, **52**, 114.
- [114] S. Nyoni, T. Mugadza, T. Nyokong, *Electrochim. Acta*, 2014, **128**, 32.
- [115] G. de la Torre, W. Blau, T. Torres, *Nanotechnology*, 2003, **14**, 765.
- [116] X. Wang, Y. Liu, W. Qiu, D. Zhu, *J. Mater. Chem.*, 2002, **12**, 1636.
- [117] X. Zuo, H. Zhang, N. Li, *Sens. Actuators, B*, 2012, **161**, 1074.
- [118] M. Shi, Z. Chen, L. Guo, X. Liang, J. Zhang, C. He, B. Wang, Y. Wu, *J. Mat. Chem., B*, 2014, **2**, 4876.

- [119] H. Hosseini, M. Mahyari, A. Bagheri, A. Shaabani, *Biosens. Bioelectron.*, 2014, **52**, 136.
- [120] I. Ohtsu<sup>1</sup>, N. Wiriyathanawudhiwong, S. Morigasaki, T. Nakatani, H. Kadokura, H. Takagi, *J. Biol. Chem.*, 2010, **285**, 17479.
- [121] S.V. Litvinenko, D. Bielobrov, V. Lysenko, T. Nychporuk, V.A. Skryshevsky, *Appl. Mater. Interfaces*, 2014, **6**, 18440.
- [122] C. Medina-Plaza, G. Revilla, R. Munoz, J.A. Fernandez-Escudero, E. Barajas, G. Medrano, J.A. de Saja, M.L. Roderiguez-Mendez, *J. Porphyrins Phthalocyanines*, 2014, **18**, 76.
- [123] K.V. Ragavan, N.K. Rastogi, M.S. Thakur, *Trends Anal. Chem.*, 2013, **52**, 248.
- [124] B.K. Kim, J.Y. Kim, D.-H. Kim, H.N. Choi, W.-Y. Lee, *Bull. Korean Chem. Soc.*, 2013, **34**, 1065.
- [125] V. Chauke, F. Matemadombo, T. Nyokong, *J. Hazard. Mater.*, 2010, **178**, 180.

---

---

# CHAPTER TWO

## Materials and Instrumentation

### 2.1 Materials

All solvents used were of analytical grade and purchased either from Merck SA or Sigma-Aldrich. Dimethylformamide (DMF) used in general synthesis and electrochemical experiments was distilled and stored over molecular sieves prior to use. All other solvents were used without further purification. All common laboratory chemicals were of analytical grade and were used as received. Refer to **Table 2.1** for the chemicals which were commercially obtained from either Sigma-Aldrich or Merck SA for use in synthesis. Refer to **Table 2.2** for the chemicals used in electrochemical experiments.

Sodium sulfate, phosphorus pentoxide ( $P_2O_5$ ), molecular sieves (4 Å), silicon dioxide (silica) for column chromatography, silica plates for thin layer chromatography, and aluminium oxide (alumina) were purchased from Merck SA. pH 4 and pH 7 buffer tablets were purchased from Sigma Aldrich. Multi-walled carbon nanotubes (MWCNTs) were acquired from Nanoshel. All metal complexes and ligands were stored over  $P_2O_5$ . Ultrapure water was obtained from an ElgaPurelab Ultra system.

**Table 2.1:** List of laboratory chemicals used for synthesis.

Name	Purity
4-Nitrophthalonitrile	99%
Potassium Carbonate	99.5%
7-Hydroxy-4-chromone	97%
7-Hydroxy-4-trifluoromethylcoumarin	98%
3-Hydroxyflavone	≥98%
(2-hydroxyphenyl)benzoxazole	98%
Tetrahydropyran-2-methanol	98%
2-Furanmethanethiol	≥98%
Cobalt(II) chloride	97%
Iron(II) chloride tetrahydrate	≥99%
Iron(II) acetate	95%
1,8-Diazabicyclo[5.4.0]undec-7-ene	98%

**Table 2.2:** List of laboratory chemicals used for electrochemistry.

Name	Purity
Tetrabutylammonium tetrafluoroborate (TBABF <sub>4</sub> )	99%
Sodium nitrite	≥97%
Dopamine hydrochloride	98%
L-cysteine	97%
Ferrocene	98%

## 2.2 Instrumentation

Fourier transform infrared (FTIR) spectra were recorded using a Bruker Alpha FTIR spectrometer equipped with an ATR platinum Diamond 1 reflectance accessory. A Varian 500 MHz spectrometer was available for nuclear magnetic resonance (NMR) spectroscopy. All NMR experiments were conducted in deuterated dimethylsulfoxide (DMSO). Ultraviolet-Visible (UV-Vis) spectroscopy was carried out using a Perkin-Elmer Spectrum 25. Melting points were recorded using a Stuart SMP3 melting point apparatus. Elemental analysis was carried out using a CHNS-O Flash 2000 Organic Elemental Analyser. Mass spectrometry (MS) was performed in both the positive and negative modes *via* direct injection of the respective samples into a Waters Micromass LCT Premier MS instrument equipped with an electrospray ionization (ESI) source and a time-of-flight (TOF) mass analyzer.

Single crystal X-ray diffraction (XRD) studies were conducted using a Bruker Apex Duo equipped with an Oxford Instruments Cryojet operating at 120( $\pm$ 2) and 100( $\pm$ 2) K and an Incoatec microsource operating at 30 W. The diffraction data was collected with Mo K $\alpha$  ( $\lambda = 0.71073 \text{ \AA}$ ) radiation at a crystal-to-detector distance of 50 mm. The following conditions were used for data collection: omega and phi scans with exposures taken at 30 W X-ray power and 0.50° frame widths using APEX2 [1]. The data were reduced with the programme SAINT [1] using outlier rejection, scan speed scaling, as well as standard Lorentz and polarization correction factors. A SADABS semi-empirical multi-scan absorption correction [2] was applied to the

data. Direct methods, SHELXS-97 [3] and WinGX [4] were used to solve the structures. All non-hydrogen atoms were located in the difference density map and refined anisotropically with SHELXL-97 [3].

Voltammetric studies on the metal complexes were conducted using an Autolab Potentiostat equipped with a three-electrode system: a Pt or glassy carbon (GC) working electrode, a pseudo Ag|AgCl reference electrode and a Pt counter electrode. The Autolab Nova 1.7 software was used for operation of the potentiostat and data analysis. The working electrode surfaces were regenerated between voltammetric scans by polishing over a slurry of alumina and ultra-pure water on Buehler and diamond polishing pads followed by rinsing with ultra-pure water and anhydrous DMF. Square wave voltammetry (SWV) was conducted by setting the step potential at 4 mV, the amplitude at 20 mV and the frequency at 25 Hz. Spectroelectrochemical experiments were undertaken using a Specac Optically Transparent Thin-Layer Electrochemical (OTTLE) cell. Chronoamperometry was employed to determine the catalytic rate constants associated with each modified electrode. Rotating disc electrode (RDE) studies were conducted using a Metrohm Autolab RDE equipped with a motor control unit. All electrochemical solutions of the complexes were prepared in deoxygenated DMF containing 0.1 M equivalents of TBABF<sub>4</sub> as a supporting electrolyte. A 1 mM solution of ferrocene containing 0.1 M TBABF<sub>4</sub> was employed as an electrochemical standard. **Fig. 2.1** shows the CVs of a Pt electrode and a GCE in ferrocene.

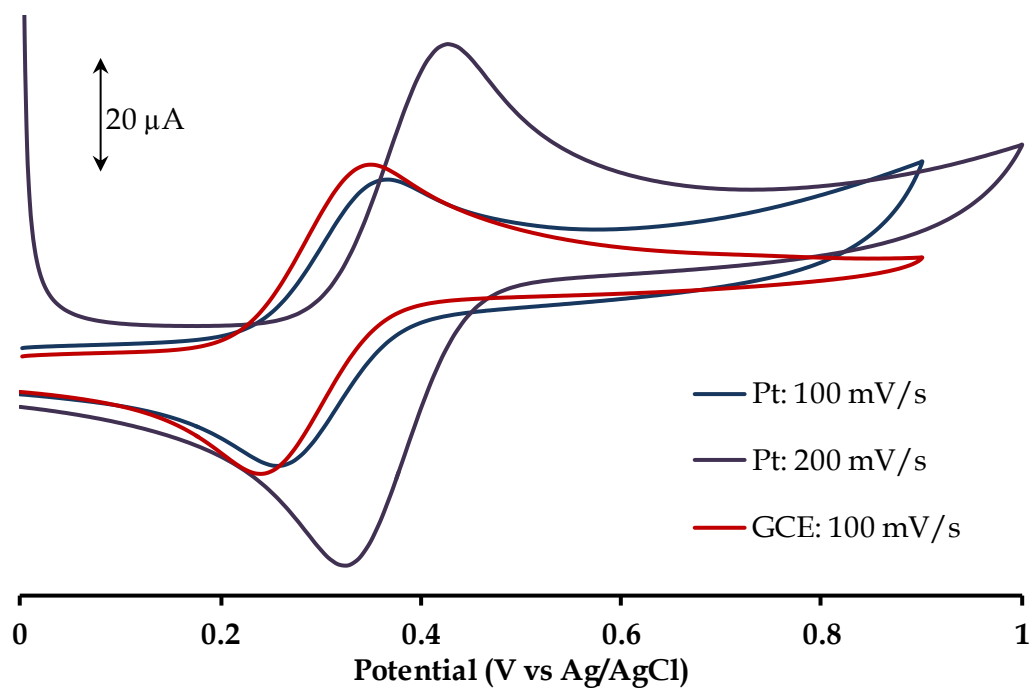


**Figure 2.1:** CV scans of the ferrocene standard on Pt and GC electrodes.

## 2.7 References

- [1] Bruker APEX2, SAINT and SADABS. Bruker AXS Inc. (2010) Madison, Wisconsin, USA.
- [2] R.H. Blessing, *Acta Cryst.*, 1995, **A51**, 33.
- [3] G.M. Sheldrick, *Acta Cryst.*, 2008, **A64**, 112.
- [4] L.J. Farrugia, *J. Appl. Cryst.*, 2012, **45**, 849.

---

---

# CHAPTER THREE

## Synthesis, Characterization and Electrocatalytic Behaviour of Novel Cobalt and Iron Phthalocyanines Bearing Chromone and Coumarin Moieties

### 3.1 Introduction

Phthalocyanines (Pcs) were originally used as dyes given their characteristic blue-green colour [1-4]. Further studies showed that their metal complexes, metallophthalocyanines (MPcs), are versatile compounds with vast applications in areas such as non-linear optics, chemical sensing, photodynamic therapy and surface modification through formation of Langmuir-Blodgett films [5-7]. MPcs form stable films on electrode surfaces which behave as active catalysts for a myriad of reactions including nitrite oxidation [8-11]. Typically, good electrocatalysts display durability, enhance electrode sensitivity and selectivity as well as lower the redox potential of an analyte [12]. These electrochemical properties can be optimized by meticulous selection of the metal centre as well as the substituents and their positions on the Pc ring [13-16].

The use of MPcs covalently linked to biologically significant substituents has been widely employed in electrocatalysis to allow the selective detection of important biological analytes [9, 17, 18]. In this study, MPcs substituted with chromones (1-benzopyran-4-one) and coumarins (1-benzopyran-2-one) were selected as they are oxygen-containing heterocyclic compounds, known as benzopyrones, which occur naturally in plants [19-22]. The biological activities of these heterocyclic compounds are modulated by different substituents to afford a wide range of properties such as anti-oxidant [23-25] and anti-coagulant activities [26, 27]. The utilization of the redox active metal centres, cobalt and iron is motivated by their ability to promote faster electron transfer kinetics for the respective MPc-modified working electrodes which is essential for electrocatalysis [28-30].

Nitrites are important biological molecules used as food preservatives and fertilizers [31, 32]. However, they combine with haemoglobin in the blood preventing oxygen from penetrating the tissues and also react with amines in the stomach to form carcinogenic nitrosamines [33-35]. The detection of nitrite concentrations is thus imperative for food quality assurance and for the determination of water resource contamination by fertilizer run-offs. Spectral analyses, chromatography and electrochemical methods have been employed for nitrite detection; the latter of which has proved to be the most time and cost effective method [33-36, 37]. In this study we report on the synthesis and characterization of peripherally benzopyrone-substituted MPcs containing redox active Fe(II) and Co(II) metal centres. In addition,

the electrocatalytic oxidation of nitrite was explored using electropolymerized MPcs on platinum working electrodes.

## 3.2 Experimental

### 3.2.1 Electrochemical Methods

A Pt working electrode was employed for all electrochemical experiments. Electrochemical studies on the complexes were conducted in deoxygenated dimethylformamide (DMF) solutions containing 0.1 M equivalents of tetrabutylammonium tetrafluoroborate (TBABF<sub>4</sub>) as a supporting electrolyte. Electropolymerization of the complexes onto a Pt electrode was achieved by repetitive cyclic voltammetry (20 cycles) in the potential window of -1.5 V to +1.5 V. The CMEs were rinsed in ultrapure water prior to use.

### 3.2.2 Synthesis

#### a) 4-(Chromone-7-oxy)phthalonitrile (**1**)

A mixture of 4-nitrophthalonitrile (1.00 g, 5.78 mmol) and 7-hydroxychromone (0.937 g, 5.78 mmol) in the presence of a basic catalyst, potassium carbonate (2.30 g, 16.6 mmol) was added to anhydrous DMF (30.0 cm<sup>3</sup>). The reaction mixture was heated while stirring at 90 °C under an inert nitrogen atmosphere for 24 h. The resultant solution was cooled to room temperature and poured into 300 cm<sup>3</sup> of a water-ice slurry. The precipitate was filtered and washed with cold ethyl acetate. A light

orange compound was obtained after purification *via* column chromatography using a 9:1 (*v:v*) ethyl acetate:hexane solvent system. The product was recrystallized by partial slow diffusion of hexane into a solution of **1** in CH<sub>3</sub>CN to give yellow-gold needle-like crystals. Yield: 46 %; m.p. (°C): 226.2-226.8; FT-IR ( $\nu_{max}$  /cm<sup>-1</sup>):  $\nu$ (C=O) 1644,  $\nu$ (C≡N) 2231,  $\nu$ (C-O-C) 1027, 1130; UV-Vis (DMF,  $\lambda_{max}$  ( $\epsilon$ , M<sup>-1</sup>cm<sup>-1</sup>)): 306 nm (11010), 295 nm (9962); <sup>1</sup>H NMR (ppm): 8.30 (d, 1H, *J* = 6.11 Hz, *H1*), 6.37 (d, 1H, *J* = 6.23 Hz, *H2*), 8.12 (d, 1H, *J* = 8.76 Hz, *H3*), 7.64 (d, 1H, *J* = 8.78 Hz, *H4*), 7.27 (d, 1H, *J* = 8.79 Hz, *H5*), 8.18 (d, 1H, *J* = 8.75 Hz, *H6*), 7.47 (s, 1H, *H7*), 8.01 (s, 1H, *H8*); <sup>13</sup>C NMR (ppm): 176.10, 159.84, 159.16, 157.77, 157.60, 136.91, 128.17, 124.59, 124.42, 121.96, 118.10, 117.43, 116.25, 115.76, 112.90, 110.28, 109.22. Molecular mass (*m/z*): Calcd: 288.26. Found: 311.32 [M+Na]<sup>+</sup>. Anal. Calc. for C<sub>17</sub>H<sub>8</sub>N<sub>2</sub>O<sub>3</sub>(%): C, 70.83; H, 2.80; N, 9.72. Found: C, 70.19; H, 2.78; N, 9.72.

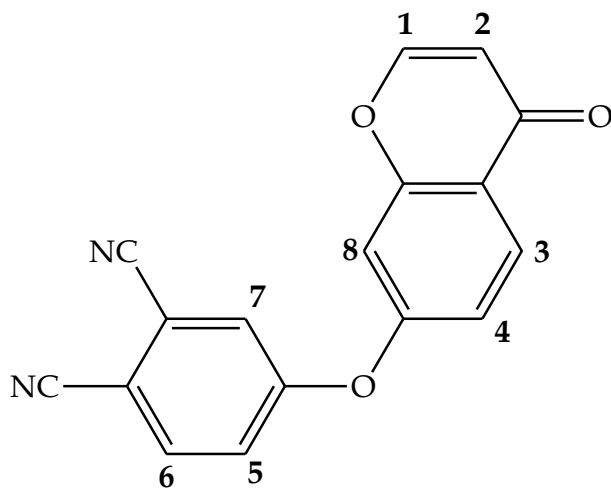


**Figure 3.1:** Structure of ligand 1.

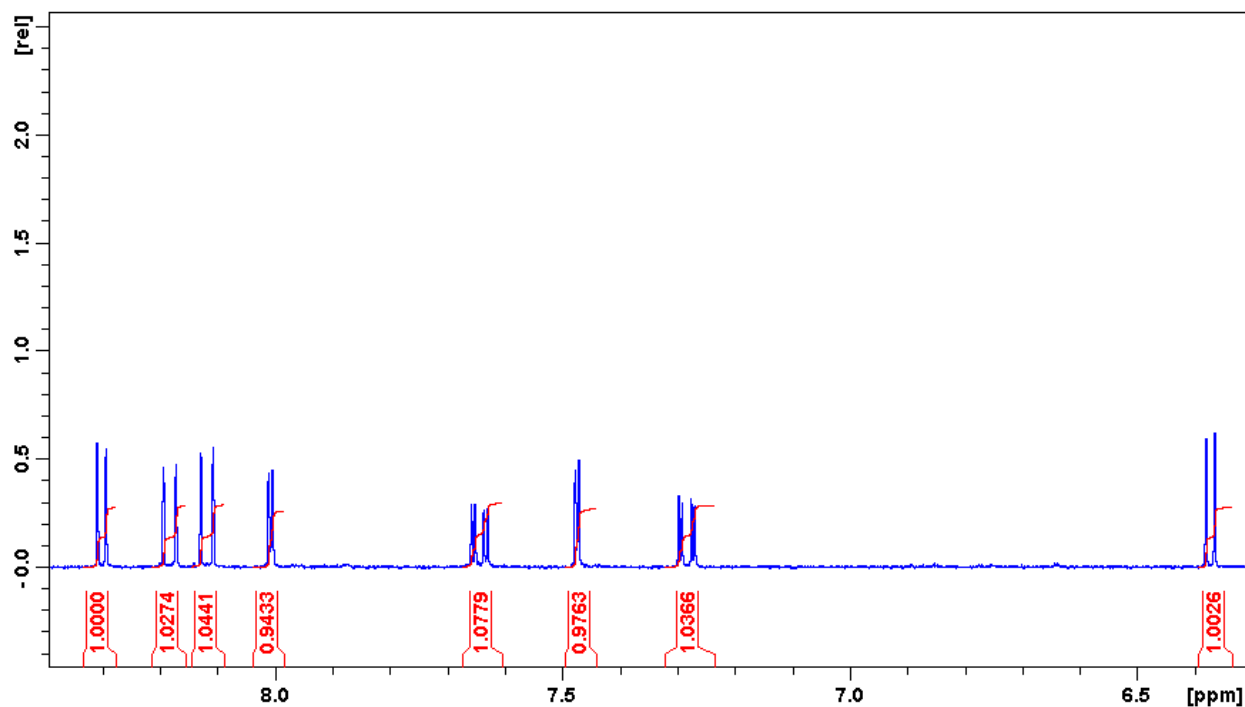


**Figure 3.2:**  $^1\text{H}$  NMR spectrum of ligand **1** in the range of 6.30-8.40 ppm.

b) 4-(4-(Trifluoromethyl)-coumarin-7-oxy)phthalonitrile (**2**)

Similarly, the reaction of 4-nitrophthalonitrile (1.00 g, 5.78 mmol) with 7-hydroxy-4-trifluoromethylcoumarin (1.33 g, 5.78 mmol) was initiated in 30.0 cm<sup>3</sup> of DMF in the presence of K<sub>2</sub>CO<sub>3</sub> (2.30 g, 16.6 mmol). The reaction mixture was heated with stirring at 90 °C under an inert nitrogen atmosphere for 24 h. Thereafter, the reaction mixture was cooled to room temperature, poured into 60.0 cm<sup>3</sup> water and extracted with CH<sub>3</sub>CN. The combined organic extracts were dried over sodium sulfate and filtered. The solvent was evaporated under reduced pressure and the remaining residue was added to 30% HCl to induce precipitation. The precipitate was then repeatedly washed with water and added to hot methanol (MeOH), filtered and dried under P<sub>2</sub>O<sub>5</sub>. Yield: 41 %; m.p. (°C): 180.0-181.8; FT-IR ( $\nu_{\text{max}}$  /cm<sup>-1</sup>):  $\nu(\text{C}=\text{O})$  1729,  $\nu(\text{C}\equiv\text{N})$

2235,  $\nu(\text{C-O-C})$  990, 1129; UV-Vis (DMF,  $\lambda_{\text{max}}$  ( $\epsilon$ ,  $\text{M}^{-1}\text{cm}^{-1}$ ): 443 nm (90), 318 nm (29875), 307 nm (33370);  $^1\text{H}$  NMR (ppm): 7.06 (s, 1H, H1), 7.99 (s, 1H, H2), 7.64 (d, 1H,  $J = 8.73$  Hz, H3), 8.19 (d, 1H,  $J = 8.74$  Hz, H4), 7.43 (s, 1H, H5), 7.28 (d, 1H,  $J = 8.80$  Hz, H6), 7.80 (d, 1H,  $J = 9.01$  Hz, H7);  $^{13}\text{C}$  NMR (ppm): 159.78, 158.74, 158.42, 156.01, 146.85, 137.01, 127.37, 124.64, 124.38, 123.44, 117.57, 117.21, 116.26, 116.11, 115.69, 110.82, 110.40, 109.04. Molecular mass ( $m/z$ ): Calcd: 356.25. Found: 379.03  $[\text{M}+\text{Na}]^+$ . Anal. Calcd. for  $\text{C}_{18}\text{H}_7\text{F}_3\text{N}_2\text{O}_3$  (%): C, 60.68; H, 1.98; N, 7.86. Found: C, 60.48; H, 2.30; N, 7.86.

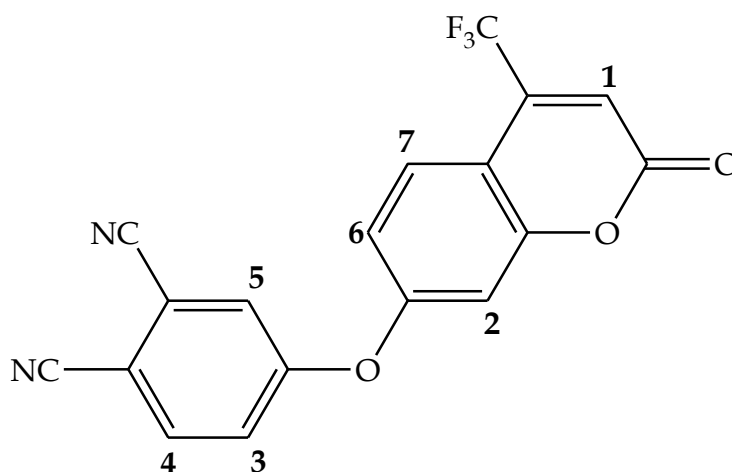


**Figure 3.3:** Structure of ligand 2.

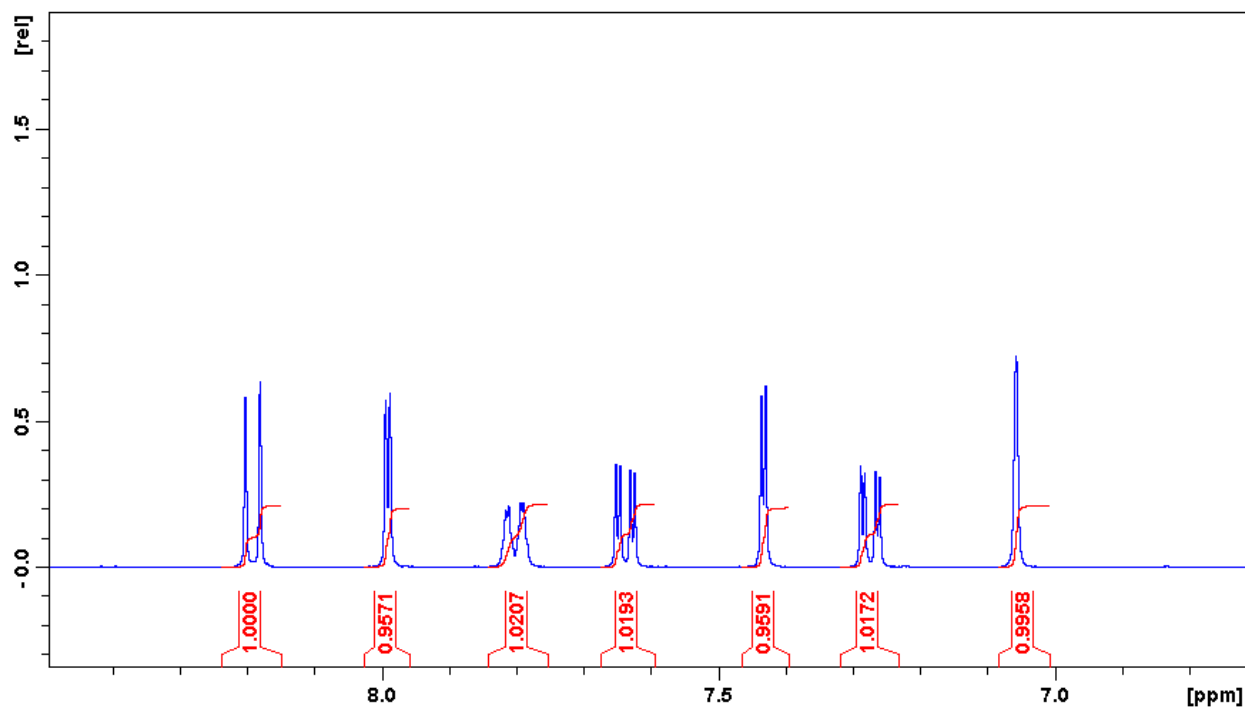


**Figure 3.4:**  $^1\text{H}$  NMR spectrum of ligand **2** in the range of 6.70-8.50 ppm.

c) *Tetra-4-(7-oxochromone phthalocyaninato)Co(II)* (*CoPc-chr*, **3**)

A mixture of **1** (0.25 g, 0.867 mmol),  $\text{CoCl}_2$  (0.0282 g, 0.217 mmol) and DBU was heated with stirring in *n*-pentanol (40.0  $\text{cm}^3$ ) at 160  $^\circ\text{C}$  under nitrogen for 16 h. The reaction mixture was then cooled to room temperature and *n*-hexane was added drop-wise to induce precipitation. The precipitate was filtered off using a millipore filtration setup and then washed with water, MeOH, ethanol (EtOH), dichloromethane (DCM) and  $\text{CH}_3\text{CN}$ . The desired product was thereafter recovered *via* column chromatography using a 50:1  $\text{CHCl}_3$ :MeOH solvent system. Yield: 51%; FT-IR ( $\nu_{\text{max}} / \text{cm}^{-1}$ ):  $\nu(\text{C}=\text{O})$  1645,  $\nu(\text{C}=\text{N})$  1592,  $\nu(\text{C}-\text{O}-\text{C})$  1073, 1131; UV-Vis (DMF,  $\lambda_{\text{max}}$  ( $\epsilon$ ,  $\text{M}^{-1}\text{cm}^{-1}$ ): 679 nm (23075), 343 nm (29176), 305 nm (82909). Molecular mass ( $m/z$ ): Calcd: 1211.15. Found: 1211.21  $[\text{M}]^+$ , 1212.22  $[\text{M}+\text{H}]^+$ , 1213.22  $[\text{M}+2\text{H}]^+$ . Anal.

Calcd. for  $C_{68}H_{32}CoN_8O_{12}$ (%): C, 67.39; H, 2.66; N, 9.25. Found: C, 66.95; H, 2.91; N, 8.97.

d) *Tetra-4-(7-oxy-4-trifluoromethylcoumarinphthalocyaninato)Fe(II) (FePc-cou, 4)*

The cyclotetramerization of **2** (0.250 g, 0.702 mmol) and  $FeCl_2 \cdot 4H_2O$  (0.0349 g, 0.175 mmol) was carried out under the same conditions as reported for **3**. The reaction mixture was allowed to cool to room temperature and *n*-hexane was added drop-wise to induce precipitation. The precipitate was filtered using a millipore filtration setup and then washed with water, MeOH, EtOH,  $CH_3CN$  and diethyl ether. The compound was purified by column chromatography using a 50:1 (*v:v*)  $CHCl_3$ :MeOH solvent system. Yield: 55%; FT-IR ( $\nu_{max}$  /  $cm^{-1}$ ):  $\nu(C=O)$  1747,  $\nu(C=N)$  1605,  $\nu(C-O-C)$  997, 1122; UV-Vis (DMF,  $\lambda_{max}$  ( $\epsilon$ ,  $M^{-1}cm^{-1}$ )): 657 nm (16891), 423 nm (17660), 328 nm (81208), 629 nm (18476), 423 nm (17660). Molecular mass ( $m/z$ ): Calcd: 1480.10. Found: 1480.19  $[M]^+$ , 1481.22  $[M+H]^+$ , 1482.21  $[M+2H]^+$ . Anal. Calcd. for  $FeC_{72}H_{28}F_{12}N_8O_{12}$ (%): C, 58.40; H, 1.91; N, 7.57. Found: C, 57.98; H, 2.15; N, 7.22.

e) *Tetra-4-(7-oxy-4-trifluoromethylcoumarinphthalocyaninato)Co(II) (CoPc-cou, 5)*

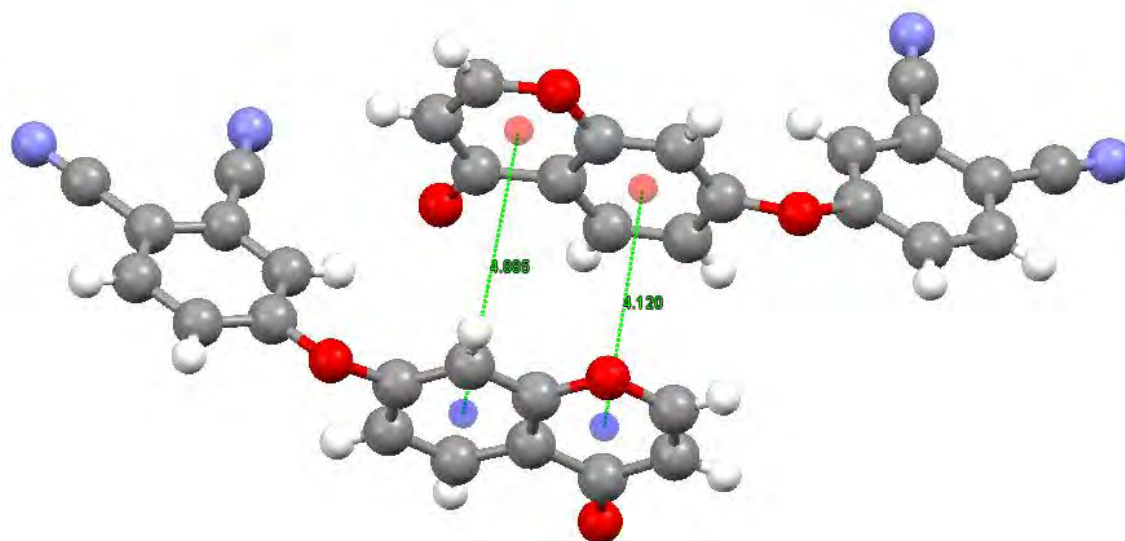
The title compound was formulated from the reaction of  $CoCl_2$  (0.0228 g, 0.175 mmol) with **2** (0.250 g, 0.702 mmol) using the same reaction conditions as specified in the isolation of the aforementioned MPcs. The reaction mixture was cooled to room temperature and *n*-hexane was added drop-wise in order to induce

precipitation. The precipitate was filtered using a millipore filtration setup and then washed with water, MeOH, EtOH, CH<sub>3</sub>CN, hexane and diethyl ether. The compound was further purified by column chromatography using a 1:50 (*v:v*) THF:CHCl<sub>3</sub> solvent system. FT-IR ( $\nu_{max}$  /cm<sup>-1</sup>):  $\nu(\text{C}=\text{O})$  1746,  $\nu(\text{C}=\text{N})$  1605,  $\nu(\text{C}-\text{O}-\text{C})$  997, 1122. Yield: 58%; UV-Vis (DMF,  $\lambda_{max}$  ( $\epsilon$ , M<sup>-1</sup>cm<sup>-1</sup>)): 669 nm (37422), 331 nm (41139), 283 nm (45899). Molecular mass ( $m/z$ ): Calcd: 1483.10. Found: 1483.09 [M]<sup>+</sup>, 1484.08 [M+H]<sup>+</sup>, 1485.07 [M+2H]<sup>+</sup>, 1486.10 [M+3H]<sup>+</sup>. Anal. Calcd. for CoC<sub>72</sub>H<sub>28</sub>F<sub>12</sub>N<sub>8</sub>O<sub>12</sub>(%): C, 58.27; H, 1.90; N, 7.55. Found: C, 57.92; H, 2.10; N, 7.12.

### 3.3 Results and Discussion

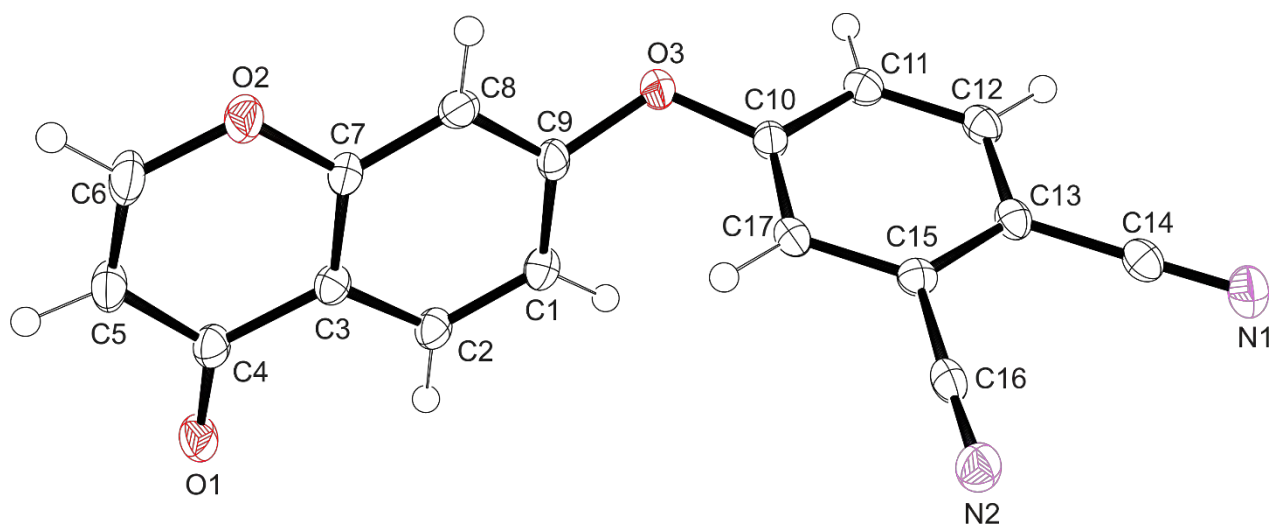
#### 3.3.1 Crystal structure of **1**

X-ray analysis of **1** revealed that it crystallizes out in a *Pc* space group with two molecules occupying a monoclinic unit cell. The crystal lattice is stabilized by interactions between co-planar chromone moieties of adjacent molecules with interplanar spacings of 4.120 Å and 4.885 Å, respectively, see **Fig. 3.5**. These intermolecular interactions ultimately lead to columns of molecules of **1** aligned parallel to the [*a*]- and [*b*]-axes. **Table 3.1** provides structure refinement data for crystal **1**.



**Figure 3.5:** A perspective view of the intermolecular interactions between the co-planar chromone moieties of adjacent molecules for **1**.

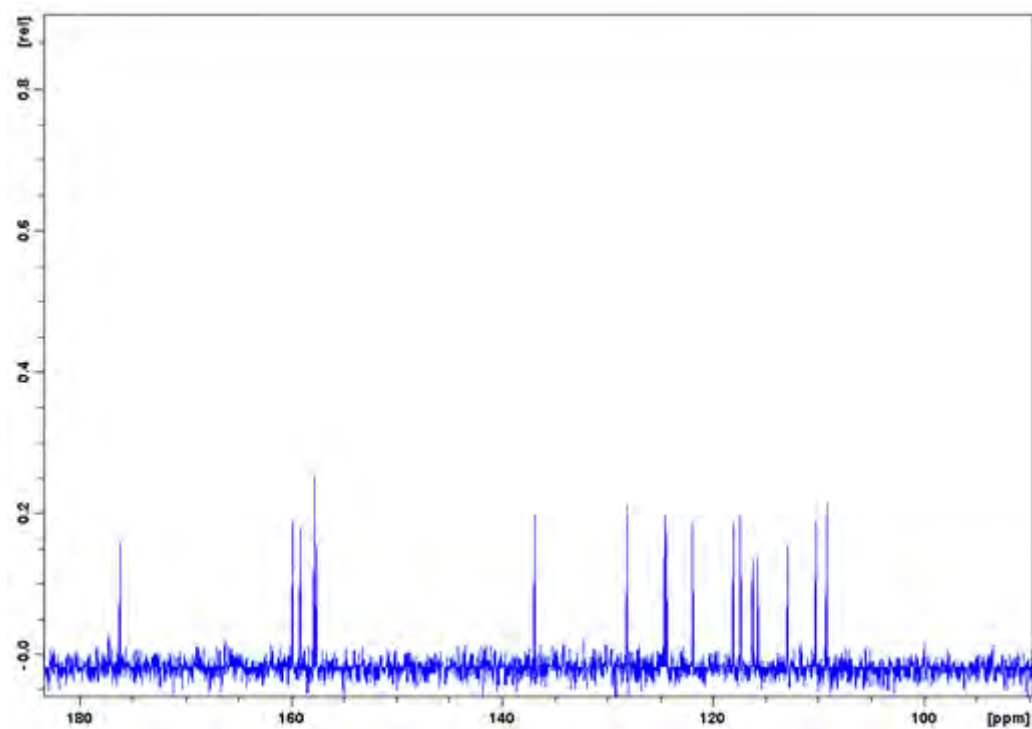
The aliphatic ether bond angle [C9-O3-C10] of  $118.9(2)^\circ$  results in the chromone moiety not lying in the same plane (deviating by  $74.51^\circ$ ) as the phthalonitrile moiety, see **Fig. 3.6**. As expected, the bond angle of the cyclic ether [C6-O2-C7 =  $117.9(2)^\circ$ ] is more constrained than the aliphatic ether but the C-O bond distances for the cyclic ether [C6-O2 =  $1.357(3)$  Å, C7-O2 =  $1.374(3)$  Å] and aliphatic ether [C9-O3 =  $1.396(2)$  Å, C10-O3 =  $1.372(3)$  Å] are still comparable. However, the C-O bond orders of the ethers and carbonyl group [C4-O1 =  $1.238(2)$  Å] are readily distinguishable based on the difference in their bond lengths. The nearly equidistant C≡N bonds are comparable to analogous bond distances of other 4-substituted phthalonitriles [38, 39]. Furthermore, the localized C1-C9 [ $1.403(3)$  Å] double bond remains intact as it is similar to the delocalized C-C (e.g. C12-C13 =  $1.402(3)$  Å) bonds found within **1**, refer to **Table 3.2**.



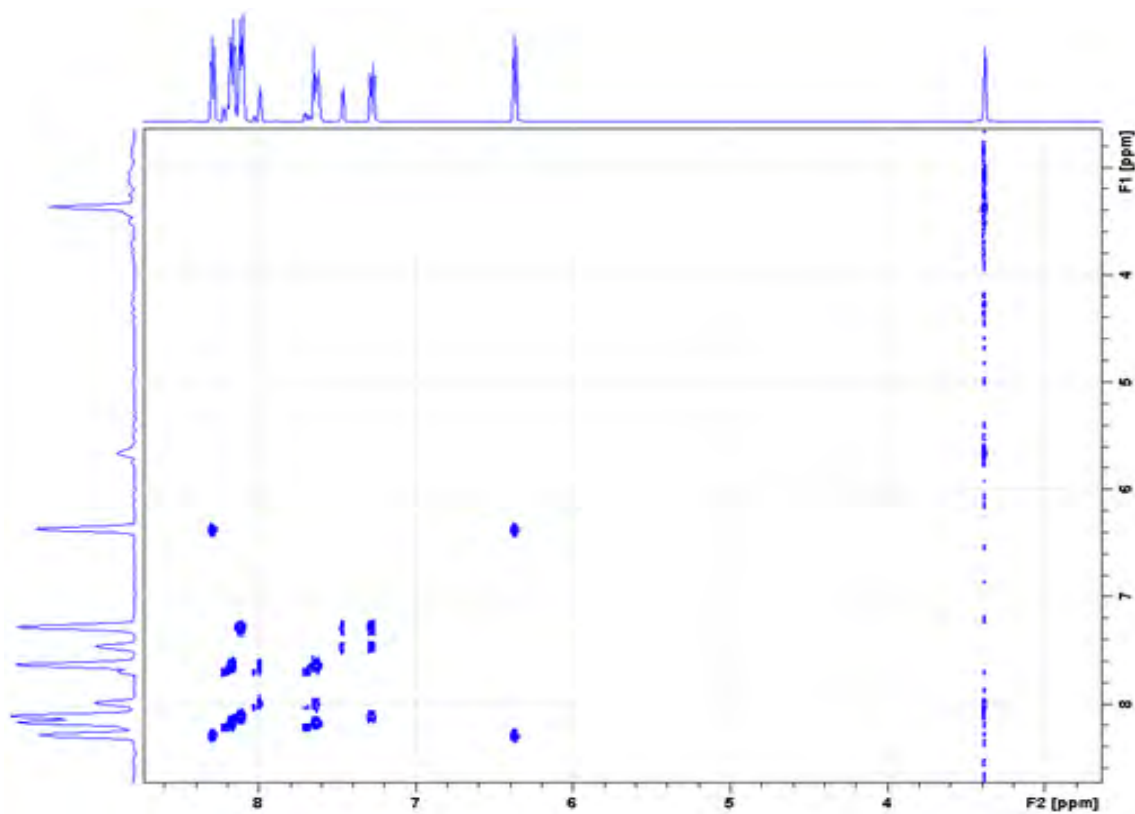
**Figure 3.6:** An ORTEP view of compound **1** showing 50 % probability displacement ellipsoids and atom labels.

### 3.3.2 Synthesis and Spectral Characterization

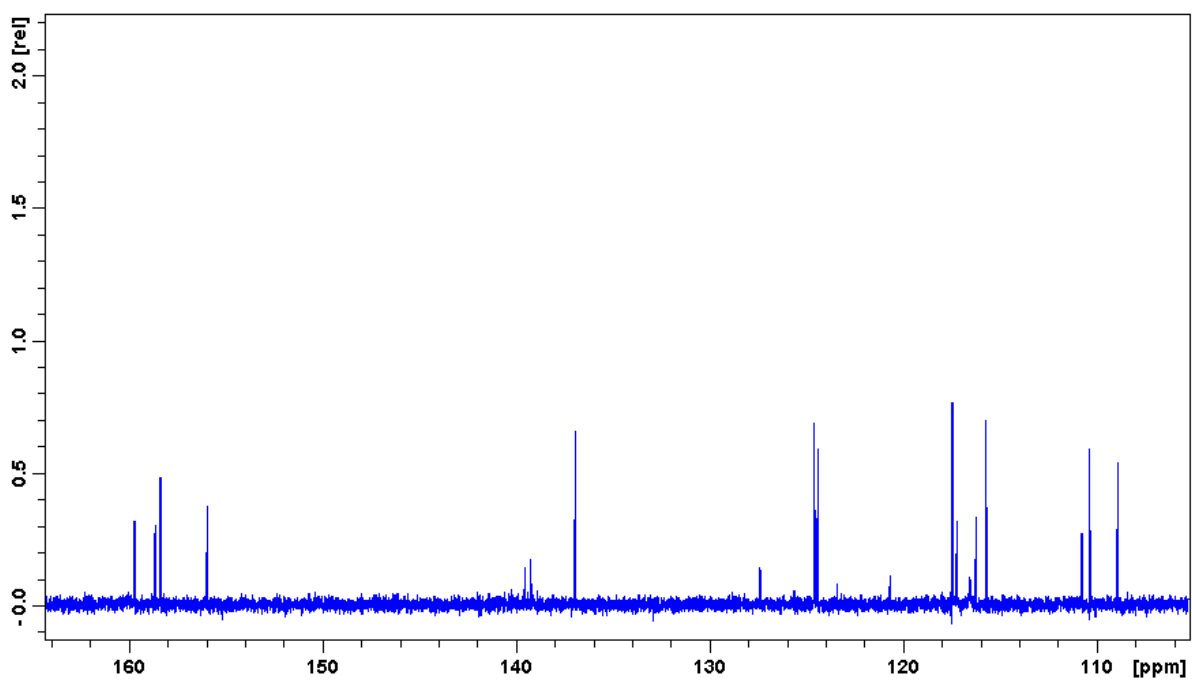
Novel benzopyrone-derivatized phthalonitriles **1** and **2** were formed *via* base catalyzed nucleophilic substitution reactions of 4-nitrophthalonitrile with 7-hydroxychromone and 7-hydroxy-4-trifluoromethylcoumarin, respectively (refer to **Scheme 3.1**). Spectral characterization of **1** and **2** unequivocally confirmed covalent linking of the individual benzopyrane moieties to the phthalonitrile groups. The  $^1\text{H}$  NMR spectra of the ligands showed well-resolved peaks in the region of 7.0 - 9.0 ppm as is expected for ligands with delocalized  $\pi$ -aromatic systems (see **Figs. 3.2** and **3.4**). The proton assignments were well supported by  $^{13}\text{C}$  and COSY NMR spectroscopy (see **Figs. 3.7-3.10**).



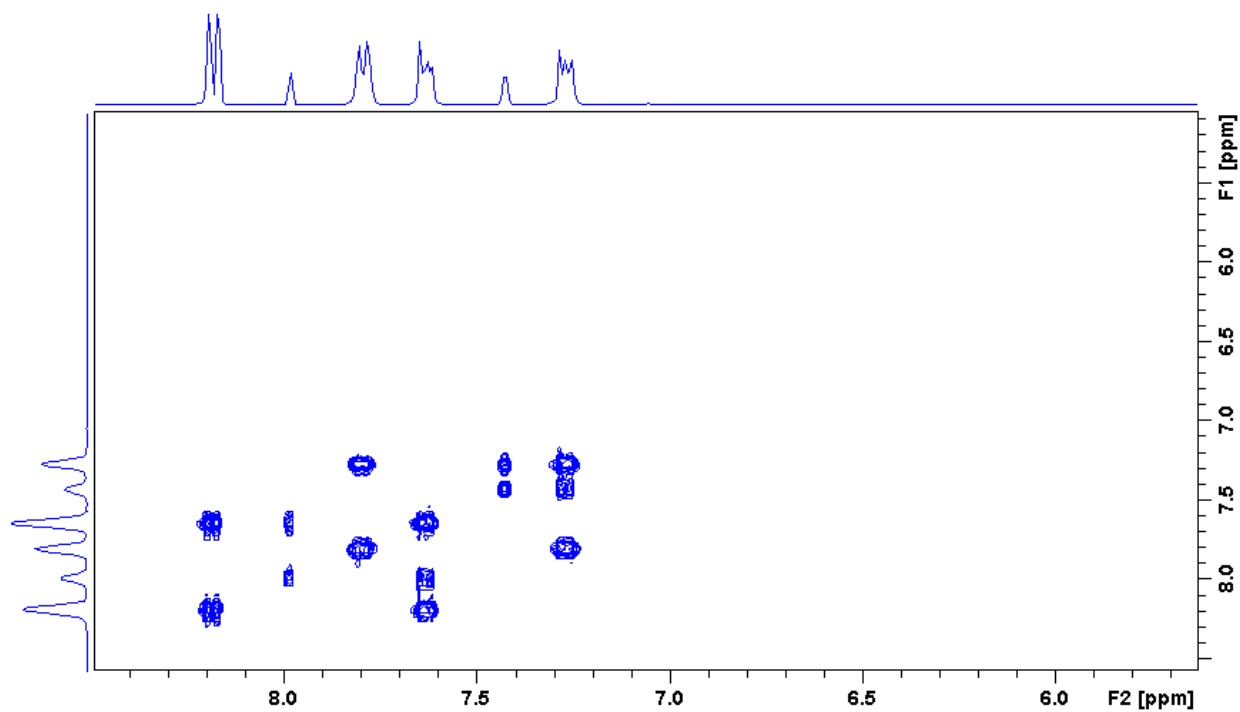
**Figure 3.7:**  $^{13}\text{C}$  NMR spectrum of ligand 1 in the range of 90 - 185 ppm.



**Figure 3.8:** COSY spectrum of ligand 1.

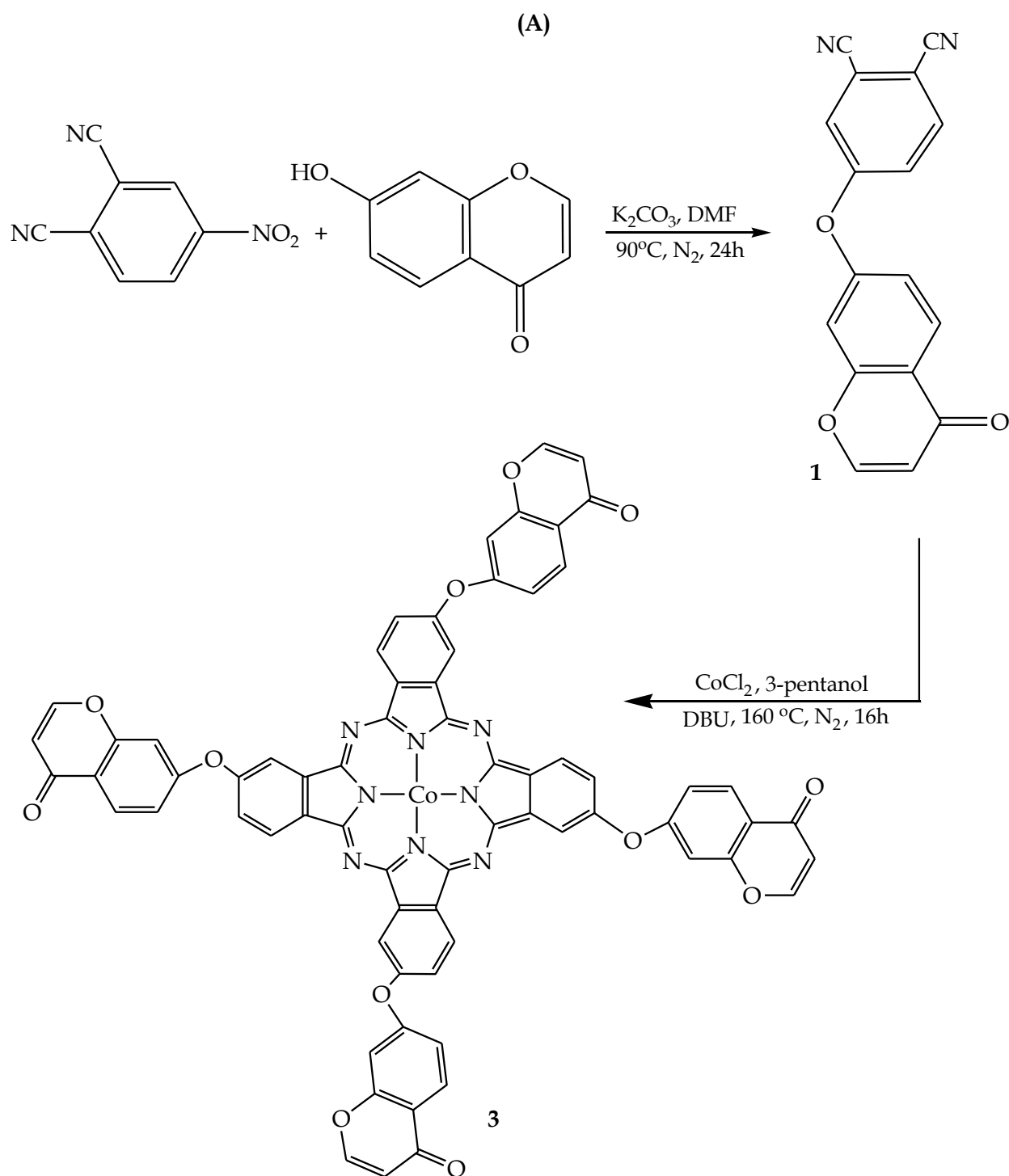


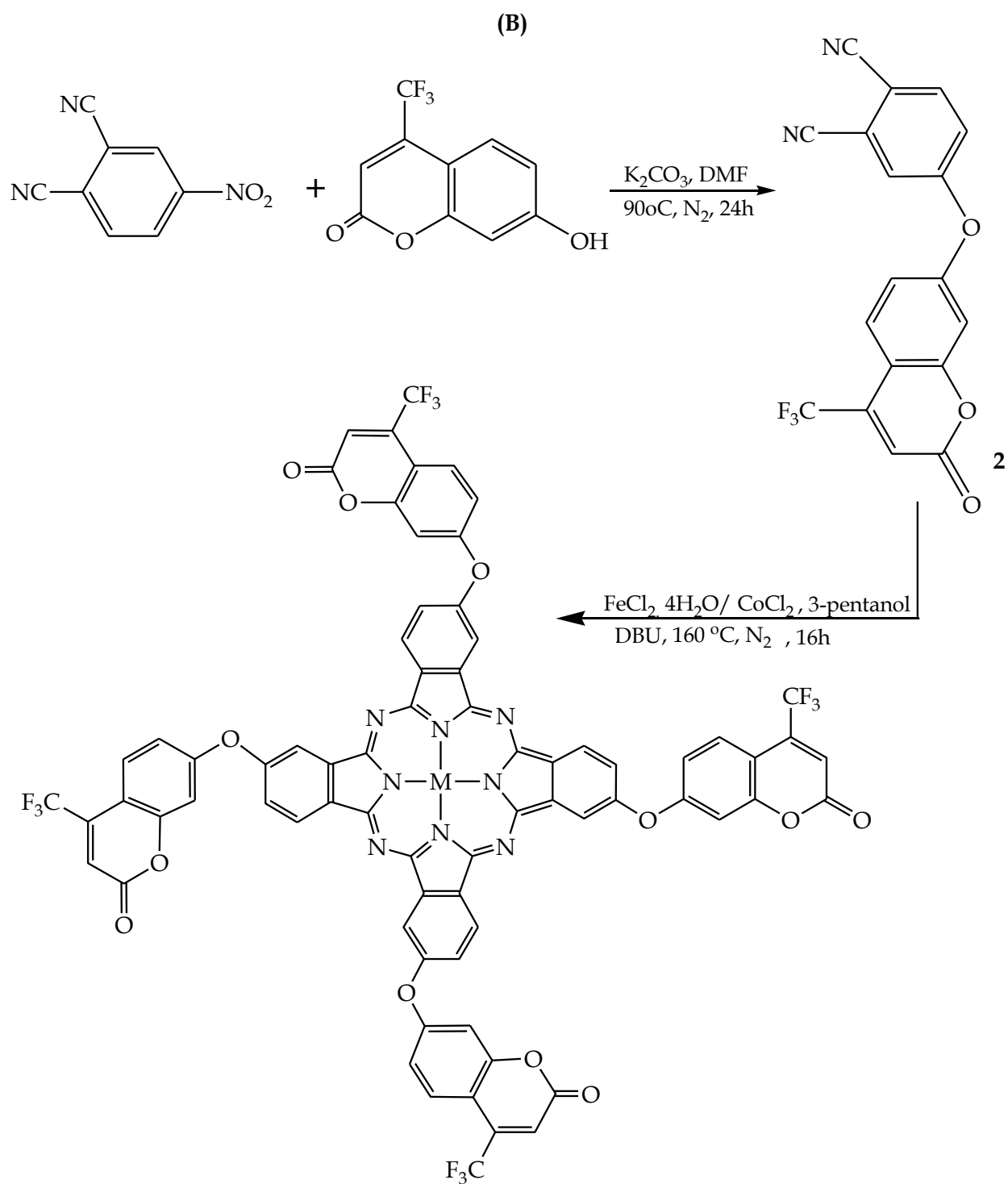
**Figure 3.9:**  $^{13}\text{C}$  NMR spectrum of ligand 2 in the range of 105 - 165 ppm.



**Figure 3.10:** COSY spectrum of ligand 2.

Template cyclotetramerization of ligands **1** and **2** in the presence of a catalyst, DBU and the desired metal salt ( $\text{CoCl}_2$  for complexes **3** and **5** and  $\text{FeCl}_2 \cdot 4\text{H}_2\text{O}$  for **4**) afforded the corresponding MPCs, refer to **Scheme 3.1**.





**Scheme 3.1:** Synthetic pathways for the respective MPcs: (A) (CoPc-*chr*, **3**), and (B) (FePc-*cou*, **4**) and (CoPc-*cou*, **5**).

Complexes **4** and **5** are soluble even in low boiling point organic solvents including THF, CHCl<sub>3</sub> and DCM while **3** is only soluble in DMF and DMSO. It is well documented that bulky or long-chain peripheral substituents improve the solubility of MPcs in organic solvents [40] and thus, as expected, **4** and **5** containing bulky trifluoromethyl groups show enhanced solubilities as compared to **3**.

The absence of the medium intensity nitrile stretches found at 2231 cm<sup>-1</sup> (for **1**) and 2235 cm<sup>-1</sup> (for **2**) in the FT-IR spectra of the MPcs is typical of cyclotetramerization (see **Figs. 3.11-3.13**). The formation of macrocyclic ring systems is also supported by the observation of strong vibrational bands, ascribed to the  $\nu(\text{C}=\text{N})$  moiety at 1592 cm<sup>-1</sup> (for **3**) and 1605 cm<sup>-1</sup> (for **4** and **5**). Commonality in some of the FT-IR bands is also observed between the ligands and their respective MPcs, an example being the ether functional group which vibrates virtually at the same frequency for both.

ESI-TOF mass spectrometry and elemental analysis provided definitive structural characterization for the ligands and their metal complexes. All molecular and cluster ion peaks were in accordance with the calculated  $m/z$  values. The mass spectra of the MPcs showed [M]<sup>+</sup> ion peaks at  $m/z$  values of 1211.21 for complex **3**, 1480.19 for **4** and 1483.09 for **5**, respectively, in addition to the protonation molecular ion peaks of the form: [M+H]<sup>+</sup>, [M+2H]<sup>+</sup> and [M+3H]<sup>+</sup> (for **5** only). The mass spectra of **2**, **3** and **5** are shown in **Figs. 3.14-3.16**.

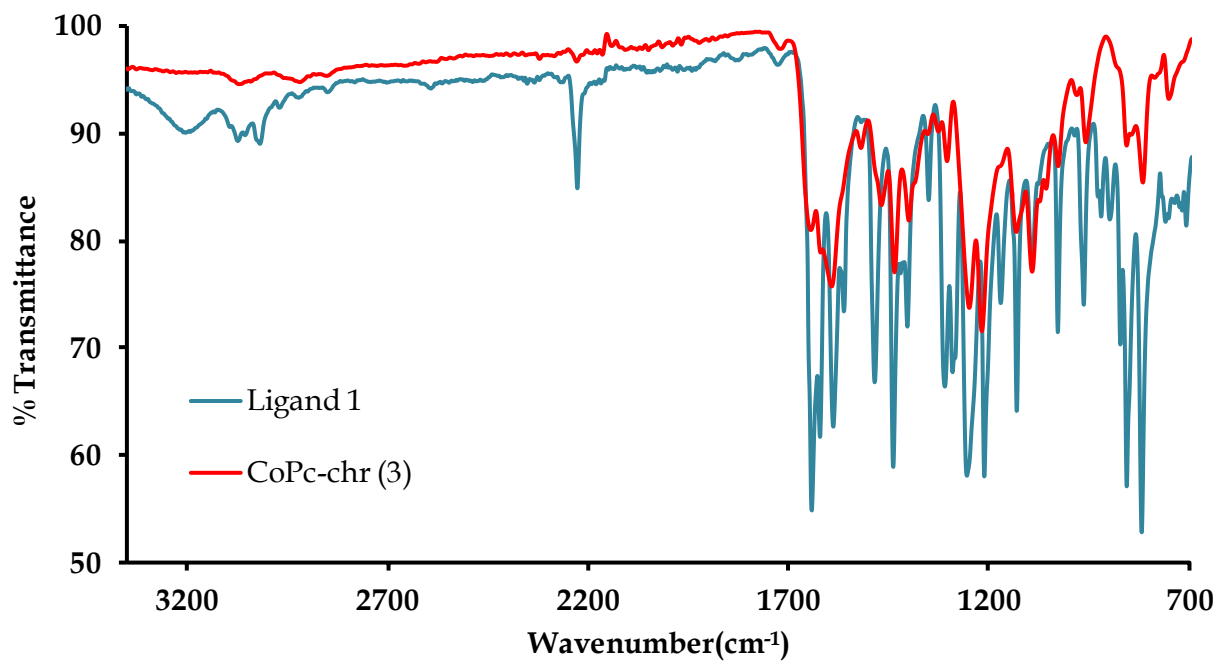


**Figure 3.11** *Overlay IR spectra of complex 3 and its free ligand, compound 1.*

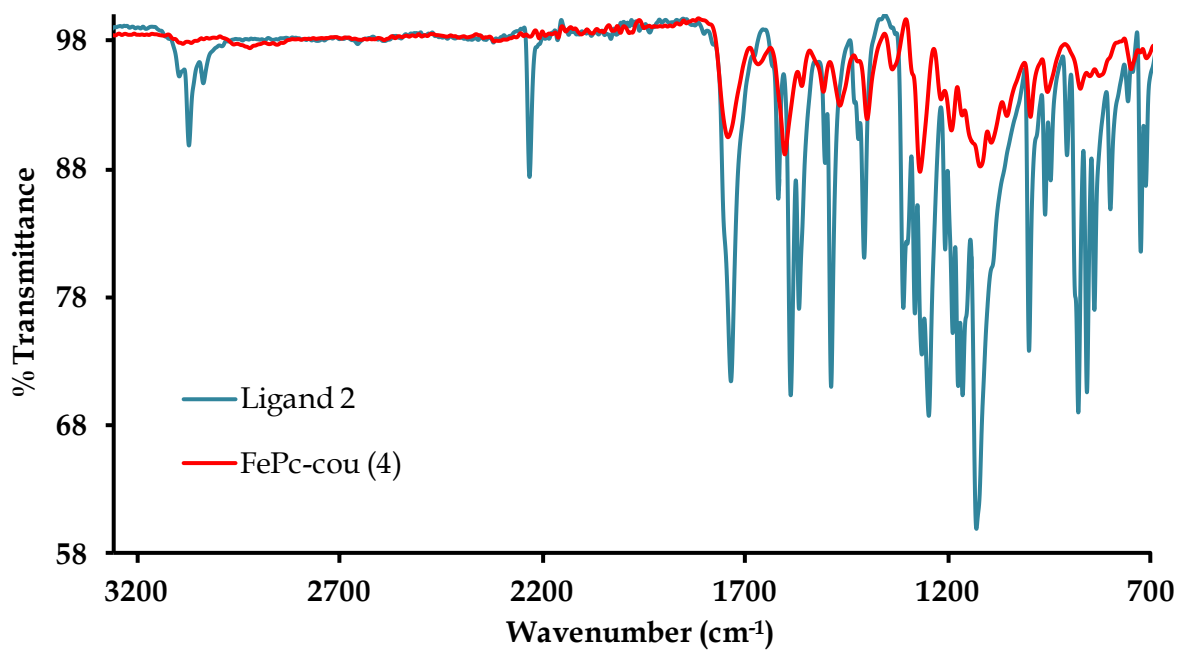


**Figure 3.12:** *Overlay IR spectra of complex 4 and its free ligand, compound 2.*

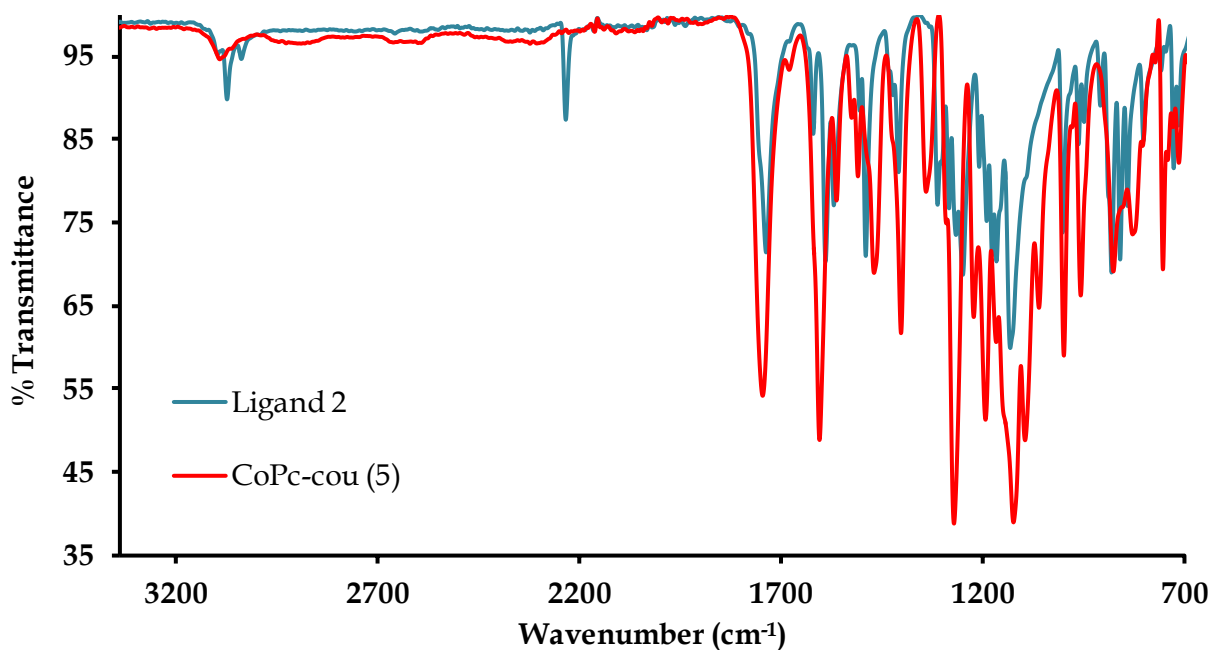


Figure 3.13: Overlay IR spectra of complex 5 and its free ligand, compound 2.

### Elemental Composition Report

Page 1

#### Single Mass Analysis

Tolerance = 5.0 PPM / DBE: min = -1.5, max = 100.0

Element prediction: Off

Number of isotope peaks used for i-FIT = 3

Monoisotopic Mass, Even Electron Ions

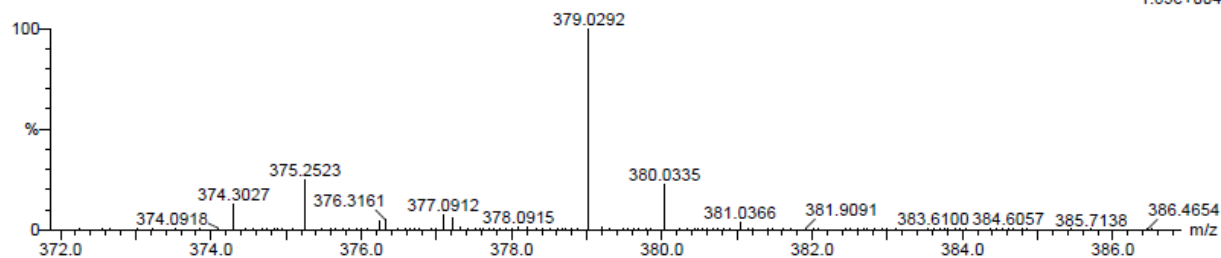
106 formula(e) evaluated with 1 results within limits (up to 20 best isotopic matches for each mass)

Elements Used:

C: 15-20 H: 5-10 N: 0-5 O: 0-5 F: 0-5 Na: 1-1

S3 +lms 60 (1.004)

TOF MS ES+



Minimum:

Maximum: 5.0 5.0 -1.5 100.0

Mass	Calc. Mass	mDa	PPM	DBE	i-FIT	i-FIT (Norm)	Formula
379.0292	379.0306	-1.4	-3.7	14.5	138.6	0.0	C18 H7 N2 O3 F3 Na

Figure 3.14: High resolution TOF-MS spectrum of 2.

Single Mass Analysis

Tolerance = 5.0 PPM / DBE: min = -1.5, max = 100.0  
 Element prediction: Off  
 Number of isotope peaks used for i-FIT = 3

Monoisotopic Mass, Even Electron Ions

17 formula(e) evaluated with 1 results within limits (up to 20 closest results for each mass)

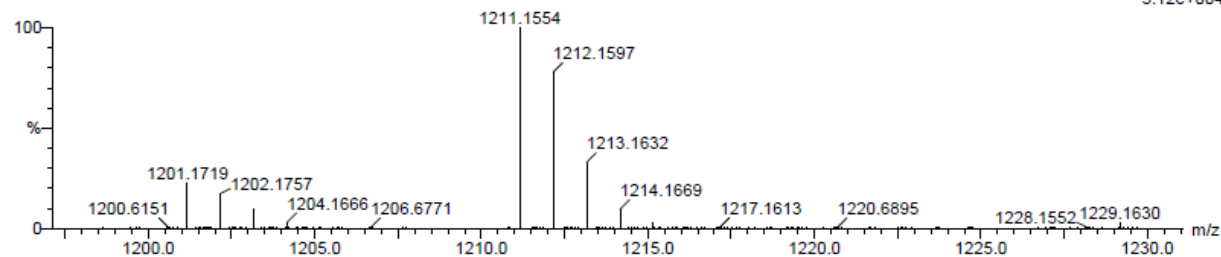
Elements Used:

C: 65-70 H: 30-35 N: 5-10 O: 10-15 Co: 0-1

S6(blue) 53 (1.755) Cm (1:61)

TOF MS ES+

5.12e+004



Minimum:

Maximum: 5.0 5.0 -1.5

Mass	Calc. Mass	mDa	PPM	DBE	i-FIT	i-FIT (Norm)	Formula
1211.1554	1211.1597	-4.3	-3.6	56.5	250.4	0.0	C69 H34 N7 O12 Co

Figure 3.15: High resolution TOF-MS spectrum of 3.

Single Mass Analysis

Tolerance = 5.0 PPM / DBE: min = -1.5, max = 100.0  
 Element prediction: Off  
 Number of isotope peaks used for i-FIT = 3

Monoisotopic Mass, Odd and Even Electron Ions

10 formula(e) evaluated with 1 results within limits (up to 20 best isotopic matches for each mass)

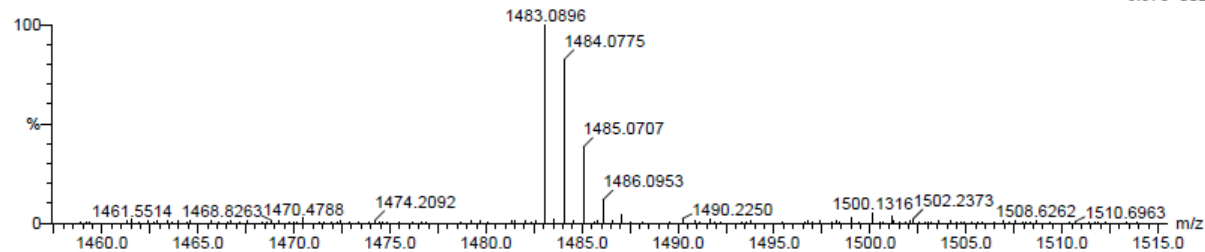
Elements Used:

C: 72-72 H: 25-30 N: 5-10 O: 12-12 F: 10-15 Co: 0-1

S10 36 (0.595)

TOF MS ES+

6.97e+002



Minimum:

Maximum: 5.0 5.0 -1.5

Mass	Calc. Mass	mDa	PPM	DBE	i-FIT	i-FIT (Norm)	Formula
1483.0896	1483.0967	-7.1	-4.8	57.0	26.2	0.0	C72 H28 N8 O12 F12 Co

Figure 3.16: High resolution TOF-MS spectrum of 5.

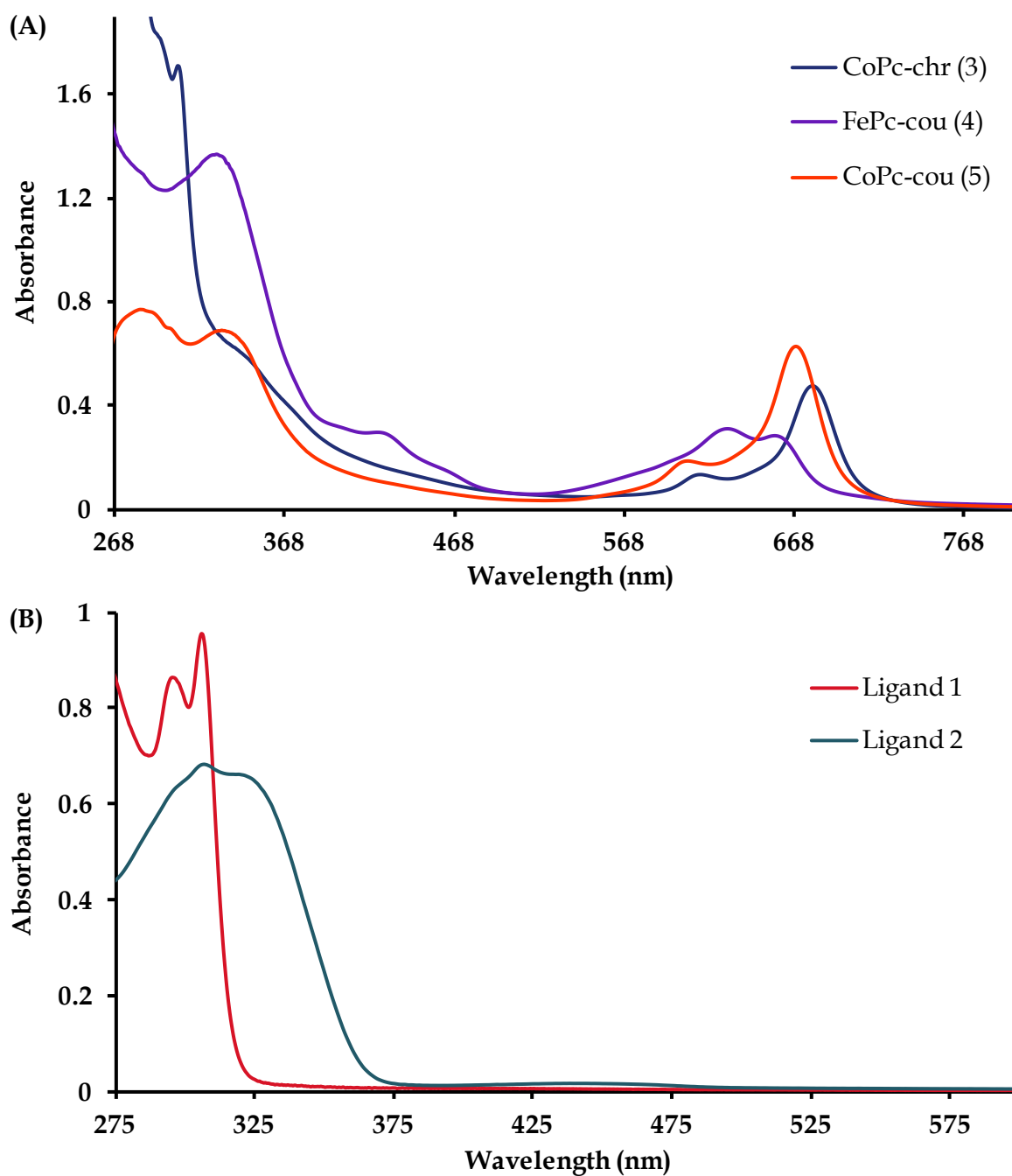
The electronic transitions observed within the UV-Vis spectra of the respective metal complexes (**3-5**) in DMF are in accordance with literature trends [12]. More specifically, the formulated MPcs showed Q- and B-bands in the regions of 600-700 nm and 300-400 nm, respectively (refer to **Table 3.3** and **Fig. 3.17**). All three complexes contain a common electron-donating oxy group on their Pc cores; however, **4** and **5** contain the strongly electron withdrawing trifluoromethyl groups which leads to blue-shifting of their electronic transitions relative to the corresponding electronic transitions of **3**.

**Table 3.3:** UV-Vis absorption wavelengths and the corresponding molar absorptivities (in parentheses) for 1-5.

Compound	Q-band (nm)	B-band (nm)	Other energy bands (nm)
<b>1</b>	-	-	306 (11010), 295 (9962)
<b>2</b>	-	-	443 (90), 318 (29875), 307 (33370)
<b>3</b>	679 (23075)	343 (29176)	305 (82909)
<b>4</b>	657 (16891)	328 (81208)	629 (18476), 423 (17660)
<b>5</b>	669 (37422)	331 (41139)	283 (45899)

The bands at 423 nm for **4** and 283 nm for **5** are ascribed to electronic transitions associated with the highly  $\pi$ -conjugated oxy-coumarin substituents as similar bands occur in the UV-Vis spectrum of **2** at 443 nm and 307 nm, respectively. Aggregation in MPcs is epitomized by a broadened or split Q-band. Splitting of the Q-band of complex **4** is indicative of aggregation occurring within solution with the band at

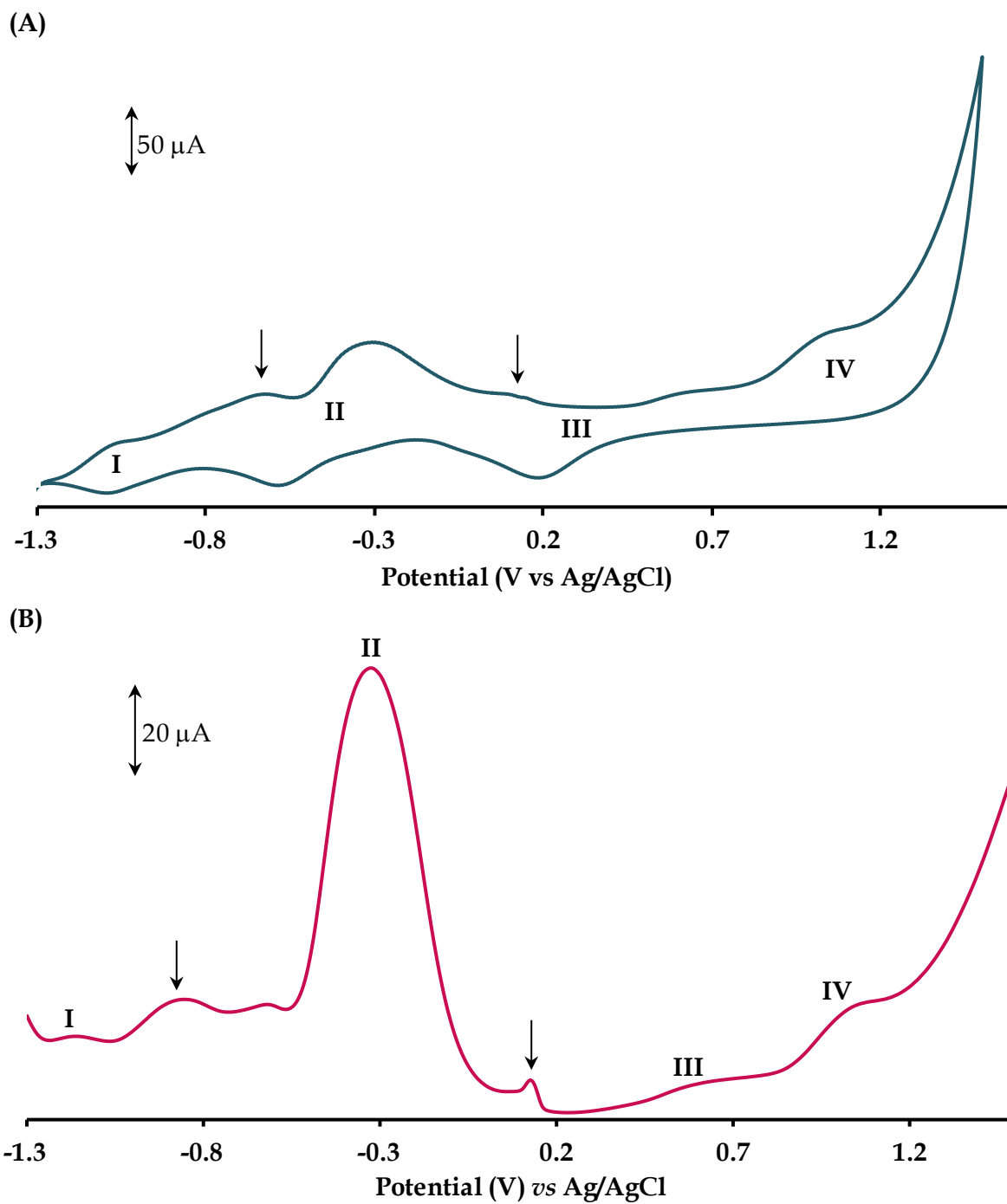
higher wavelengths due to the monomer (at 657 nm) and the one at a lower wavelength (at 632 nm) due to the aggregate [41].



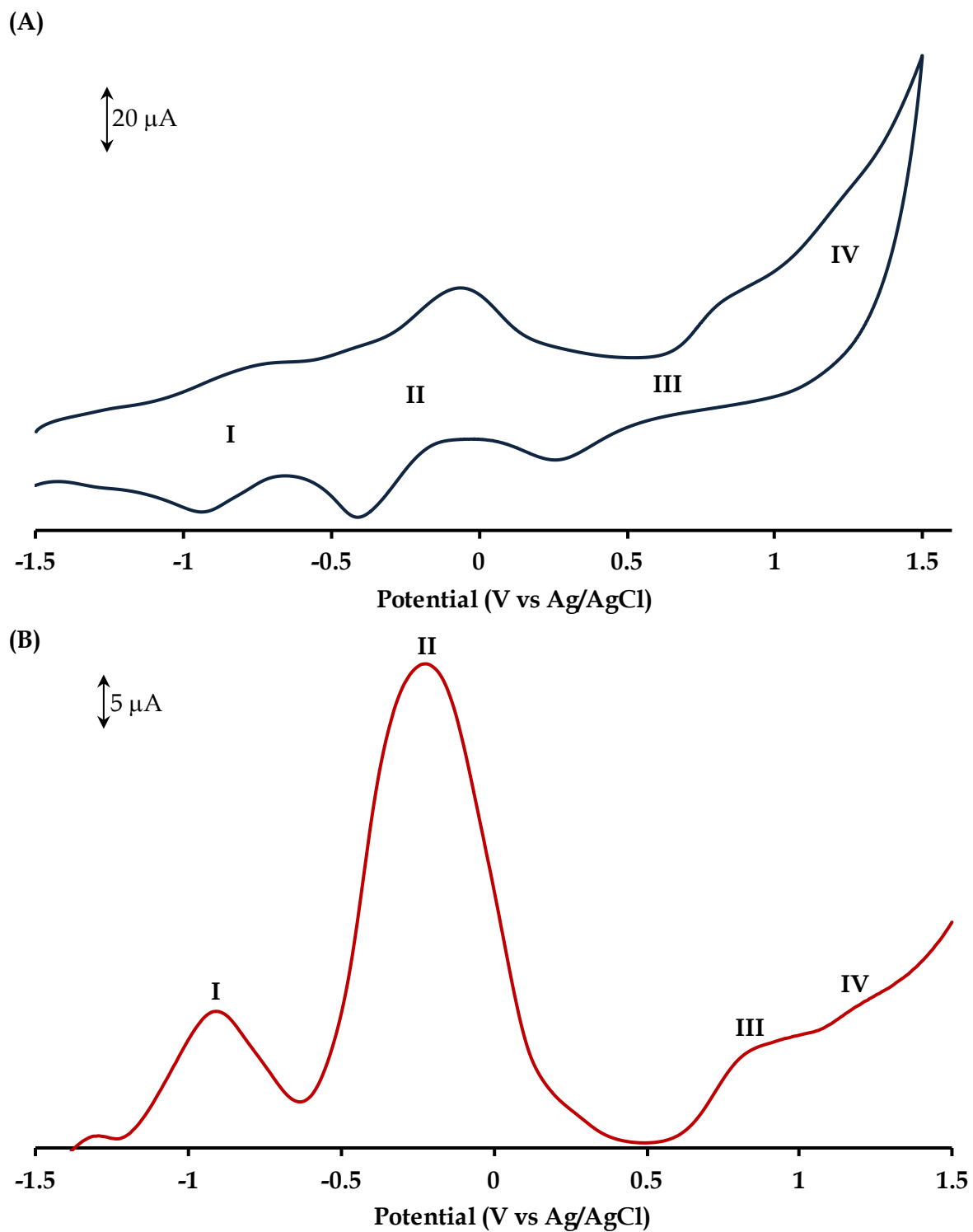
**Figure 3.17:** UV-Vis spectra of (A) complexes 3-5 at concentrations of 20.6  $\mu\text{M}$ , 16.9  $\mu\text{M}$  and 16.9  $\mu\text{M}$ , respectively and (B) ligands 1 and 2 at concentrations of 86.7  $\mu\text{M}$  and 35.1  $\mu\text{M}$ , respectively.

### 3.3.3 Voltammetry and Spectroelectrochemistry

The solution redox properties of the metal complexes were probed *via* cyclic and square-wave voltammetry in dried DMF. The MPcs exhibited similar redox behavior with four distinct redox processes which were observed in their respective cyclic (CVs) and square-wave voltammograms (SWVs), see **Figs. 3.18, 3.19** and **3.20**. The redox processes denoted as **I, II** and **III** are quasi-reversible as their  $\Delta E$  values are larger than 103 mV ( $\Delta E$  value for the standard, Ferrocene at 200 mV/s), indicating slower electron transfer kinetics compared to the standard [**41-43**]. These redox processes are ascribed to the  $Pc^{2-}/Pc^{3-}$  reduction,  $M^{2+}/M^+$  reduction and  $M^{2+}/M^{3+}$  oxidation whilst the irreversible redox process denoted as **IV** is due to  $Pc^{2-}/Pc^{1-}$  oxidation and the remaining peaks are attributed to aggregation. These assignments are based on comparable redox potentials observed for reported CoPcs containing coumarin-derived substituents (refer to **Table 3.4**) [**41, 44-46**]. Aggregation also resulted in broadened redox couples for couple **III**, while **3** also displays distinct splitting in both the forward and reverse signals, see **Fig. 3.18**. Noteworthy, the aggregation phenomena were also common to the  $\beta$ -tetra[7-oxo-4-(methoxyphenyl)-8-methylcoumarin] (oxpcou) CoPc for which broadened redox processes and split Q-bands were observed in its CV and UV-Vis spectrum, respectively [**43**]. Despite the influence of aggregation on the voltammograms, the plots of peak current against square root of scan rate for each complex displayed linear relationships indicating that the redox couples are all diffusion-controlled, see **Figs. 3.21** and **3.22** for the CV scans of complexes **3** and **4** at incrementing scan rates.



**Figure 3.18:** (A) CV and (B) SWV of complex 3 at 200 mV/s. The arrows denote peaks associated with aggregation.



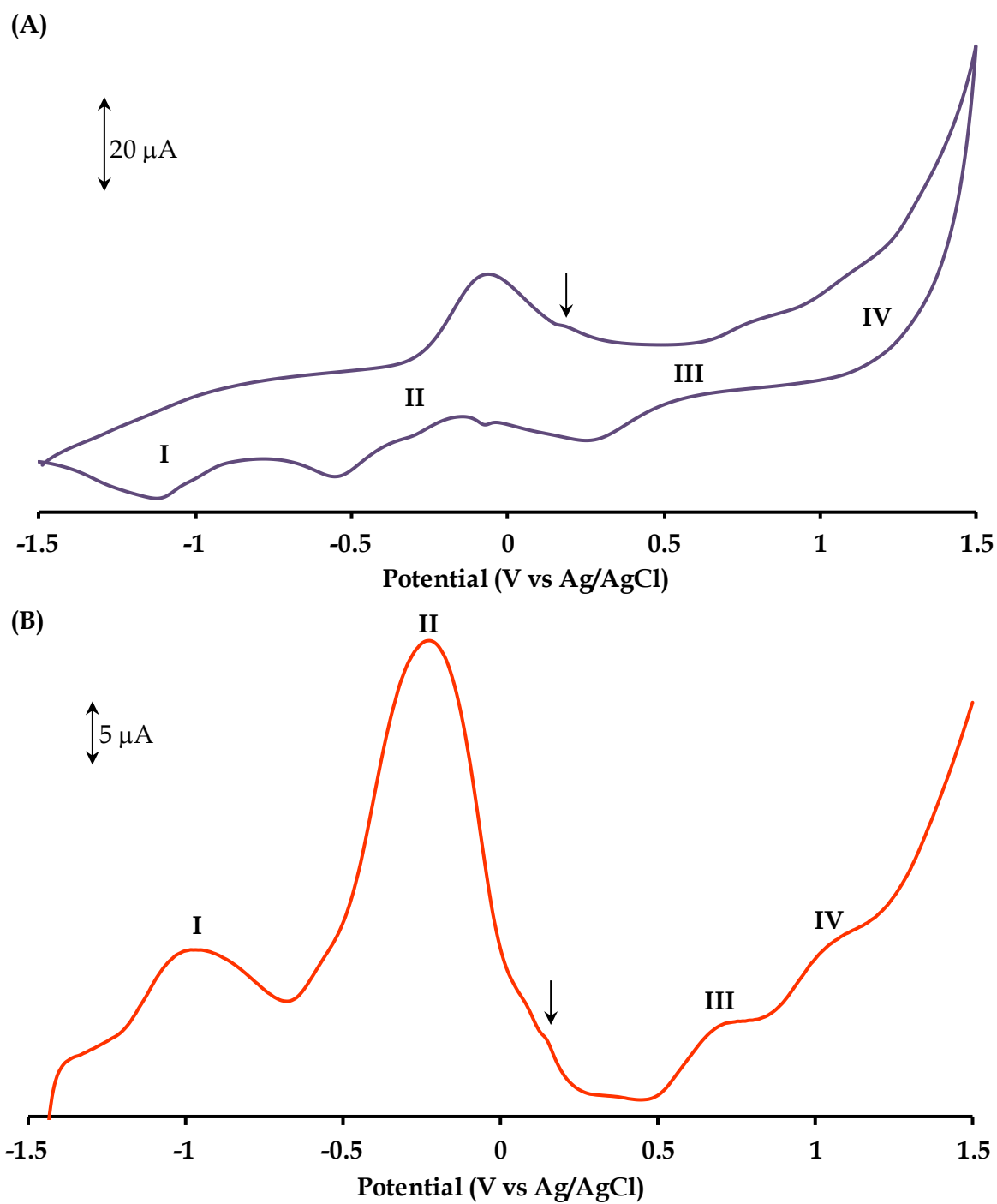


**Figure 3.20:** (A) CV and (B) SWV of complex 5 at 200 mV/s. The arrows denote peaks associated with aggregation.

**Table 3.4:** Comparison of the voltammetric data (in V) between the novel MPcs 3-5 as well as other tetrasubstituted CoPcs attained from literature.

	M <sup>I</sup> Pc <sup>2-</sup> /M <sup>I</sup> Pc <sup>3-</sup> <b>I</b>	M <sup>II</sup> Pc <sup>2-</sup> /M <sup>I</sup> Pc <sup>2-</sup> <b>II</b>	M <sup>II</sup> Pc <sup>2-</sup> /M <sup>III</sup> Pc <sup>2-</sup> <b>III</b>	M <sup>III</sup> Pc <sup>2-</sup> / M <sup>III</sup> Pc <sup>1-</sup> <b>IV</b>
<b>CoPc-chr (3)</b>	-1.11 <sup>[a]</sup>	-0.44 <sup>[a]</sup>	0.40 <sup>[a]</sup>	1.03 <sup>[b]</sup>
<b>FePc-cou (4)</b>	-0.84 <sup>[a]</sup>	-0.24 <sup>[a]</sup>	0.55 <sup>[a]</sup>	1.23 <sup>[b]</sup>
<b>CoPc-cou (5)</b>	-1.00 <sup>[a]</sup>	-0.46 <sup>[a]</sup>	0.42 <sup>[a]</sup>	1.08 <sup>[b]</sup>
<b>(β)-CoPc-ochr</b>	-1.11	-0.44	0.40	1.03
<b>(β)-CoPc- ofcou</b>	-1.00	-0.46	0.42	1.08
<b>(β)-CoPc-cfcou</b>	-0.81	-0.47	0.48	0.91
<b>(α)-CoPc-cfcou</b>	-0.86	-0.35	0.42	1.00

[a]  $E_{1/2} = \frac{E_{pa} + E_{pc}}{2}$

[b]  $E_{pa}$

cfcou = 7-oxo-3-(2-chloro-4-fluorophenyl)coumarin

ochr = 7-oxychromone

ofcou = 7-oxy-4-trifluoromethylcoumarin

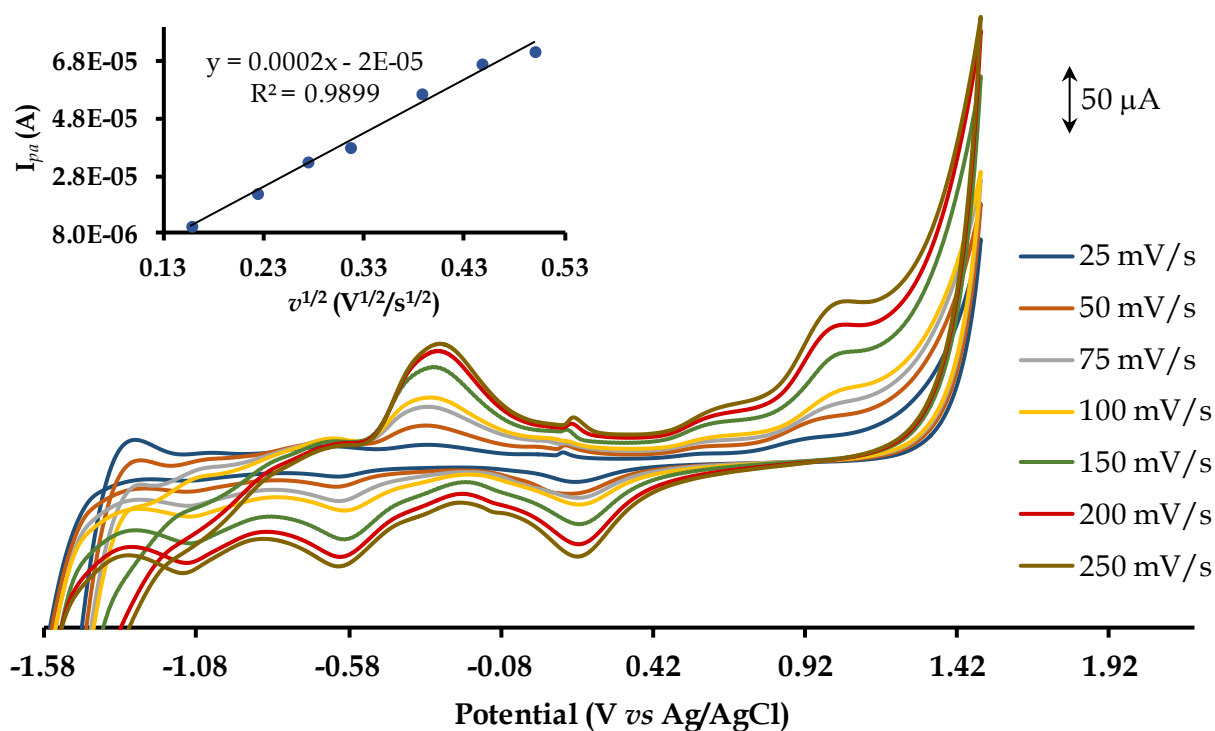


**Figure 3.21:** Overlay CVs of 3 at incrementing scan rates. Inset: Plot of  $I_{pa}$  against the square root of the scan rate (couple II) showing diffusion-controlled behavior.

Spectroelectrochemical experiments were conducted on the MPCs to verify the voltammetric assignments. The UV-Vis spectral changes of the CoPcs (3 and 5) are similar, thus, only the spectroelectrochemical data of 4 and 5 will be elaborated on, see Figs. 3.23A-D and 3.24A-D. Firstly, any differences in the starting spectra as compared to the original UV-Vis spectrum (see Fig. 3.17A) are accounted for by the extent of aggregation as a result of varying concentrations of the aggregate and monomer as well as the presence of supporting electrolyte [47].

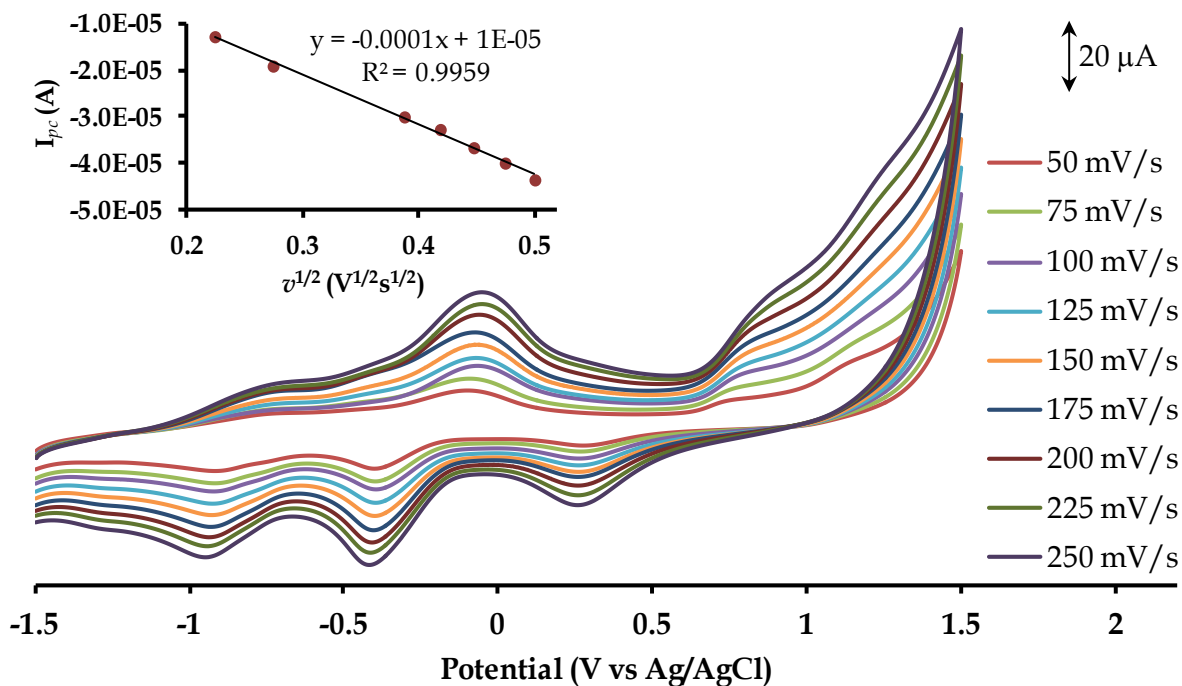


**Figure 3.22:** Overlay CVs of **4** at incrementing scan rates. Inset: Plot of  $I_{pc}$  against square root scan rate (couple **II**) showing diffusion-controlled behavior.

Investigating the first reduction (denoted as redox couple **II**), the UV-Vis spectral changes of **5** indicates that significant disaggregation occurs resulting in the formation of a well-defined monomeric and red-shifted Q-band at 703 nm, see **Fig. 3.23A**. The aforementioned UV-Vis spectral changes are accompanied by the formation of a new charge transfer band found at 473 nm. It is well documented that the red-shifting of the Q-band and a new peak forming at around 480 nm is typical of  $\text{Co}^{\text{I}}$  species [48], hence the redox couple **II** assigned to  $\text{Co}^{\text{II}}\text{Pc}^{-2}/\text{Co}^{\text{I}}\text{Pc}^{-2}$  is confirmed. Furthermore, the presence of diffuse isosbestic points (at 389 nm, 554 nm and 679 nm) is characteristic of mixed valence species in solution. Nearly 80% regeneration of the initial CoPc species was achieved when a zero voltage was applied. Upon application of negative overpotentials relative to the redox couple **I**,

the Q- and B-band decreases and a shift of the charge transfer band to a higher wavelength (at 493 nm) is observed, see **Fig 3.23B**. This redox behavior is typical of  $\text{Pc}^{2-}$  reduction and the formation of  $\text{Pc}^{3-}$  species [49], thereby confirming that these UV-Vis spectral changes are associated with the  $\text{Co}^{\text{I}}\text{Pc}^{2-}/\text{Co}^{\text{I}}\text{Pc}^{3-}$  redox couple.

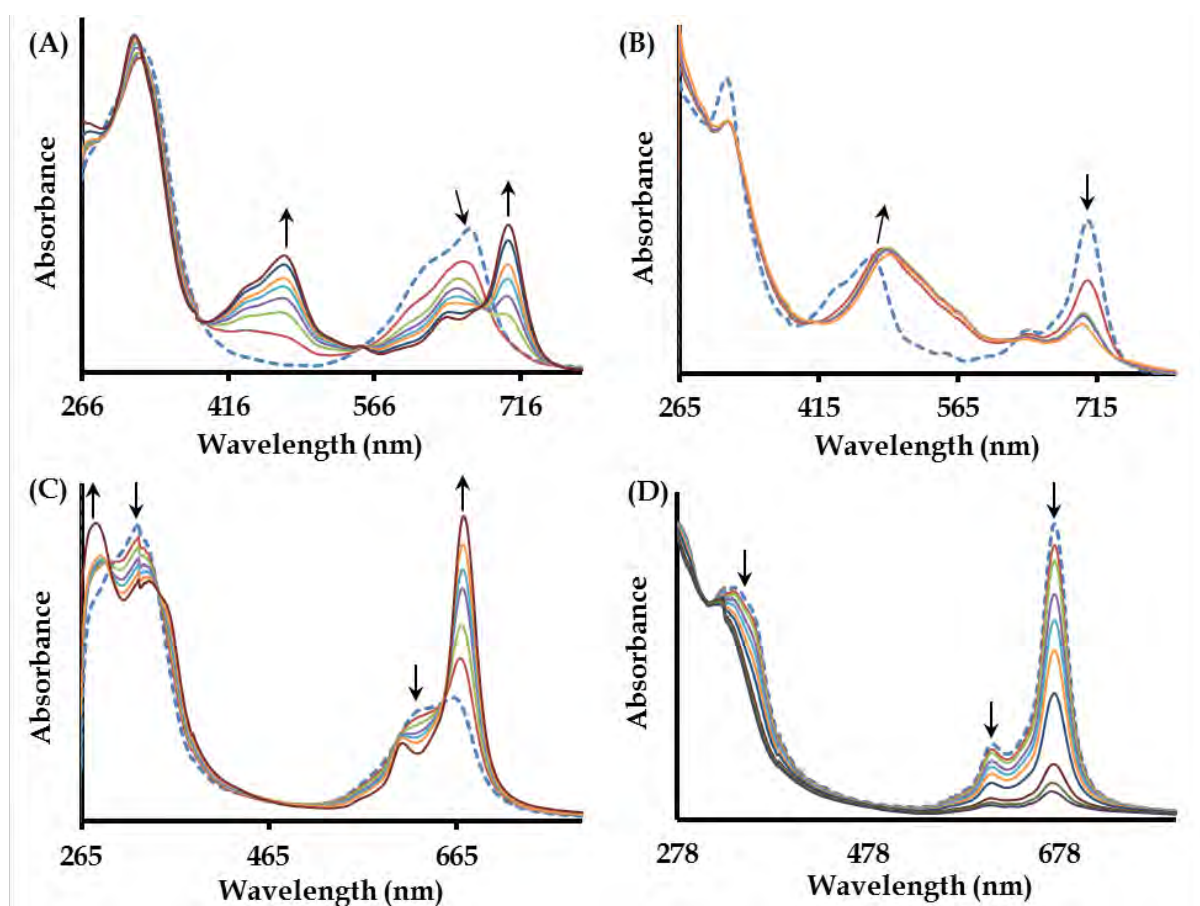


**Figure 3.23:** UV-Vis spectral changes of complex 5 at overpotentials applied at (A)  $-0.25\text{ V}$ , (B)  $-1.3\text{ V}$ , (C)  $0.78\text{ V}$  and (D)  $1.06\text{ V}$ . The initial spectrum is shown as a dashed line.

Thereafter, new sample was injected into the OTTLE cell to investigate the nature of the redox couples within a positive potential window. Examining the UV-Vis spectral changes of redox couple **III**, disaggregation of the Q-band followed by a

red-shift and an increase in the intensity of the monomer occurs which is indicative of metal oxidation within the  $\text{Co}^{\text{II}}\text{Pc}$  core [50], see **Fig. 3.23C**. Hence, the voltammetric assignment of redox couple **III** (ascribed to the  $\text{Co}^{\text{II}}\text{Pc}^{2-}/\text{Co}^{\text{III}}\text{Pc}^{2-}$  redox process) is corroborated by the attained spectroelectrochemical data. The characteristic increase in the *Q*-band is accompanied by the disappearance of the electronic transition associated with the aggregate and a decrease of the *B*-band leading to well-defined isosbestic points at 349 nm, 474 nm and 651 nm. Upon applying positive overpotentials relative to redox couple **IV**, decomposition occurs as indicated by the decrease in *Q*- and *B*-band intensities and a lack of increase in the 500 nm region. Similar behavior has previously been reported [51]. Redox couple **IV** is expected to be due to  $\text{Co}^{\text{III}}\text{Pc}^{2-}/\text{Co}^{\text{III}}\text{Pc}^{1-}$ , see **Fig. 3.23D**.

Compound **4** was also subjected to spectroelectrochemical experiments to validate its voltammetric assignments, see **Fig. 3.24**. Similar to the  $\text{CoPcs}$  **3** and **5**, the UV-Vis spectral behaviour for the metal-based reduction of **4** shows a red-shift in the *Q*-band from 657 nm to 663 nm (see **Fig. 3.24A**). Subsequently, this leads to significant disaggregation justified by the progressive decrease in the intensity of the aggregate peak (at 633 nm). It is well documented that a shift in the position of the *Q*-band indicates metal-based electron transfer, [52, 53] thereby confirming that redox couple **II** is due to  $\text{Fe}^{\text{II}}\text{Pc}^{2-}/\text{Fe}^{\text{I}}\text{Pc}^{2-}$ . Application of negative overpotentials relative to redox couple **I** ( $E_{1/2} = -1.00$  V), resulted in a decrease in the intensity of its *Q*- and *B*-band as well as the formation of a charge transfer band in the 500-600 nm region (see **Fig.**

3.24B). These changes are consistent with Pc ring reduction [53], hence couple I is assigned to  $\text{Fe}^{\text{II}}\text{Pc}^{2-}/\text{Fe}^{\text{III}}\text{Pc}^{3-}$ .

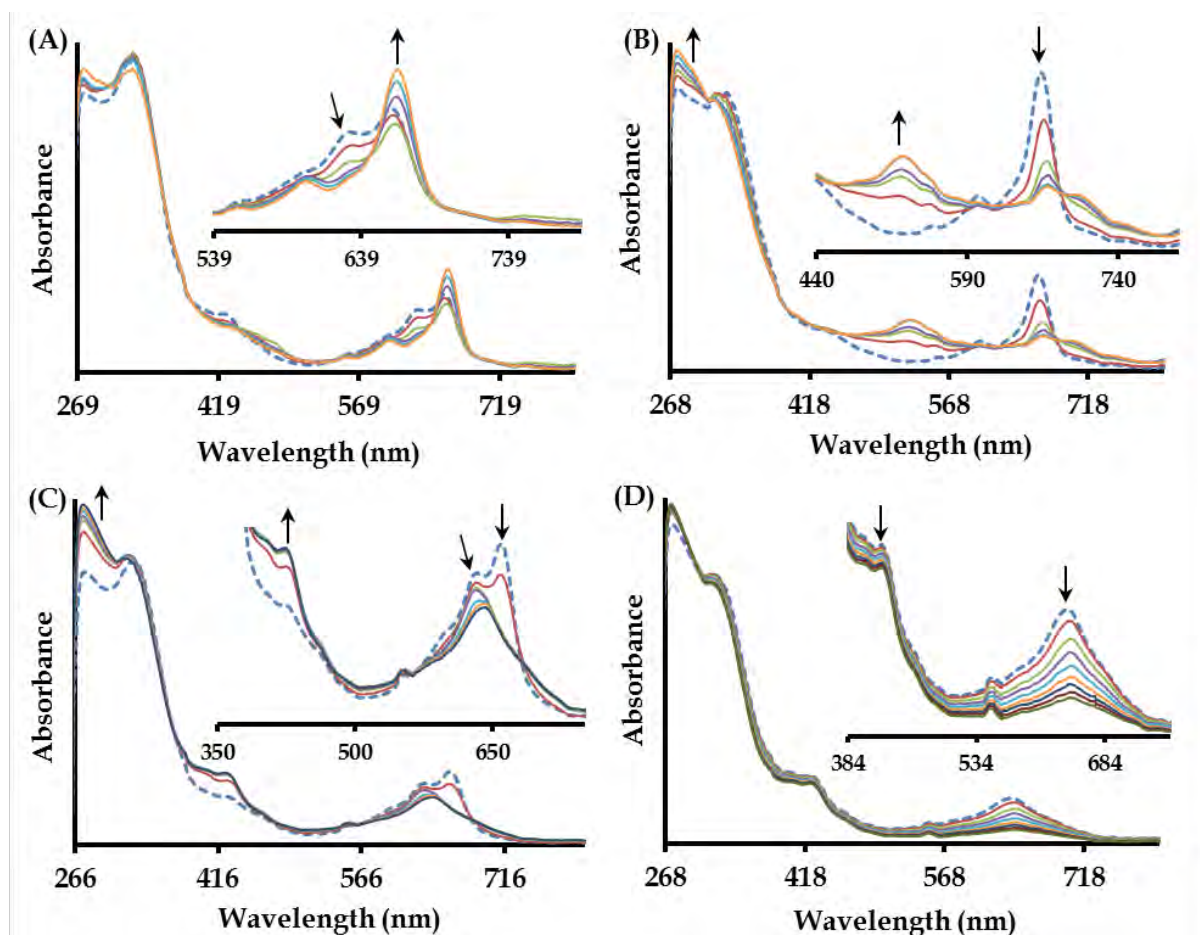


**Figure 3.24:** UV-Vis spectral changes of complex 4 at overpotentials applied at (A)  $-0.30$  V, (B)  $-0.92$  V, (C)  $0.45$  V and (D)  $1.06$  V. The initial spectrum is shown as a dashed line.

Investigating the redox couple III, coalescence of the Q-bands associated with the monomeric and aggregated species into a single broad Q-band indicates that the resultant  $\text{Fe}^{\text{III}}\text{Pc}^{2-}$  species are aggregated. Furthermore, blue-shifting of the monomeric Q-band is indicative of the metal-based oxidative process associated with the  $\text{Fe}^{\text{II}}\text{Pc}^{2-}/\text{Fe}^{\text{III}}\text{Pc}^{2-}$  redox couple (see Fig. 3.24C). Upon the application of an

overpotential of 1.22 V, ring oxidation (for the couple  $\text{Fe}^{\text{III}}\text{Pc}^{2-}/\text{Fe}^{\text{III}}\text{Pc}^{1-}$ ) and subsequent Pc decomposition is expected to have occurred as with the previous complex (see **Fig. 3.24D**) [51, 54].

### 3.3.4 Electropolymerization and Electrocatalysis

Complexes **3-5** were deposited on respective Pt working electrodes *via* electropolymerization. **Figs. 3.25 - 3.27** show the evolution of the CVs over 20 repetitive scans at 100 mV/s. The general increase in currents and shift of peak potentials is typical of electropolymerization of MPcs on electrode surfaces [55, 56]. In addition, for complex **5** (see **Fig. 3.25**), intensification of the peaks associated with the aggregate is observed and ascribed to the progressive elongation of the polymer chain on the Pt electrode surface. Furthermore, the new peak which forms near 0.40 V displays a concomitant increase in intensity as well as a shift towards more positive potentials and is ascribed to the electropolymerized MPc. The shift to positive potentials implies an increase in the electrical resistance of the polymer film, necessitating a larger overpotential to overcome the current inhibition [57].

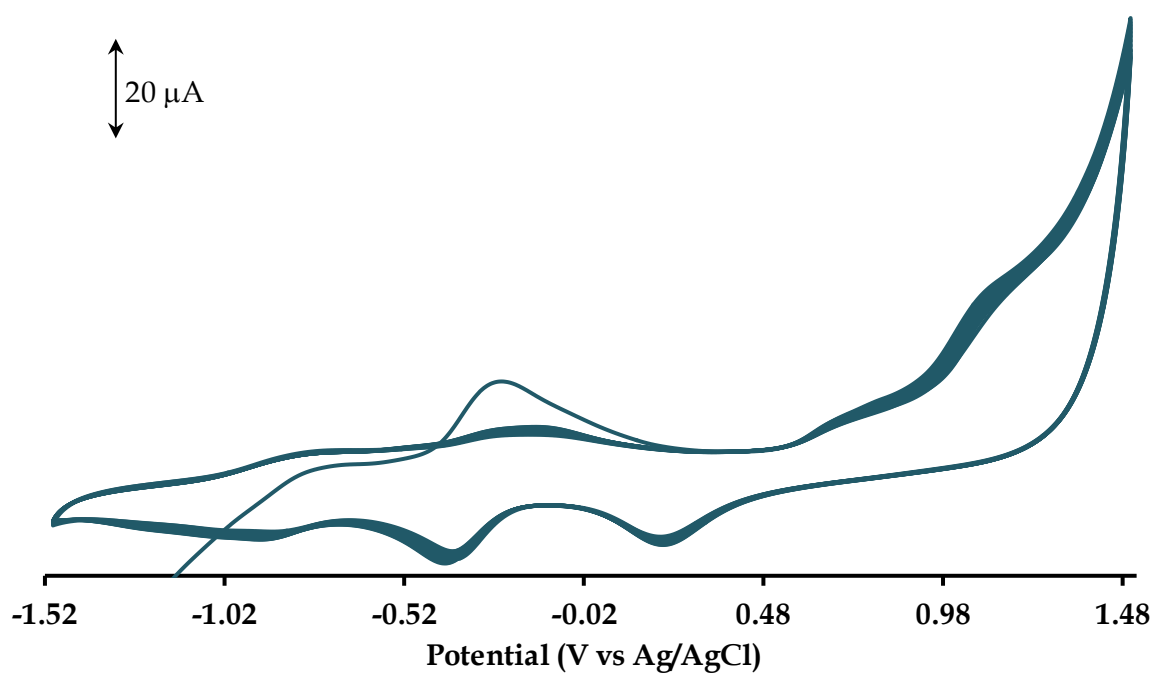


**Figure 3.25:** Electropolymerization of complex 5 at 100 mV/s for 20 CV scans.

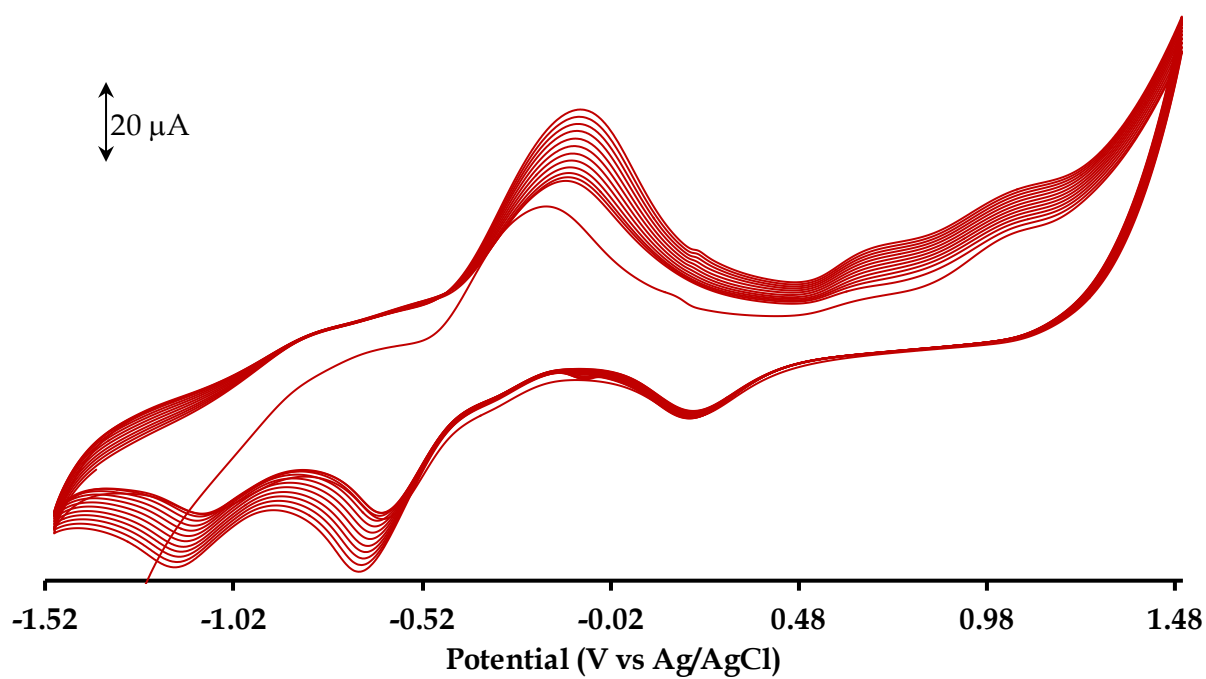


**Figure 3.26:** Electropolymerization of complex 4 at 100 mV/s for 20 CV scans.

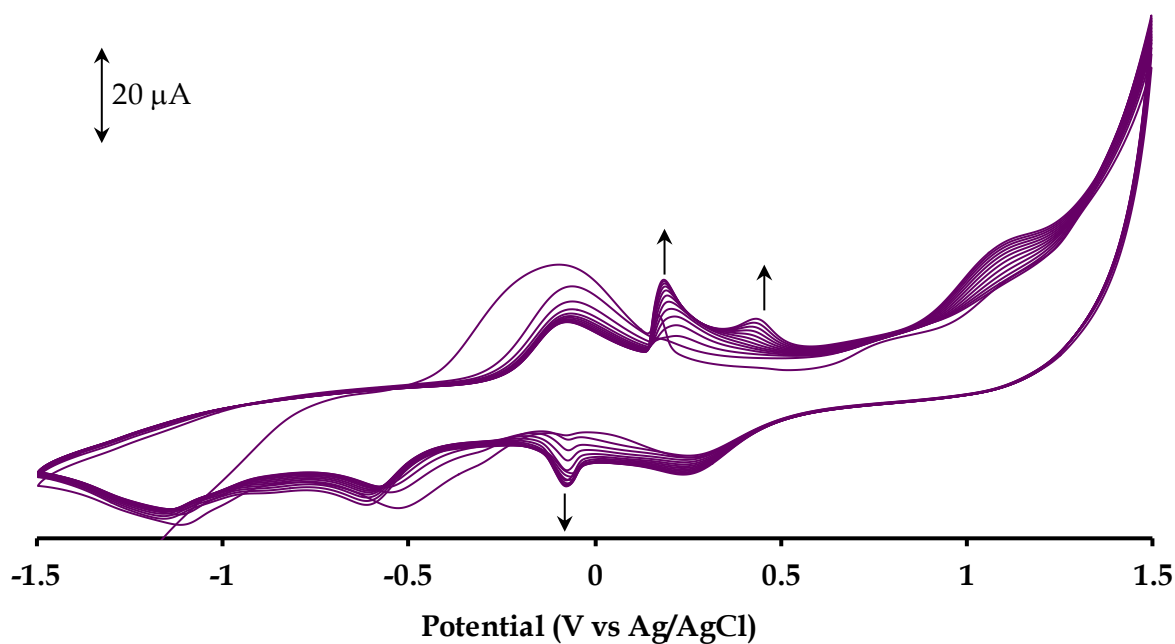


**Figure 3.27:** Electropolymerization of complex 5 at 100 mV/s for 20 scans. The arrows denote progressive increases in the aggregate peaks and the formation of a new peak.

To confirm modification of the respective working electrode (*viz.* 3-Pt, 4-Pt and 5-Pt), CVs at incrementing scan rates were run in a pH 7 buffer solution; see Figs. 3.28-3.30. The motivation behind the use of a neutral pH stems from the fact that the disproportionation of nitrite to NO is insignificant at this pH. The CVs of the respective modified electrodes (*viz.* 3-Pt, 4-Pt and 5-Pt) in a pH 7 buffer revealed the presence of the distinctive redox couple II (for  $\text{Co}^{\text{II}}/\text{Co}^{\text{I}}$ ) in the negative potential window. In addition, the 3-Pt and 5-Pt modified working electrodes showed sharp peaks which are similar to the aggregate peaks observed upon polymerization of the respective MPcs. Furthermore, commonality between the modified working electrodes (3-Pt and 5-Pt) is also observed with the appearance of irreversible metal oxidation peaks (for  $\text{Co}^{\text{II}}/\text{Co}^{\text{III}}$ ) found at positive potentials.

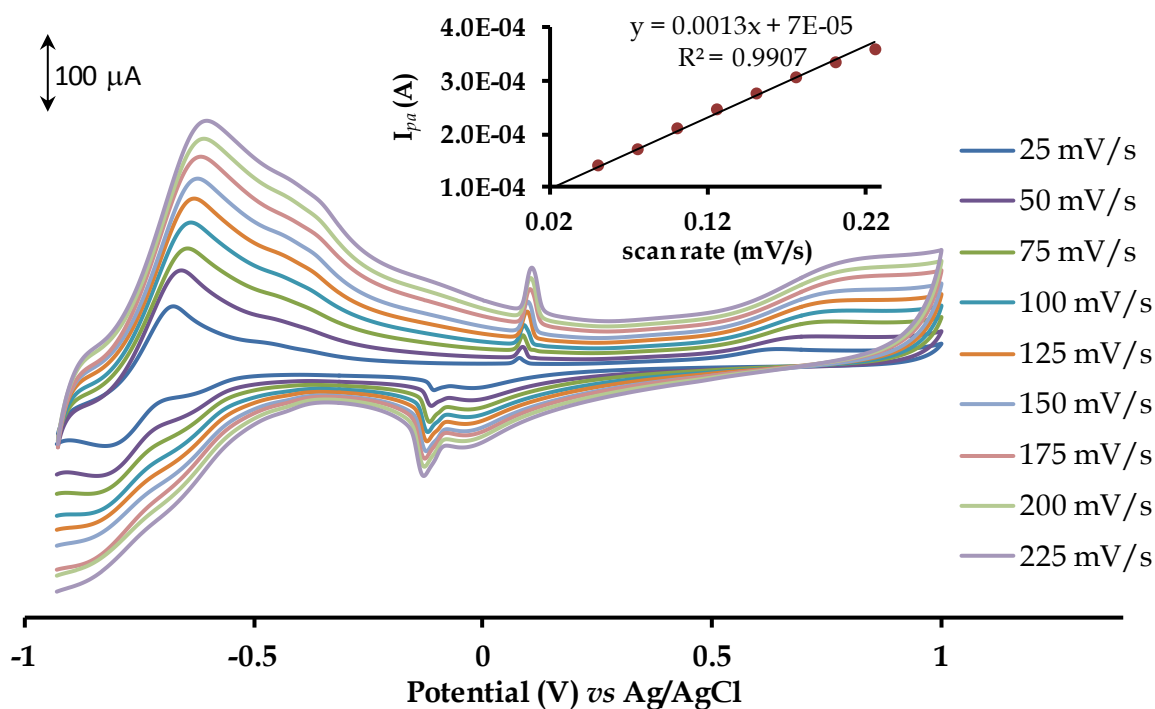


**Figure 3.28:** Overlay CVs of 3-Pt in pH 7 buffer solution at incrementing scan rates from 25 mV/s to 225 mV/s. Inset: Plot of  $I_{pa}$  vs scan rate measured at the redox couple II.

Further confirmation of electrode modification is ascertained from the fact that the degree of ion-permeability for each modified working electrode is different from each other and the standard (ferrocene) as can be seen by their peak to peak separations ( $\Delta E$ ): 120 mV for 3-Pt, 290 mV for 4-Pt, 510 mV for 5-Pt and 103 mV for the bare Pt electrode, see **Fig. 3.31**. The surface coverages of the respective modified platinum working electrodes were calculated using the following equation [58]:

$$I_p = \frac{n^2 F^2 A \Gamma(v)}{4RT} \quad (1)$$

where  $I_p$  is the peak current of redox couple II,  $n$  is the number of electrons and  $A$  is the real surface area (0.132 cm<sup>2</sup>) of the bare platinum electrode. A correlation between the surface coverages and the electrocatalytic activities of the modified

electrodes indicates that a higher surface coverage ( $3.34 \times 10^{-8}$  mol/cm<sup>2</sup> for 3-Pt,  $2.64 \times 10^{-8}$  mol/cm<sup>2</sup> for 4-Pt and  $1.87 \times 10^{-8}$  mol/cm<sup>2</sup> for 5-Pt) resulted in a lower electrocatalytic oxidation potential of nitrite (0.75 V for 3-Pt, 0.77 V for 4-Pt and 0.78 V for 5-Pt), see Fig. 3.30.

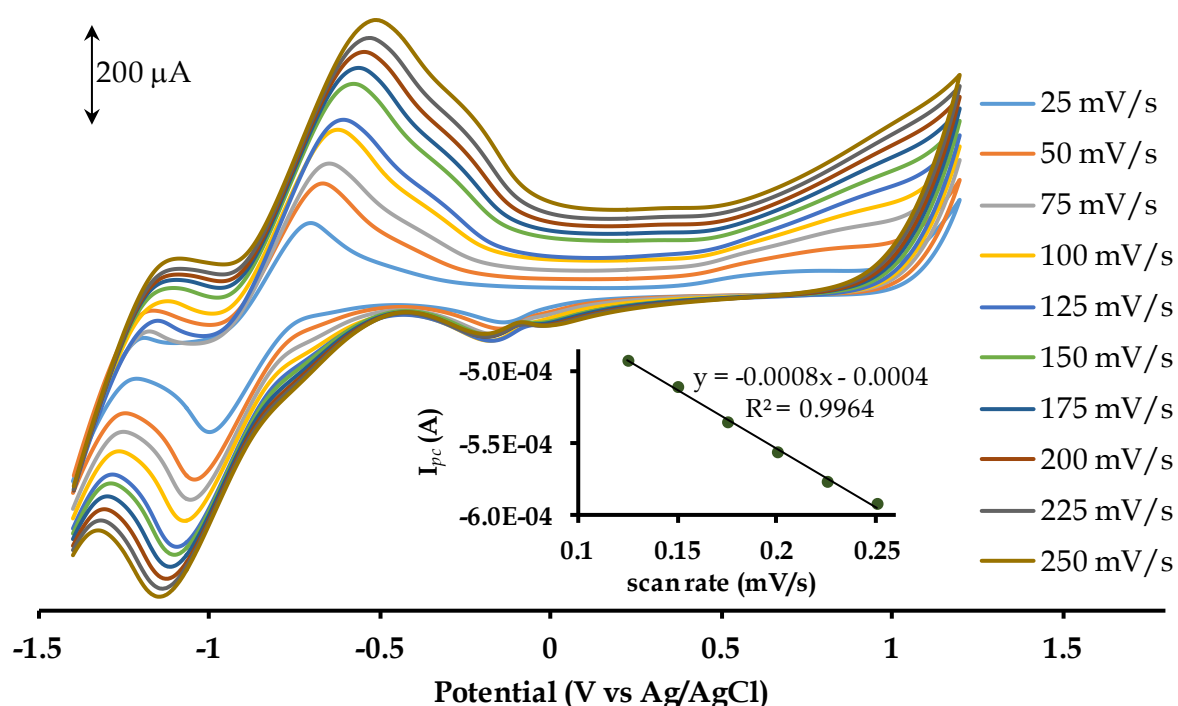


**Figure 3.29:** Overlay CVs of 4-Pt in pH 7.4 buffer solution at incrementing scan rates from 25 mV/s to 250 mV/s. Inset: Plot of  $I_{pc}$  vs scan rate measured at the redox couple II.

The surface coverage values of the modified electrodes are higher than typical surface coverage values obtained for a monolayer deposited flat on an electrode surface ( $1 \times 10^{-10}$  mol/cm<sup>2</sup>) [59], which is suggestive of electropolymerization. In conjunction with the lowering of the oxidation potentials of nitrite, larger oxidation currents were observed for the modified electrodes as compared to the bare platinum electrode (peak at 0.79 V). The larger current for the modified electrodes is

promoted by the metal oxidation couple (*i.e.* Co<sup>III</sup>/Co<sup>II</sup>) which is found in the same vicinity as the electrocatalytic potentials of nitrite using the respective modified electrodes. A linear relationship was established between the oxidation peak currents ( $I_{pa}$ ) and the square root of the scan rates ( $v^{1/2}$ ) for the oxidation peak potentials which affirms diffusion controlled behaviour.

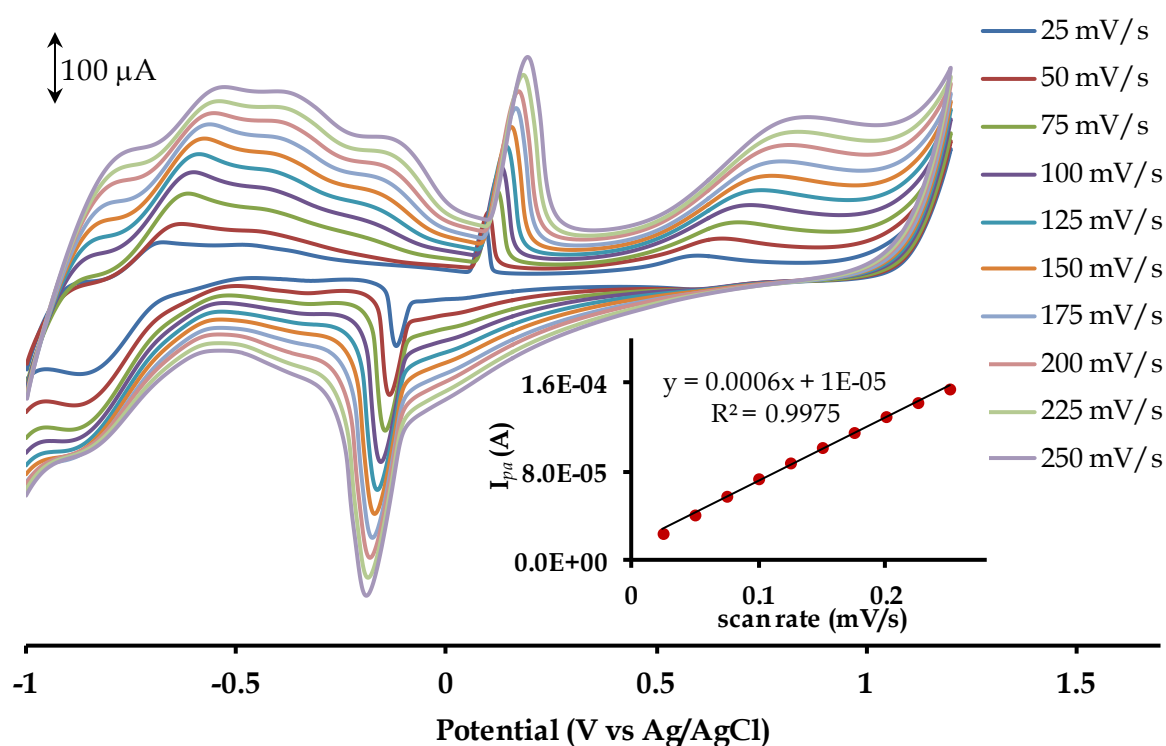


**Figure 3.30:** Overlay CVs of 5-Pt in pH 7.4 buffer solution at incrementing scan rates from 25 mV/s to 250 mV/s. Inset: Plot of  $I_{pa}$  vs scan rate measured at the redox couple II.

To gain more insight into the mechanism of electrocatalytic oxidation of nitrite, the Tafel slopes were calculated using equation (2):

$$E_p = \frac{2.3RT}{2(1-\alpha)Fn_\alpha} \text{Log } v + K \quad (2)$$

where  $\alpha$  is the transfer coefficient,  $\nu$  is the scan rate,  $n_{\alpha}$  is the number of electrons in the rate-determining step and  $K$  is the intercept. Tafel slopes were obtained from the plots of  $E_p$  vs  $\text{Log } \nu$ , see **Figs 3.33-3.35**. The large Tafel slope of 279 mV/decade for 4-Pt in comparison with 3-Pt (116 mV/decade) and 5-Pt (102 mV/decade) which are in the normal range of 30-120 mV/decade, indicates that electrocatalytic oxidation using 4-Pt has no kinetic meaning and is rather suggestive of substrate-catalyst interaction [60]. However, the Tafel slopes of the electropolymerized CoPcs, *viz.* 3-Pt and 5-Pt are close to 118 mV/decade which implies that the first one-electron transfer is rate-determining [61].

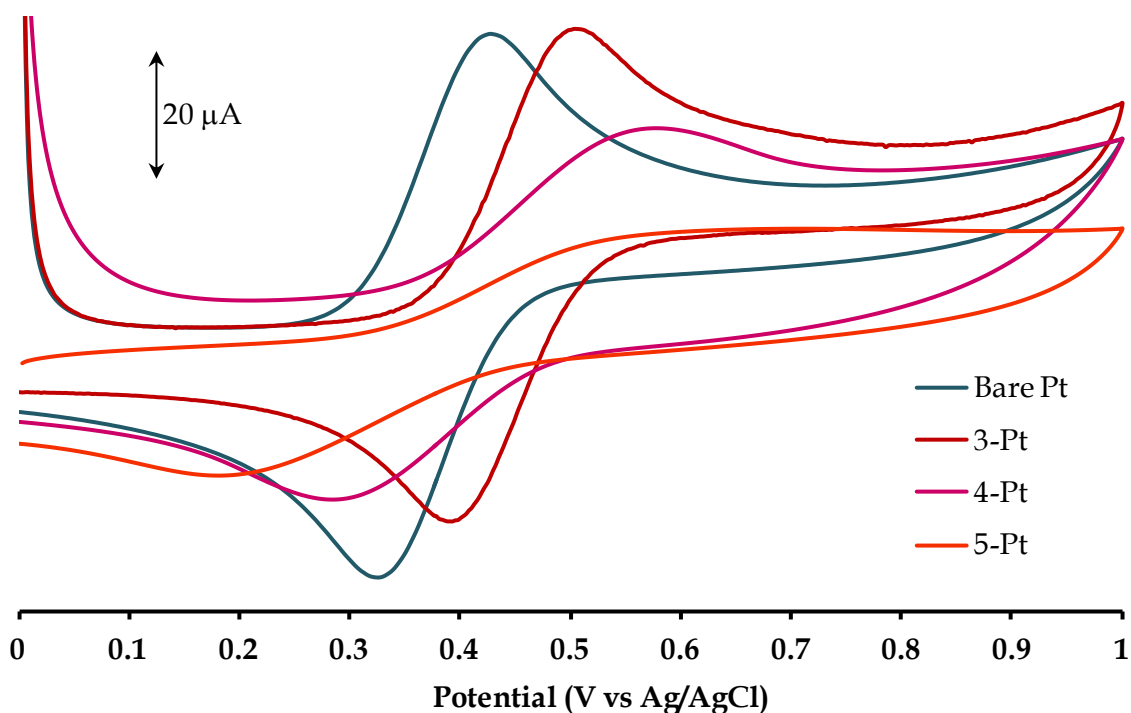


**Fig. 3.31:** Overlay CVs in 1 mM Ferrocene using the bare, 3-Pt, 4-Pt and 5-Pt working electrodes at 100 mV/s.

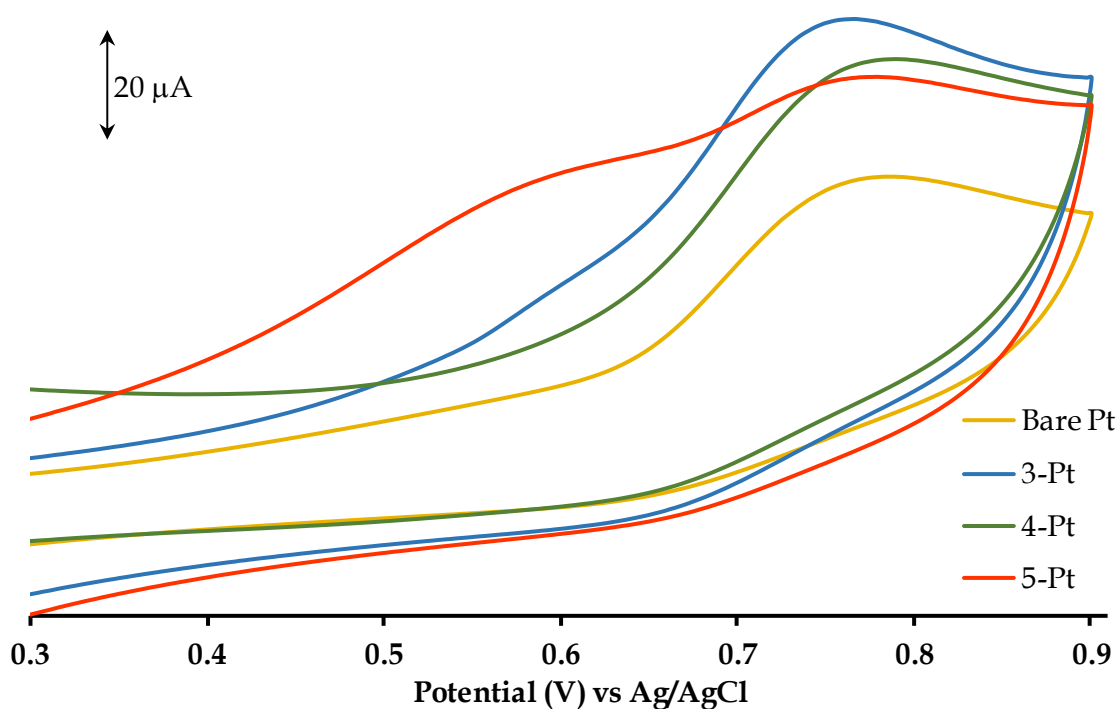


**Figure 3.32:** Electrocatalytic oxidation of 1 mM nitrite ion in pH 7 buffer solution at 100 mV/s using the bare and respective modified working electrodes.

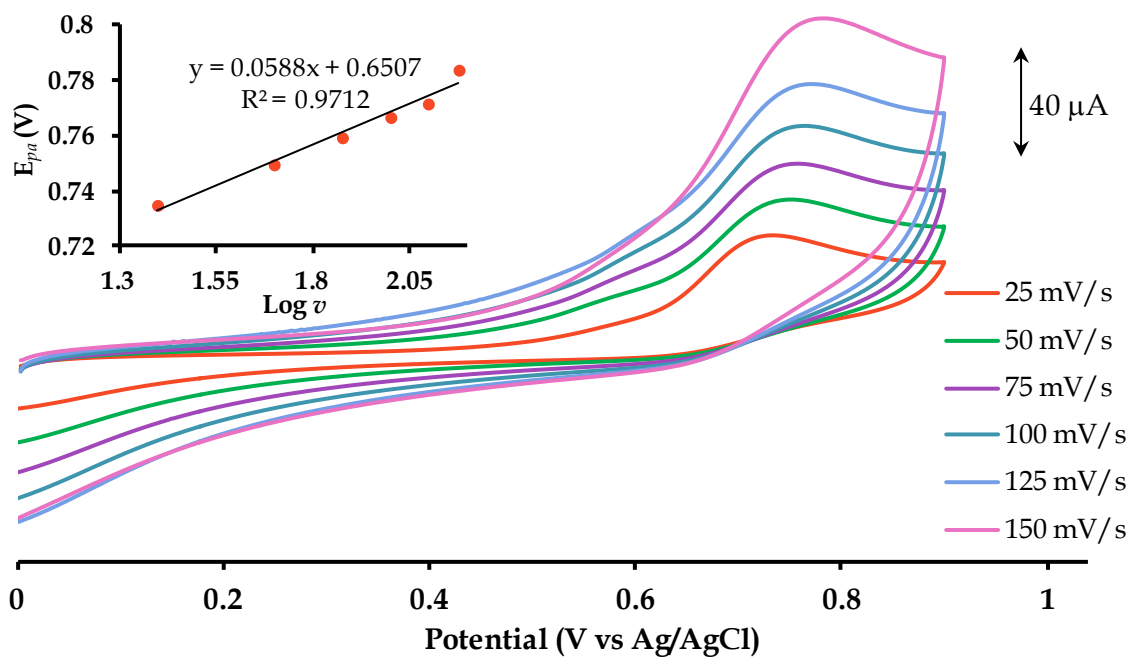


**Figure 3.33:** The electrocatalytic oxidation of nitrite (1 mM) using 3-Pt in pH 7 buffer solution at incrementing scan rates. Inset: Plot of  $E_{pa}$  vs  $\text{Log } v$ .

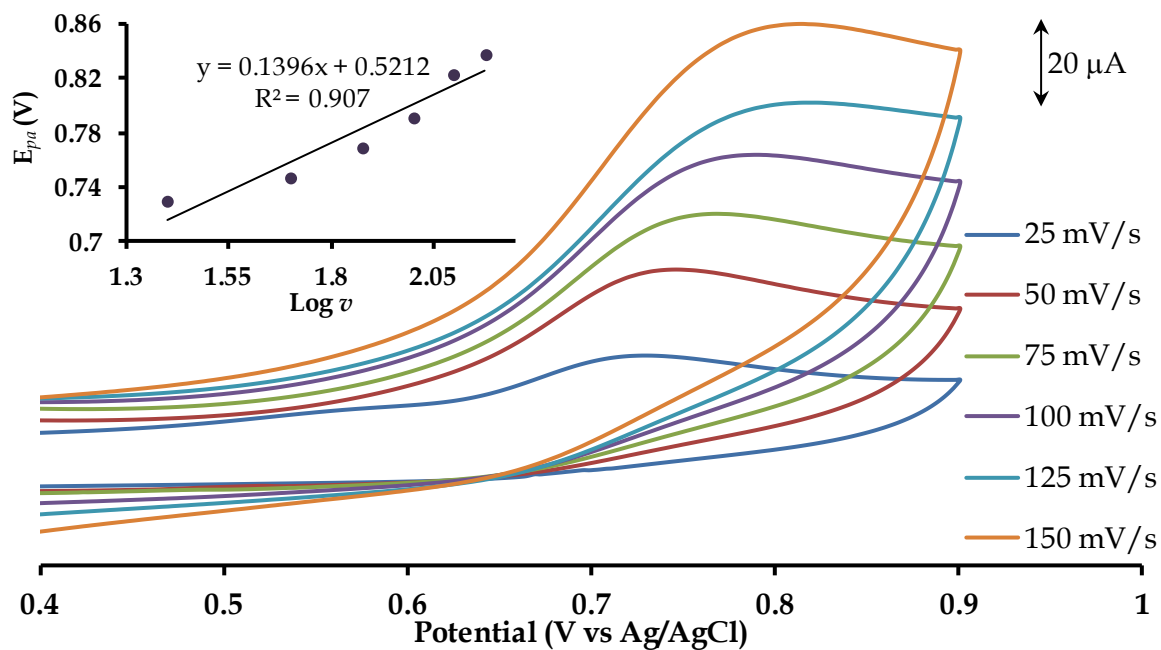


**Figure 3.34:** The electrocatalytic oxidation of nitrite (1 mM) using 4-Pt in pH 7 buffer solution at incrementing scan rates. Inset: Plot of  $E_{pa}$  vs  $\text{Log } v$ .

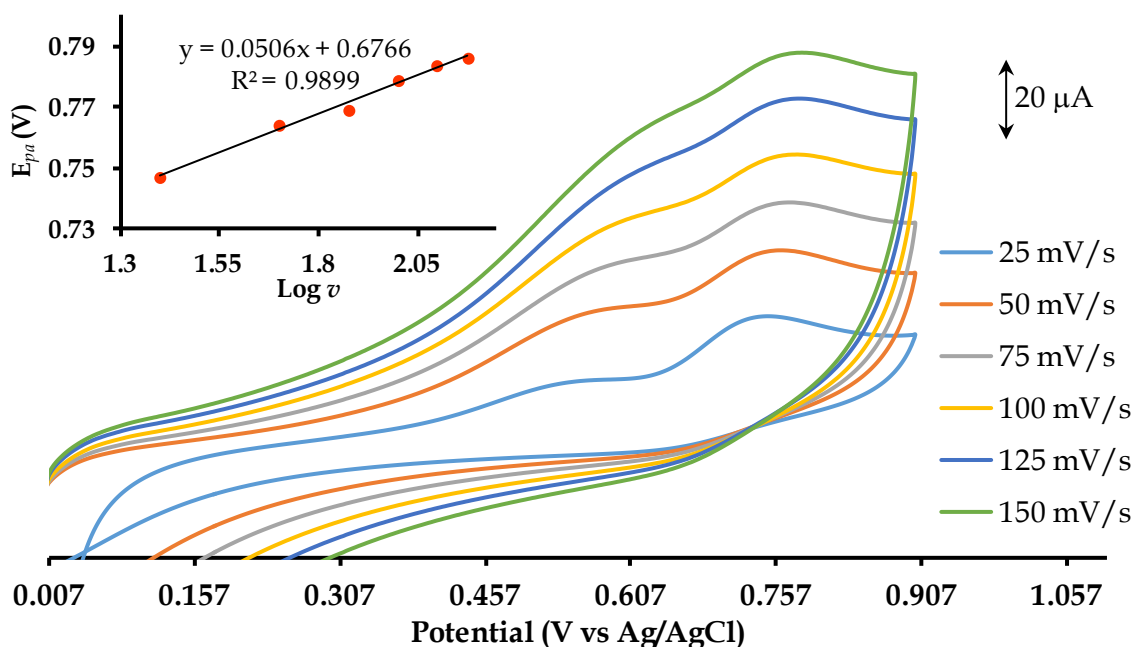


**Figure 3.35:** The electrocatalytic oxidation of nitrite (1 mM) using 5-Pt in pH 7 buffer solution at incrementing scan rates. Inset: Plot of  $E_{pa}$  vs  $\text{Log } v$ .

### 3.4 Conclusion

Novel Co and Fe MPcs bearing chromone and coumarin substituents were synthesized and spectroscopically characterized. The MPcs exhibited similar redox behavior as was deduced from their voltammetric analysis. Voltammetric assignments were well corroborated by UV-Vis spectroelectrochemical data and were comparable to those reported in literature for similar tetra-substituted mononuclear Co and FePcs. Surface modification of bare Pt microelectrodes was achieved readily *via* electropolymerization (in 20 successive CV cycles). These electropolymerized MPc surfaces acted as electron mediators in the electrocatalytic oxidation of nitrite.

**Table 3.1** *Crystal data and structure refinement data.*

Chemical formula	C <sub>17</sub> H <sub>8</sub> N <sub>2</sub> O <sub>3</sub>
Formula weight	288.25
Temperature (K)	100(2)
Crystal system	Monoclinic
Space group	<i>Pc</i>
Unit cell dimensions (Å, °)	$a = 5.2704(4)$ $b = 14.0315(10)$ $c = 8.9561(6)$ $\alpha = 90.000(5)$ $\beta = 94.340(4)$ $\gamma = 90.000(5)$
Crystal size (mm)	0.60 x 0.14 x 0.09
V(Å <sup>3</sup> )	660.42(8)
Z	2
Density (calc.) (Mg/m <sup>3</sup> )	1.450
Absorption coefficient (mm <sup>-1</sup> )	0.102
<i>F</i> (000)	296
$\theta$ range for data collection	1.5; 26.1
Index ranges	$-6 \leq h \leq 5$ $-17 \leq k < 16$ $-10 \leq l \leq 11$
Reflections measured	5668
Observed reflections [ $I > 2\sigma(I)$ ]	1284
Independent reflections	1306
Data/Restraints/parameters	1306/2/199
Goodness of fit on $F^2$	1.115
Observed $R$ , $wR^2$	0.0268; 0.0716
$R_{int}$	0.022

**Table 3.2:** Selected bond lengths [ $\text{\AA}$ ] and bond angles [ $^\circ$ ] for **1**.

C6-O2	1.357(3)
C7-O2	1.374(3)
C9-O3	1.396(2)
C10-O3	1.372(3)
C4-O1	1.238(2)
C1-C9	1.403(3)
C12-C13	1.402(3)
C9-O3-C10	118.9(2)
C6-O2-C7	117.9(2)

### 3.5 References

- [1] K.M. Kadish, K.M. Smith, R. Guilard, *The Porphyrin Handbook*, Academic Press, San Diego, 2003, **19**, 105.
- [2] D. Wöhrle, G. Schnurpfeil, S.G. Makarov, A. Kazarin, O.N. Suvorova, *Macroheterocycles*, 2012, **5**, 191.
- [3] H. Cakici, A.A. Esenpinar, M. Bulut, *Polyhedron*, 2008, **27**, 3625.
- [4] E.T. Saka, D. Cakir, Z. Biyiklioglu, H. Kantekin, *Dyes and Pigments*, 2013, **98**, 255.
- [5] N. Sekkat, H. v.d. Bergh, T. Nyokong, N. Lange, *Molecules*, 2012, **17**, 98.

- [6] M. Burghard, M. Schmelzer, S. Roth, P. Haisch, M. Hanack, *Langmuir*, 1994, **10**, 4265.
- [7] S. Yang, L. Fan, S. Yang, *J. Phys. Chem. B*, 2003, **107**, 8403.
- [8] W.J.R. Santos, P.R. Lima, A.A. Tanaka, S.M.C.N. Tanaka, L.T. Kubota, *Food Chem.*, 2009, **113**, 1206.
- [9] J.H. Zagal, S. Griveau, J.F. Silva, T. Nyokong, F. Bedioui, *Coord. Chem. Rev.*, 2010, **254**, 2755.
- [10] I. Booyesen, F. Matemadombo, M. Durmuş, T. Nyokong, *Dyes and Pigments*, 2011, **89**, 111.
- [11] J. Obirai, N.P. Rodrigues, F. Bedioui, T. Nyokong, *J. Porphyrins Phthalocyanines*, 2003, **7**, 508.
- [12] T. Nyokong, *N<sub>4</sub>-Macrocyclic Metal Complexes*, ed. J.H. Zagal, F. Bedioui, J.-P. Dodelet, Springer Science + Business Media, LLC, New York, 2006, ch. 7, pp. 315-361.
- [13] A.I. Adebayo, T. Nyokong, *Polyhedron*, 2009, **28**, 2831.
- [14] B. Ceken, M. Kandaz, A. Koca, *J. Coord. Chem.*, 2012, **65**, 3383.
- [15] S. Seelan, M.S. Agashe, D. Srinivas, S. Sivasanker, *J. Mol. Catal. A: Chem.*, 2001, **168**, 61.
- [16] C. Barrera, I. Zhukov, E. Villagra, F. Bedioui, M.A. Páez, J. Costamagna, J.H. Zagal, *J. Electroanal. Chem.*, 2006, **589**, 212.
- [17] J. C. Obirai, T. Nyokong, *J. Electroanal. Chem.*, 2007, **600**, 251.
- [18] V. Mani, R. Devasenathipathy, S. -M. Chen, S. -T. Huang, V.S. Vasantha, *Enzyme Microb. Technol.*, 2014, **66**, 60.

- [19] B.H. Havsteen, *Pharmacol. Ther.*, 2002, **96**, 67.
- [20] M. Camur, M. Bulut, M. Kandaz, O. Guney, *Polyhedron*, 2009, **28**, 233.
- [21] S.K. Sharma, S. Kumar, K. Chand, A. Kathuria, A. Gupta, R. Jain, *Curr. Med. Chem.*, 2011, **18**, 3825.
- [22] C. Zwergel, S. Valente, A. Salvato, Z. Xu, O. Talhi, A. Mai, A. Silva, L. Altucci, G. Kirsch, *Med. Chem. Commun.*, 2013, **4**, 1571.
- [23] Y. Li, Z. Yang, Z. Liao, Z. Han, Z. Liu, *Inorg. Chem. Commun.*, 2010, **13**, 1213.
- [24] A. Zwergel, S. Valente, A. Salvato, Z. Xu, O. Talhi, A. Mai, A. Silva, L. Altucci, G. Kirsch, *Med. Chem. Commun.*, 2013, **4**, 1571.
- [25] S.H. Kim, Y.H. Lee, S.Y. Jung, H.J. Kim, C. Jin, Y.S. Lee, *Eur. J. Med. Chem.*, 2011, **46**, 1721.
- [26] M.M. Ghoneim, A. Tawfik, *Anal. Chim. Acta*, 2004, **511**, 63.
- [27] M. Camur, M. Bulut, *Dyes and Pigments*, 2008, **77**, 165
- [28] A.S. Başak, A.R. Özkaya, A. Altındal, B. Salih, A. Şengüld, Ö. Bekaroğlu, *Dalton Trans.*, 2014, **43**, 5858.
- [29] R. Baker, D.P. Wilkinson, J. Zhang, *Electrochim. Acta*, 2008, **53**, 6906.
- [30] S. Nyoni, T. Mugadza, T. Nyokong, *Electrochim. Acta*, 2014, **128**, 32.
- [31] A. Caro, F. Beddioui, J.H. Zagal, *Electrochim. Acta*, 2002, **47**, 1489.
- [32] A. Lin, A. Balamurugan, Y. Lai, K. Ho, *Talanta*, 2010, **82**, 1905.
- [33] R. Cammack, C.L. Joannou, X.Y. Cui, C.T. Martinez, S.R. Maraj, M.N. Hughes, *Biochim. Biophys. Acta*, 1999, **1411**, 475.
- [34] H. Özena, U. Kamber, M. Karaman, S. Gül, E. Atakis, K. Özcan, O. Atakisi, *Exp. Toxicol. Pathol.*, 2014, **66**, 367.

- [35] A. Cockburn, C.W. Heppner, J.L.C.M. Dorne, *Encyclopedia of Food Safety*, 2014, **2**, 332.
- [36] H. Zhang, S. Qi, Y. Dong, X. Chen, Y. Xu, Y. Ma, X. Chen, *Food Chem.*, 2014, **151**, 429.
- [37] D. Yu, D. Yong, S. Dong, *J. Environ. Sci.*, 2013, **25**, 785.
- [38] A. Hori, Y. Inoue, H. Yuge, *Acta Crystallogr., Sect. C*, 2011, **67**, o154.
- [39] M. Dinçer, A. Agar, N. Akdemir, E. Agar, N. Özdemir, *Acta Crystallogr., Sect. E*, 2004, **60**, o79.
- [40] E. Guzel, A. Atsay, S. Nalbantoglu, N. Saki, A.L. Dogan, A. Gul, M.B. Kocak, *Dyes and Pigments*, 2013, **97**, 238.
- [41] S. Altun, A.R. Özkaya, M. Bulut, *Polyhedron*, 2012, **48**, 31.
- [42] A. Alemdar, A.R. Özkaya, M. Bulut, *Polyhedron*, 2009, **28**, 3788.
- [43] Z. Odabaş, H. Kara, A.R. Özkaya, M. Bulut, *Polyhedron*, 2012, **39**, 38.
- [44] Y. Ipeka, H. Dincer, A. Koca, *Sens. Actuators, B*, 2014, **193**, 830.
- [45] M. Kandaz, M.N. Yarasir, A. Koca, *Polyhedron*, 2009, **28**, 257.
- [46] M. Sevim, M.N. Yaras, A. Koca, M. Kandaz, *Dyes and Pigments*, 2014, **111**, 190.
- [47] A. Erdoğan, I.A. Akinbulu, T. Nyokong, *Polyhedron*, 2010, **29**, 2352.
- [48] A. Erdoğan, I.N. Booyesen, T. Nyokong, *Synth. Met.*, 2011, **161**, 241.
- [49] I.A. Akinbulu, T. Nyokong, *Polyhedron*, 2010, **29**, 1257.
- [50] G. Özgül, A. Taştemel, A.R. Özkaya, M. Bulut, *Polyhedron*, 2015, **85**, 181.
- [51] B.O. Agboola, K.I. Ozoemena, T. Nyokong, *Electrochim. Acta*, 2006, **51**, 4379.
- [52] M. Arici, D. Arican, A.L. Ugur, A. Erdogmus, A. Koca, *Electrochim. Acta*, 2013, **87**, 554

- [53] I. Özçeşmeci, A.K. Burat, Y. İpek, A. Koca, Z. Aayır, *Electrochim. Acta*, 2013, **89**, 270.
- [54] A. Alemdar, A.R. Özkaya, M. Bulut, *Synth. Met.*, 2010, **160**, 1556.
- [55] V. Çakır, H. Kantekin, Z. Bıyıklıoğlu, A. Koca, *Polyhedron*, 2014, **81**, 525.
- [56] Z. Bıyıklıoğlu, V. Çakır, F. Demir, A. Koca, *Synth. Met.*, 2014, **196**, 166.
- [57] B.O. Agboola, K.I. Ozoemena, T. Nyokong, *Electrochim. Acta*, 2006, **51**, 6470.
- [58] A. Maringa, E. Antunes, T. Nyokong, *Electrochim. Acta*, 2014, **121**, 93
- [59] F. Matemadombo, T. Nyokong, *Electrochim. Acta*, 2007, **52**, 6856.
- [60] F. Bedioui, S. Griveau, T. Nyokong, A.J. Appleby, C.A. Caro, M. Gulppi, G. Ochoae, J.H. Zagal, *Phys. Chem. Chem. Phys.*, 2007, **9**, 3383.
- [61] N. Nombona, P. Tau, N. Sehlotho, T. Nyokong, *Electrochim. Acta*, 2008, **53**, 3139

---

---

# CHAPTER FOUR

## Cobalt $\beta$ -Tetra(3-oxyflavone/2-(2-oxyphenyl)benzoxazole)phthalocyanines and Their Carbon Nanotube Conjugates: Formation, Characterization and Dopamine Electrocatalysis

### 4.1 Introduction

Dopamine (DA) is a naturally occurring catecholamine which behaves as a neurotransmitter in mammals [1]. It plays a significant role in the functioning of the central nervous, renal and hormonal systems [2]. Abnormally low or high levels of dopamine may result in disorders like Parkinson's disease or Schizophrenia; hence, their detection in human physiological fluids is of paramount importance in clinical diagnosis [3]. Electrochemical methods have proved to be quite advantageous for this purpose with minimal costs, low detection limits, high accuracy and fast detection times [4, 5].

Metallophthalocyanines (MPcs) are promising candidates for application in biosensors by virtue of their optimal electrochemical properties [6]. Transition metal

phthalocyanines in particular are well recognized for their excellent electrocatalytic behaviour towards various biological analytes [7]. The preparation of MPc modified electrodes with immobilized carbon nanotube (CNT) films has gained particular interest over the years. CNTs are known to promote electron transfer reactions due to their high electrical conductivity and enhanced mechanical properties [8]. MPcs can be non-covalently adsorbed *via*  $\pi$ - $\pi$  stacking onto CNTs to produce MPc-CNT conjugate films that possess the catalytic properties of MPcs while preserving the electronic structures and properties of CNTs [9, 10]. The electrocatalysis of many analytes such as dopamine, asulam and ascorbic acid have been reported using this method [10-12].

MPcs containing biologically relevant substituents have been used for developing biosensors that exhibit enhanced selectivity and sensitivity towards biological analytes [13]. Flavonoids found in plant pigments are known to have cytotoxic, anti-inflammatory and antiviral activities [14], while benzoxazoles have attracted pharmacological application in the synthesis of antifungal, antibacterial and anti-cancer drugs [15]. In this study, we report on the synthesis and characterization of Co(II) phthalocyanines substituted with biologically relevant flavone (flav) and benzoxazole (bo) moieties. In addition, we explore the comparative electrocatalytic capabilities of MPc modified glassy carbon electrodes (GCEs) and GCEs modified with multi-walled carbon nanotubes (MWCNTs) adsorbed onto MPcs, toward dopamine.

## 4.2 Experimental

### 4.2.1 Electrochemical Methods

A Pt working electrode was employed for voltammetric studies while a GCE was used in the preparation of chemically modified electrodes (CMEs). Electrodeposition was carried out by running 30 repetitive cyclic voltammetry (CV) scans on a GCE immersed in the appropriate CoPc solution (**3** or **4**) from -1.4 V to 1.5 V at 100 mV/s to produce **3**-GCE and **4**-GCE, respectively. Electrodes modified with MWCNTs were prepared *via* adsorption of the MWCNTs onto both a bare GCE and electrodeposited films of the metal complexes. The MWCNTs (1 mg) were first dispersed in 2 cm<sup>3</sup> dimethylformamide (DMF) by ultrasonication for 1 hr. Thereafter, 2 × 10<sup>-3</sup> cm<sup>3</sup> of the black suspension was transferred onto each GCE and allowed to dry at 100 °C for 24 hrs. The nanofabricated CMEs (MWCNT-GCE, **3**-MWCNT-GCE and **4**-MWCNT-GCE) were rinsed in ultrapure prior to use. A 1 mM solution of dopamine was prepared in a pH 7 phosphate buffer solution (PBS) for electrocatalysis.

### 4.2.2 Synthesis

#### a) 4-(Flavone-3-oxy)phthalonitrile (**1**)

A mixture of 4-nitrophthalonitrile (1.00 g, 5.78 mmol), 3-hydroxyflavone (1.38 g, 5.78 mmol) and potassium carbonate (2.30 g, 16.64 mmol) was stirred into anhydrous DMF (30.0 cm<sup>3</sup>) at 90 °C under N<sub>2</sub> for 48 hrs after which it was cooled to room

temperature and poured into 300 cm<sup>3</sup> of a water-ice slurry. The resulting precipitate was filtered and washed with methanol (MeOH) as well as ethanol (EtOH) to produce a fluffy white compound. Yield: 41 %; m.p. (°C): 214.1-215.5; FT-IR ( $\nu_{max}/\text{cm}^{-1}$ ):  $\nu(\text{C}\equiv\text{N})$  2231,  $\nu(\text{C}=\text{O})$  1641,  $\nu(\text{C}-\text{O}-\text{C})$  1248, 1187; UV-Vis (DMF,  $\lambda_{max}$  ( $\epsilon$ ,  $\text{M}^{-1}\text{cm}^{-1}$ ): 296 nm (1443), 303 nm (1434), 317 nm (1171); <sup>1</sup>H NMR (ppm): 8.11-8.05 (m, 3H, H4, H7, H9), 7.94-7.85 (m, 4H, H2, H6, H11, H12), 7.70-7.67 (d, 1H, H8), 7.61-7.54 (m, 4H, H1, H3, H5, H10); <sup>13</sup>C NMR (ppm): 172.24, 160.62, 157.56, 155.81, 136.49, 135.11, 134.95, 132.16, 129.83, 129.39, 128.75, 126.01, 125.56, 124.00, 121.73, 121.30, 119.17, 116.96, 116.33, 115.85, 108.73. Molecular mass ( $m/z$ ): Calcd: 364.35. Found: 365.09 [M+H]<sup>+</sup>. Anal. Calcd for C<sub>23</sub>H<sub>12</sub>N<sub>2</sub>O<sub>3</sub>(%): C, 75.82; H, 3.32; N, 7.69. Found: C, 75.50; H, 3.48; N, 7.86.

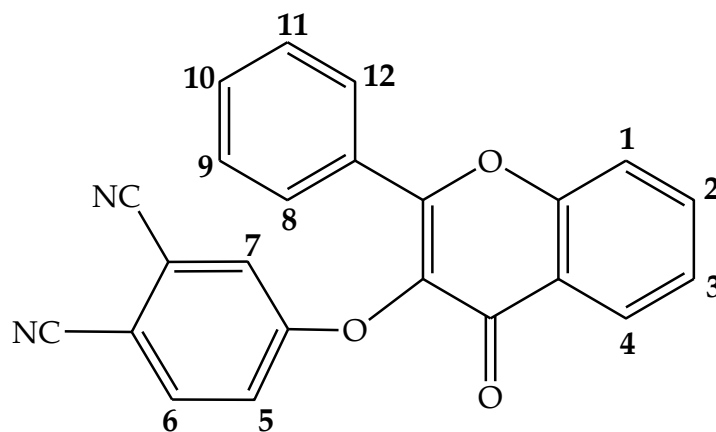


**Figure 4.1:** Structure of ligand 1.

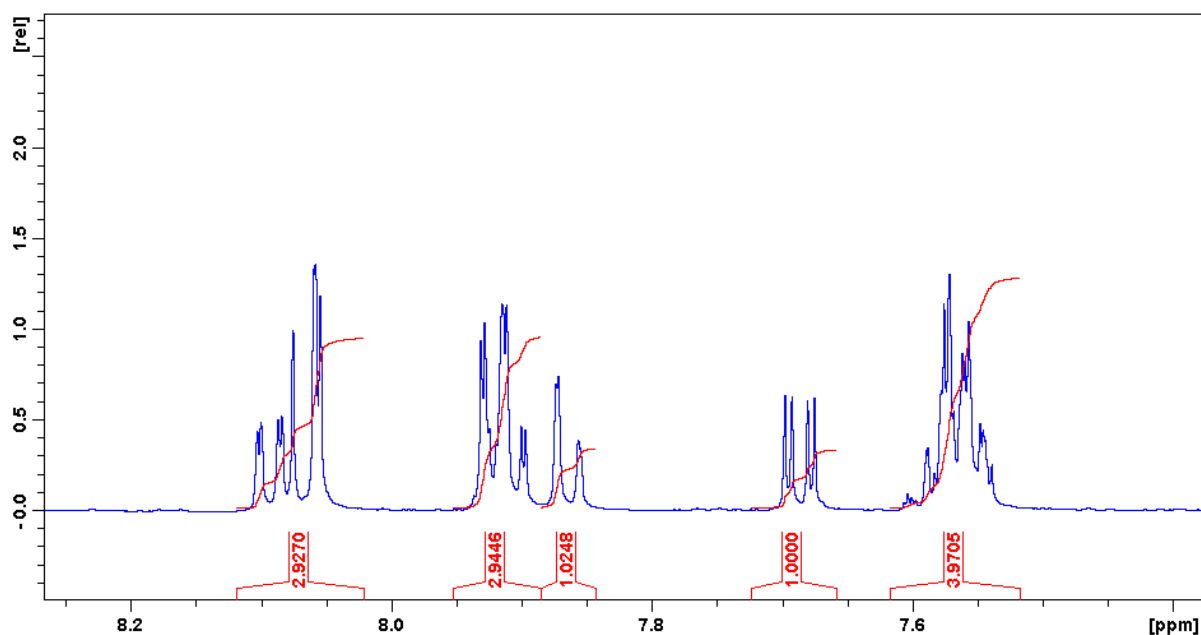


**Figure 4.2:**  $^1\text{H}$  NMR spectrum of ligand **1** in the range of 7.35 - 8.30 ppm.

b) 4-(2-(Benzoxazol-2-yl)phenoxy)phthalonitrile (**2**)

The synthetic procedure of **2** is similar to that of **1**, with the addition of 2-(2-hydroxyphenyl)benzoxazole (1.22 g, 5.78 mmol) in place of 3-hydroxyflavone. After addition of the reaction mixture to 300 cm<sup>3</sup> of a water-ice slurry, the resulting precipitate was collected and thoroughly washed with MeOH to produce the desired white compound. Yield: 54 %; m.p. (°C): 175.7-176.0; FT-IR ( $\nu_{\text{max}}/\text{cm}^{-1}$ ):  $\nu(\text{C}\equiv\text{N})$  2233,  $\nu(\text{C}=\text{N})_{\text{Heterocyclic}}$  1595,  $\nu(\text{C}-\text{O}-\text{C})$  1249, 1039; UV-Vis (DMF,  $\lambda_{\text{max}}$  ( $\epsilon$ , M<sup>-1</sup>cm<sup>-1</sup>)): 295 nm (31829), 302 nm (26951), 317 nm (14300);  $^1\text{H}$  NMR (ppm): 8.34 (d, 1H, *H*8), 8.07 (d, 1H, *H*11), 7.85 (d, 1H, *H*1), 7.79-7.71 (m, 2H, *H*6, *H*9), 7.67 (d, 1H, *H*4), 7.59 (t, 1H, *H*7), 7.46-7.35 (m, 4H, *H*2, *H*3, *H*5, *H*10);  $^{13}\text{C}$  NMR (ppm): 161.88, 159.62, 151.99, 150.31, 141.48, 136.66, 134.49, 131.77, 127.88, 126.34, 125.40, 123.71, 122.75, 122.01, 120.46, 120.09, 117.08, 116.33, 115.83, 111.31, 108.58. Molecular mass (*m/z*): Calcd: 337.33.

Found: 338.09 [M+H]<sup>+</sup>. Anal. Calcd for C<sub>21</sub>H<sub>11</sub>N<sub>3</sub>O<sub>2</sub>(%): C, 74.77; H, 3.29; N, 12.46.

Found: C, 74.24; H, 3.09; N, 12.40.

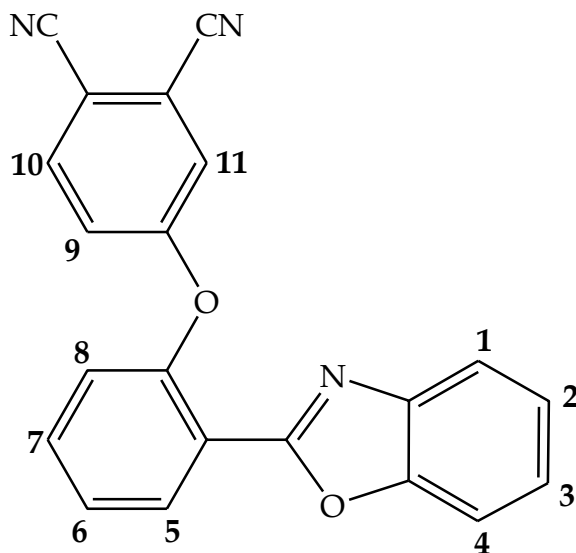


**Figure 4.3:** Structure of ligand 2.

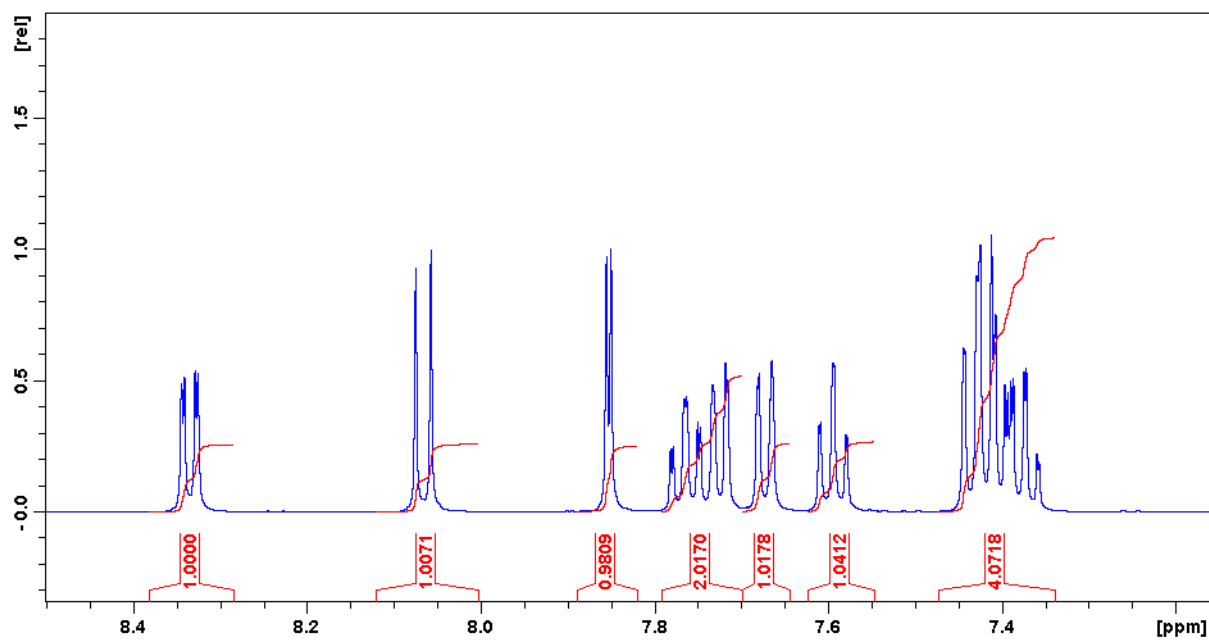


**Figure 4.4:** <sup>1</sup>H NMR spectrum of ligand 2 in the range of 7.15 - 8.50 ppm.

c) *Tetra-4-(3-oxyflavonephthalocyaninato)Co(II) (CoPc-flav, 3)*

A mixture of **1** (0.250 g, 0.686 mmol), CoCl<sub>2</sub> (0.0223 g, 0.172 mmol) and DBU was heated with stirring in *n*-pentanol (40.0 cm<sup>3</sup>) at 160 °C under nitrogen for 16 hrs. The reaction mixture was then cooled to room temperature and *n*-hexane was added drop-wise to induce precipitation. The precipitate was filtered using a millipore filtration setup and then washed with water, MeOH, EtOH, hexane and acetonitrile. The desired product was thereafter recovered *via* column chromatography using a 1:1 (*v:v*) CHCl<sub>3</sub>:tetrahydrofuran (THF) solvent system. Yield: 15%; IR ( $\nu_{max}/\text{cm}^{-1}$ ):  $\nu(\text{C}=\text{O})$  1646,  $\nu(\text{C}=\text{N})$  1605,  $\nu(\text{C}-\text{O}-\text{C})$  1219, 1093; UV-Vis (DMF,  $\lambda_{max}$  ( $\epsilon$ , M<sup>-1</sup>cm<sup>-1</sup>)): 668 nm (163402), 318 nm (174636), 304 nm (173305). Molecular mass ( $m/z$ ): Calcd: 1516.35. Found: 1515.27 [M-H]<sup>+</sup>, 1516.27 [M]<sup>+</sup>, 1517.28 [M+H]<sup>+</sup>, 1518.28 [M+2H]<sup>+</sup>. Anal. Calcd for C<sub>92</sub>H<sub>48</sub>CoN<sub>8</sub>O<sub>12</sub> (%): C, 72.87; H, 3.19; N, 7.39. Found: C, 70.37; H, 3.32; N, 7.23.

d) *Tetra-4-(2-(2-oxyphenyl)benzoxazolephthalocyaninato)Co(II) (CoPc-bo, 4)*

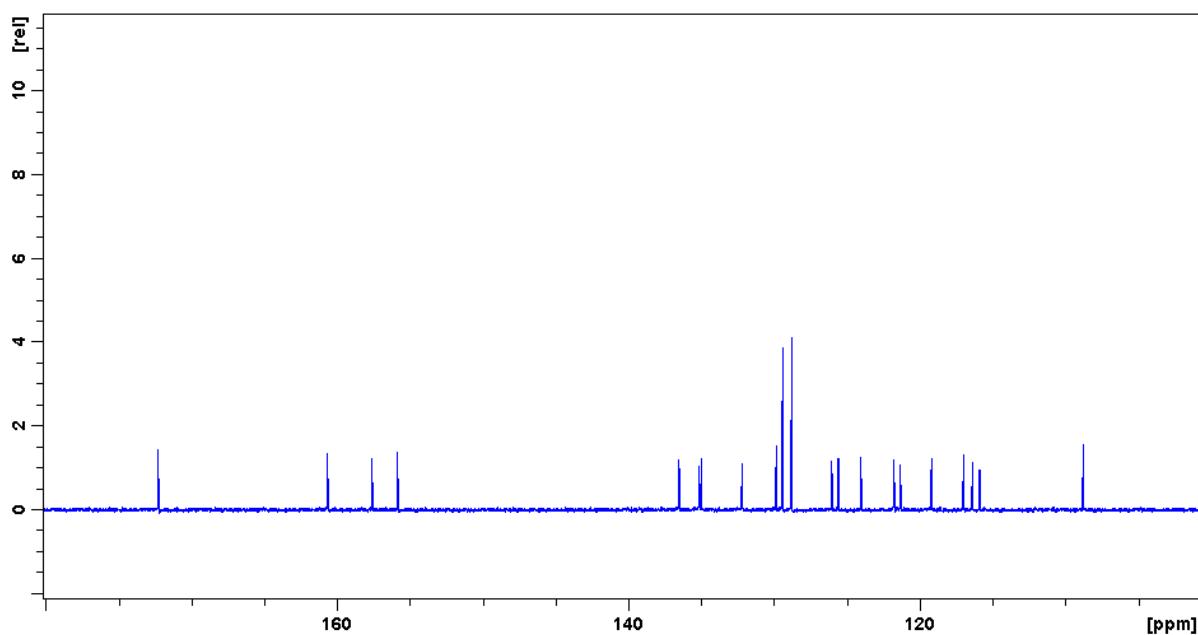
For the synthesis of **4**, compound **2** (0.250 g, 0.741 mmol) was added to CoCl<sub>2</sub> (0.024 g, 0.185 mmol) and DBU in *n*-pentanol (40.0 cm<sup>3</sup>) under the specified reaction conditions of **3**. The product was washed with water, MeOH, EtOH, dichloromethane (DCM), CHCl<sub>3</sub>, hexane and CH<sub>3</sub>CN and further purified *via* column chromatography using CH<sub>3</sub>Cl as the eluent. Yield: 22%; IR ( $\nu_{max}/\text{cm}^{-1}$ ):  $\nu(\text{C}=\text{N})_{\text{MPc}}$  1608,  $\nu(\text{C}=\text{N})_{\text{Heterocyclic}}$  1579,  $\nu(\text{C}-\text{O}-\text{C})$  1230, 1091; UV-Vis (DMF,  $\lambda_{max}$  ( $\epsilon$ , M<sup>-1</sup>cm<sup>-1</sup>)): 666 nm (64178), 332 nm (54837), 294 nm (82117), 304 nm (75954), 318 nm

(63996). Molecular mass ( $m/z$ ): Calcd: 1408.26. Found: 1407.29  $[M-H]^+$ , 1408.29  $[M]^+$ , 1409.29  $[M+H]^+$ , 1410.29  $[M+2H]^+$ . Anal. Calcd for  $C_{84}H_{44}CoN_{12}O_8$  (%): C, 71.64; H, 3.15; N, 11.94. Found: C, 69.45; H, 2.94; N, 11.40.

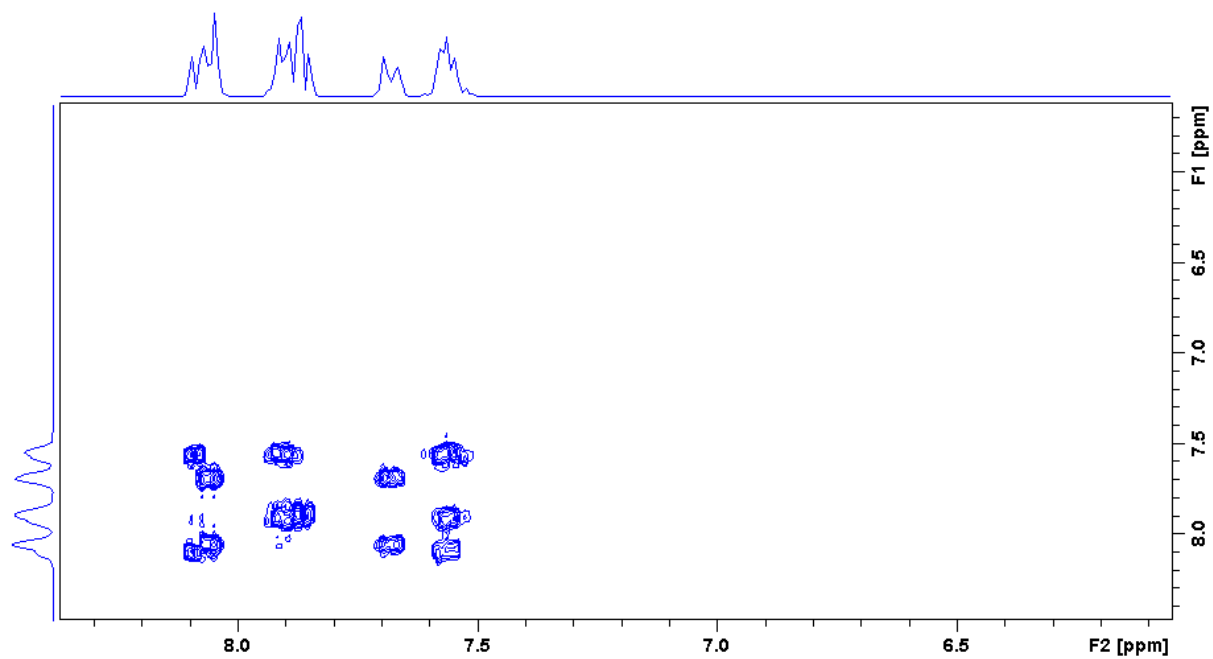
## 4.3 Results and Discussion

### 4.3.1 Synthesis and Spectral Characterization

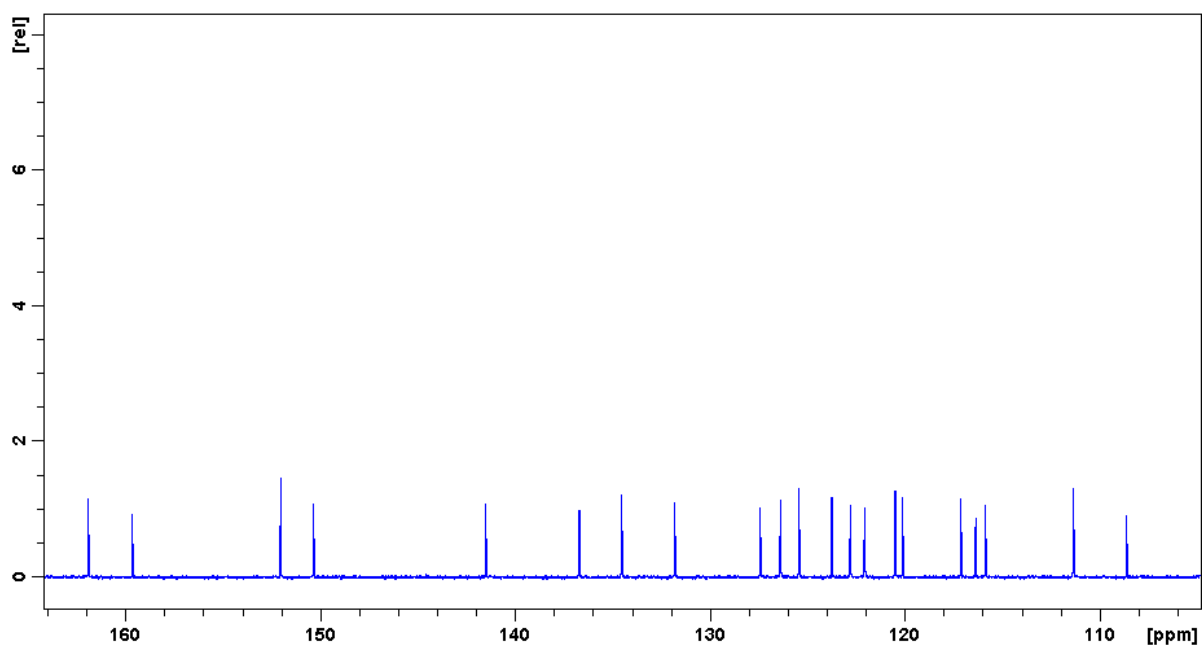
The  $^1H$  NMR spectra for the derivatized phthalonitriles **1** and **2** (see **Figs. 4.2** and **4.4**) showed well resolved peaks in the region of 7.0–9.0 ppm as is expected for compounds with delocalized  $\pi$ -aromatic systems. The proton NMR assignments were well supported by  $^{13}C$  NMR spectroscopy and homonuclear correlation spectroscopy (COSY) (see **Figs. 4.5-4.8**).



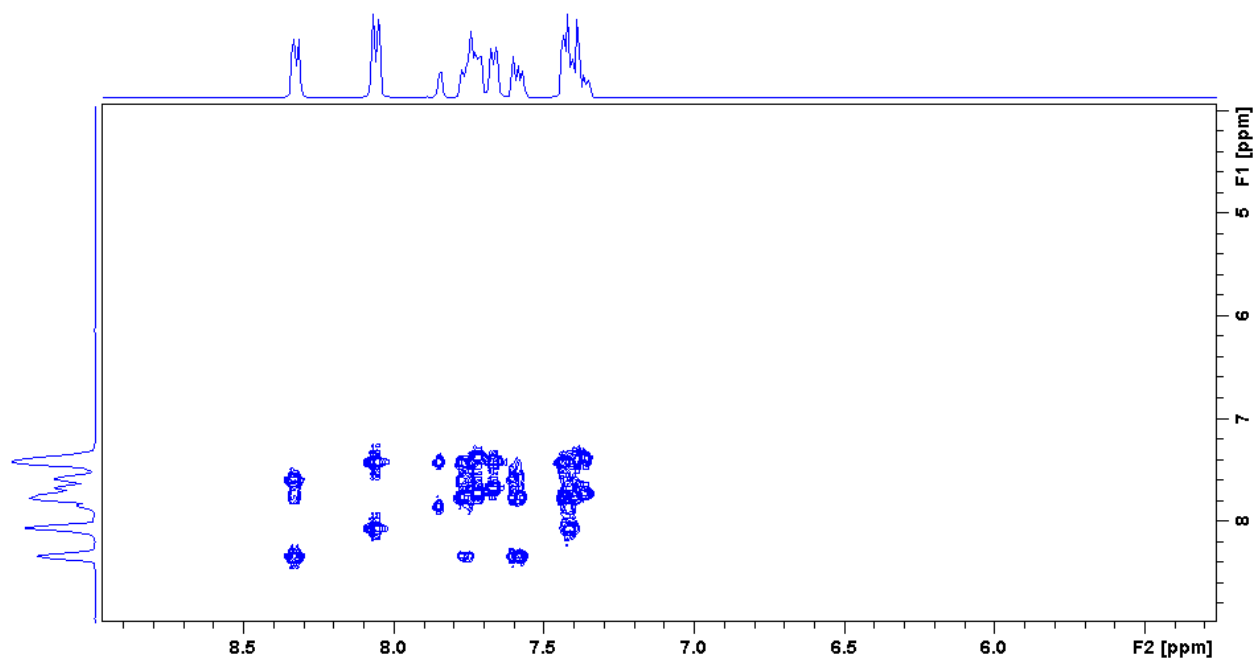
**Figure 4.5:**  $^{13}C$  NMR spectrum of ligand **1** in the range of 100 - 180 ppm.



**Figure 4.6:** *Cosy spectrum of ligand 1.*

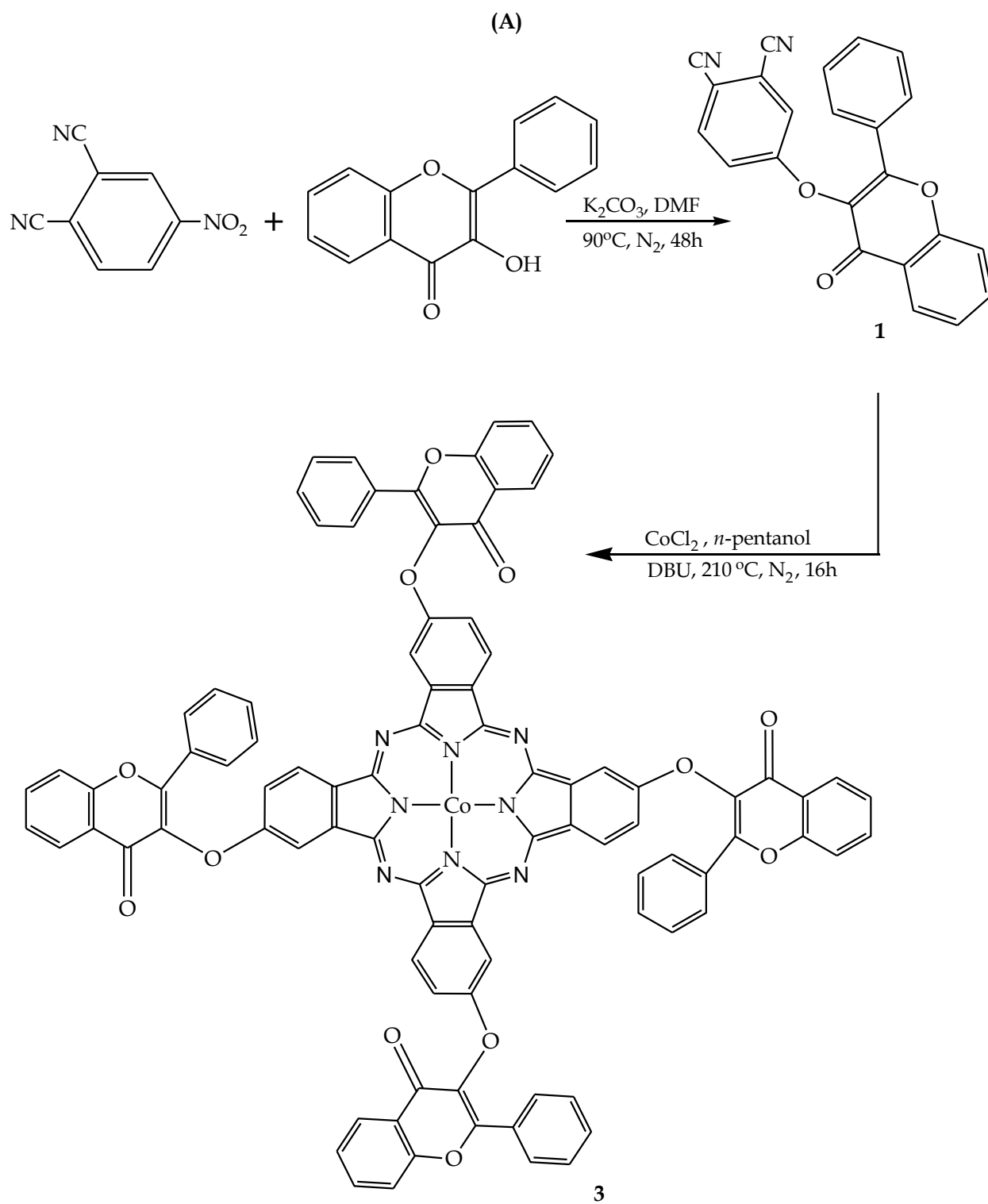


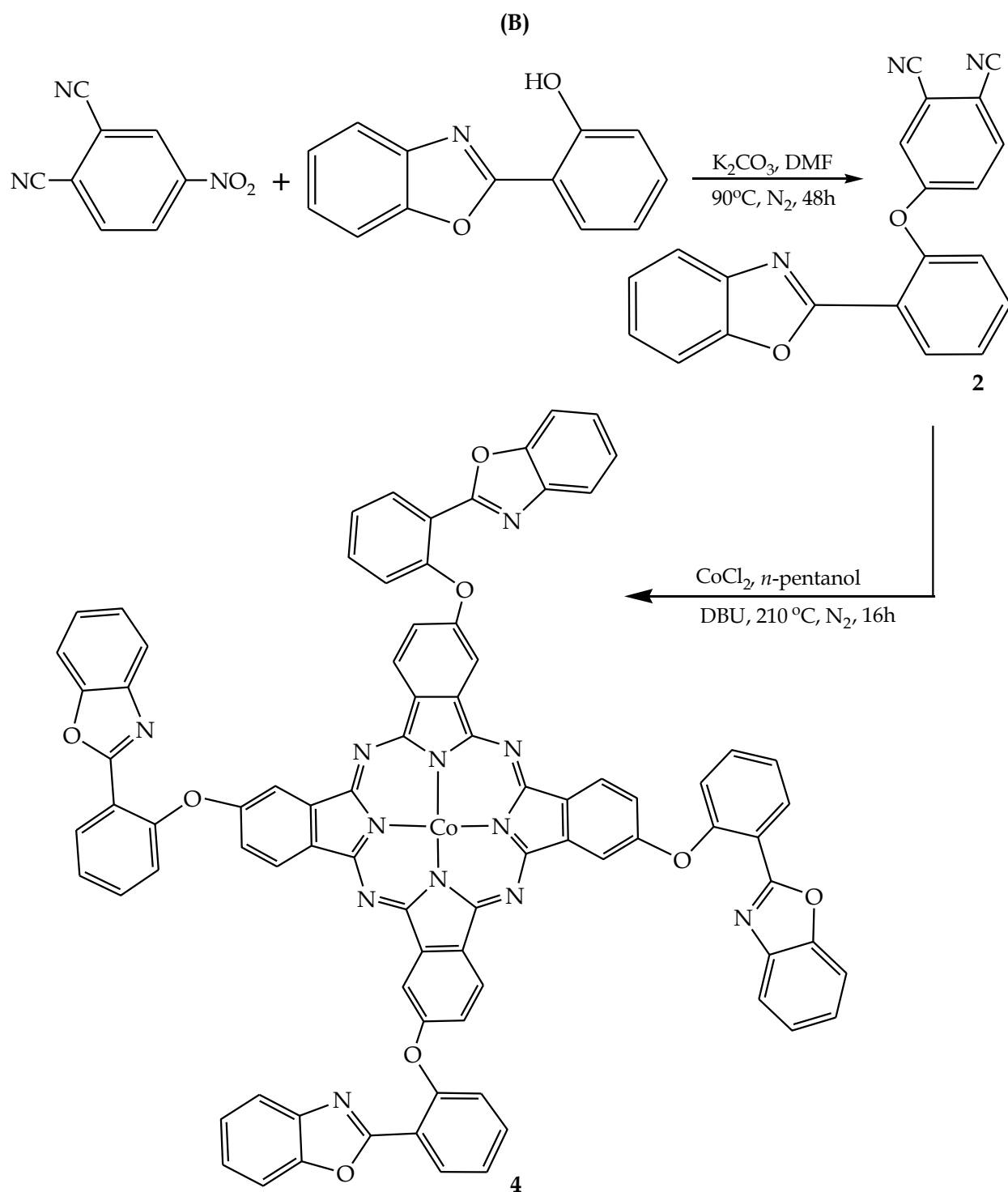
**Figure 4.7:** <sup>13</sup>C NMR spectrum of ligand 2 in the range of 102 - 164 ppm.



**Figure 4.8:** *Cosy spectrum of ligand 2.*

Template cyclotetramerization of ligands **1** and **2** in the presence of a catalyst, 1, 8-diazabicyclo[5.4.0]undec-7-ene (DBU) afforded the corresponding MPcs **3** or **4**, refer to **Scheme 4.1**. Complex **3** was found to be soluble in low boiling point organic solvents including THF,  $\text{CHCl}_3$  and DCM while **4** displayed good solubility in THF, DMF and DMSO. It is well documented that bulky or long-chain peripheral substituents improve the solubility of MPcs in organic solvents [16], thus, as expected, **3**, which contains more bulky aromatic groups exhibits enhanced solubility compared to **4**.





**Scheme 4.1:** Synthetic pathways for the CoPcs: (a) (CoPc-flav, 3) and (b) (CoPc-bo, 4).

The absence of the medium intensity nitrile stretches found at  $2231\text{ cm}^{-1}$  (for **1**) and  $2233\text{ cm}^{-1}$  (for **2**) in the FT-IR spectra of the MPcs is typical of cyclotetramerization (see **Figs. 4.9** and **4.10**). The formation of macrocyclic ring systems is further supported by the observation of strong C=N vibrational bands at  $1605\text{ cm}^{-1}$  (for **3**) and  $1608\text{ cm}^{-1}$  (for **4**). Commonality is observed between the IR spectra of the ligands [ $\nu(\text{C}=\text{O})$   $1641\text{ cm}^{-1}$  (for **1**) and  $\nu(\text{C}=\text{N})_{\text{Heterocyclic}}$   $1595\text{ cm}^{-1}$  (for **2**)] and their respective CoPcs [ $\nu(\text{C}=\text{O})$   $1646\text{ cm}^{-1}$  (for **3**) and  $\nu(\text{C}=\text{N})_{\text{Heterocyclic}}$   $1579\text{ cm}^{-1}$  (for **4**)] affirming the presence of the biologically significant moieties in **3** and **4**.

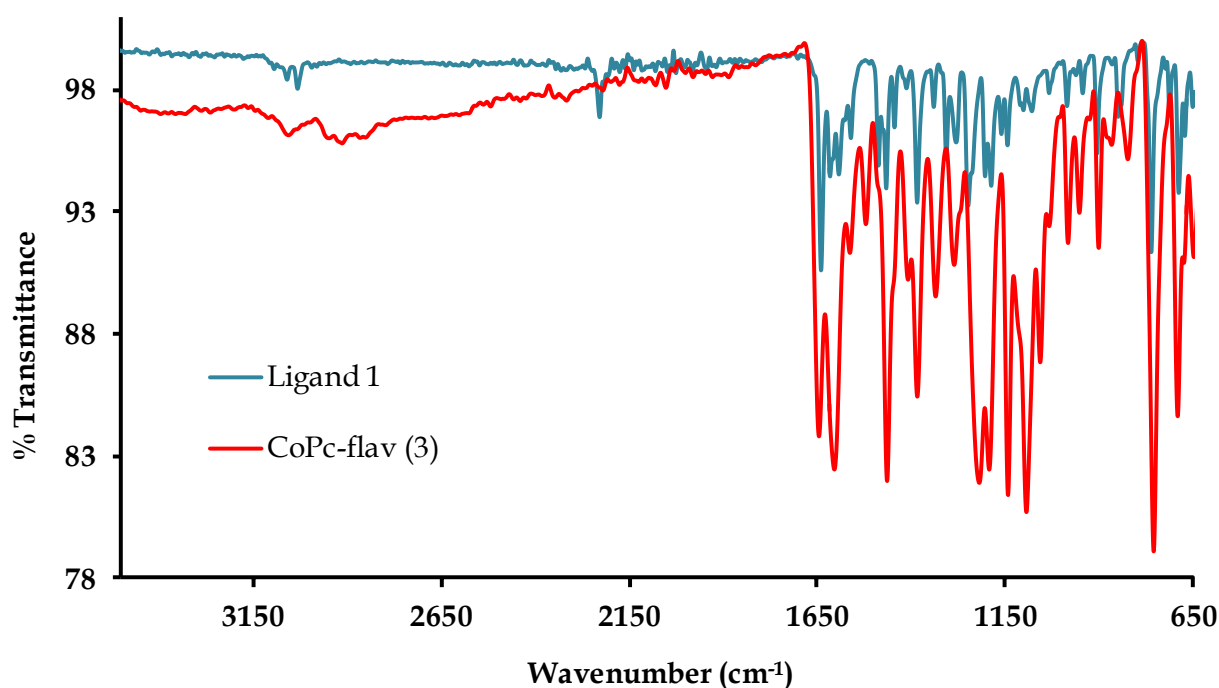


**Figure 4.9:** *Overlay IR spectrum of complex 3 and its free ligand, compound 1.*

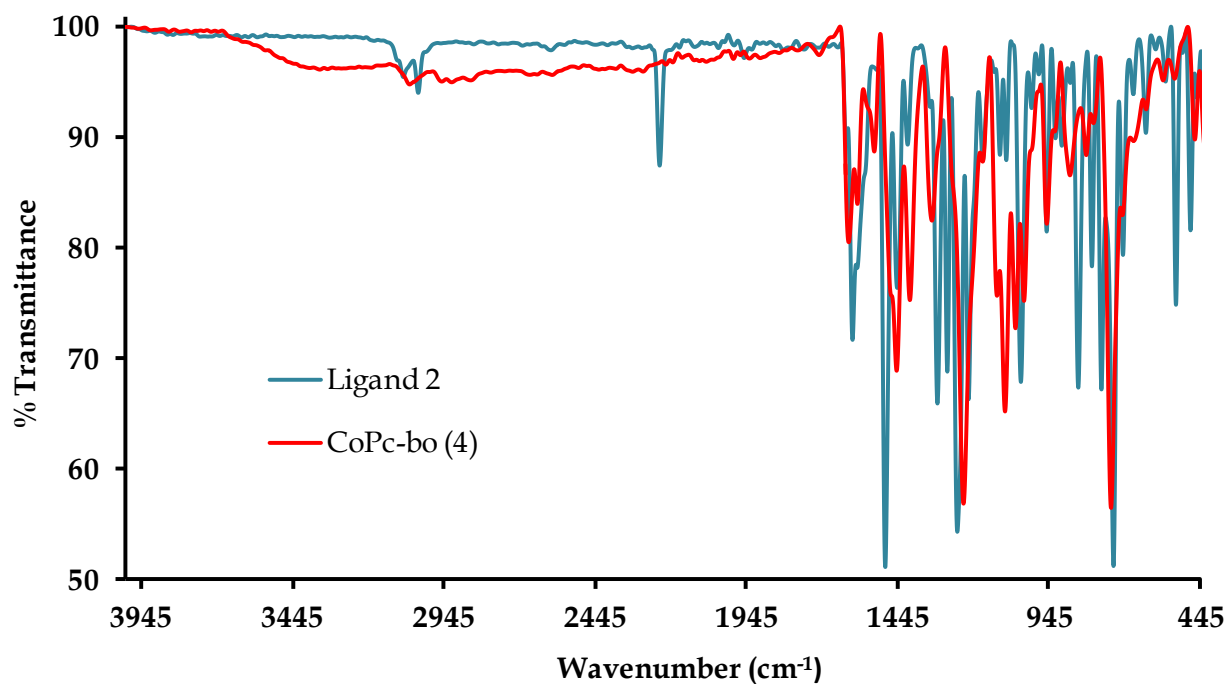


**Figure 4.10:** Overlay IR spectrum of complex **4** and its free ligand, compound **2**.

Data obtained from ESI-TOF mass spectrometry (Figs. 4.11-4.14) and elemental analysis provided definitive structural characterization for the ligands and metal complexes. All molecular and cluster ion peaks were in accordance with the calculated  $m/z$  values. The mass spectra of the MPcs showed  $[M]^+$  ion peaks at  $m/z$  values of 1516.27 for complex **3** and 1408.29 for **4**, in addition to the protonation molecular ion peaks of the form:  $[M+H]^+$ ,  $[M+2H]^+$  and  $[M-H]^+$ .

Elemental Composition Report

Single Mass Analysis

Tolerance = 5.0 PPM / DBE: min = -1.5, max = 100.0

Element prediction: Off

Number of isotope peaks used for i-FIT = 3

Monoisotopic Mass, Even Electron Ions

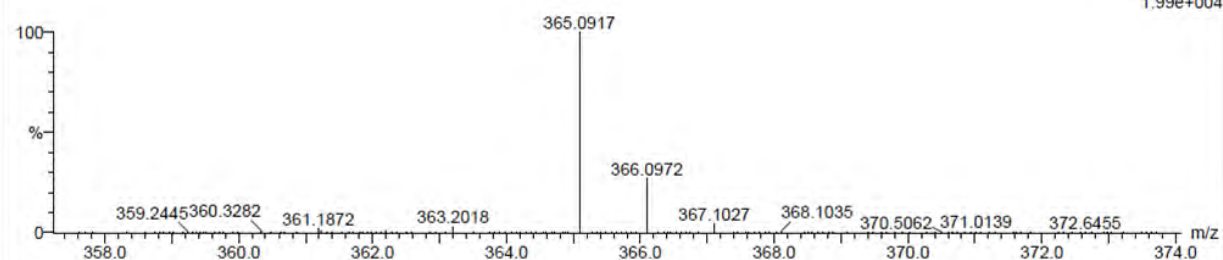
12 formula(e) evaluated with 1 results within limits (up to 20 best isotopic matches for each mass)

Elements Used:

C: 20-25 H: 10-15 N: 0-5 O: 0-5

S2 +rms 55 (0.919)

TOF MS ES+



Mass	Calc. Mass	mDa	PPM	DBE	i-FIT	i-FIT (Norm)	Formula
365.0917	365.0926	-0.9	-1.5	18.5	137.0	0.0	C23 H13 N2 O3

Figure 4.11: High resolution TOF-MS spectrum of 1.

Elemental Composition Report

Single Mass Analysis

Tolerance = 5.0 PPM / DBE: min = -1.5, max = 100.0

Element prediction: Off

Number of isotope peaks used for i-FIT = 3

Monoisotopic Mass, Even Electron Ions

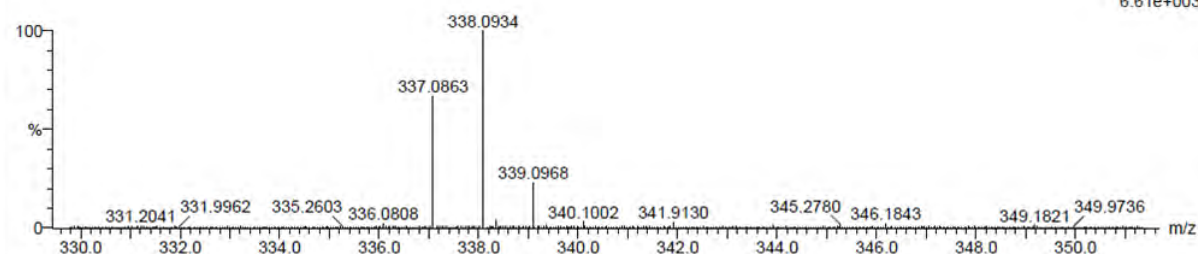
18 formula(e) evaluated with 1 results within limits (up to 20 closest results for each mass)

Elements Used:

C: 20-25 H: 10-15 N: 0-5 O: 0-5

S13 56 (0.939) Cm (1:60)

TOF MS ES+



Mass	Calc. Mass	mDa	PPM	DBE	i-FIT	i-FIT (Norm)	Formula
338.0934	338.0930	0.4	1.2	17.5	390.1	0.0	C21 H12 N3 O2

Figure 4.12: High resolution TOF-MS spectrum of 2.

Single Mass Analysis

Tolerance = 5.0 PPM / DBE: min = -1.5, max = 100.0

Element prediction: Off

Number of isotope peaks used for i-FIT = 3

Monoisotopic Mass, Even Electron Ions

8 formula(e) evaluated with 1 results within limits (up to 20 best isotopic matches for each mass)

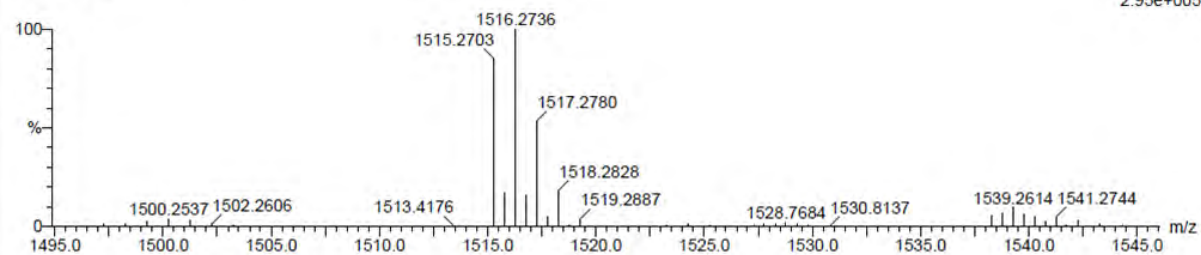
Elements Used:

C: 85-92 H: 45-50 N: 5-9 O: 10-15 Co: 0-1

S8-b2-MS 56 (1.854) Cm (1:61)

TOF MS ES+

2.95e+005



Mass	Calc. Mass	mDa	PPM	DBE	i-FIT	i-FIT (Norm)	Formula
1516.2736	1516.2802	-6.6	-4.4	72.5	113.0	0.0	C92 H49 N8 O12 Co

Figure 4.13: High resolution TOF-MS spectrum of 3.

Single Mass Analysis

Tolerance = 5.0 PPM / DBE: min = -1.5, max = 100.0

Element prediction: Off

Number of isotope peaks used for i-FIT = 3

Monoisotopic Mass, Even Electron Ions

11 formula(e) evaluated with 1 results within limits (up to 20 closest results for each mass)

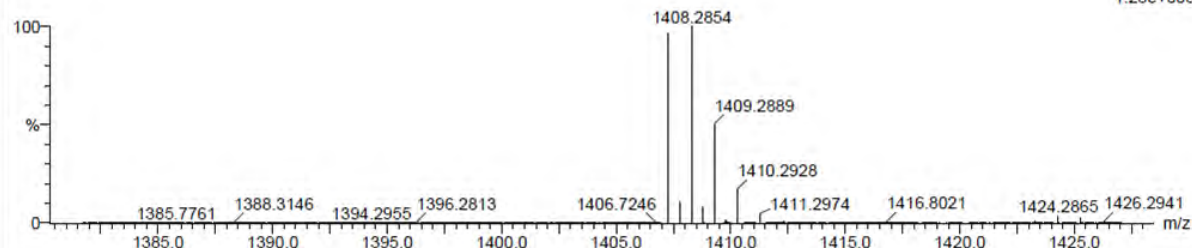
Elements Used:

C: 80-85 H: 40-45 N: 10-15 O: 5-10 Co: 0-1

S14THF 8 (0.234) Cm (1:61)

TOF MS ES+

1.28e+005



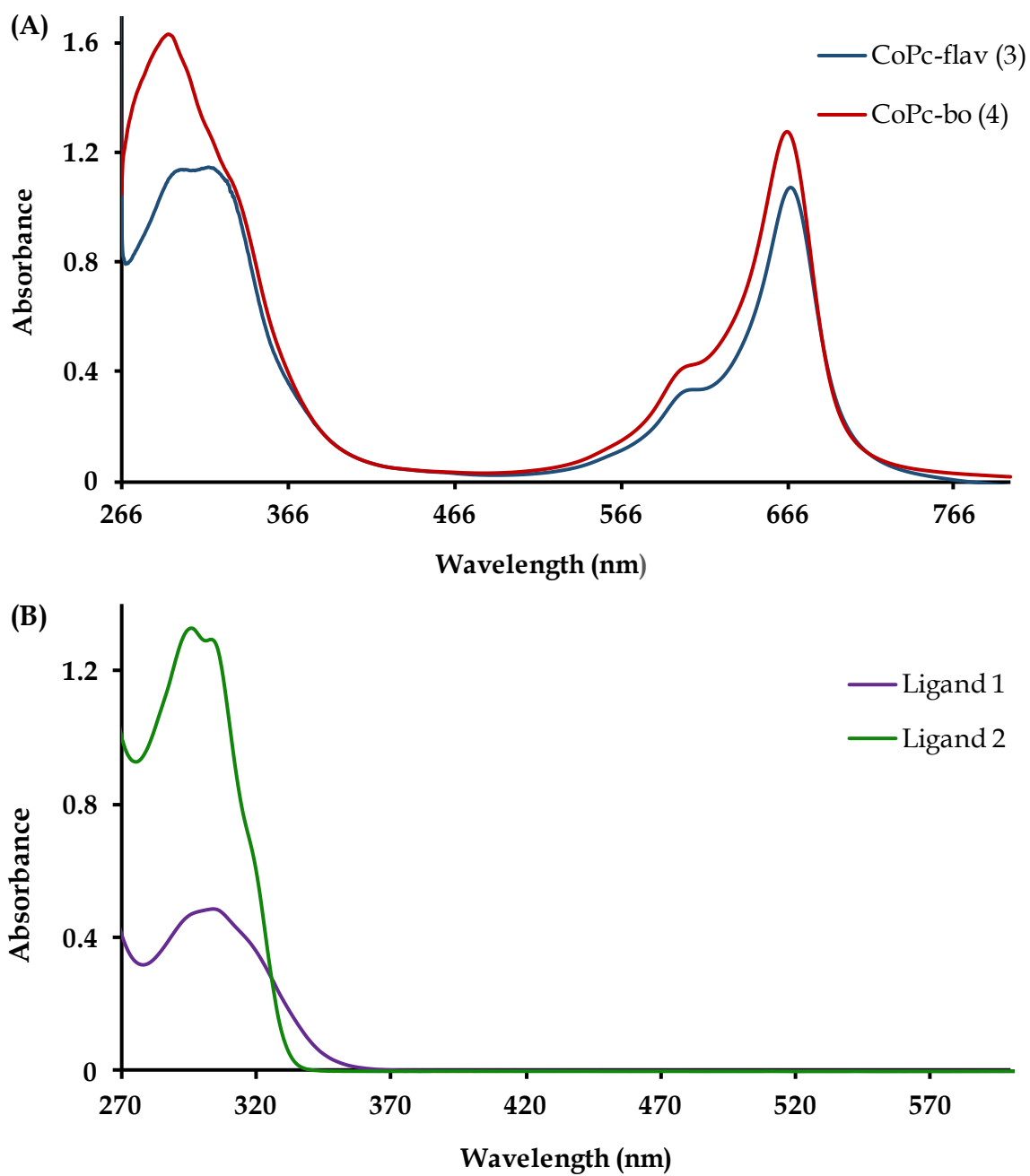
Mass	Calc. Mass	mDa	PPM	DBE	i-FIT	i-FIT (Norm)	Formula
1408.2854	1408.2815	3.9	2.8	68.5	195.6	0.0	C84 H45 N12 O8 Co

Figure 4.14: High resolution TOF-MS spectrum of 4.

The formulated MPcs showed Q- and B-bands in the regions of 600-700 nm and 300-400 nm, respectively in accordance with literature [17] (refer to **Table 4.1**). The Q-bands of the metal complexes do not differ significantly in wavelength but complex **3** is slightly red-shifted due to the presence of the electron donating imine groups in **3** (see **Fig. 4.15**). Both metal complexes display absorption bands in their electronic spectra that are characteristic of their corresponding ligands. The broadened B-band of **3** at 318 nm arises from an overlap of  $\pi$ - $\pi^*$  electronic transitions of the Pc ring and its corresponding phthalonitrile (317 nm) while the absorption band of **3** at a lower wavelength (304 nm) is also common to **1** (303 nm). The B-band of complex **4** (332 nm) is not well defined due to dampening by the intense absorption band at 294 nm which originates from **2**.

**Table 4.1:** UV-Vis absorption wavelengths and the corresponding molar absorptivities (in parentheses) for **1-4**.

Compound	Q-band (nm)	B-band (nm)	Higher energy bands (nm)
<b>1</b>	-	-	296 (1443), 303 (1434), 317(1171)
<b>2</b>	-	-	295 (31829), 302 (26951), 317(14300)
<b>3</b>	668 (163402)	318 (174636)	304 (173305)
<b>4</b>	666 (64178)	332 (54837)	294 (82117), 304 (75954), 318 (63996)



**Figure 4.15:** UV-Vis spectra of (A) complexes **3** and **4** at concentrations of  $6.6 \mu\text{M}$  and  $20 \mu\text{M}$ , respectively and (B) ligands **1** and **2** at concentrations of  $329 \mu\text{M}$  and  $48.1 \mu\text{M}$ , respectively.

### 4.3.2 Voltammetry and Spectroelectrochemistry

The solution redox properties of the complexes were investigated *via* cyclic and square-wave voltammetry in dry DMF. Both MPcs exhibited four redox processes which were observed in their respective cyclic and square-wave voltammograms, see **Figs. 4.16** and **4.17**. The difference between the anodic and cathodic peak potentials of a redox couple, denoted as  $\Delta E$ , gives an indication of the rate of electron transfer of the corresponding redox process. Redox couples that have peak current ratios ( $I_{pa}/I_{pc}$ ) approaching one and  $\Delta E$  values that are equal to those of a standard like ferrocene ( $\Delta E = 105$  mV at 100 mV/s on a Pt electrode) indicate optimal electron transfer kinetics and such redox couples are classified as reversible. However, the large  $\Delta E$  values ( $\Delta E > 105$  mV) of redox couples **I**, **II** and **III** indicate slower electron transfer kinetics as compared to that of the standard, hence these processes are considered to be quasi-reversible [18]. Redox couple **IV** is irreversible. Typically, MPcs with redox active transition metals (*e.g.* Fe, Co and Mn) have accessible *d*-orbitals that lie between the HOMO and LUMO gap of the Pc ring. Consequently, this class of MPcs can vary their electrochemical behaviour according to the coordination environment of the metal centre. For instance, the use of a donor solvent allows for axial coordination of the MPc to produce a stable 6-coordinate complex which promotes metal oxidation and reduction redox processes [19]. Hence, redox couples **I** to **IV** were assigned according to literature trends (refer to **Table 4.2**) [13, 20, 21] as  $Pc^{2-}/Pc^{3-}$  and  $M^{2+}/M^+$  reductions as well as  $M^{3+}/M^{2+}$  and  $Pc^{1-}/Pc^{2-}$

oxidations, respectively. The broadened metal reduction couples and any unassigned peaks are attributed to aggregation.

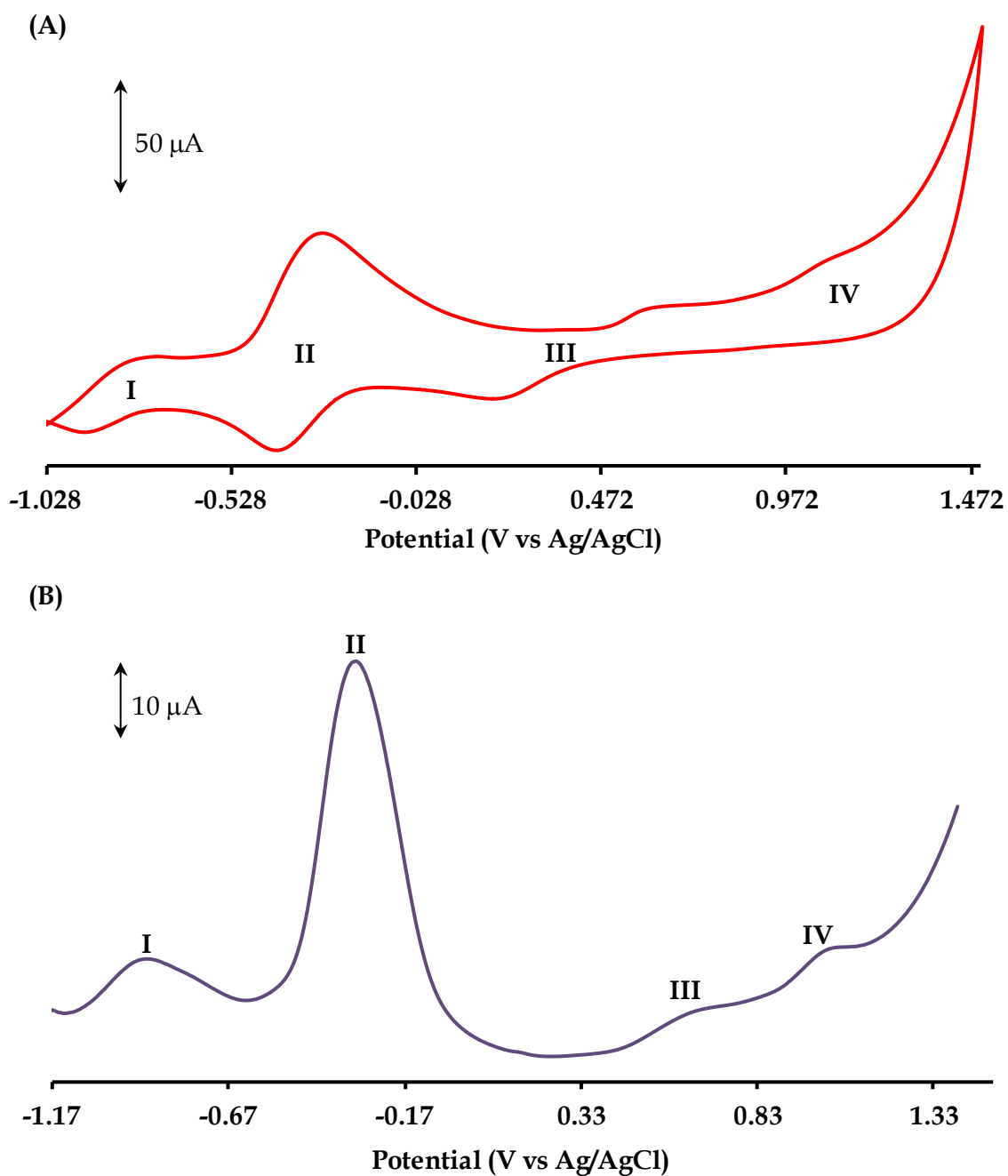


**Figure 4.16:** (A) CV and (B) SWV of complex 3 at 100 mV/s.

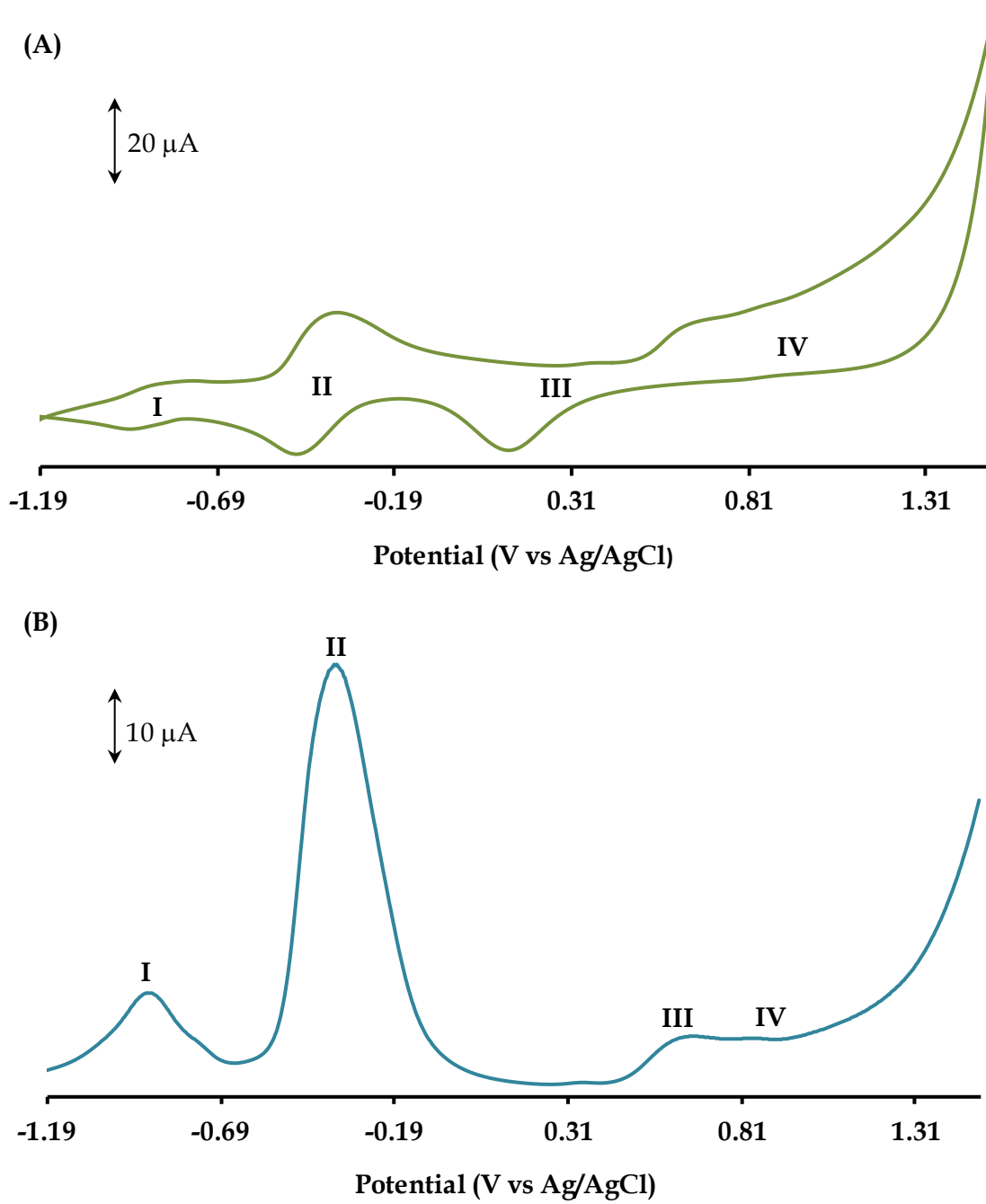


**Figure 4.17:** (A) CV and (B) SWV of complex 4 at 100 mV/s.

**Table 4.2:** Comparison of the voltammetric data (in V) between the novel MPcs **3** and **4** as well as other tetrasubstituted CoPcs attained from literature.

	M <sup>I</sup> Pc <sup>2-</sup> /M <sup>I</sup> Pc <sup>3-</sup> <b>I</b>	M <sup>II</sup> Pc <sup>2-</sup> /M <sup>I</sup> Pc <sup>2-</sup> <b>II</b>	M <sup>II</sup> Pc <sup>2-</sup> /M <sup>III</sup> Pc <sup>2-</sup> <b>III</b>	M <sup>III</sup> Pc <sup>2-</sup> / M <sup>III</sup> Pc <sup>1-</sup> <b>IV</b>
<b>CoPc-flav (3)</b>	-0.85 <sup>[a]</sup>	-0.37 <sup>[a]</sup>	0.41 <sup>[a]</sup>	1.06 <sup>[b]</sup>
<b>CoPc-bo (4)</b>	-0.91 <sup>[a]</sup>	-0.41 <sup>[a]</sup>	0.41 <sup>[a]</sup>	0.85 <sup>[b]</sup>
<b>(β)-CoPc-ochr</b>	-1.11	-0.44	0.40	1.03
<b>(β)-CoPc- ofcou</b>	-1.00	-0.46	0.42	1.08
<b>(β)-CoPc-cfcou</b>	-0.81	-0.47	0.48	0.91
<b>(α)-CoPc-cfcou</b>	-0.86	-0.35	0.42	1.00

[a]  $E_{1/2} = \frac{E_{pa} + E_{pc}}{2}$

[b]  $E_{pa}$

cfcou = 7-oxo-3-(2-chloro-4-fluorophenyl)coumarin

ochr = 7-oxychromone

ofcou = 7-oxy-4-trifluoromethylcoumarin

The assigned redox couples were further corroborated using spectroelectrochemistry. Both **3** and **4** exhibited similar UV-Vis spectral changes (Figs. 4.18 and 4.19); hence, only the spectroelectrochemical data of **4** will be elaborated on. The *in situ* spectroelectrochemical behaviour of CoPcs is well documented. It is known that a red shift in the Q-band and the formation of a charge transfer (CT) band between 450 and 500 nm is reminiscent of Co(I) species in solution [22, 23]. Upon application of negative overpotentials to redox couple **II**, disaggregation and red-shifting of the Q-band occurs to produce a well-defined monomeric peak at 705 nm. Furthermore, a CT-band occurs at 474 nm thereby confirming that the first redox couple occurs as a result of metal reduction ( $\text{Co}^{\text{II}}\text{Pc}^{2-}/\text{Co}^{\text{I}}\text{Pc}^{2-}$ ), see Fig. 4.19A. These spectral changes are accompanied by well-defined isosbestic points which are observed at 328 nm, 387 nm, 561 nm and 690 nm suggesting that the metal reduction process results in the formation of only one species in solution.

Spectral changes associated with redox couple **I** include a decrease in the Q- and B-bands as well as a shift in the CT-band to a higher wavelength (at 491 nm), see Fig. 4.19B. This behaviour is typical of Pc ring-based reduction and confirms the assignment of the  $\text{Co}^{\text{I}}\text{Pc}^{2-}/\text{Co}^{\text{I}}\text{Pc}^{3-}$  redox couple [24]. Following the application of positive overpotentials to redox couple **III**, considerable disaggregation of the Q-band and a subsequent increase in its intensity was observed. The emergence of an electronic transition band at 362 nm was noted. These spectral changes are consistent with metal oxidation; hence confirming the assignment of couple **III** to

$\text{Co}^{\text{II}}\text{Pc}^{2-}/\text{Co}^{\text{III}}\text{Pc}^{2-}$ , see Fig. 4.19C. Spectral changes accompanying couple IV are shown in Fig. 4.19D. A significant decrease in the Q-band and an increase in the 450 nm region is observed for 3 which suggests  $\text{Pc}^{2-}$  oxidation and confirms the assignment of the redox couple IV to  $\text{Co}^{\text{III}}\text{Pc}^{2-}/\text{Co}^{\text{III}}\text{Pc}^{1-}$  [25]. For complex 4, no increase is observed near 500 nm hence decomposition is expected to have occurred.

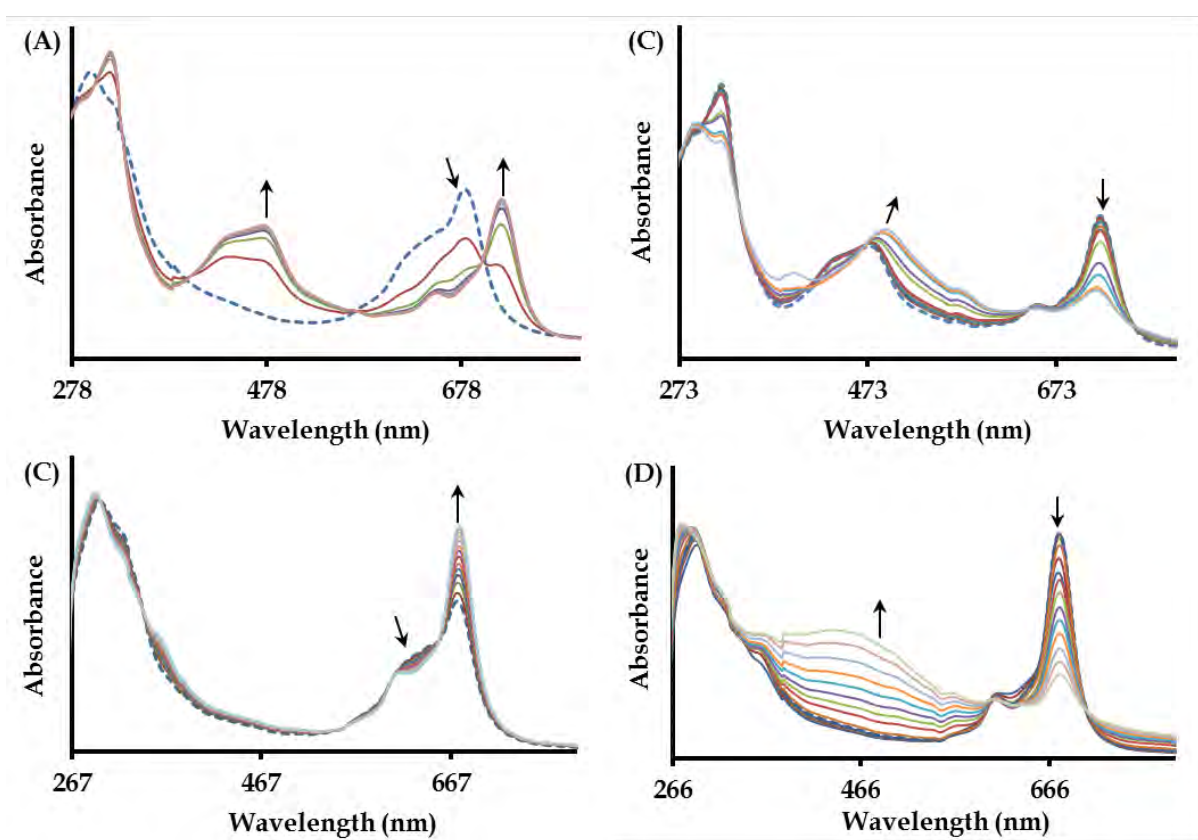


**Figure 4.18:** UV-Vis spectral changes of complex 3 at overpotentials applied at (A)  $-0.30$  V, (B)  $-0.96$  V, (C)  $0.50$  V and (D)  $1.08$  V. The initial spectrum is shown as a dashed line.

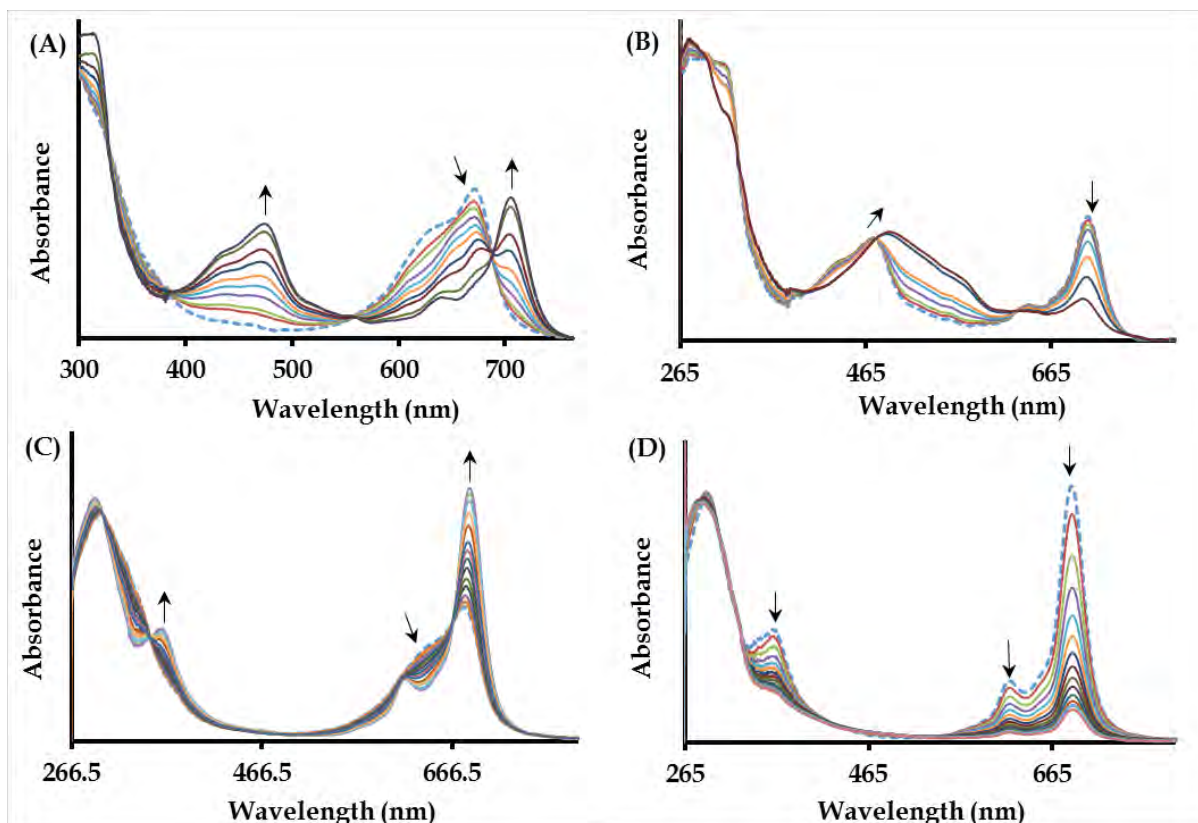


**Figure 4.19:** UV-Vis spectral changes of complex 4 at overpotentials applied at (A)  $-0.30$  V, (B)  $-0.92$  V, (C)  $0.45$  V and (D)  $1.06$  V. The initial spectrum is shown as a dashed line.

#### 4.3.3 Characterization of Modified Electrodes

Complexes 3 and 4 were deposited on respective GCEs *via* electrodeposition as inferred by the lack of new peaks synonymous with electropolymerization. Figs. 4.20 and 4.21 show the evolution of the CVs over 30 consecutive scans at  $100$  mV/s. The general increase in currents is typical of electrodeposition of MPCs on electrode surfaces [26].

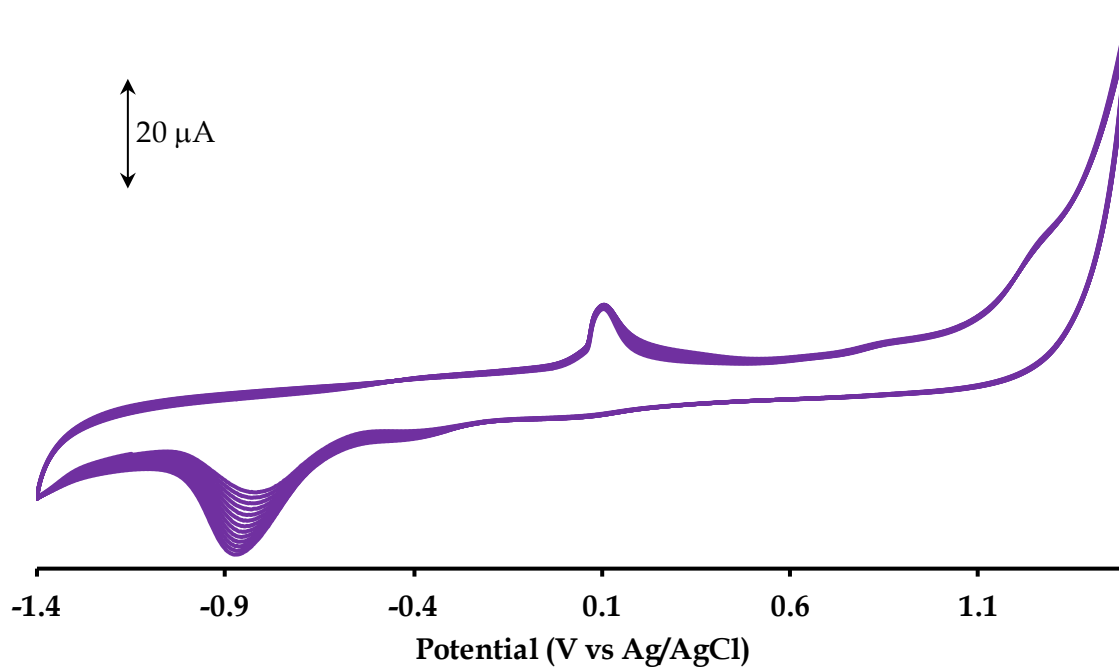


**Figure 4.20:** Electrodeposition of **3** via 30 repetitive CV scans at 100 mV/s.

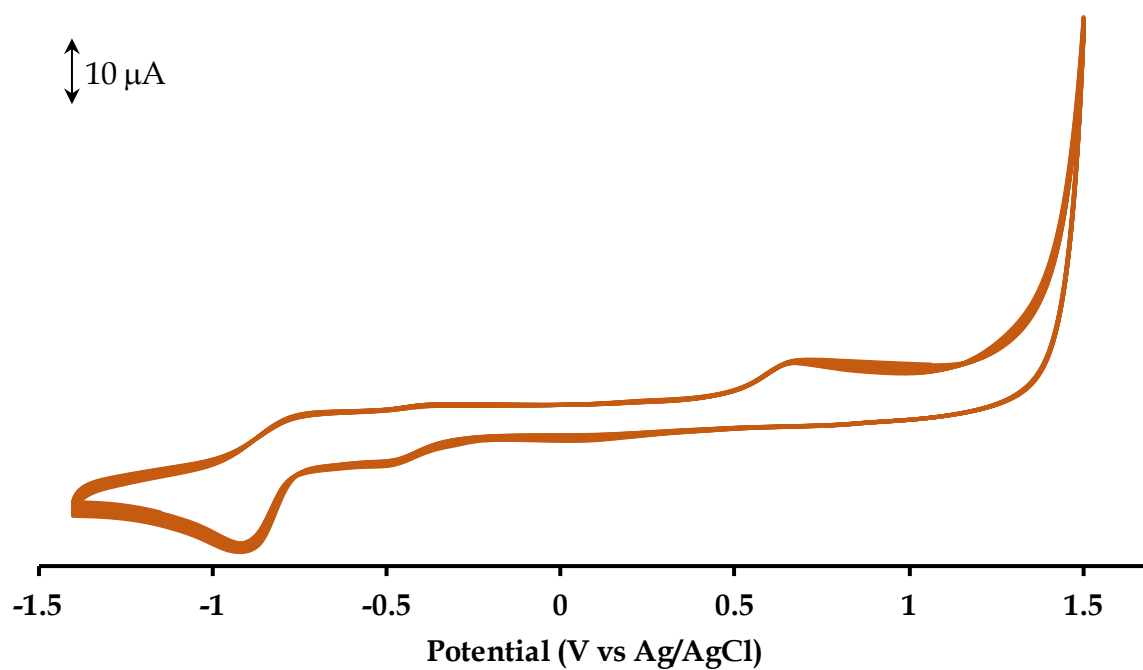


**Figure 4.21:** Electrodeposition of **4** via 30 repetitive CV scans at 100 mV/s.

Following electrodeposition; CVs at incrementing scan rates in pH 7 buffer were obtained for the working electrodes (**3-GCE** and **4-GCE**) to confirm electrode modification, see **Figs. 4.22** and **4.23**. The CVs of the modified electrodes (*viz.* **3-GCE** and **4-GCE**) in pH 7 buffer revealed peaks distinctive of redox couple **II** (for  $\text{Co}^{\text{II}}/\text{Co}^{\text{I}}$ ) in the negative potential window. In addition, **3-GCE** showed sharp peaks indicative of adsorbed species.

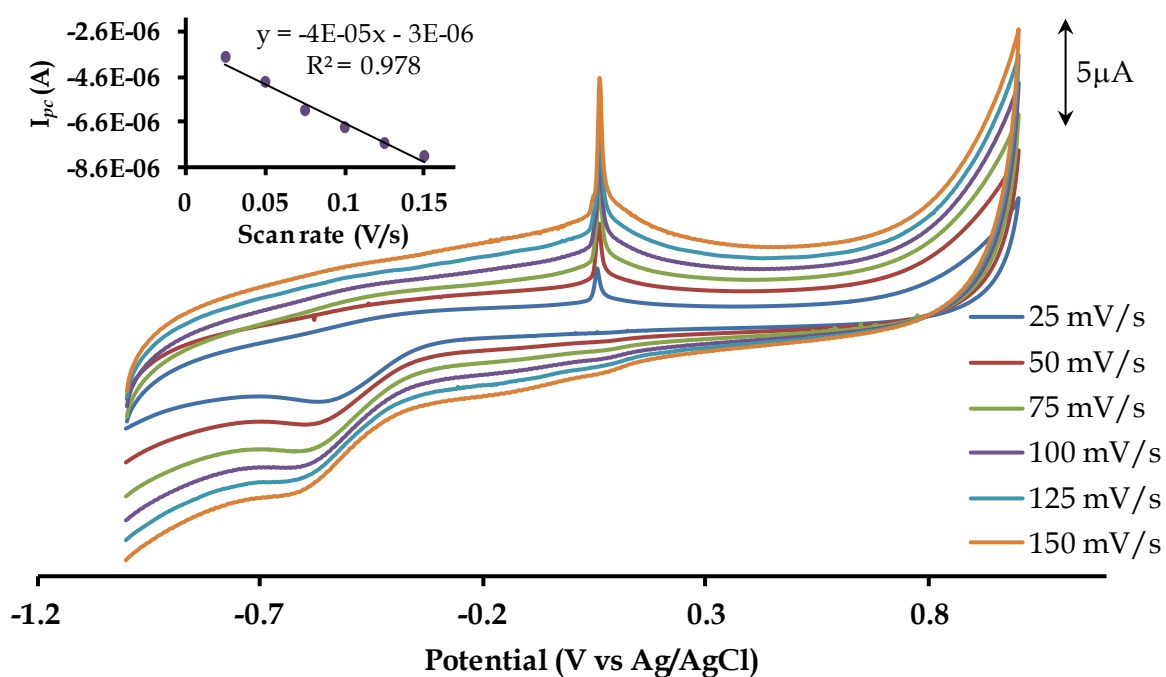


**Figure 4.22:** Overlay CVs at incrementing scan rates of **3-GCE** in pH 7 buffer solution.

*Inset: The linear relationship between reduction peak currents ( $I_{pc}$ ) vs. scan rates measured at the redox couple **II**.*

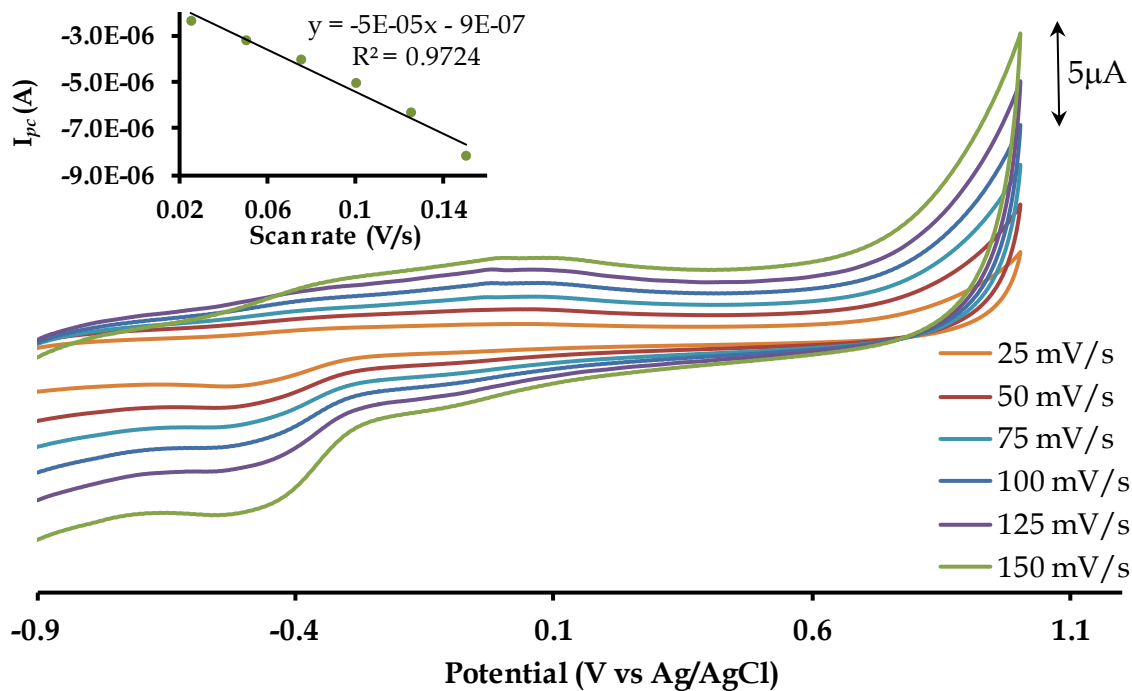


**Figure 4.23:** Overlay CVs at incrementing scan rates of 4-GCE in pH 7 buffer solution.

*Inset: The linear relationship between reduction peak currents ( $I_{pc}$ ) vs. scan rates measured at the redox couple II.*

Further confirmation of electrode modification is ascertained from the fact that the degree of ion-permeability for each modified working electrode is different from the other as is implied by their peak to peak separations (103 mV for 3-GCE and 122 mV for 4-GCE), see Fig. 4.24. In addition, these values differ from those obtained for the bare GCE ( $\Delta E = 107$  mV). The surface coverage values of the respective modified working electrodes were calculated using the following equation [27]:

$$I_p = \frac{n^2 F^2 A \Gamma(v)}{4RT} \quad (1)$$

where  $I_p$  is the peak current of redox couple II,  $n$  is the number of electrons and  $A$  is the real surface area (0.0707 cm<sup>2</sup>) of the bare GCE. The calculated surface coverage

values of the modified electrodes ( $5.29 \times 10^{-10}$  mol/cm<sup>2</sup> for **3**-GCE and  $6.80 \times 10^{-10}$  mol/cm<sup>2</sup> for **4**-GCE) correspond well with surface coverage values obtained for a monolayer electrodeposited flat on an electrode surface ( $1 \times 10^{-10}$  mol/cm<sup>2</sup>) [28].

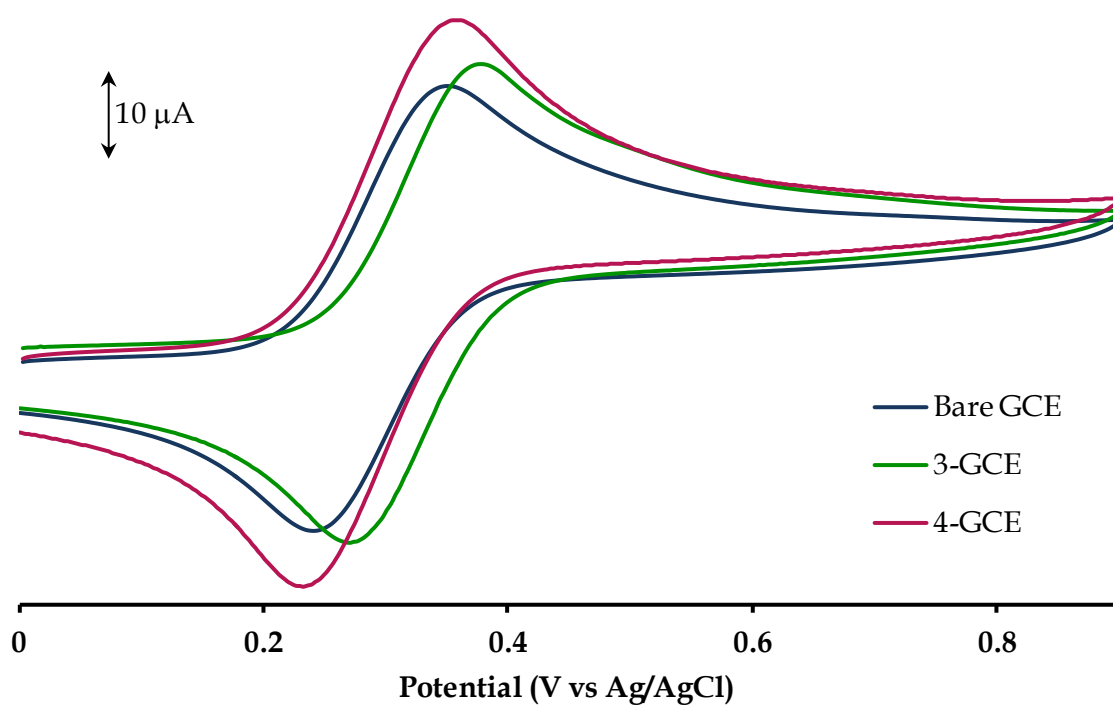


**Figure 4.24:** Overlay CVs of the bare electrode, **3**-GCE and **4**-GCE at 100 mV/s in 1 mM ferrocene.

#### 4.3.4 Electrocatalysis of Dopamine

The electrocatalytic behaviour of the modified electrodes towards dopamine was studied using cyclic voltammetry. **Fig. 4.25** compares the CVs obtained for **3**-GCE and **4**-GCE with that of the bare electrode. The anodic peak potential for dopamine oxidation appears at 0.19 V on a bare GCE. The CMEs were found to have both

lower oxidation potentials and higher catalytic currents as compared to the bare GCE, see **Table 4.3**.

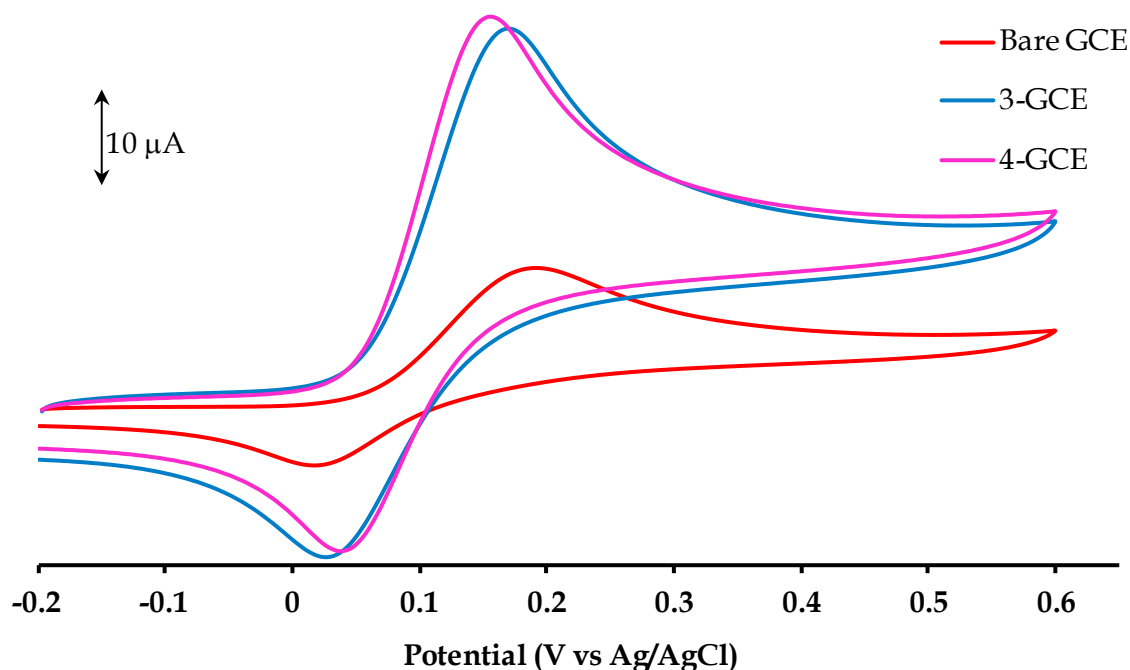


**Figure 4.25:** *Electrocatalytic oxidation of 1 mM dopamine in pH 7 buffer solution using the modified and bare electrodes at 100 mV/s.*

Furthermore, the  $\Delta E$  values of both CMEs (139 mV for 3-GCE and 115 mV for 4-GCE) are lower than that of the bare GCE (168 mV) indicating relatively faster electron transfer. The catalytic activity of the CoPcs is promoted by the metal oxidation couple (*i.e.*  $\text{Co}^{\text{III}}/\text{Co}^{\text{II}}$ ) which is found in the same vicinity as the redox potentials of dopamine using the respective modified electrodes. It can be noted that in the case of these CMEs, a higher surface coverage produces a lower  $\Delta E$  value for dopamine oxidation. A linear relationship was established between the oxidation

peak currents ( $I_{pa}$ ) and the square root of the scan rates ( $v^{1/2}$ ) which suggests diffusion-controlled behaviour.

**Table 4.3:** Cyclic voltammetric parameters for dopamine oxidation at 100 mV/s.

<i>Electrode</i>	<i>E<sub>pa</sub> (V vs Ag/AgCl)</i>	<i>ΔE (mV)</i>	<i>I<sub>pa</sub> (10<sup>-5</sup> A)</i>
<i>Bare GCE</i>	<i>0.19</i>	<i>168</i>	<i>1.53</i>
<i>MWCNT-GCE</i>	<i>0.14</i>	<i>88</i>	<i>3.34</i>
<i>3-GCE</i>	<i>0.17</i>	<i>139</i>	<i>4.14</i>
<i>3-MWCNT-GCE</i>	<i>0.14</i>	<i>90</i>	<i>5.43</i>
<i>4-GCE</i>	<i>0.15</i>	<i>115</i>	<i>4.27</i>
<i>4-MWCNT-GCE</i>	<i>0.15</i>	<i>90</i>	<i>6.15</i>

To gain more insight into the mechanism of the electrocatalytic oxidation of dopamine, the Tafel slopes were calculated using equation (2):

$$E_p = \frac{2.3RT}{2(1-\alpha)Fn_\alpha} \text{Log } v + K \quad (2)$$

where  $\alpha$  is the transfer coefficient,  $v$  is the scan rate,  $n_\alpha$  is the number of electrons in the rate-determining step,  $E_p$  is the peak potential and  $K$  is the intercept. Tafel slopes were obtained from the plots of  $E_p$  vs  $\text{Log } v$ , see **Figs. 4.26** and **4.27**. The large tafel slope of 244 mV/decade for 3-GCE is outside the normal range of 30-120

mV/decade which indicates that electrocatalytic oxidation using **3**-GCE has no kinetic meaning and is rather suggestive of substrate-catalyst interaction [29]. However, the tafel slope of 106 mV/decade for **4**-GCE is close to 118 mV/decade which implies that the first one-electron transfer process is rate-determining [30].

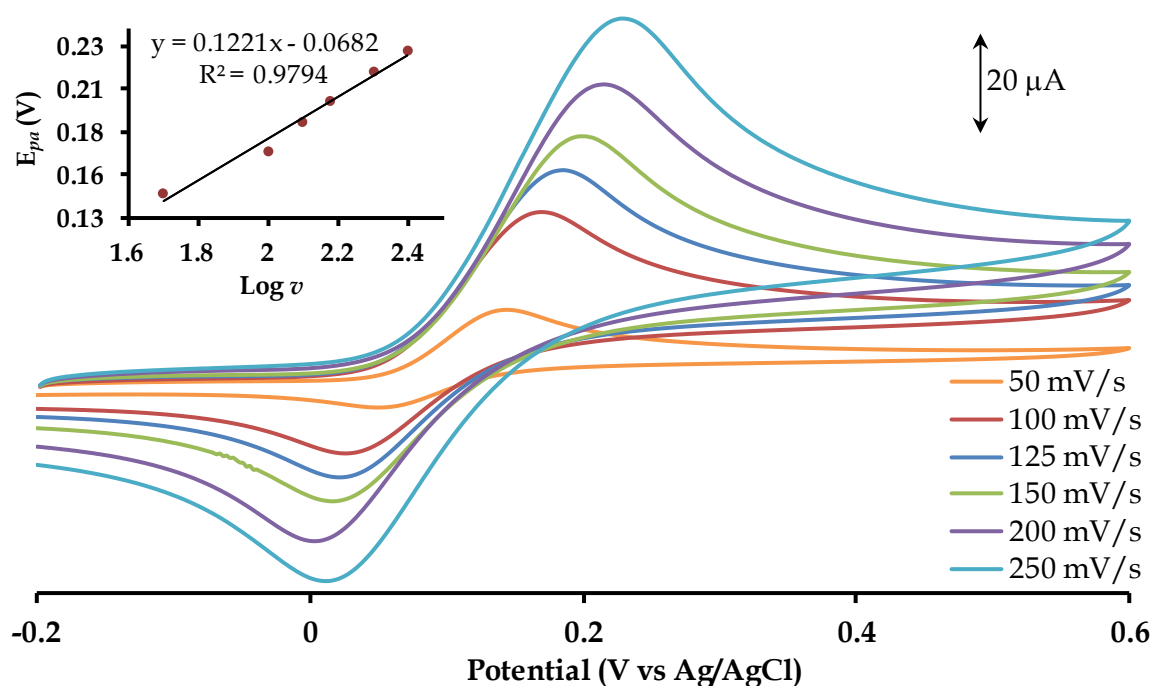


**Figure 4.26:** Electrocatalytic oxidation of 1 mM dopamine in pH 7 buffer solution by **3**-GCE at incrementing scan rates from 50 mV/s to 250 mV/s. Inset: Plot of  $E_{pa}$  vs  $\text{Log } v$ .

The electrocatalytic behaviour of electrodes modified with both an electrodeposited film and MWCNTs (**3**-MWCNT-GCE and **4**-MWCNT-GCE) were then explored. It was found that these electrodes produced even higher catalytic currents and lower oxidation potentials, see **Figs. 4.28** and **4.29**. The peak to peak separation for both modified electrodes was 90 mV, showing a remarkable enhancement in catalytic activity as compared to **3**-GCE and **4**-GCE. The higher anodic peak current of **4**-

MWCNT-GCE as compared to 3-MWCNT-GCE (refer to **Table 4.3**) indicates that the former is more electrocatalytically active since the anodic peak potentials of both CMEs are similar.

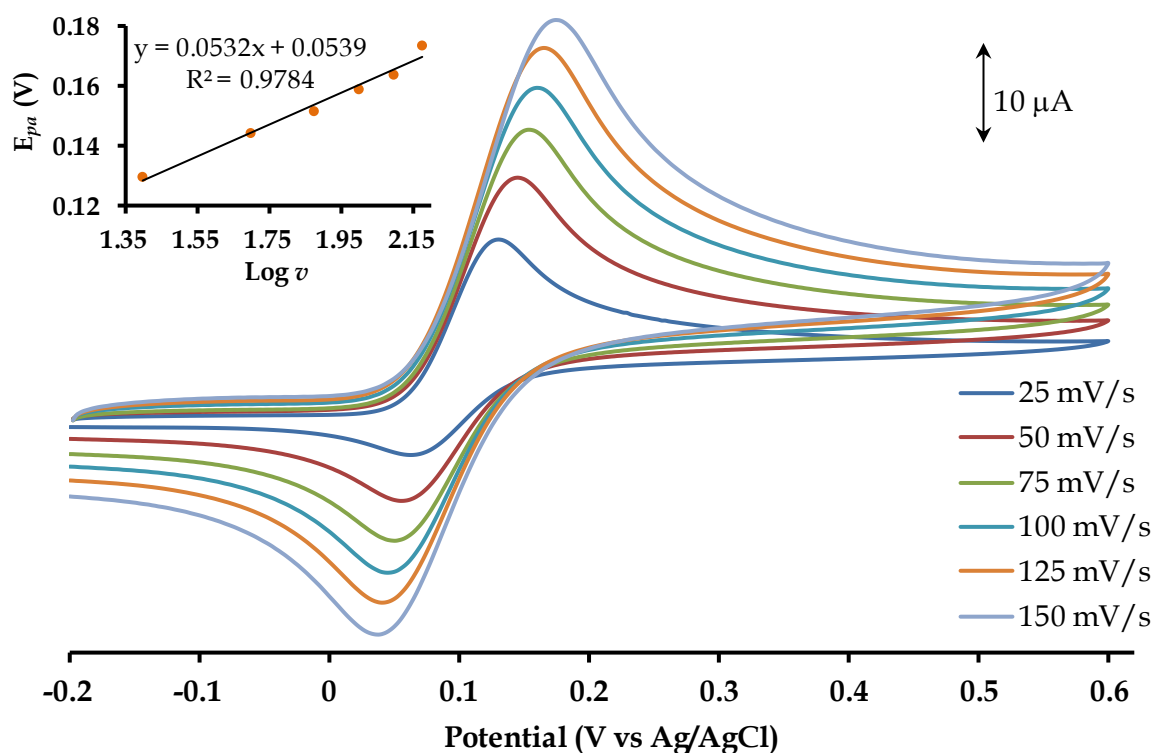


**Figure 4.27:** Electrocatalytic oxidation of 1 mM dopamine in pH 7 buffer solution by 4-GCE at incrementing scan rates from 25 mV/s to 150 mV/s. Inset: Plot of  $E_{pa}$  vs  $\text{Log } v$ .

The electrocatalytic activities of some previously reported MPCs towards dopamine oxidation are documented in **Table 4.4** [2, 12, 31-33]. The anodic peak potential for each of these compounds under the specified conditions is used as an indicator of their electrocatalytic activities. Both 3-MWCNT-GCE and 4-MWCNT-GCE have  $E_{pa}$  values that are equal to or lower than the reported  $E_{pa}$  values for other MPCs. Hence, these CMEs possess higher electrocatalytic activities for dopamine oxidation as compared to most of the reported MPCs in **Table 4.4**.

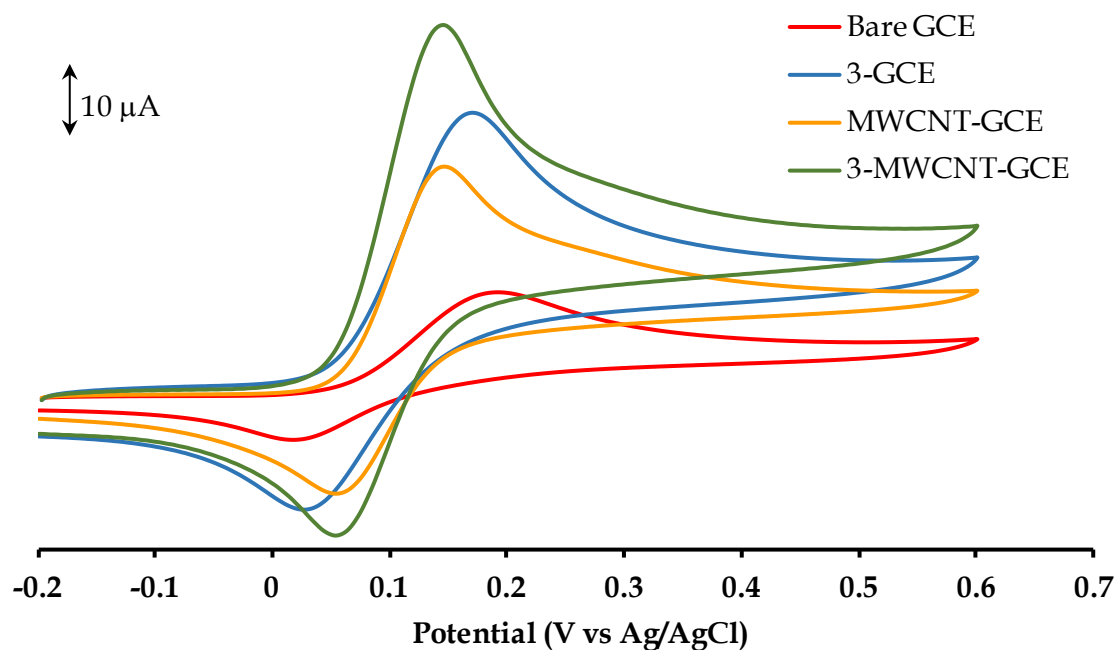


**Figure 4.28:** Comparison of the electrocatalytic oxidation of 1 mM dopamine by 3-GCE, MWCNT-GCE, 3-MWCNT-GCE and the bare electrode in pH 7 buffer at 100 mV/s.

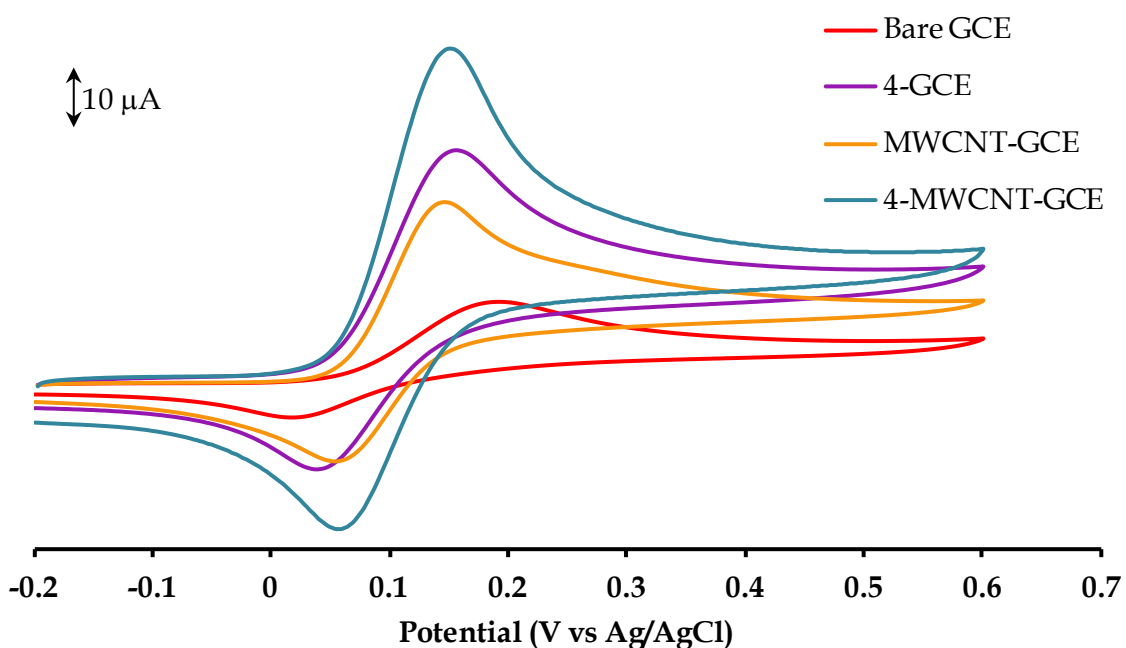


**Figure 4.29:** Comparison of the electrocatalytic oxidation of 1 mM dopamine by 4-GCE, MWCNT-GCE, 4-MWCNT-GCE and the bare electrode in pH 7 buffer at 100 mV/s.

**Table 4.4:** Cyclic voltammetric parameters of previously reported MPcs for dopamine oxidation.

Electrode	$E_{pa}$ (V vs Ag/AgCl)	Buffer	Scan rate (mV/s)	[dopamine] (M)
fMWCNT-nanoFeTSPc (GCE)	0.21	pH 7  PBS	50	0.10
MWCNT-NH <sub>2</sub> 4β(SO <sub>3</sub> ) (GCE)	0.15	pH 6.8  PBS	20	0.24
p-NiTAPc/GC (GCE)	0.19	pH 7.4  PBS	60	1.0
FeTSPc-CPE (carbon paste electrode)	0.32	pH 4  HCl/NaOH	100	0.10
MWCNT/CoPc (carbon paste electrode)	0.39	pH 4  PBS	50	1.0

fMWCNT = MWCNTs functionalized with sulfonic acid

FeTSPc = iron(II) tetrasulfophthalocyanine

NH<sub>2</sub>4β(SO<sub>3</sub>) = copper(II) tetrasulfonatephthalocyanine

p-NiTAPc = β-(tetraaminophthalocyaninato) nickel(II)

#### 4.3.5 Chronoamperometry Studies

Double-step chronoamperometry was used to determine the catalytic rate-constants for **3**-GCE, **4**-GCE, **3**-MWCNT-GCE and **4**-MWCNT-GCE in 1 mM dopamine. The chronoamperograms were obtained by setting the forward and reverse potentials on the CMEs to 0.20 and 0.00 V, respectively. **Fig. 4.30** displays the double-step chronoamperograms for the modified electrodes.

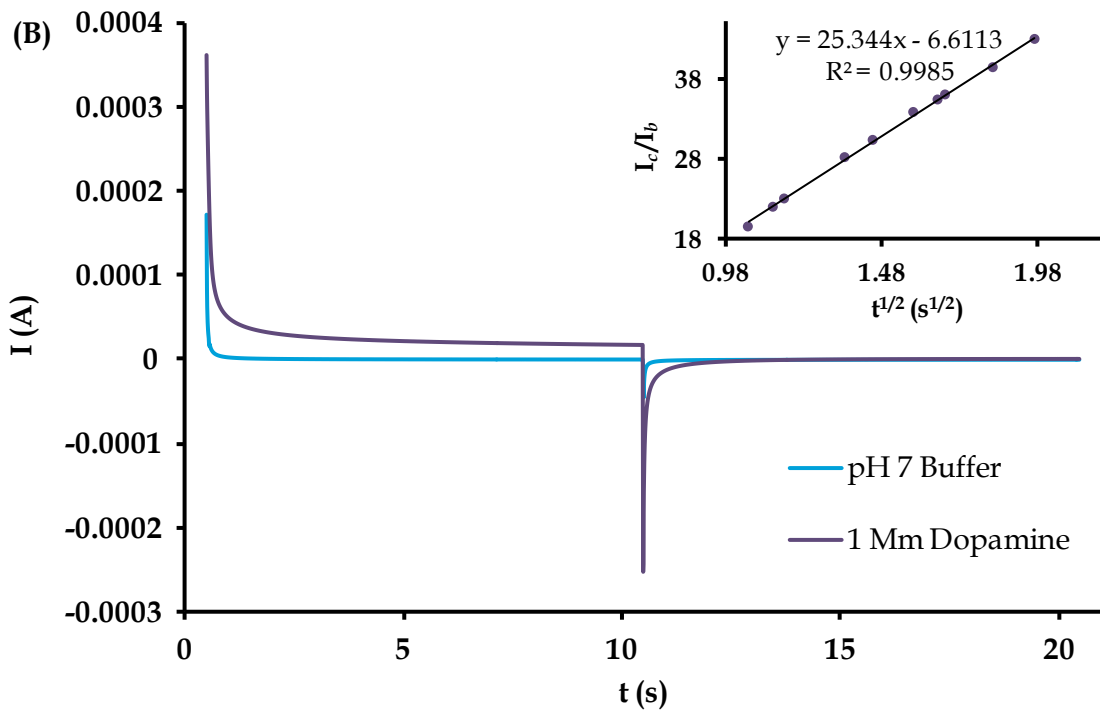
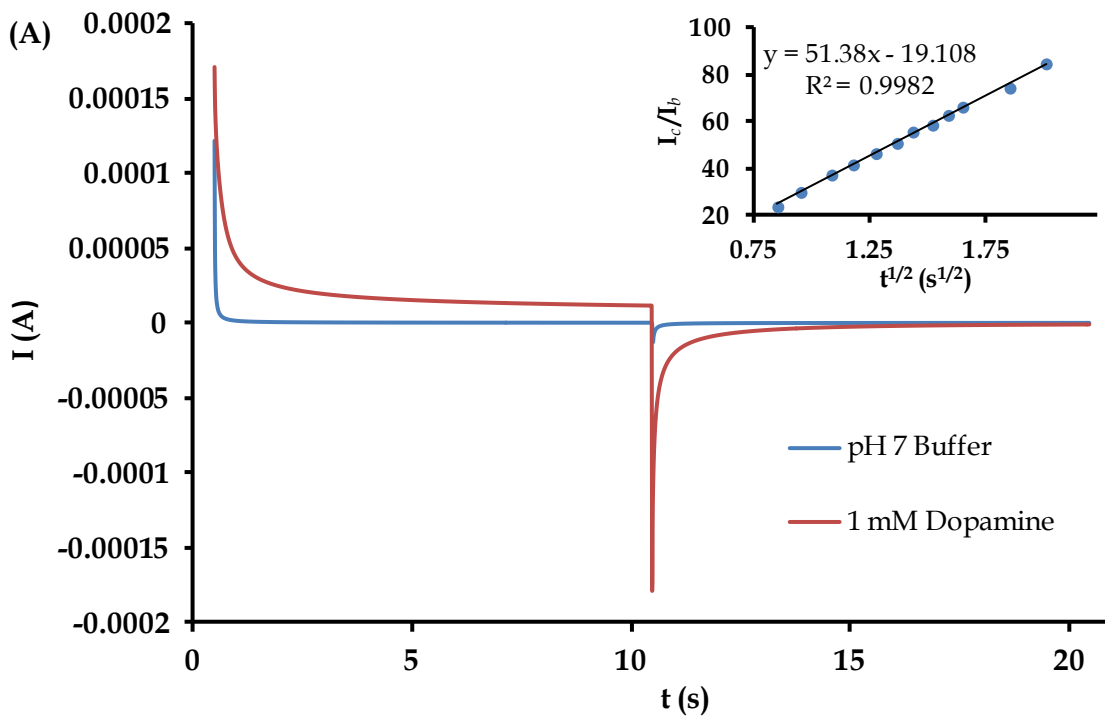
At intermediate times ( $t = 0.4 - 4$  s), the catalytic current is dominated by the rate of the electrocatalyzed oxidation of dopamine [34] and the rate constants for the chemical reaction between dopamine and the redox sites of the modifiers on the CMEs were calculated according to literature methods [35, 36]:

$$\frac{I_c}{I_b} = \gamma^{1/2} \left[ \pi^{1/2} \operatorname{erf}(\gamma^{1/2}) + \frac{\exp(-\gamma)}{\gamma^{1/2}} \right] \quad (3)$$

where  $\gamma = kC_0t$  ( $C_0$  is the bulk concentration of dopamine) and  $\operatorname{erf}^{1/2}$  is the error function. In cases where  $\gamma$  exceeds 2, the error function is almost equal to 1 and the above equation reduces to:

$$\frac{I_c}{I_b} = \sqrt{\gamma\pi} = \sqrt{\pi k C_0 t} \quad (4)$$

where  $I_c$  and  $I_b$  are the currents in the presence and in the absence of dopamine,  $t$  is the time elapsed (s) and  $k$  is the rate constant ( $\text{M}^{-1} \text{s}^{-1}$ ).



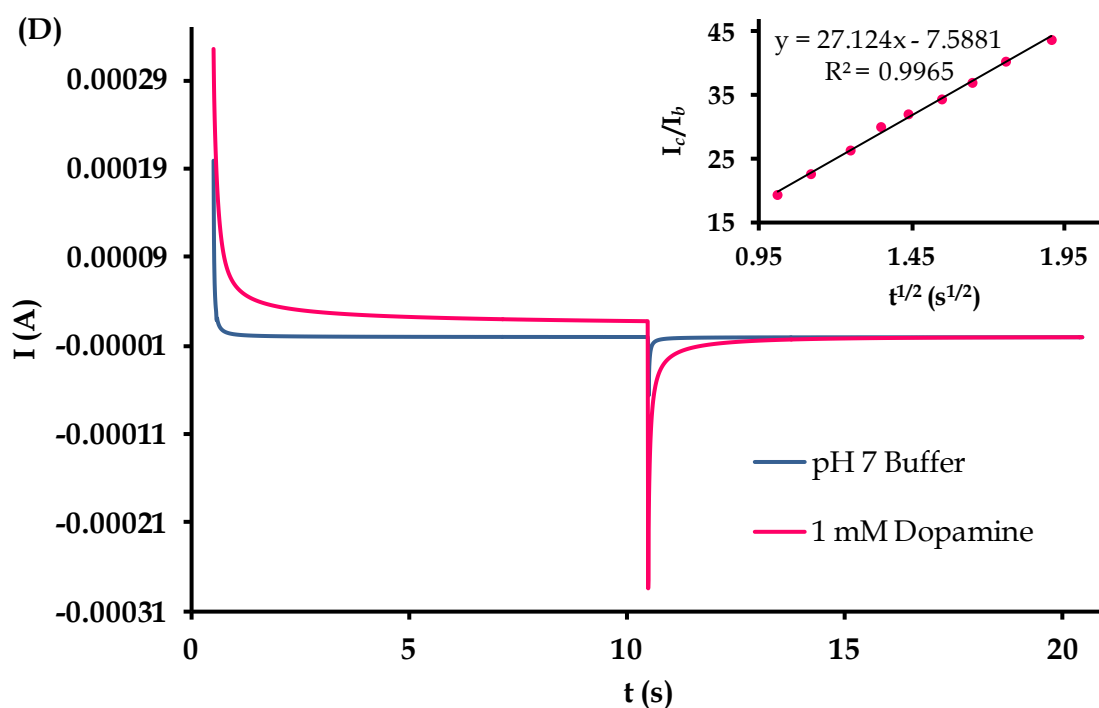
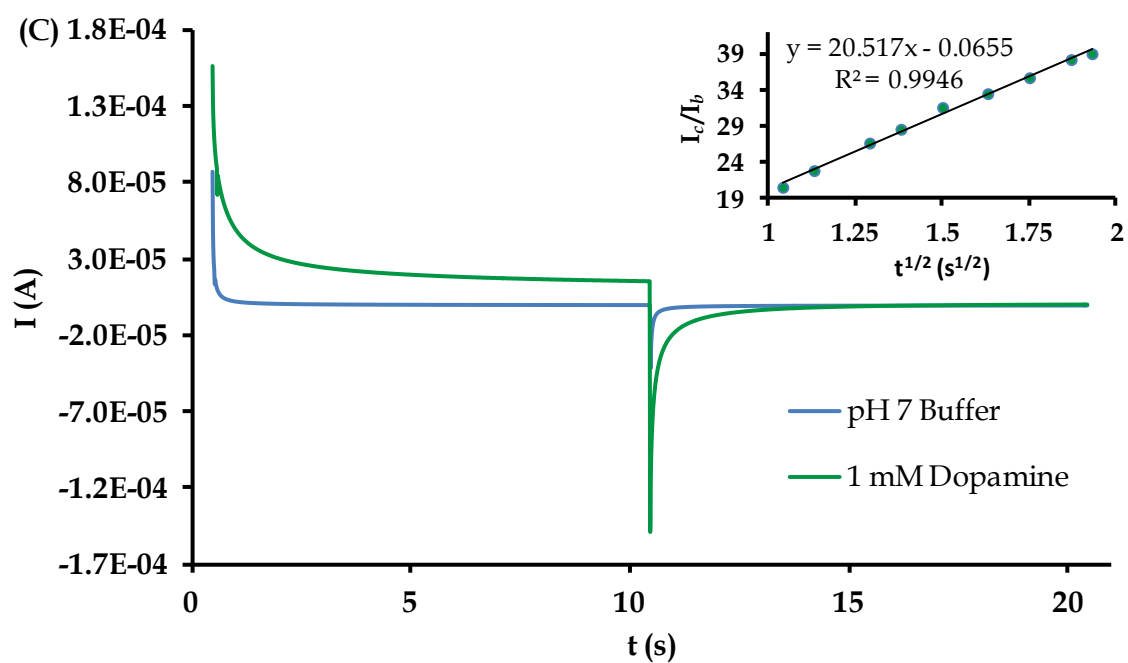


**Figure 4.30:** Double-step chronoamperograms of 1 mM dopamine on (A) 3-GCE, (B) 3-MWCNT-GCE, (C) 4-GCE and (D) 4-MWCNT-GCE in pH 7 buffer solution. Insets: Plots of  $I_c/I_b$  against  $t^{1/2}$  obtained from the corresponding chronoamperograms.

From the slopes of the plots of  $\frac{I_c}{I_b}$  against  $t^{1/2}$  (see insets **Fig. 4.30**), the values of  $k$  were determined as  $7.83 \times 10^5 \text{ M}^{-1} \text{ s}^{-1}$  for **3**-GCE,  $2.10 \times 10^5 \text{ M}^{-1} \text{ s}^{-1}$  for **3**-MWCNT-GCE,  $1.45 \times 10^5 \text{ M}^{-1} \text{ s}^{-1}$  for **4**-GCE and  $2.29 \times 10^5 \text{ M}^{-1} \text{ s}^{-1}$  for **4**-MWCNT-GCE. In comparison to previously reported rate constants for dopamine electrocatalysis by modified electrodes [**8, 37-39**]:  $1.82 \times 10^4 \text{ M}^{-1} \text{ s}^{-1}$ ,  $3.50 \times 10^2 \text{ M}^{-1} \text{ s}^{-1}$ ,  $8.33 \times 10^4 \text{ M}^{-1} \text{ s}^{-1}$  and  $3.46 \times 10^3 \text{ M}^{-1} \text{ s}^{-1}$ ; the calculated rate constants are of order  $10^5 \text{ M}^{-1} \text{ s}^{-1}$ , emphasizing their electrocatalytic superiority.

#### 4.4 Conclusion

CoPcs bearing flavone and benzoxazole substituents were synthesized and spectroscopically characterized. The CoPcs exhibited similar redox behaviour which was deduced from their voltammetric analysis. Voltammetric assignments were effectively corroborated by UV-Vis spectroelectrochemical experiments and were comparable to those reported for similar tetra-substituted mononuclear CoPcs. Surface modification of bare GCEs was achieved readily *via* electrodeposition (over 30 successive CV cycles) followed by casting of MWCNTs onto the electrodeposited films. Both the electrodeposited MPc surfaces and the films with the MWCNTs acted as electron mediators in the oxidation of dopamine.

## 4.5 References

- [1] G.-S. Lai, H.-L. Zhang, D.-Y. Han, *Anal. Letters*, 2008, **41**, 3088.
- [2] M. Sancy, J.F. Silva, J. Pavez, J.H. Zagal, *J. Chil. Chem. Soc.*, 2013, **58**, 2117.
- [3] S.B.A. Barros, A. Rahim, A.A. Tanaka, L.T. Arenas, R. Landers, Y. Gushikem, *Electrochim. Acta*, 2013, **87**, 140.
- [4] C. Wang, Q. Liu, X. Shao, X. Hu, *Anal. Lett.*, 2007, **40**, 689.
- [5] R. Suresh, K. Giribabu, R. Manigandan, S.P. Kumar, S. Munusamy, S. Muthamizh, A. Stephen, V. Narayanan, *Sens. Actuators, B*, 2014, **202**, 440.
- [6] T. Nyokong, *N<sub>4</sub>-Macrocyclic Metal Complexes*, ed. J.H. Zagal, F. Bedioui, J.-P. Dodelet, Springer Science + Business Media, LLC, New York, 2006, ch. 7, pp. 315-361.
- [7] J.H. Zagal, S. Griveau, J.F. Silva, T. Nyokong, F. Bedioui, *Coord. Chem. Rev.*, 2010, **254**, 2755.
- [8] R.E. Sabzi, K. Rezapour, N. Samadi, *J. Serb. Chem. Soc.*, 2010, **75**, 537.
- [9] S. Nyoni, T. Mugadza, T. Nyokong, *Electrochim. Acta*, 2014, **128**, 32.
- [10] M.P. Siswana, K.I. Ozoemena, T. Nyokong, *Electrochim. Acta*, 2006, **52**, 114.
- [11] X. Zuo, H. Zhang, N. Li, *Sens. Actuators, B*, 2012, **161**, 1074.
- [12] O.O. Fashedemi, K.I. Ozoemena, *Sens. Actuators, B*, 2011, **160**, 7.
- [13] S. Chohan, I.N. Booyesen, A. Mambanda, M.P. Akerman, *J. Coord. Chem.*, 2015, **68**, 1829.
- [14] J.-H. Kim, M. Song, G.-H. Kang, E.-R. Lee, H.-Y. Choi, C. Lee, J.-H. Kim, Y. Kim, B.-N. Koo, S.-G. Cho, *Leukemia Research*, 2012, **36**, 1157.

- [15] A. Bouchoucha, A. Terbouche, A. Bourouina, S. Djebbar, *Inorg. Chim. Acta*, 2014, **418**, 187.
- [16] E. Guzel, A. Atsay, S. Nalbantoglu, N. Saki, A.L. Dogan, A. Gul, M.B. Kocak, *Dyes and Pigments*, 2013, **97**, 238.
- [17] N. Sehlotho, M. Durmus, V. Ahsen, T. Nyokong, *Inorg. Chem. Commun.*, 2008, **11**, 479.
- [18] S. Altun, A.R. Özkaya, M. Bulut, *Polyhedron*, 2012, **48**, 31.
- [19] B. Koksoy, O. Soyer, E.B. Orman, A.R. Ozkaya, M. Bulut, *Dyes and Pigments*, 2015, **118**, 166.
- [20] M. Sevim, M.N. Yaras, A. Koca, M. Kandaz, *Dyes and Pigments*, 2014, **111**, 190.
- [21] Z. Odabaş, H. Kara, A.R. Özkaya, M. Bulut, *Polyhedron*, 2012, **39**, 38.
- [22] M.B. Kiliçaslan, H. Kantekin, A. Koca, *Dyes and Pigments*, 2014, **103**, 95.
- [23] I.A. Akinbulu, T. Nyokong, *Polyhedron*, 2009, **28**, 2831.
- [24] V. Cakir, H. Kantekin, Z. Biyiklioglu, A. Koca, *Polyhedron*, 2014, **81**, 525.
- [25] I.A. Akinbulu, T. Nyokong, *Polyhedron*, 2010, **29**, 1257.
- [26] A. Erdogmus, I.N. Booyesen, T. Nyokong, *Synth. Met.*, 2011, **161**, 241.
- [27] A. Maringa, E. Antunes, T. Nyokong, *Electrochim. Acta*, 2014, **121**, 93.
- [28] F. Matemadombo, T. Nyokong, *Electrochim. Acta*, 2007, **52**, 6856.
- [29] F. Bedioui, S. Griveau, T. Nyokong, A.J. Appleby, C.A. Caro, M. Gulppi, G. Ochoa, J.H. Zagal, *Phys. Chem. Chem. Phys.*, 2007, **9**, 3383.
- [30] N. Nombona, P. Tau, N. Sehlotho, T. Nyokong, *Electrochim. Acta*, 2008, **53**, 3139.
- [31] T-F. Kang, G.L. Shang, R-Q. Yu, *Anal. Chim. Acta*, 1997, **354**, 343.

- [32] J. Oni, T. Nyokong, *Anal. Chim. Acta*, 2001, **434**, 9.
- [33] F.C. Moraes, M.F. Cabral, S.A.S. Machado, L.H. Mascaro, *Electroanal.*, 2008, **20**, 851.
- [34] T. Mugadza, T. Nyokong, *Electrochim. Acta*, 2011, **56**, 1995.
- [35] J.B. Raof, R. Ojani, H. Beitollahi, *Int. J. Electrochem. Sci.*, 2007, **2**, 534.
- [36] M.H. Pournaghi-Azar, R. Sabzi, *J. Electroanal. Chem.*, 2003, **543**, 115.
- [37] R.E. Sabzi, S. Zare, K. Farhadi, G. Tabrizivanda, *J. Chin. Chem. Soc.*, 2005, **52**, 1079.
- [38] S.S.L. Castro, R.J. Mortimer, M.F. de Oliveira, N.R. Stradiotto, *Sensors*, 2008, **8**, 1950.
- [39] M. Mazloun-Ardakani, S.H. Ahmadi, Z.S. Mahmoudabadi, K.T. Haydar, B.F. Mirjalili, *Anal. Methods*, 2013, **5**, 6982.

---

---

# CHAPTER FIVE

## Formulation, Characterization and Electrochemical Properties of Novel Tetrasubstituted Cobalt Phthalocyanines Bearing Tetrahydropyran, Furan and Coumarin Moieties

### 5.1 Introduction

*L*-cysteine is an amino acid that plays a crucial role in biological systems for the functioning of various proteins [1]. It has several applications in the pharmaceutical and food industries for the formulation of drugs and the production of antibiotics and antioxidants [2]. A deficiency in *L*-cysteine is associated with many health issues such as liver damage, skin lesions, hair depigmentation and muscle loss; hence, its detection is of great importance for physiological and clinical diagnosis [3, 4]. Electrochemical methods have proved to be the preferred choice for this purpose above other techniques like chromatographic separation and spectrometric methods [5, 6] due to their simplicity, enhanced selectivity and high sensitivity [7]. The detection of *L*-cysteine on bare electrodes requires high overpotentials which results in sluggish responses, surface fouling and interference from other analytes [3, 7, 8].

To overcome these shortcomings, researchers are focusing on the development of chemically modified electrodes (CMEs) to electrocatalytically enhance the detection of L-cysteine [9, 10].

Metallophthalocyanines (MPcs) are versatile materials that are particularly useful in the preparation of biosensors [11-13]. The high chemical, thermal, and mechanical stability of these metal complexes makes them an attractive choice for such application [14, 15]. In many instances, electrodes modified with MPcs have shown excellent electrocatalytic behaviour towards various biologically important analytes [16]. MPc modified electrodes can be prepared in various ways such as the drop-dry method, formation of Langmuir-Blodgett films, self-assembled monolayers, electropolymerization and electrodeposition [17-20].

Optimization of the electrochemical properties of MPcs can be achieved by modification of the substituents and metal centres [21, 22]. Redox active metal centres like Co, Fe and Mn promote electron mediation [23] while biosensors prepared with MPcs containing biologically active substituents have been reported to show improved selectivity and sensitivity towards biological analytes [24, 25]. Furan derivatives are known to possess anti-bacterial, anti-tumor and analgesic properties [26, 27] while pyrans have been discovered to have antimicrobial and antioxidant activities [28, 29]. In this study, we report on the synthesis and characterization of Co(II) phthalocyanines substituted with biologically relevant tetrahydropyran (thp) and furan (fur) moieties. In addition, we explore the

comparative electrocatalytic capabilities of glassy carbon electrodes (GCEs) modified with MPCs containing thp and coumarin (cou) moieties, towards *L*-cysteine.

## 5.2 Experimental

### 5.2.1 Electrochemical Methods

Both a Pt working electrode and GCE were employed for voltammetric studies while a GCE was used in the preparation of CMEs. Adsorption of the MPCs onto a GCE was achieved *via* the drop-dry method. Concentrated solutions of the metal complexes were prepared in dichloromethane (DCM) and a drop of each metal complex was transferred onto the electrode surfaces which were then dried for 1 hr at 100 °C. The CMEs were rinsed with DCM, ethanol (EtOH) and ultrapure water prior to use. A 1 mM solution of *L*-cysteine was prepared in pH 4 buffer for electrocatalysis. Tetra-4-(7-oxy-4-trifluoromethylcoumarinphthalocyaninato)Co(II) (CoPc-cou, **5**) used in the preparation of CMEs was synthesized as previously reported in chapter three [30].

### 5.2.2 Synthesis

#### a) 4-(Tetrahydropyran-2-methoxy)phthalonitrile (**1**)

A mixture of tetrahydropyran-2-methanol (0.653 cm<sup>3</sup>, 5.78 mmol) and potassium carbonate (2.30 g, 16.64 mmol) was stirred in anhydrous dimethylformamide (DMF) (30.0 cm<sup>3</sup>) at room temperature under N<sub>2</sub> for 1 hr. Thereafter, to the resultant

reaction mixture, 4-nitrophthalonitrile (1.00 g, 5.78 mmol) was added. The reaction mixture was removed after 48 hrs and poured into 300 cm<sup>3</sup> of a water-ice slurry. The resulting precipitate was filtered and purified *via* column chromatography using a 1:1 (*v:v*) ethyl acetate:hexane solvent system to produce a white compound. Yield: 20 %; m.p (°C): 62.3-62.9; FT-IR ( $\nu_{max}$  /cm<sup>-1</sup>):  $\nu(\text{C}\equiv\text{N})$  2240,  $\nu(\text{C-O-C})$  1252, 1090, 1027; UV-Vis (DMF,  $\lambda_{max}$  ( $\epsilon$ , M<sup>-1</sup>cm<sup>-1</sup>)): 306 nm (13081), 299 (12647); <sup>1</sup>H NMR (ppm): 8.04 (d, 1H, H14), 7.78 (d, 1H, H13), 7.47 (d, 1H, H12), 4.06-4.14 (m, 2H, H10, H11), 3.85-3.92 (m, 1H, H8), 3.62-3.70 (m, 1H, H9), 3.35-3.42 (m, 1H, H7), 1.78-1.87 (m, 1H, H4), 1.59-1.67 (m, 1H, H2), 1.42-1.59 (m, 3H, H3, H5, H6), 1.26-1.38 (m, 1H, H1); <sup>13</sup>C NMR (ppm): 22.92, 25.87, 27.67, 67.74, 72.57, 75.41, 106.38, 116.20, 116.69, 116.74, 120.57, 120.83, 136.20, 162.48. Molecular mass (*m/z*): Calcd: 242.27. Found: 265.10 [M+Na]<sup>+</sup>. Anal. Calcd for C<sub>14</sub>H<sub>14</sub>N<sub>2</sub>O<sub>2</sub> (%): C, 69.41; H, 5.82; N, 11.56. Found: C, 64.32; H, 4.91; N, 10.73.

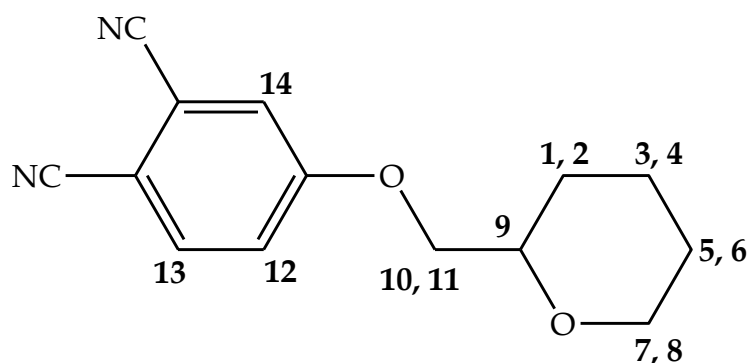


**Figure 5.1:** Structure of ligand 1.

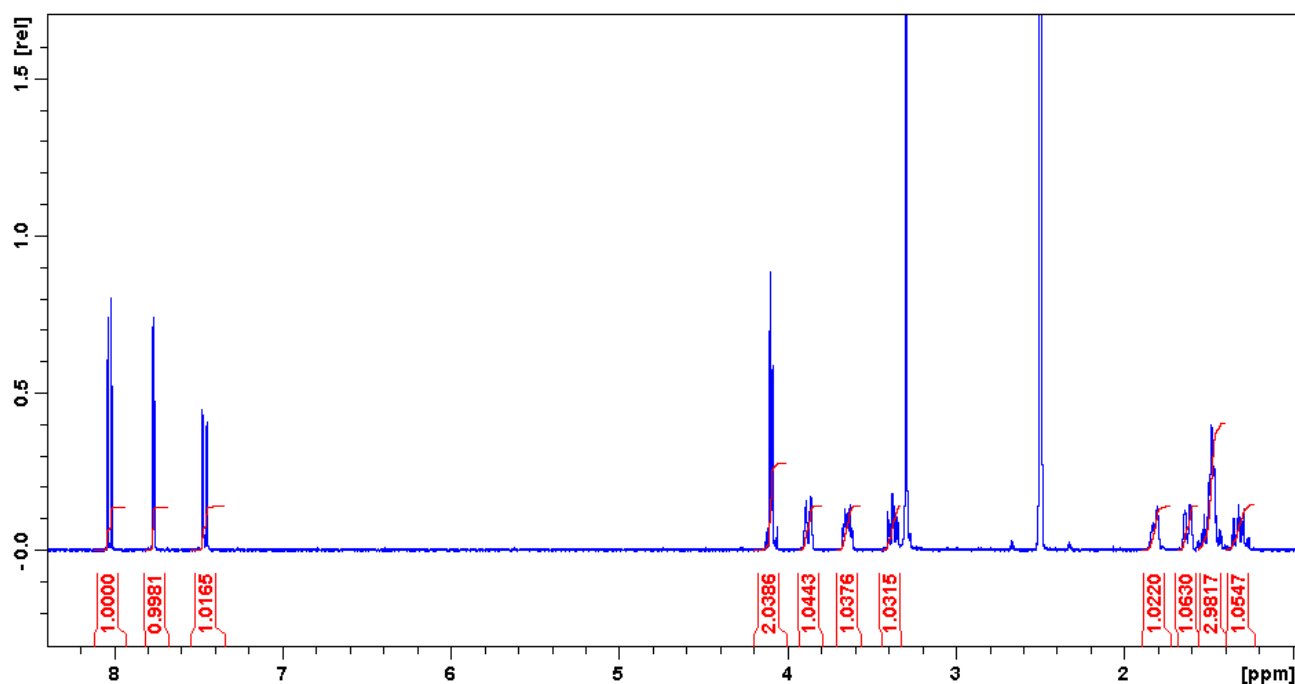


**Figure 5.2:**  $^1\text{H}$  NMR spectrum of ligand **1** in the range of 1.00-8.40 ppm.

b) 4-(Furan-2-methylthio)phthalonitrile (**2**)

A mixture of 4-nitrophthalonitrile (1.00 g, 5.78 mmol), 2-furanmethanethiol (0.583 cm<sup>3</sup>, 5.78 mmol) and potassium carbonate (2.30 g, 16.64 mmol) was added to anhydrous DMF (30.0 cm<sup>3</sup>). The reaction mixture was stirred at 90 °C under N<sub>2</sub> for 48 hrs after which it was cooled to room temperature and poured into 300 cm<sup>3</sup> of a water-ice slurry. The resulting white precipitate was filtered and recrystallized from hot methanol (MeOH). Yield: 80 %; m.p (°C): 127.8-128.5; FT-IR ( $\nu_{\text{max}}/\text{cm}^{-1}$ ):  $\nu(\text{C}\equiv\text{N})$  2228,  $\nu(\text{C}-\text{O}-\text{C})$  1249, 1061; UV-Vis (DMF,  $\lambda_{\text{max}}$  ( $\epsilon$ , M<sup>-1</sup>cm<sup>-1</sup>)): 323 nm (76752), 295 (137469);  $^1\text{H}$  NMR (ppm): 8.15 (d, 1H, *H*7), 8.01 (d, 1H, *H*8), 7.85 (d, 1H, *H*6), 7.60 (m, 1H, *H*3), 6.40 (m, 2H, *H*1, *H*2), 4.56 (s, 2H, *H*4, *H*5);  $^{13}\text{C}$  NMR (ppm): 28.10, 109.37, 110.73, 111.23, 115.52, 116.07, 116.49, 131.40, 131.47, 131.19, 143.58, 145.85, 149.77. Molecular mass (*m/z*): Calcd: 240.28. Found: 263.03 [M+Na]<sup>+</sup>. Anal. Calcd for

C<sub>13</sub>H<sub>8</sub>N<sub>2</sub>OS (%): C, 64.98; H, 3.36; N, 11.66; S, 13.34. Found: C, 65.10; H, 3.36; N, 11.64; S, 13.05.

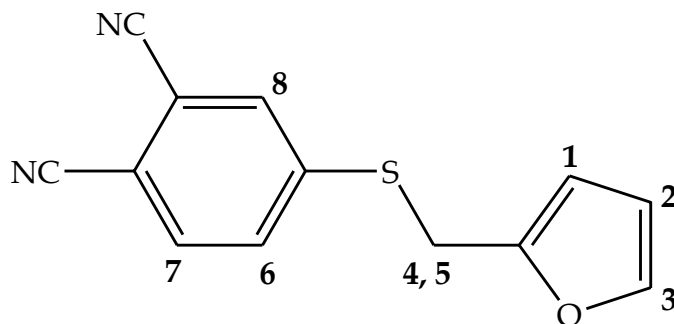


Figure 5.3: Structure of ligand 2.

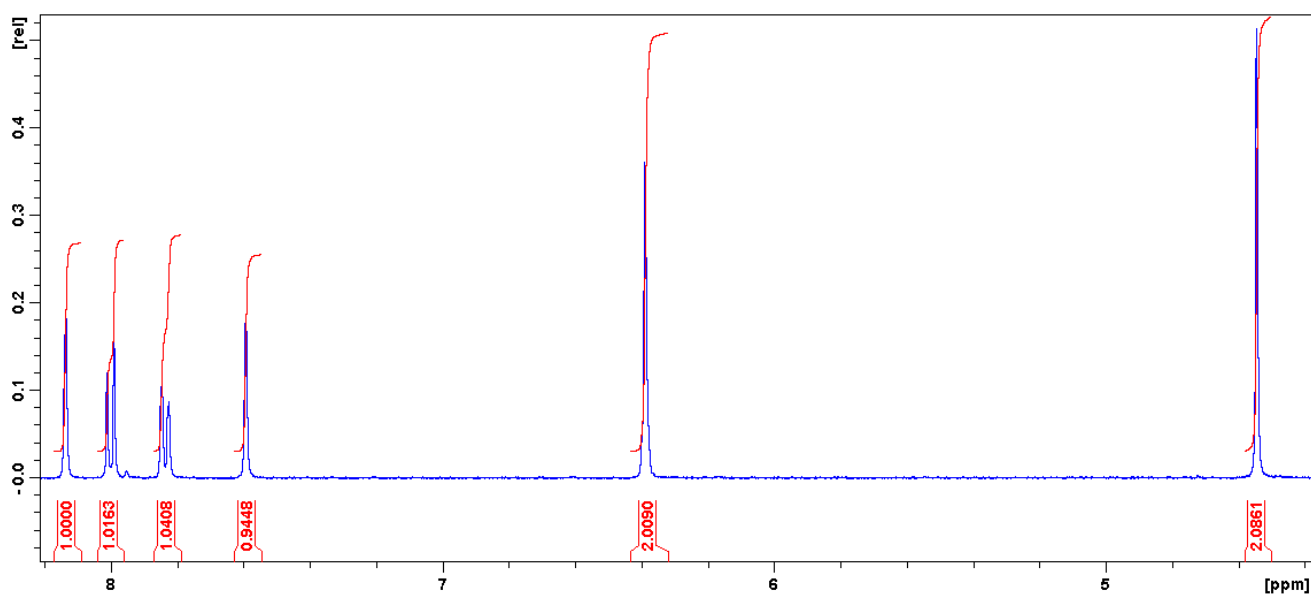


Figure 5.4: <sup>1</sup>H NMR spectrum of ligand 2 in the range of 4.40-8.20 ppm.

c) Tetra-4-(tetrahydropyran-2-methoxyphthalocyaninato)Co(II) (CoPc-thp, 3)

A mixture of **1** (0.125 g, 0.516 mmol), CoCl<sub>2</sub> (0.0167 g, 0.129 mmol) and DBU was heated with stirring in *n*-pentanol (20.0 cm<sup>3</sup>) at 160 °C under nitrogen for 16 hrs. The reaction mixture was then cooled to room temperature and *n*-hexane was added

drop-wise to induce precipitation. The precipitate was filtered off using a millipore filtration setup and then washed with water, MeOH, EtOH, hexane and acetonitrile. The desired product was thereafter recovered *via* column chromatography using a 1:10 (*v:v*) tetrahydrofuran (THF):CHCl<sub>3</sub> solvent system. Yield: 15%; IR ( $\nu_{max}$  /cm<sup>-1</sup>):  $\nu(\text{C}=\text{N})$  1601,  $\nu(\text{C}-\text{O}-\text{C})$  1232, 1123, 1088; UV-Vis (DMF,  $\lambda_{max}$  ( $\epsilon$ , M<sup>-1</sup>cm<sup>-1</sup>)): 667 nm (285321), 330 nm (189512), 307 (163949). Molecular mass ( $m/z$ ): Calcd: 1028.03. Found: 1027.36 [M-H]<sup>+</sup>, 1028.36 [M]<sup>+</sup>, 1029.36 [M+H]<sup>+</sup>, 1030.37 [M+2H]<sup>+</sup>. Anal. Calcd for C<sub>56</sub>H<sub>56</sub>CoN<sub>8</sub>O<sub>8</sub> (%): C, 65.43; H, 5.49; N, 10.90. Found: C, 65.43; H, 5.02; N, 10.60.

d) *Tetra-4-(2-furanmethylthiophthalocyaninato)Co(II)* (*CoPc-fur*, **4**)

The synthesis of **4** includes the addition of **2** (0.125 g, 0.520 mmol) to CoCl<sub>2</sub> (0.0169 g, 0.130 mmol) under the specified reaction conditions of **3**. The product was washed with water, MeOH, EtOH, ethyl acetate, hexane and acetonitrile and further purified *via* column chromatography using a 1:10 (*v:v*) THF:CHCl<sub>3</sub> solvent system. Yield: 60%; IR ( $\nu_{max}$  /cm<sup>-1</sup>):  $\nu(\text{C}=\text{N})$  1596,  $\nu(\text{C}-\text{O}-\text{C})$  1271, 1071; UV-Vis (DMF,  $\lambda_{max}$  ( $\epsilon$ , M<sup>-1</sup> cm<sup>-1</sup>)): 676 nm (161757), 331 nm (106668). Molecular mass ( $m/z$ ): Calcd: 1020.05. Found: 1019.08 [M-H]<sup>+</sup>, 1020.08 [M]<sup>+</sup>, 1021.08 [M+H]<sup>+</sup>, 1022.08 [M+2H]<sup>+</sup>. Anal. Calcd for C<sub>52</sub>H<sub>32</sub>FeN<sub>8</sub>O<sub>4</sub>S<sub>4</sub> (%): C, 61.23; H, 3.16; N, 10.99; S, 12.57. Found: C, 60.65; H, 2.93; N, 10.51; S, 12.14.

## 5.3 Results and Discussion

### 5.3.1 Crystal Structure of **2**

The X-ray data obtained for ligand **2** shows that it crystallizes out in a  $P2_1/n$  space group with four molecules aligned parallel to the  $[b]$ -axis occupying a monoclinic unit cell. The ORTEP view of **2** is presented in Fig. 5.5. The crystal lattice is stabilized by interactions between co-planar furan moieties of adjacent molecules with interplanar spacings of 4.609 Å. These intermolecular interactions are not reflective of  $\pi$ - $\pi$  stacking given that the interplanar spacings exceed 3.5 Å.

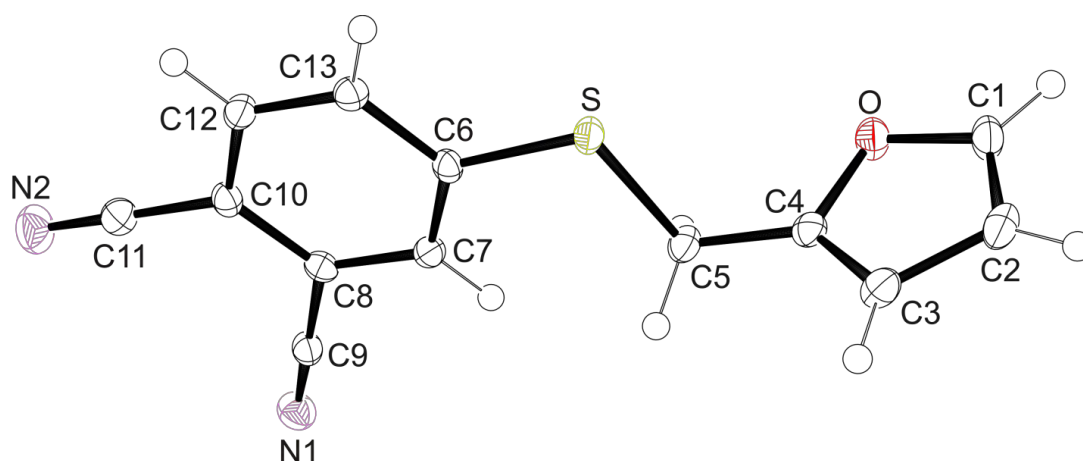


**Fig. 5.5:** An ORTEP view of compound **2** showing 50 % probability displacement ellipsoids and atom labels.

The aromatic ether bond angle [C1-O-C4] of  $106.09(1)^\circ$  is similar to previously reported C-O-C angles for furans [31]. This angle is lower than the previously reported C-O-C angle of  $117.90(2)^\circ$  obtained for the chromone derivative in chapter three [30]. The larger bond length [C2-C3] of  $1.432(2)$  Å as compared to the adjacent

bond lengths implies that the double bonds of the furan moiety are localized. The nearly equidistant C≡N bonds were comparable to analogous bond distances of other 4-substituted phthalonitriles [32, 33].

### 5.3.2 Synthesis and Spectral Characterization

The  $^1\text{H}$  NMR spectra of the derivatized phthalonitriles **1** and **2** are shown in **Figs. 5.2** and **5.4**. Both spectra contain aromatic proton peaks between 6.0–9.0 ppm as well as methyl proton peaks further upfield. The proton NMR assignments were well supported by  $^{13}\text{C}$  NMR spectroscopy and homonuclear correlation spectroscopy (COSY) (see **Figs. 5.6-5.9**).

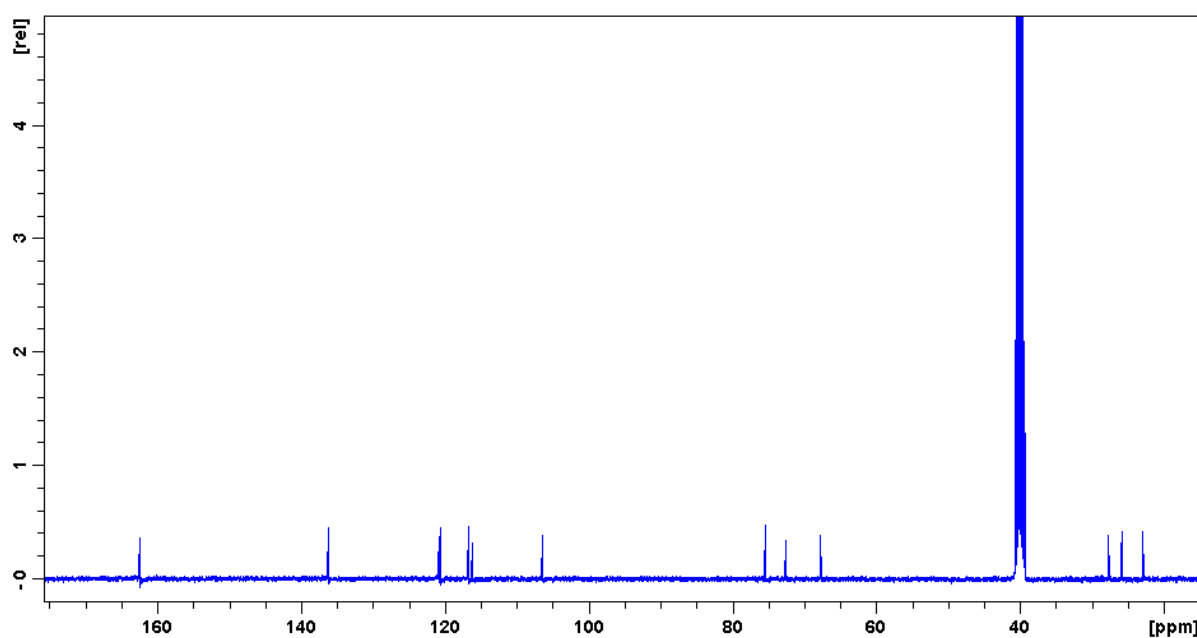


**Figure 5.6:**  $^{13}\text{C}$  NMR spectrum of ligand **1** in the range of 15 - 175 ppm.

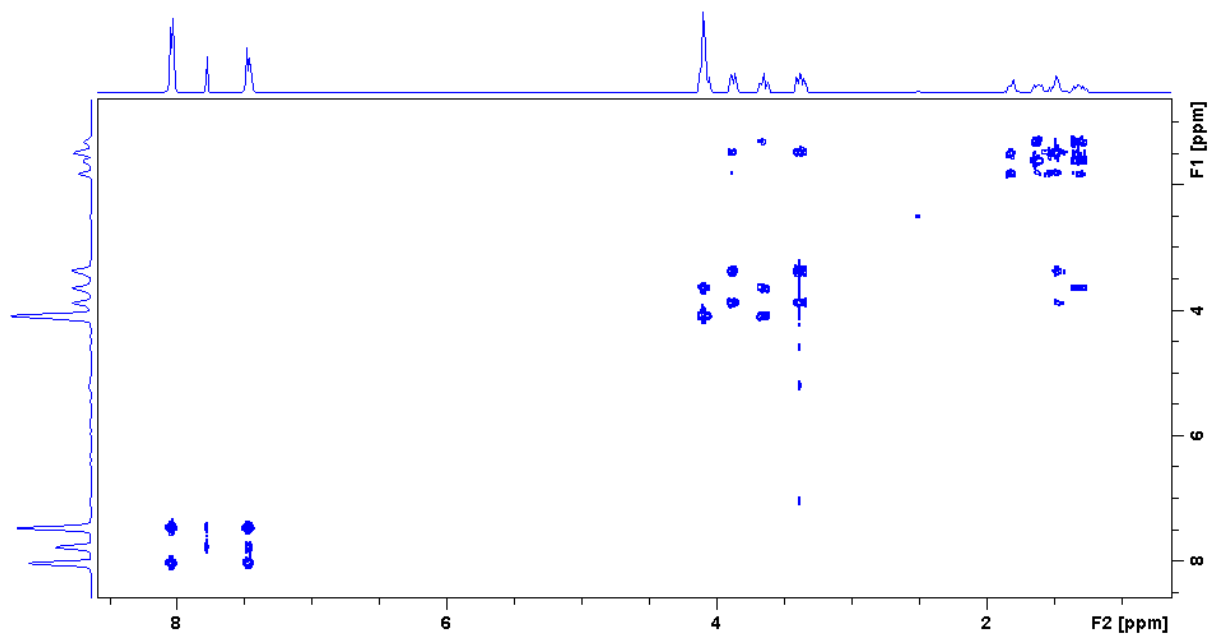


Figure 5.7: COSY spectrum of ligand 1.

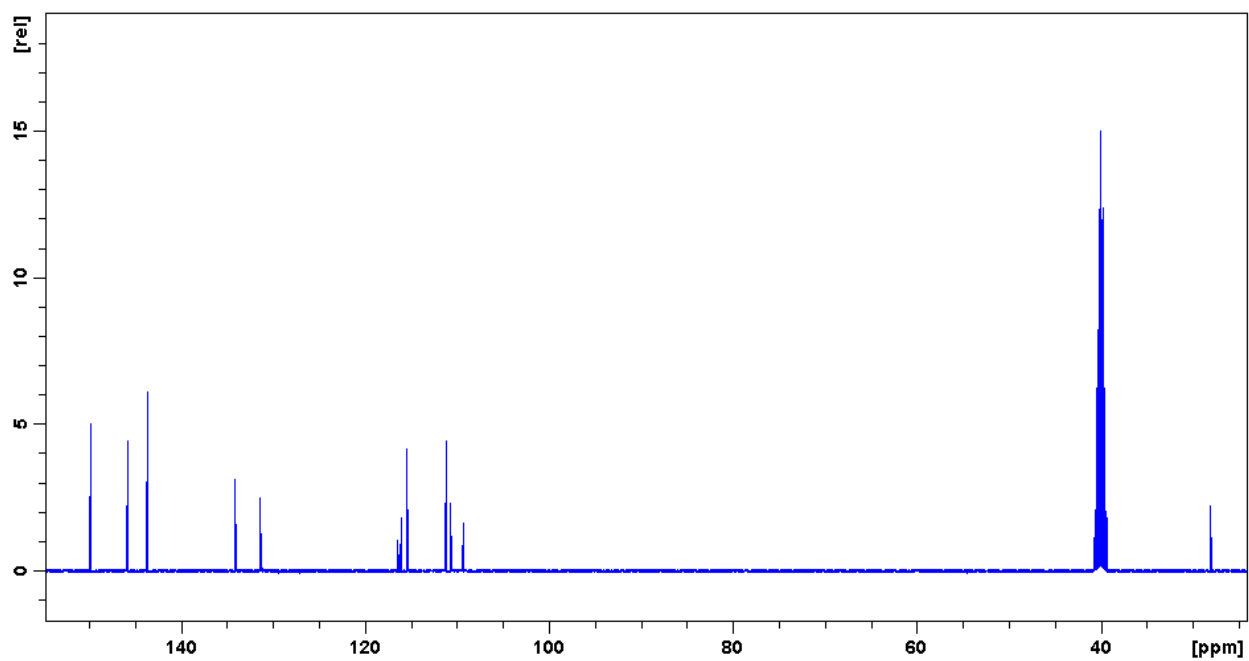
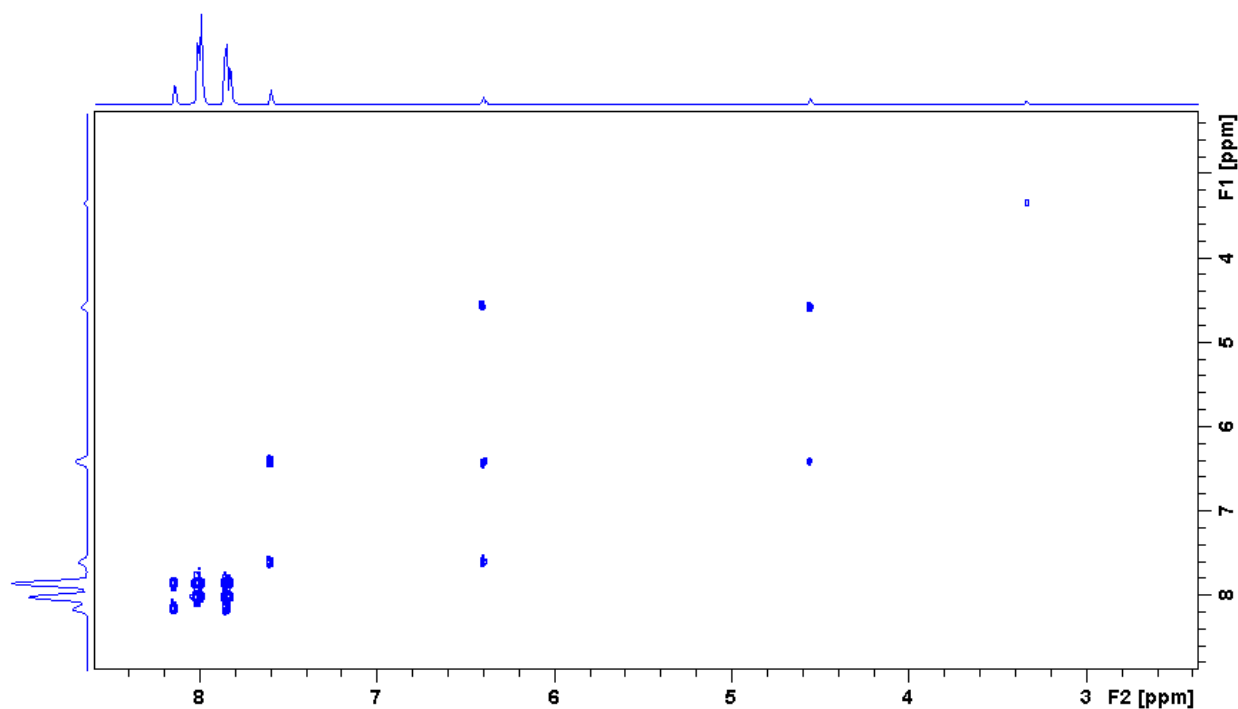


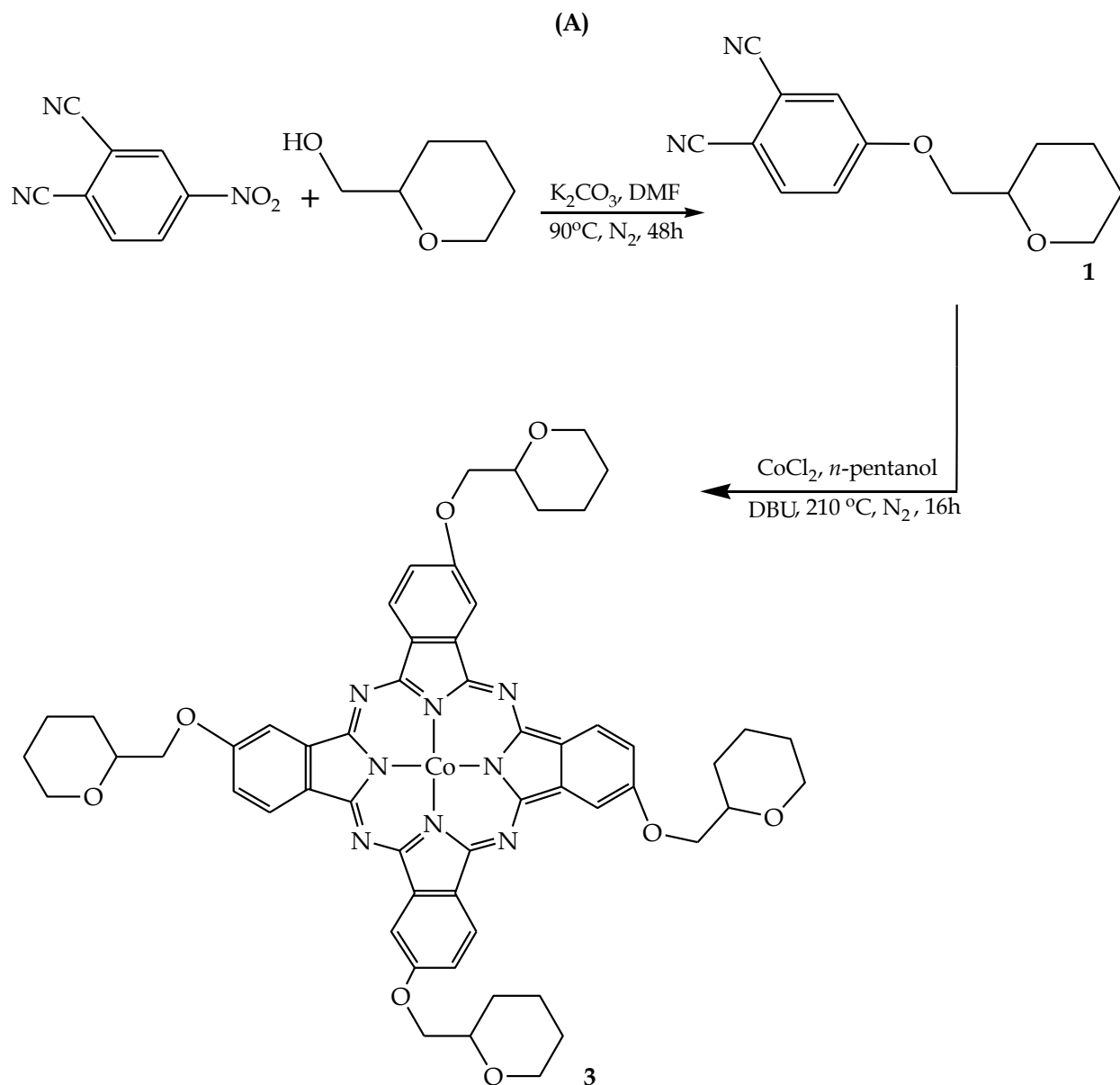
Figure 5.8:  $^{13}\text{C}$  NMR spectrum of ligand 2 in the range of 25 - 155 ppm.



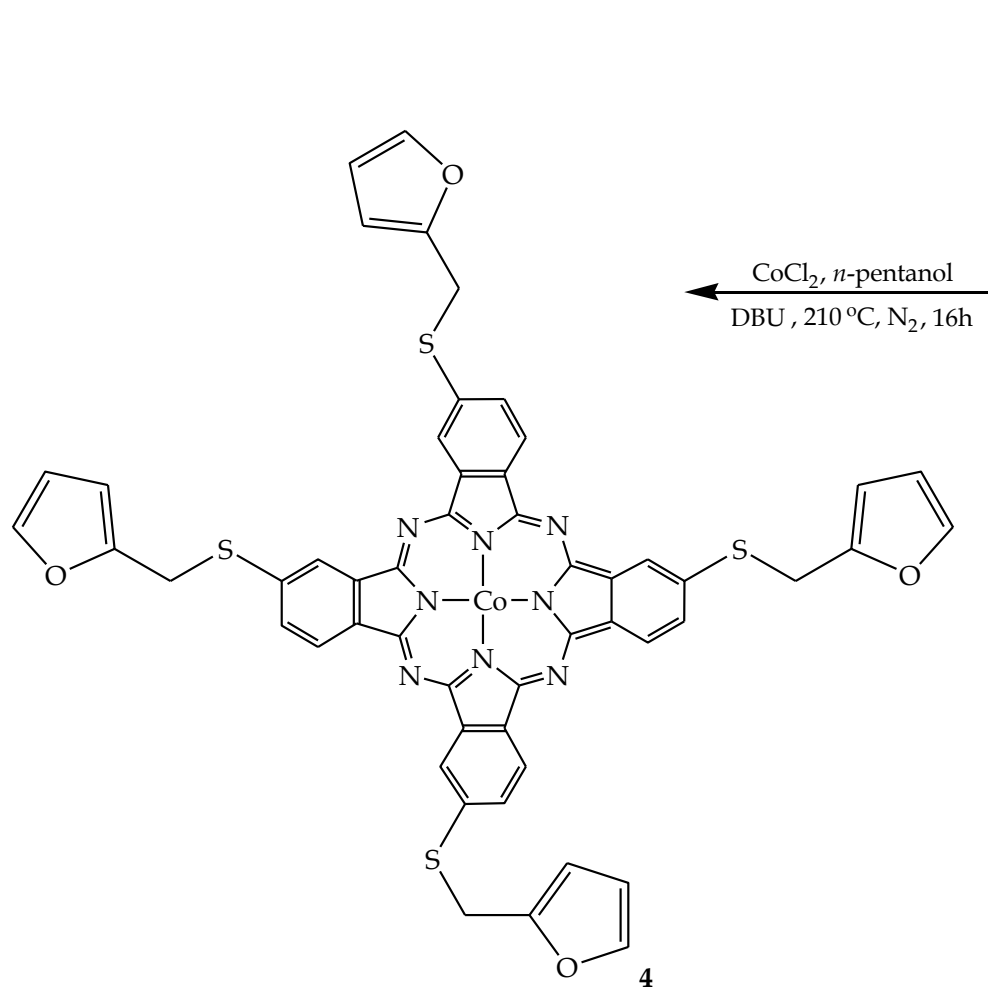
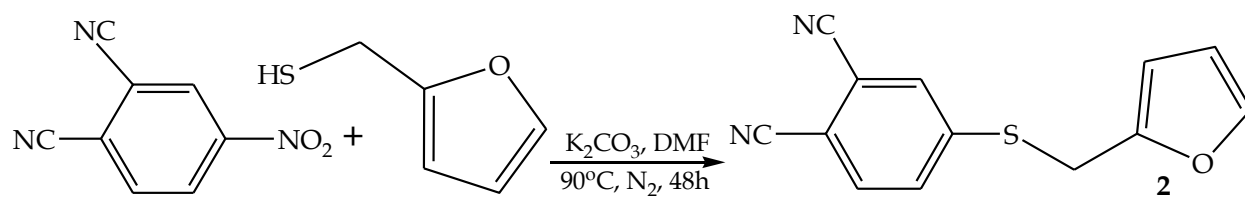
**Figure 5.9:** COSY spectrum of ligand **2**.

Template cyclotetramerization of ligands **1** and **2** in the presence of a catalyst, DBU and  $\text{CoCl}_2$  afforded the corresponding MPcs, refer to **Scheme 5.1**. The metal complexes displayed good solubility in low boiling point organic solvents including THF, chloroform and DCM. The FT-IR spectra of the MPcs (see **Figs. 5.10** and **5.11**) showed disappearance of the medium intensity nitrile stretches found at  $2240\text{ cm}^{-1}$  (for **1**) and  $2228\text{ cm}^{-1}$  (for **2**) which is typical of cyclotetramerization. ESI-TOF mass spectrometry provided definitive structural characterization for the ligands (see **Figs 5.12** and **5.13**) and their metal complexes (see **Figs 5.14** and **5.15**). The elemental composition of ligand **2** and the complexes were consistent with the calculated values; however, the hygroscopic nature of **1** resulted in an elemental composition that was different from the theoretical values. All molecular and cluster ion peaks were in accordance with the calculated  $m/z$  values. For example, the mass spectra of the MPcs showed  $[\text{M}]^+$  ion peaks at  $m/z$  values of 1028.36 (for **3**) and 1020.08 (for **4**),

in addition to the protonation molecular ion peaks of the form:  $[M+H]^+$ ,  $[M+2H]^+$  and  $[M-H]^+$ .



(B)



**Scheme 5.1:** Synthetic pathways for the CoPcs: (A) (CoPc-thp, **3**) and (B) (CoPc-fur, **4**).

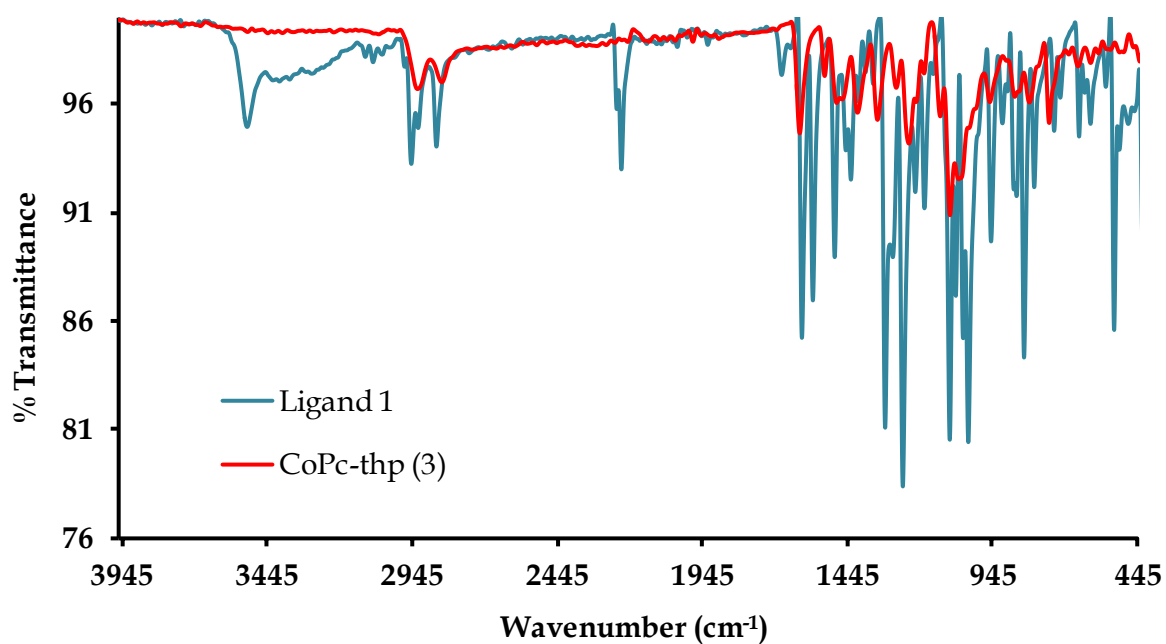


**Figure 5.10:** *Overlay IR spectrum of complex 3 and its free ligand, compound 1.*

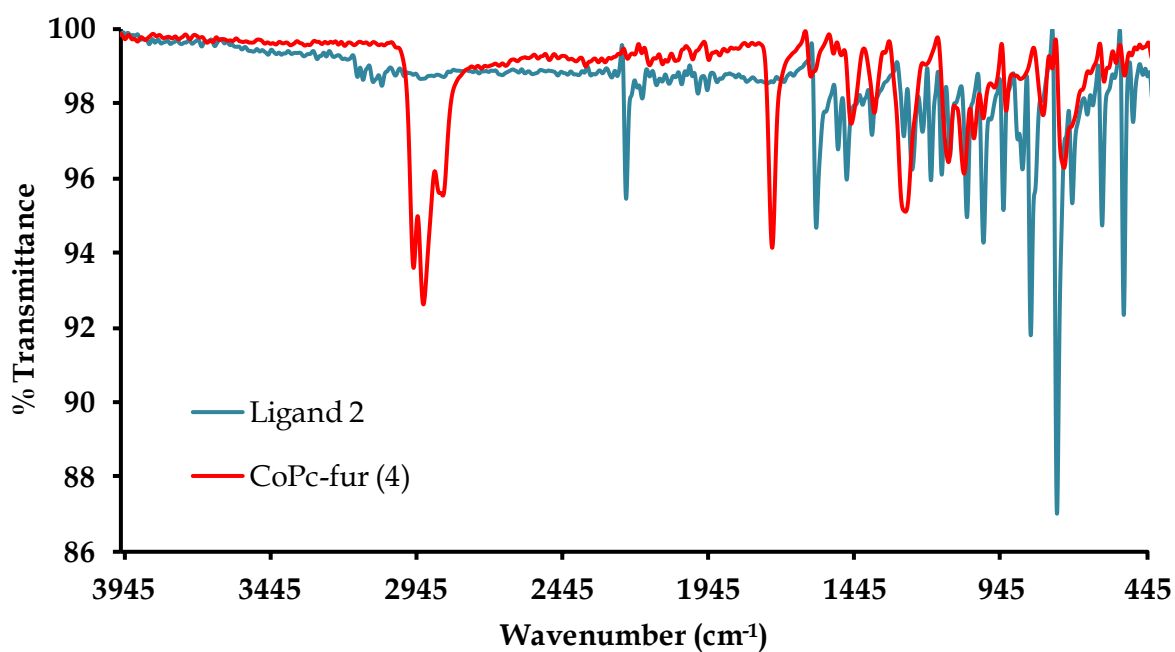


**Figure 5.11:** *Overlay IR spectrum of complex 4 and its free ligand, compound 2.*

Single Mass Analysis

Tolerance = 5.0 PPM / DBE: min = -1.5, max = 100.0

Element prediction: Off

Number of isotope peaks used for i-FIT = 3

Monoisotopic Mass, Even Electron Ions

15 formula(e) evaluated with 1 results within limits (up to 20 closest results for each mass)

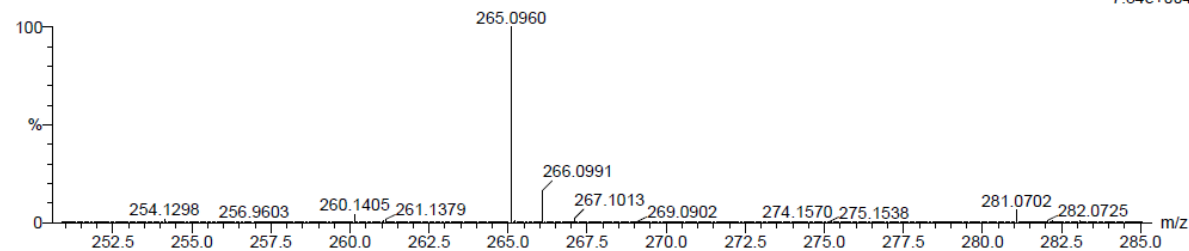
Elements Used:

C: 10-15 H: 10-15 N: 0-5 O: 0-5 Na: 1-1

S42 31 (1.054) Cm (1:58)

TOF MS ES+

7.84e+004



Minimum: -1.5  
Maximum: 5.0 5.0 100.0

Mass	Calc. Mass	mDa	PPM	DBE	i-FIT	i-FIT (Norm)	Formula
265.0960	265.0953	0.7	2.6	8.5	550.9	0.0	C14 H14 N2 O2 Na

Figure 5.12: High resolution TOF-MS spectrum of 1.

Single Mass Analysis

Tolerance = 5.0 PPM / DBE: min = -1.5, max = 100.0

Element prediction: Off

Number of isotope peaks used for i-FIT = 3

Monoisotopic Mass, Even Electron Ions

144 formula(e) evaluated with 1 results within limits (up to 20 closest results for each mass)

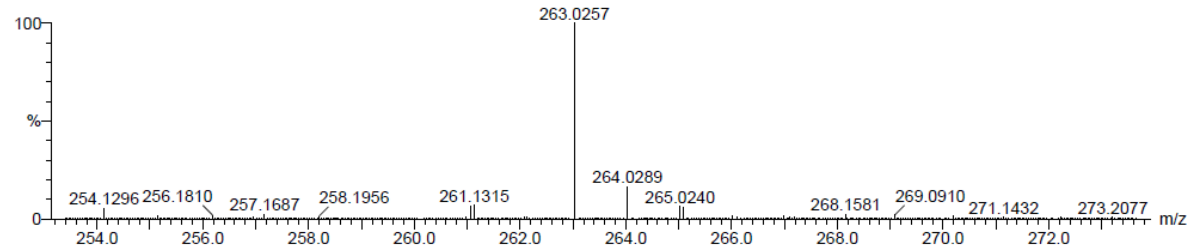
Elements Used:

C: 10-15 H: 5-10 N: 0-5 O: 0-5 Na: 1-1 S: 0-5

S5(2) 40 (1.371) Cm (1:58)

TOF MS ES+

2.98e+005



Minimum: -1.5  
Maximum: 5.0 5.0 100.0

Mass	Calc. Mass	mDa	PPM	DBE	i-FIT	i-FIT (Norm)	Formula
263.0257	263.0255	0.2	0.8	10.5	599.1	0.0	C13 H8 N2 O Na S

Figure 5.13: High resolution TOF-MS spectrum of 2.

Single Mass Analysis

Tolerance = 5.0 PPM / DBE: min = -1.5, max = 100.0

Element prediction: Off

Number of isotope peaks used for i-FIT = 3

Monoisotopic Mass, Odd and Even Electron Ions

14 formula(e) evaluated with 1 results within limits (up to 20 closest results for each mass)

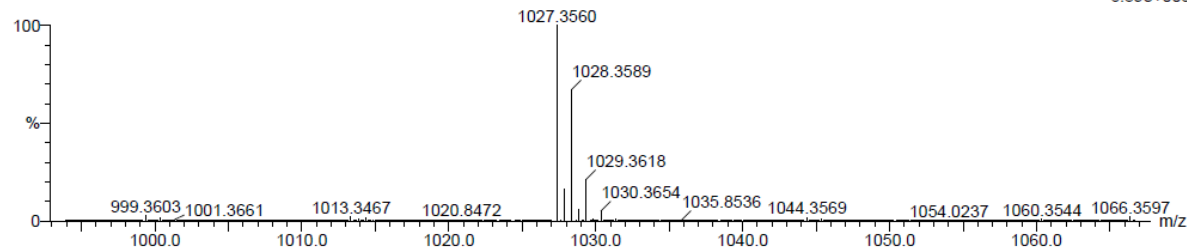
Elements Used:

C: 55-60 H: 55-60 N: 6-10 O: 5-10 Co: 0-1

S17 36 (1.121) Cm (1:64)

TOF MS ES+

6.39e+005



Mass	Calc. Mass	mDa	PPM	DBE	i-FIT	i-FIT (Norm)	Formula
1027.3560	1027.3553	0.7	0.7	33.0	172.7	0.0	C56 H56 N8 O8 Co

Figure 5.14: High resolution TOF-MS spectrum of 3.

Single Mass Analysis

Tolerance = 5.0 PPM / DBE: min = -1.5, max = 100.0

Element prediction: Off

Number of isotope peaks used for i-FIT = 3

Monoisotopic Mass, Odd Electron Ions

161 formula(e) evaluated with 1 results within limits (up to 20 closest results for each mass)

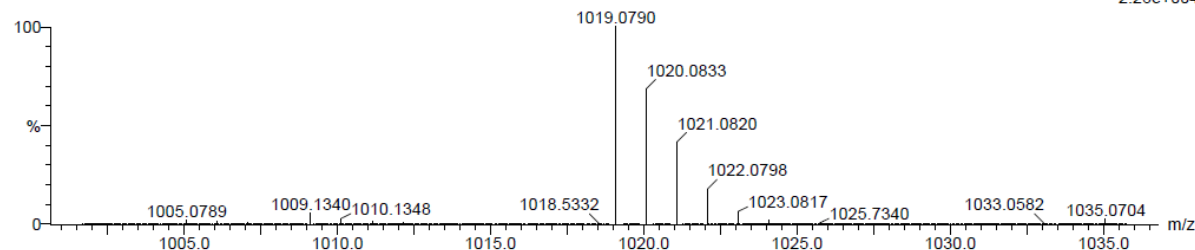
Elements Used:

C: 50-55 H: 30-35 N: 5-10 O: 0-5 S: 0-5 Co: 0-1

S11F1WEA 54 (1.788) Cm (1:61)

TOF MS ES+

2.26e+004



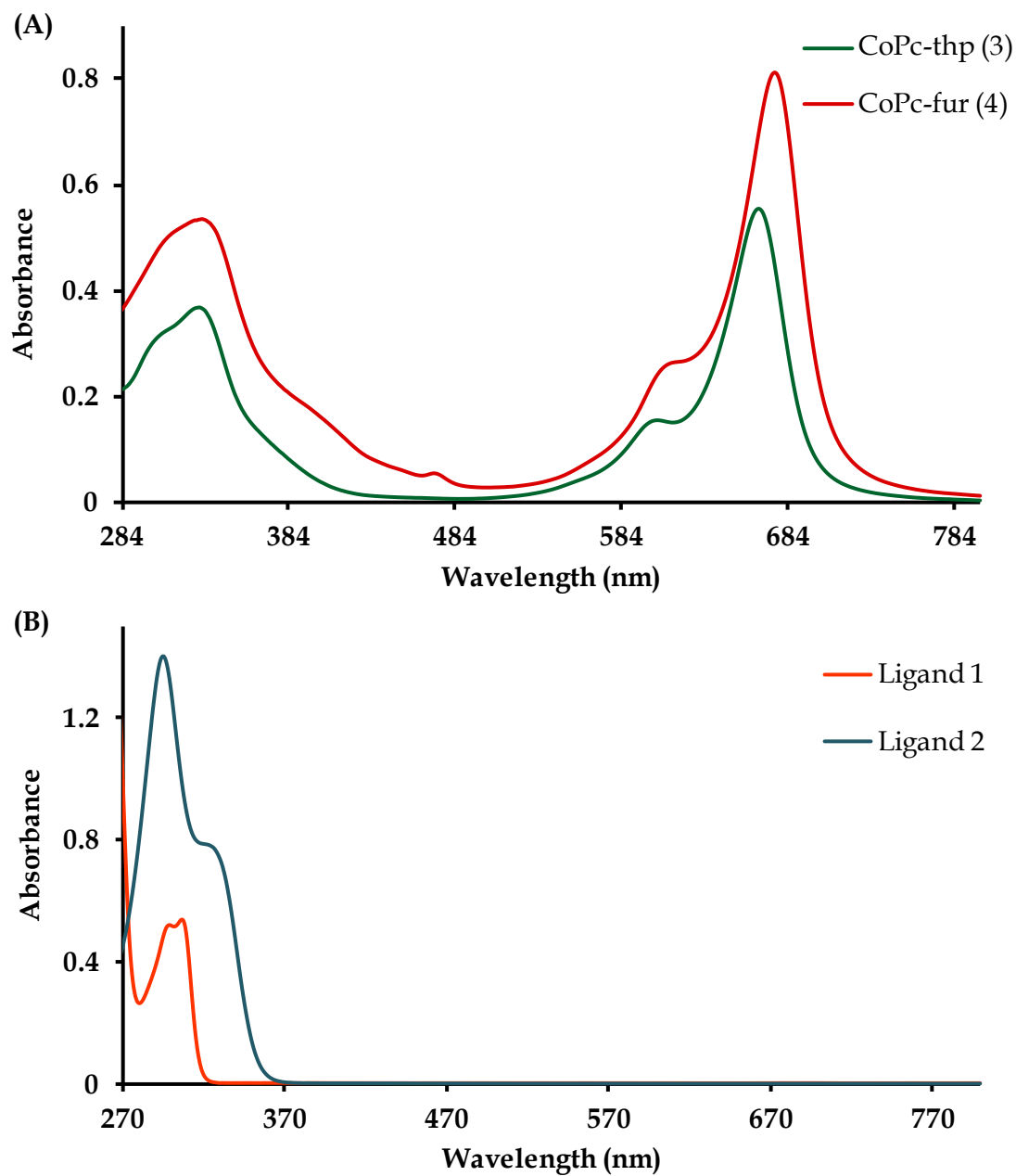
Mass	Calc. Mass	mDa	PPM	DBE	i-FIT	i-FIT (Norm)	Formula
1019.0790	1019.0761	2.9	2.8	41.0	266.0	0.0	C52 H32 N8 O4 S4 Co

Figure 5.15: High resolution TOF-MS spectrum of 4.

The formulated MPcs showed Q- and B-bands in the regions of 600-700 nm and 300-400 nm, respectively, in accordance with literature [34] (refer to **Table 5.3**). The Q-bands of the metal complexes do not differ significantly in wavelength but complex **4** is slightly red-shifted due to the presence of the electron donating sulfur atoms (see **Fig. 5.15**). Both metal complexes display absorption bands in their electronic spectra that are characteristic of their corresponding ligands. The band of complex **3** appearing at 307 nm resembles the band of **1** which appears at a lower energy (306 nm) while the broadened B-band of **4** at 331 nm arises from an overlap of  $\pi$ - $\pi^*$  electronic transitions of the Pc ring and its corresponding phthalonitrile (323 nm).

**Table 5.3:** UV-Vis absorption wavelengths and the corresponding molar absorptivities (in parentheses) for **1-4**.

Compound	Q-band (nm)	B-band (nm)	Higher energy bands (nm)
<b>1</b>	-	-	299 (12647), 306 (13081)
<b>2</b>	-	-	295 (137469), 323 (76752)
<b>3</b>	667 (285321)	330 (189512)	307 (163949)
<b>4</b>	676 (161757)	331 (106668)	-



**Figure 5.16:** UV-Vis spectra of (A) complexes **3** and **4** at concentrations of  $1.95 \mu\text{M}$  and  $5.03 \mu\text{M}$ , respectively and (B) ligands **1** and **2** at concentrations of  $41.1 \mu\text{M}$  and  $10.2 \mu\text{M}$ , respectively.

### 5.3.3 Voltammetry and Spectroelectrochemistry

The solution redox properties of the complexes were investigated *via* cyclic and square-wave voltammetry. Both complexes **3** and **4** displayed four redox processes as observed in their respective cyclic and square-wave voltammograms, see **Figs. 5.17** and **5.18**. The redox couples **I**, **II** and **III** have larger peak to peak separations ( $\Delta E$  values) and hence slower electron transfer kinetics as compared to the ferrocene standard ( $\Delta E > 107$  mV on a GCE or  $\Delta E > 105$  mV on a Pt electrode, at 100 mV/s), thus these processes are considered to be quasi-reversible [35]. Redox couple **IV** is irreversible. The use of donor solvents in electrocatalysis is known to promote metal oxidation and reduction redox processes above Pc-based electron transfer in MPcs with redox active metal centres (*e.g.* Fe, Co and Mn) [36]. Hence, redox couples **I** to **IV** were assigned according to literature trends (refer to **Table 5.4**) [30, 37, 38] as  $\text{Pc}^{2-}/\text{Pc}^{3-}$  and  $\text{M}^{2+}/\text{M}^{+}$  reductions as well as  $\text{M}^{3+}/\text{M}^{2+}$  and  $\text{Pc}^{1-}/\text{Pc}^{2-}$  oxidations, respectively. Any unassigned peaks are attributed to aggregation. The reverse peak of couple **II** for complex **4** is slightly sharper than the forward peak and is indicative of adsorption. Plots of peak current against square root of scan rate for both complexes were linear indicating that the redox couples are diffusion-controlled (see **Figs. 5.19** and **5.20**).

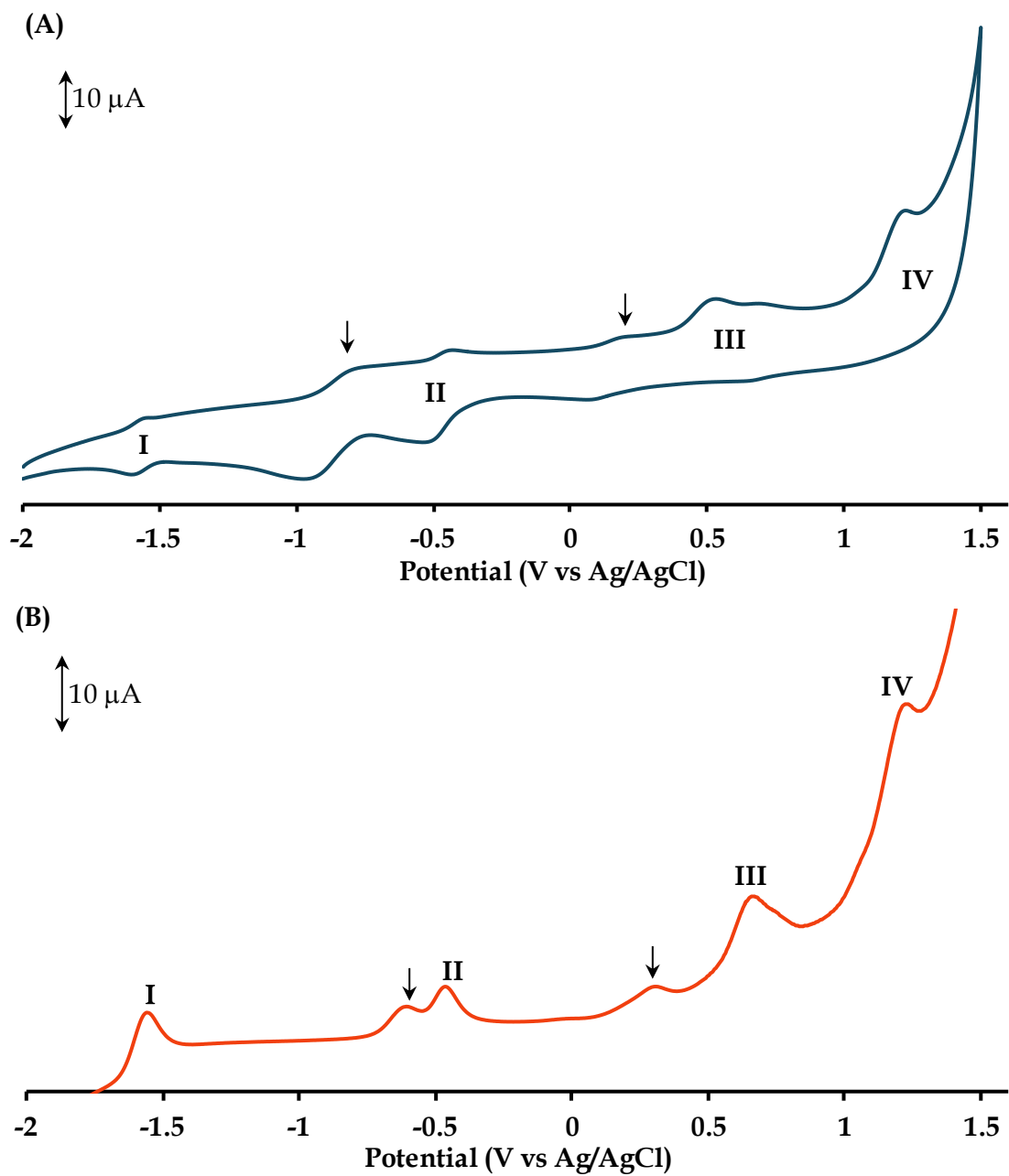


**Figure 5.17:** (A) CV and (B) SWV of complex 3 at 100 mV/s. The arrows denote aggregate peaks.

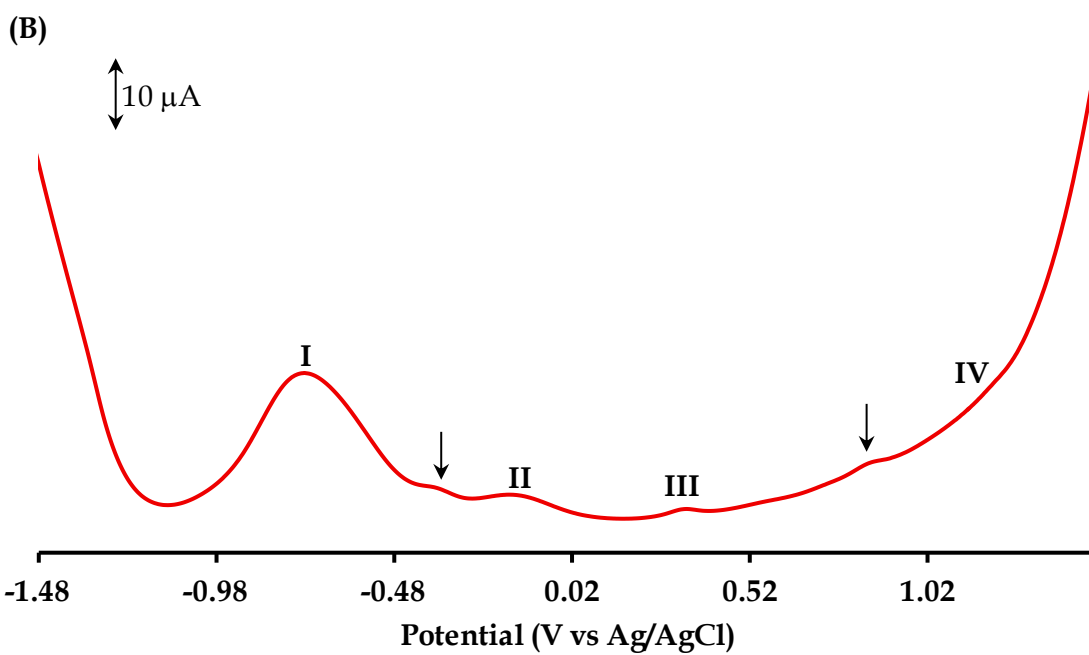
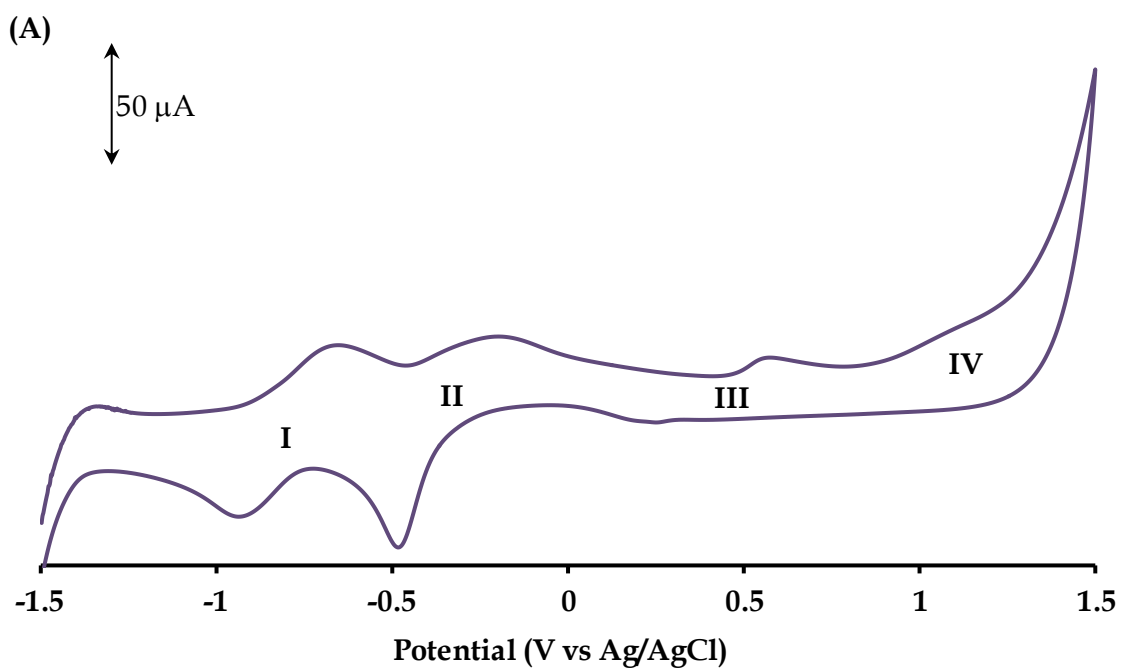


**Figure 5.18:** (A) CV and (B) SWV of complex **4** at 100 mV/s. The arrows denote aggregate peaks.

**Table 5.4:** Comparison of the voltammetric data (in V) between the novel CoPcs **3** and **4** as well as other tetrasubstituted CoPcs attained from literature.

	$M^I Pc^{2-}/M^I Pc^{3-}$ <b>I</b>	$M^{II} Pc^{2-}/M^I Pc^{2-}$ <b>II</b>	$M^{II} Pc^{2-}/M^{III} Pc^{2-}$ <b>III</b>	$M^{III} Pc^{2-}/M^{III} Pc^{1-}$ <b>IV</b>
<b>CoPc-thp (3)</b>	-0.870 <sup>[a]</sup>	-0.477 <sup>[a]</sup>	0.677 <sup>[a]</sup>	1.22 <sup>[b]</sup>
<b>CoPc-fur (4)</b>	-0.796 <sup>[a]</sup>	-0.345 <sup>[a]</sup>	0.411 <sup>[a]</sup>	1.07 <sup>[b]</sup>
<b>(β)-CoPc-ochr</b>	-1.11	-0.44	0.40	1.03
<b>(β)-CoPc-ofcou</b>	-1.00	-0.46	0.42	1.08
<b>(β)-CoPc-cfcou</b>	-0.81	-0.47	0.48	0.91
<b>(α)-CoPc-cfcou</b>	-0.86	-0.35	0.42	1.00

[a]  $E_{1/2} = \frac{E_{pa} + E_{pc}}{2}$

[b]  $E_{pa}$

cfcou = 7-oxo-3-(2-chloro-4-fluorophenyl)coumarin

ochr = 7-oxychromone

ofcou = 7-oxy-4-trifluoromethylcoumarin

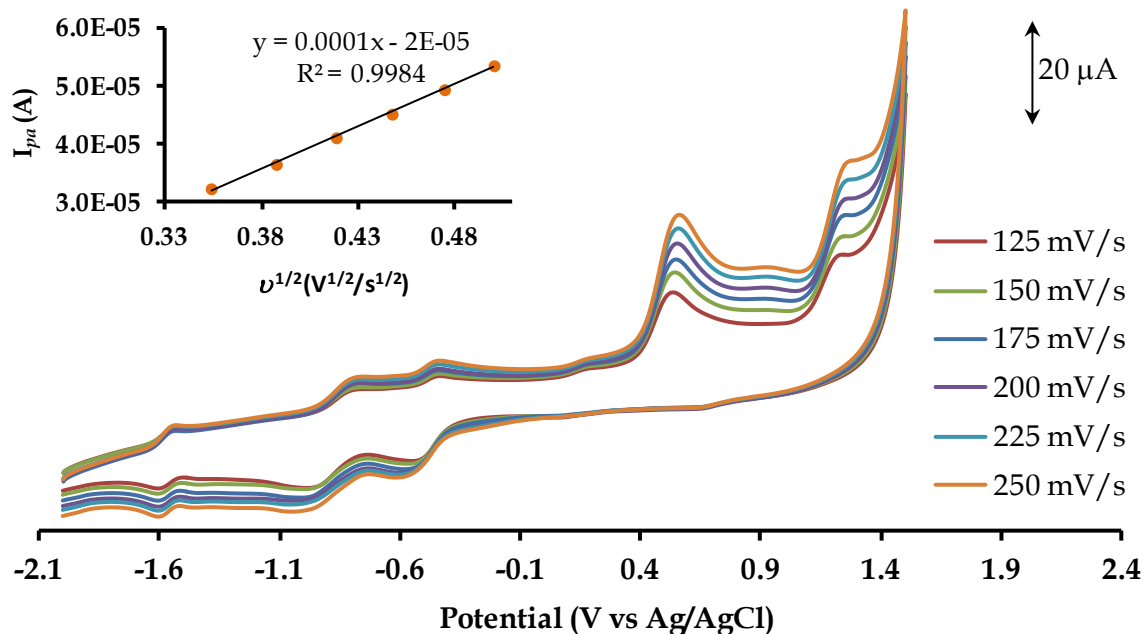


**Figure 5.19:** Overlay CVs of 3 at incrementing scan rates. Inset: Plot of  $I_{pa}$  against square root scan rate (redox couple III) showing diffusion-controlled behaviour.

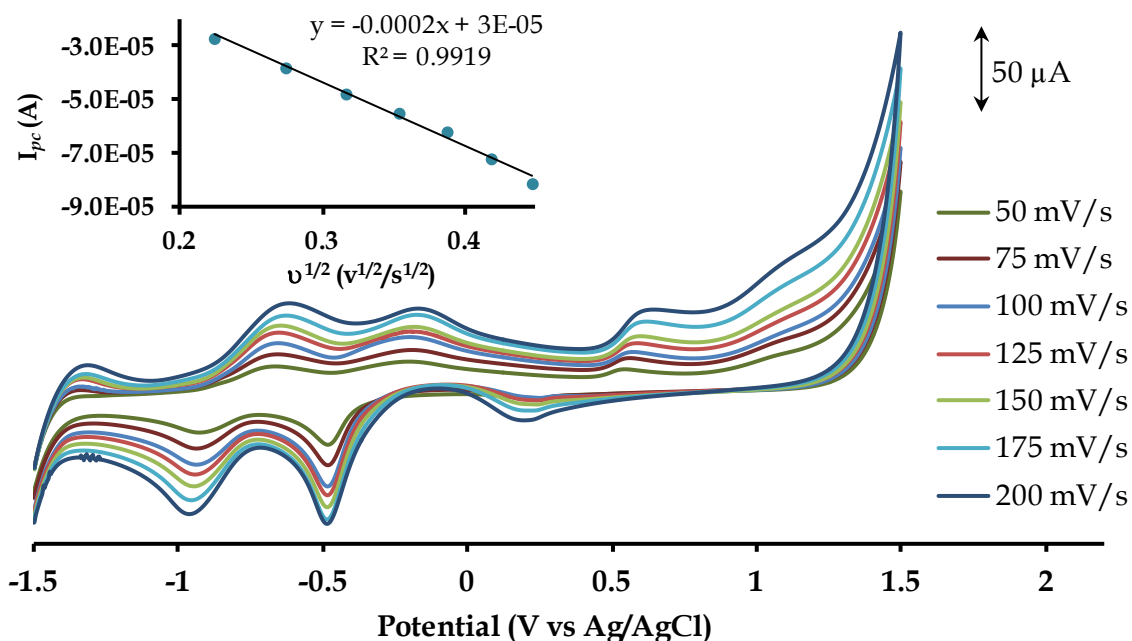


**Figure 5.20:** Overlay CVs of 4 at incrementing scan rates. Inset: Plot of  $I_{pc}$  against square root scan rate (redox couple I) showing diffusion-controlled behaviour.

Spectroelectrochemical experiments were conducted on the MPcs to verify the voltammetric assignments. The UV-Vis spectral changes of the CoPcs are similar, thus, only the spectroelectrochemical data of **3** will be elaborated on. **Figs. 5.21A-D** and **5.22A-D** illustrate the spectral changes accompanying the redox processes of complexes **3** and **4**, respectively. The *in situ* spectroelectrochemical behaviour of CoPcs is well documented. It is known that a red shift in the Q-band and the formation of a CT-band between 450 and 500 nm is reminiscent of Co(I) species in solution [23, 39]. Upon application of negative overpotentials to redox couple **II**, disaggregation and red-shifting of the Q-band occurs to produce a well-defined monomeric peak at 705 nm. Furthermore, a CT-band develops at 474 nm thereby confirming that the first redox couple occurs as a result of metal reduction ( $\text{Co}^{\text{II}}\text{Pc}^{-2}/\text{Co}^{\text{I}}\text{Pc}^{-2}$ ), see **Fig 5.21A**. These spectral changes are accompanied by well-defined isosbestic points which are observed at 328 nm, 387 nm, 561 nm and 690 nm suggesting that the metal reduction process proceeds to afford only one species in solution. Spectral changes associated with redox couple **I** include a decrease in the Q- and B-band and a red shift of the charge transfer band to 491 nm, see **Fig. 5.21B**. This redox behaviour is typical of  $\text{Pc}^{2-}$  reduction and the formation of  $\text{Pc}^{3-}$  species [40], thereby confirming that these UV-Vis spectral changes are associated with the  $\text{Co}^{\text{I}}\text{Pc}^{-2}/\text{Co}^{\text{I}}\text{Pc}^{-3}$  redox couple.

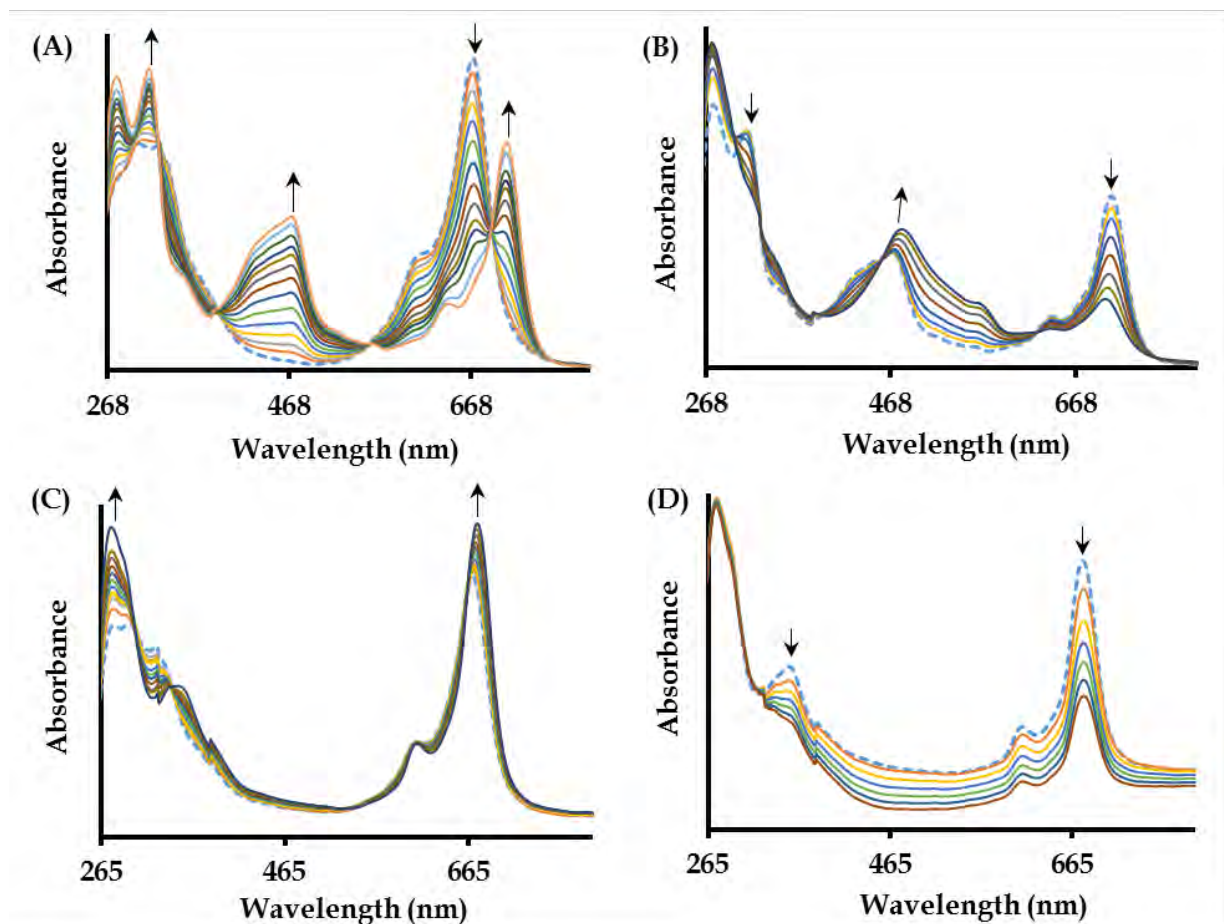


**Figure 5.21:** UV-Vis spectral changes of complex 3 at overpotentials applied at (A)  $-0.35$  V, (B)  $-1.10$  V, (C)  $0.60$  V and (D)  $1.20$  V. The initial spectrum is shown as a dashed line.

Following the application of positive overpotentials to redox couple **III**, considerable disaggregation accompanied by an increase in the intensity of the Q-band was observed and a new electronic transition band at  $362$  nm appeared. These spectral changes are consistent with metal oxidation [21]; hence the assignment of redox couple **III** to  $\text{Co}^{\text{II}}\text{Pc}^{2-}/\text{Co}^{\text{III}}\text{Pc}^{2-}$  is confirmed, see **Fig. 5.21C**. The spectral changes associated with redox couple **IV** included a decrease in the intensities of the Q- band and the band at  $362$  nm, see **Fig. 5.21D**. A loss in the intensity of the Q-band with no appreciable increase in the  $500$  nm region, which is typical of Pc oxidation, suggests

that decomposition has occurred. This has previously been reported for cobalt complexes [41]. Redox couple IV is expected to be due to  $\text{Co}^{\text{III}}\text{Pc}^{2-}/\text{Co}^{\text{III}}\text{Pc}^{1-}$ .

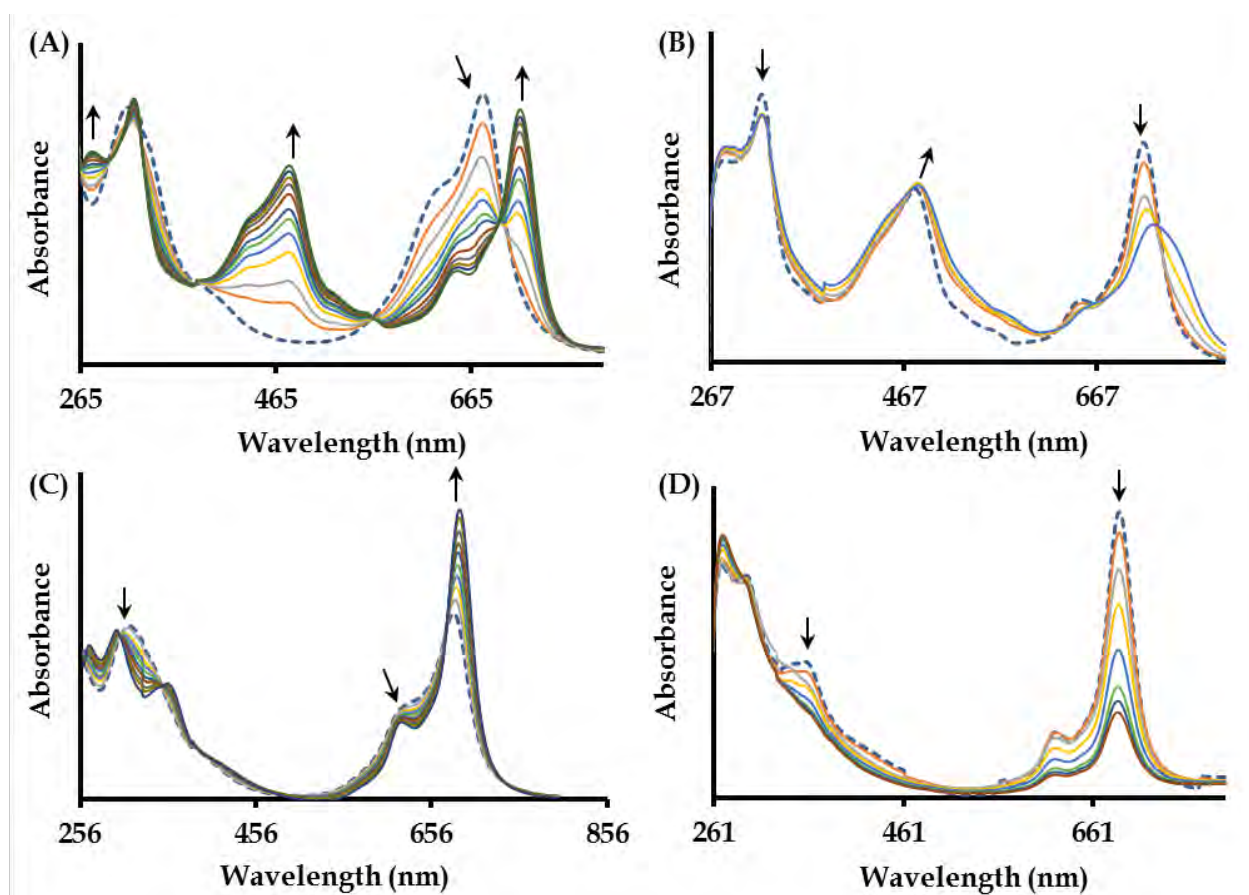


**Figure 5.22:** UV-Vis spectral changes of complex 4 at overpotentials applied at (A)  $-0.14$  V, (B)  $-0.85$  V, (C)  $0.42$  V and (D)  $1.10$  V. The initial spectrum is shown as a dashed line.

#### 5.3.4 Characterization of Modified Electrodes

Complex 4 did not show any electrocatalytic activity towards the biological analyte *L*-cysteine used in this study and is hence omitted from the following sections. Complexes 3 and 5 were adsorbed onto respective GCEs *via* the drop-dry method. CVs at incrementing scan rates were obtained for each CME in pH 4 buffer solution

to confirm electrode modification, see **Figs. 5.23** and **5.24**. The CVs revealed broadened redox couples attributed to redox process **II** ( $\text{Co}^{\text{III}}/\text{Co}^{\text{II}}$ ) thereby corroborating modification of the GCEs.

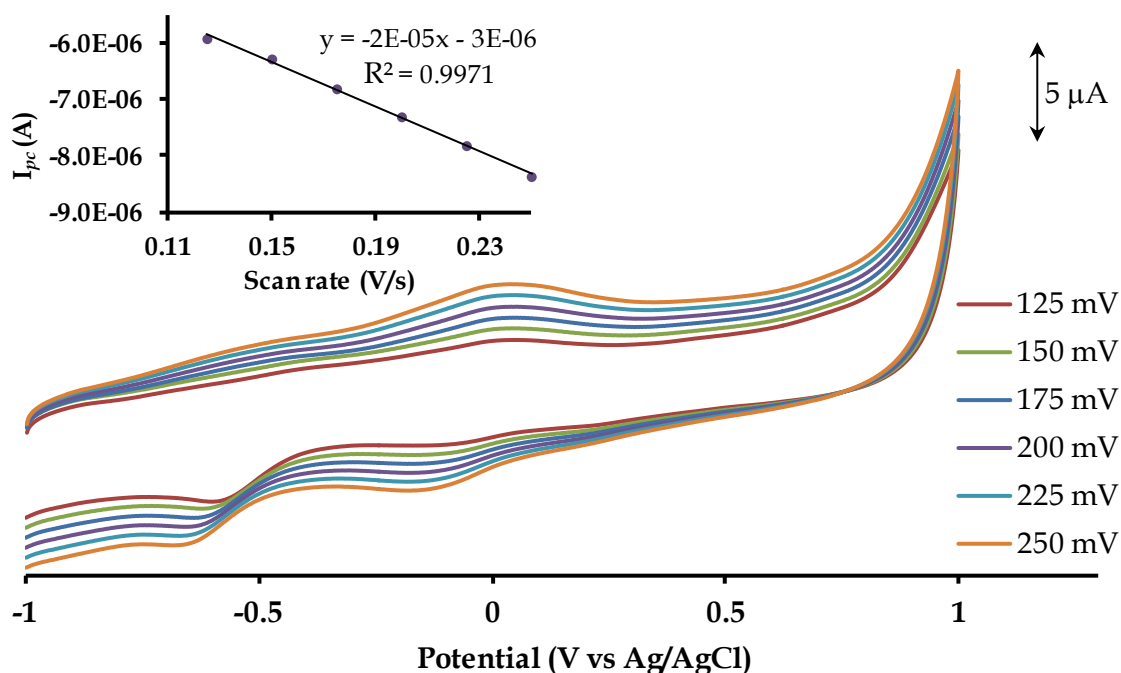


**Figure 5.23:** Overlay CVs at incrementing scan rates of 3-GCE in pH 4 buffer solution.

*Inset: The linear relationship between reduction peak currents ( $I_{pc}$ ) vs. scan rates measured at the redox couple **II**.*

Further confirmation of electrode modification is ascertained from the fact that the degree of ion-permeability for the modified working electrodes ( $\Delta E = 107$  mV) is different from that of the bare electrode ( $\Delta E = 107$  mV), see **Fig. 5.25**. The surface coverages of the respective modified working electrodes were calculated from the overlay CVs in using the following equation [42]:

$$I_p = \frac{n^2 F^2 A \Gamma(v)}{4RT} \quad (1)$$

where  $I_p$  is the peak current of redox couple II,  $n$  is the number of electrons and  $A$  is the real surface area ( $0.0707 \text{ cm}^2$ ) of the bare GCE. The surface coverage values of the modified electrodes ( $2.97 \times 10^{-10} \text{ mol/cm}^2$  for 3-GCE,  $6.53 \times 10^{-10} \text{ mol/cm}^2$  for 5-GCE) correspond well with surface coverage values previously obtained for a monolayer electrodeposited flat on an electrode surface ( $1 \times 10^{-10} \text{ mol/cm}^2$ ) [43].

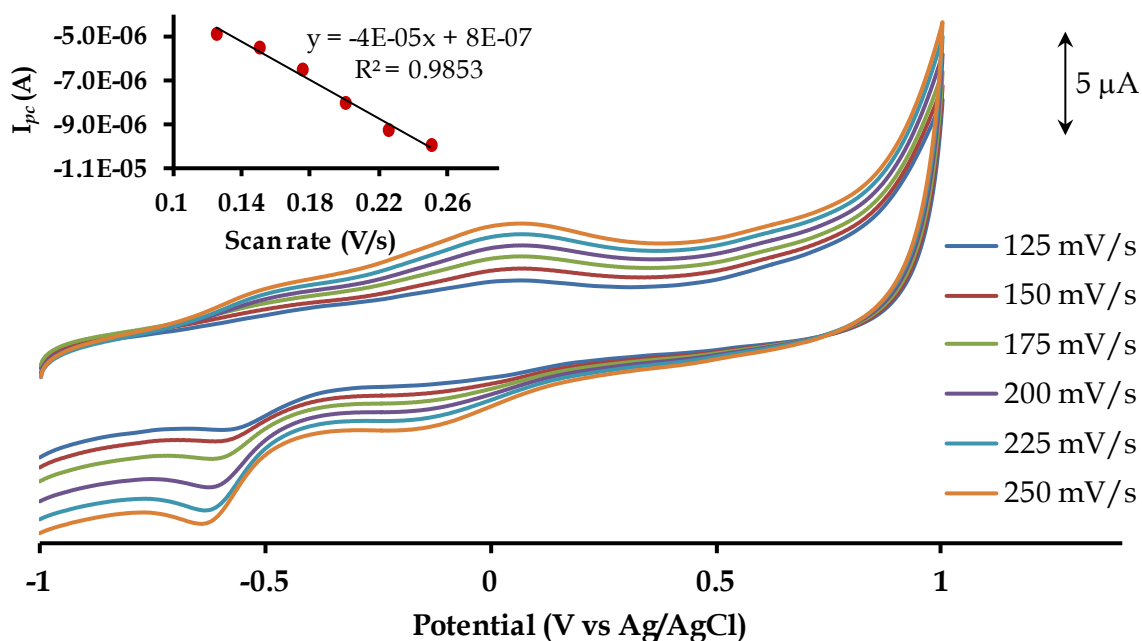


**Figure 5.24:** Overlay CVs at incrementing scan rates of 5-GCE in pH 4 buffer solution.

*Inset: The linear relationship between reduction peak currents ( $I_{pc}$ ) vs. scan rates measured at the redox couple II.*

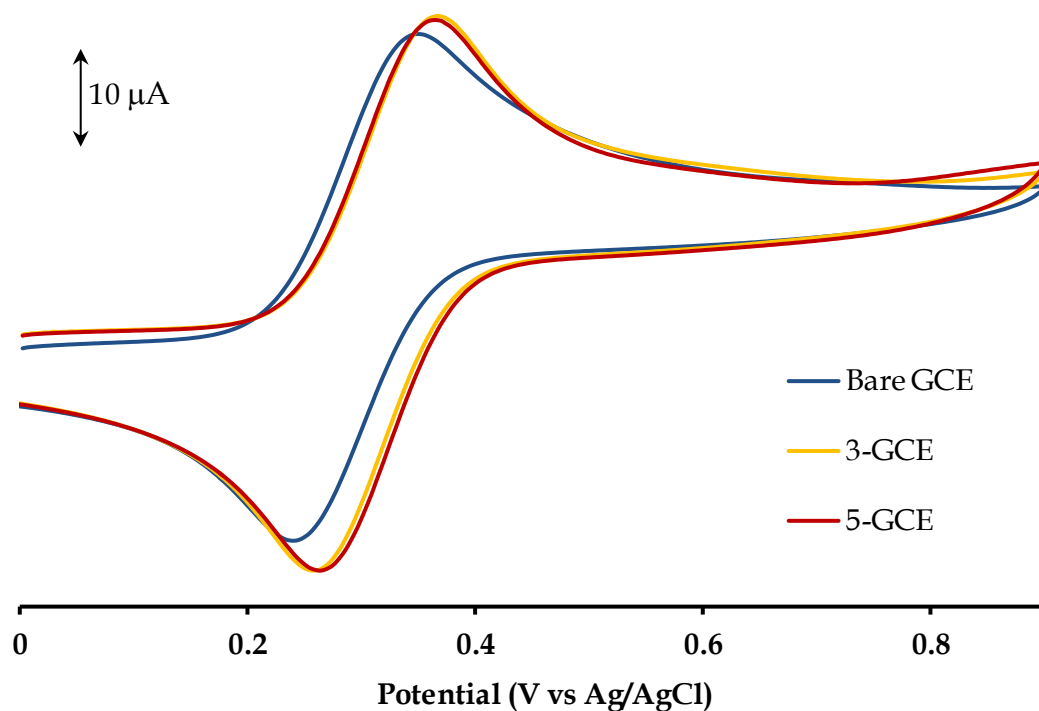


**Fig. 5.25:** Overlay CVs in 1 mM ferrocene of the bare electrode, 3-GCE and 5-GCE at 100 mV/s.

### 5.3.5 Electrocatalysis of *L*-cysteine

In contrast to the modified electrodes 3-GCE and 5-GCE, a bare GCE does not display any oxidation peak for *L*-cysteine within the potential window of 0.0 V to 0.7 V, see Fig. 5.26. The appearance of *L*-cysteine oxidation peaks at low potentials for the modified electrodes suggests that this process is promoted by the metal oxidation couple (*i.e.* Co<sup>III</sup>/Co<sup>II</sup>) which is found in the same vicinity as the electrocatalytic potential of *L*-cysteine using the respective modified electrodes (in pH 4 buffer).

The cyclic voltammograms of the CMEs in *L*-cysteine show a well defined peak at 0.42 V for 3-GCE and a broad peak at 0.52 V for 5-GCE. Furthermore, the peak current for 3-GCE is larger than 5-GCE indicating that the former is more catalytically active. A linear increase in the oxidation peak currents ( $I_{pa}$ ) with the square root of the scan rates ( $v^{1/2}$ ) was observed for the peak potentials which affirms diffusion-controlled behaviour.

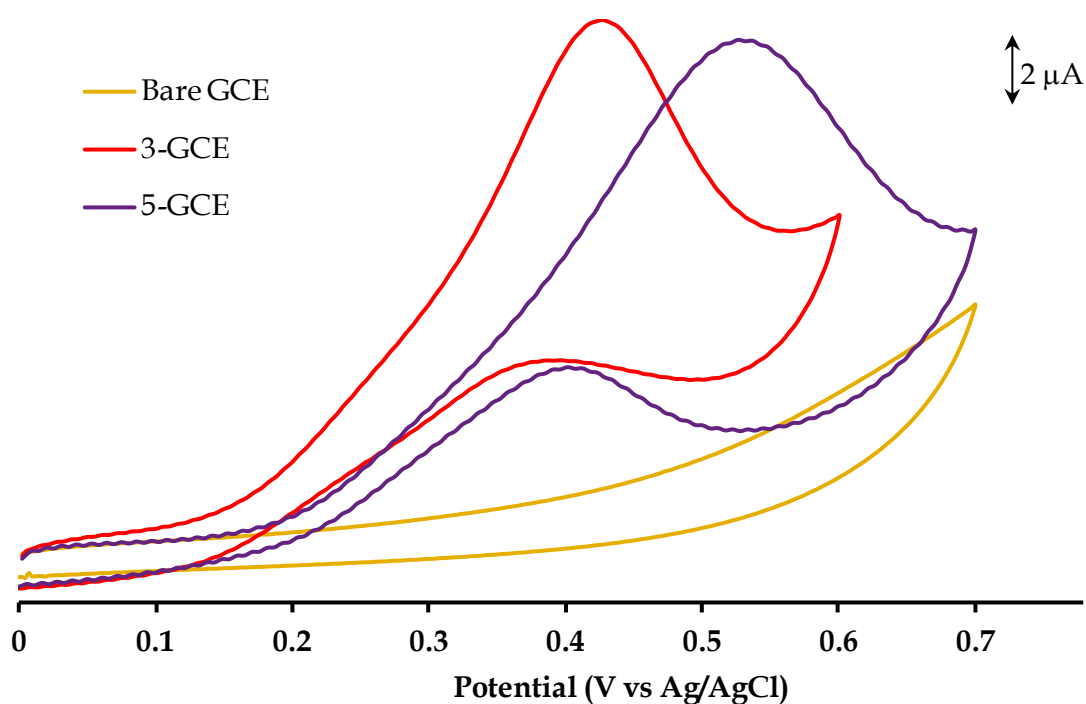


**Fig. 5.26:** Electrocatalytic oxidation of 1 mM *L*-cysteine in pH 4 buffer solution using the modified and bare electrodes at 100 mV/s.

Tafel plots (see **Figs. 5.27** and **5.28**) were constructed to obtain mechanistic information about the electrocatalyzed oxidation of *L*-cysteine. The Tafel slopes were obtained from plots of  $E_p$  vs  $\text{Log } v$  using equation (2):

$$E_p = \frac{2.3RT}{2(1-\alpha)Fn_\alpha} \text{Log } v + K \quad (2)$$

where  $\alpha$  is the transfer coefficient,  $\nu$  is the scan rate,  $n_{\alpha}$  is the number of electrons in the rate-determining step and  $K$  is the intercept.

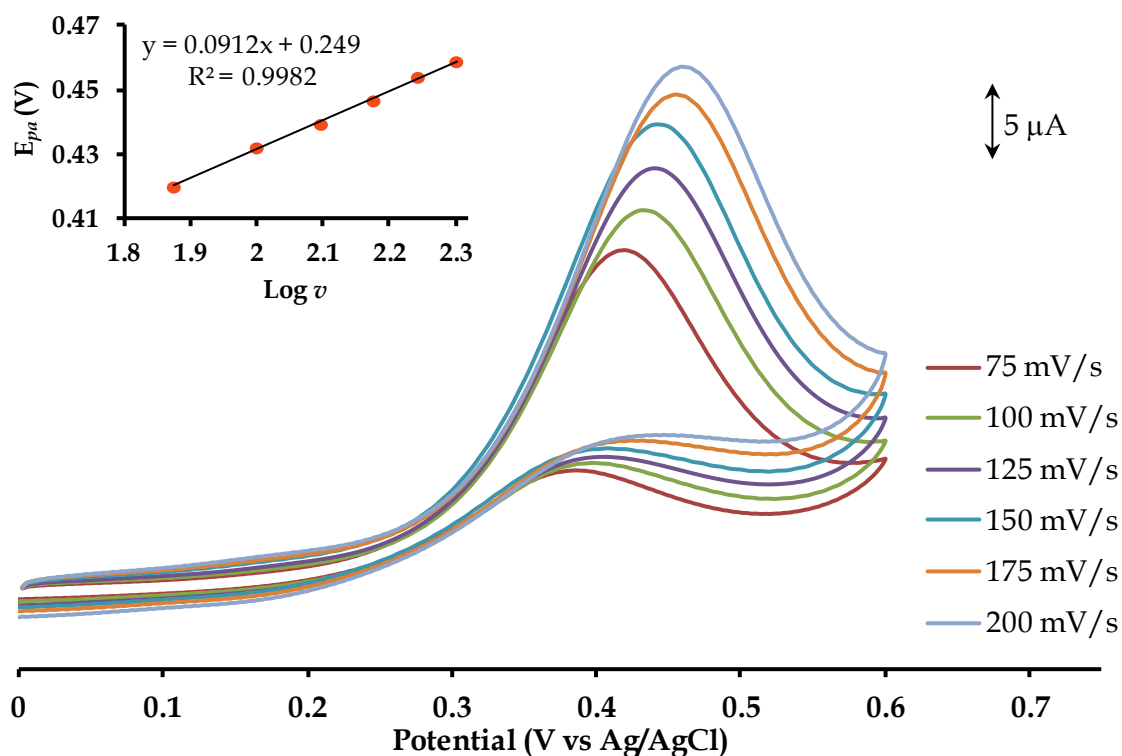
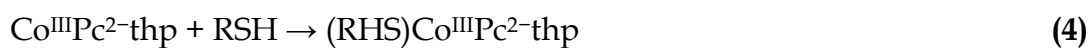


**Figure 5.27:** Electrocatalytic oxidation of 1 mM L-cysteine in pH 4 buffer solution by 3-GCE at incrementing scan rates from 75 mV/s to 200 mV/s. Inset: Plot of  $E_{pa}$  vs  $\text{Log } \nu$ .

The large Tafel slopes obtained for 3-GCE (182 mV/decade) and 5-GCE (237 mV/decade) are outside the normal range of 30-120 mV/decade which is known to be due to substrate-catalyst interactions, where the substrate (*L*-cysteine) binds very strongly to the catalyst (CoPc) during oxidation [44, 45]. Given that the oxidation of *L*-cysteine is promoted by the  $\text{Co}^{\text{III}}/\text{Co}^{\text{II}}$  couple, the following reaction mechanism is proposed from literature using CoPc-thp as an example [45]:



where RSH is *L*-cysteine and RS• is cystine.

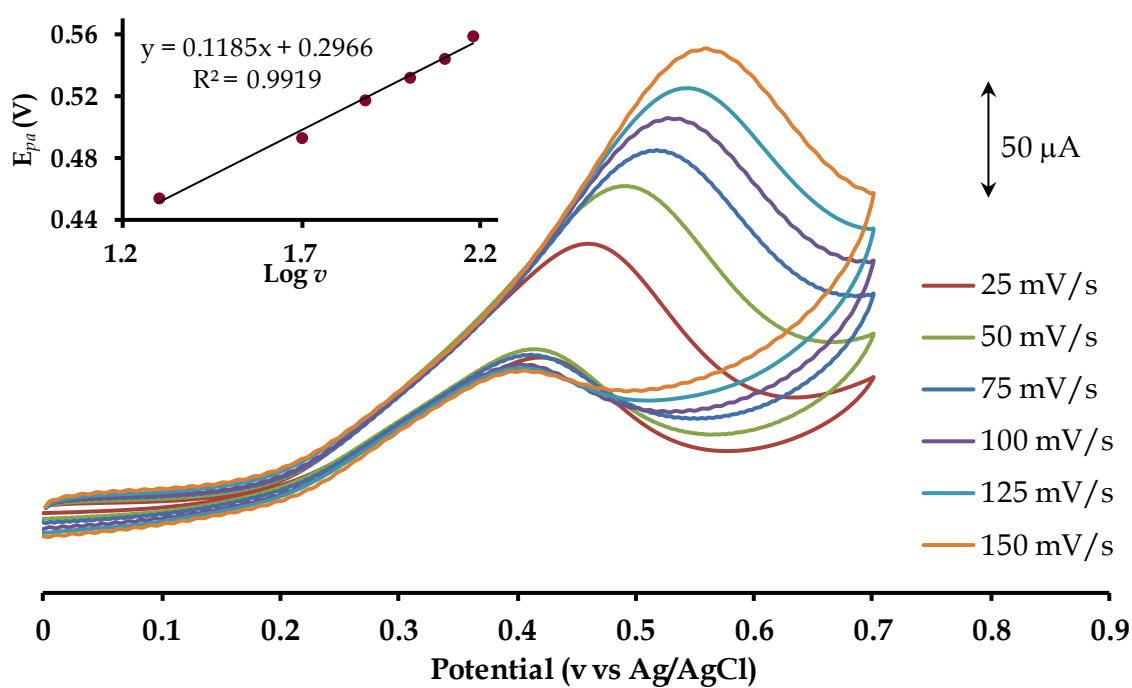


**Figure 5.28:** Electrocatalytic oxidation of 1 mM *L*-cysteine in pH 4 buffer solution by 5-GCE at incrementing scan rates from 75 mV/s to 200 mV/s. Inset: Plot of  $E_{pa}$  vs  $\text{Log } v$ .

### 5.3.6 Chronoamperometry Studies

Chronoamperometry was used to determine the catalytic rate-constants for 3-GCE and 5-GCE in 1 mM *L*-cysteine. The chronoamperograms were obtained by setting the over potentials on the CMEs to 0.45 and 0.53 V for 3-GCE and 5-GCE, respectively. Figs. 5.29 and 5.30 display the chronoamperograms for the modified electrodes.

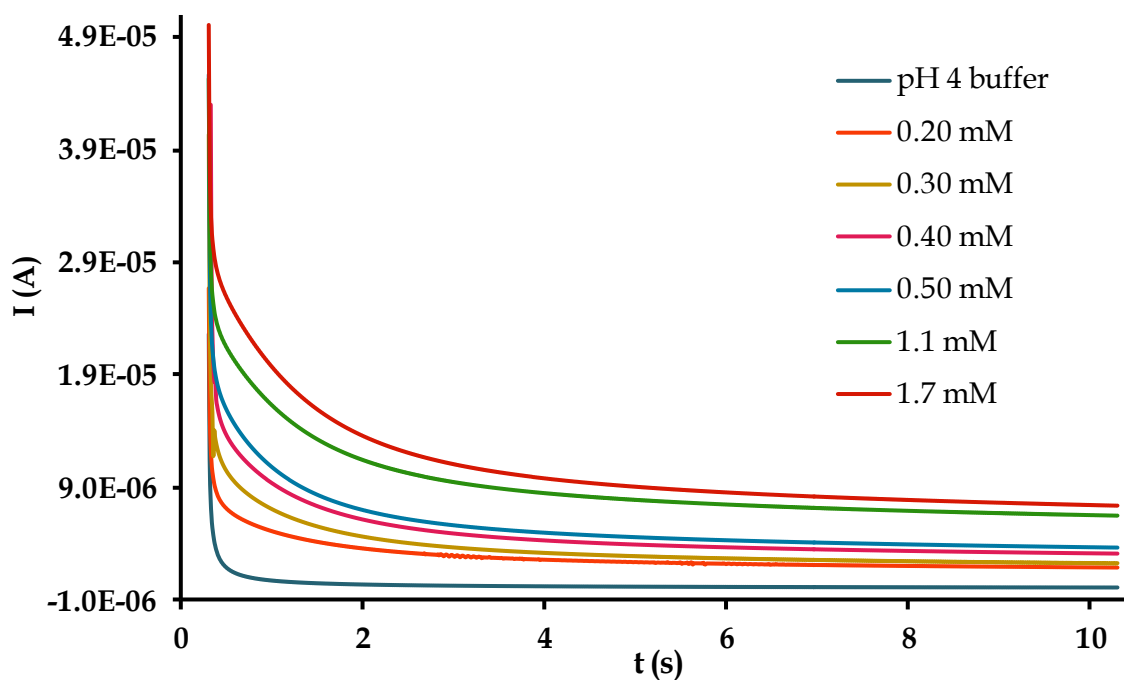


Fig. 5.29: Chronoamperograms of 3-GCE in pH 4 buffer at different concentrations of *L*-cysteine.

At intermediate times ( $t = 0.4 - 1.0$  s), the catalytic current is dominated by the rate of the electrocatalyzed oxidation of *L*-cysteine [46] and the rate constants for the

chemical reaction between *L*-cysteine and the redox sites of the modifiers on the CMEs were calculated according to literature methods [47, 48]:

$$\frac{I_c}{I_b} = \gamma^{1/2} \left[ \pi^{1/2} \operatorname{erf}(\gamma^{1/2}) + \frac{\exp(-\gamma)}{\gamma^{1/2}} \right] \quad (7)$$

Where  $\gamma = kC_0t$  ( $C_0$  is the bulk concentration of *L*-cysteine) and  $\operatorname{erf}^{1/2}$  is the error function. In cases where  $\gamma$  exceeds 2, the error function is almost equal to 1 and the above equation reduces to:

$$\frac{I_c}{I_b} = \sqrt{\gamma\pi} = \sqrt{\pi k C_0 t} \quad (8)$$

Where  $I_c$  and  $I_b$  are the currents in the presence and in the absence of *L*-cysteine,  $t$  is the time elapsed (s) and  $k$  is the rate constant ( $M^{-1}S^{-1}$ ).

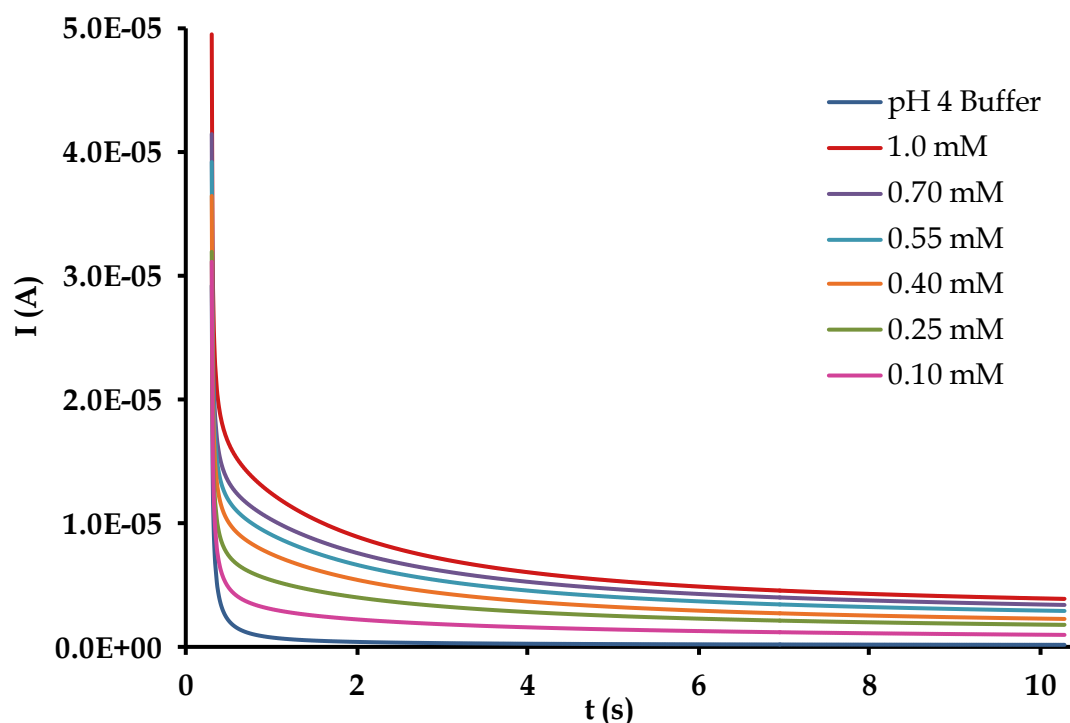


**Fig. 5.30:** Chronoamperograms of 5-GCE in pH 4 buffer at different concentrations of *L*-cysteine.

Plots of  $I_c/I_b$  against  $t^{1/2}$  (see Figs. 5.31A and 5.32A) for different concentrations of L-cysteine were constructed from the chronoamperograms.

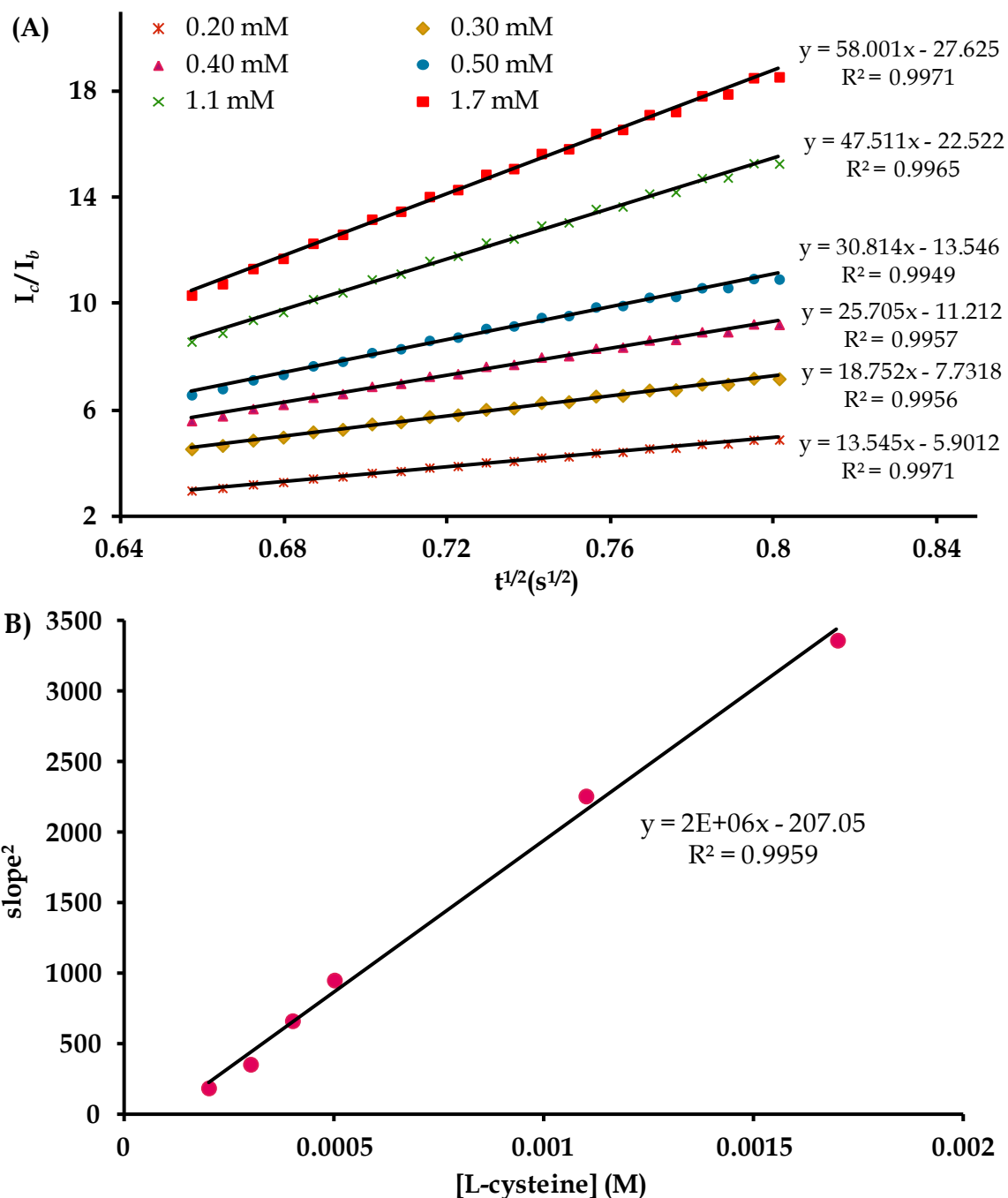


**Figure 5.31:** (A) Plot of  $I_c/I_b$  against  $t^{1/2}$  and (B) Plot of  $\text{slope}^2$  against [L-cysteine] for 3-GCE.

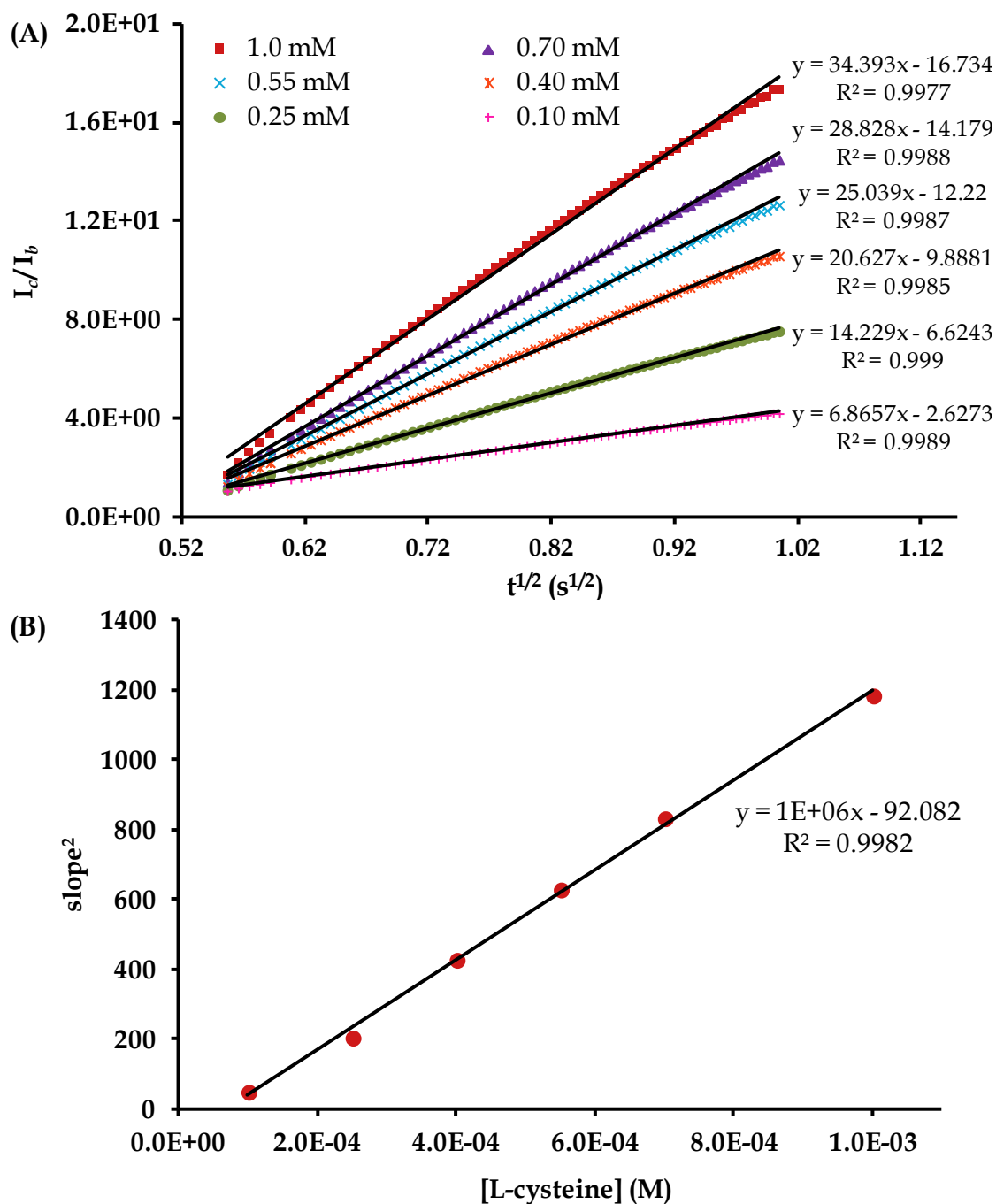


**Figure 5.32:** (A) Plot of  $I_c/I_b$  against  $t^{1/2}$  and (B) Plot of slope<sup>2</sup> against [L-cysteine] for 5-GCE.

The slopes obtained from these plots were plotted against the concentration of L-cysteine to afford a linear relationship. The rate constants were subsequently determined from the slopes of **Figs. 5.31B** and **5.32B** to be as  $6.83 \times 10^5 \text{ M}^{-1}\text{s}^{-1}$  for 3-GCE and  $3.83 \times 10^5 \text{ M}^{-1}\text{s}^{-1}$  for 5-GCE. It can be noted that the higher surface coverage of 5-GCE produced a higher L-cysteine oxidation potential and a lower rate constant

as compared to 3-GCE. The rate constants are much higher than previously reported studies, *e.g.* indigocarmin ( $5.90 \times 10^4 \text{ M}^{-1}\text{s}^{-1}$ ), poly(4-vinylpyridine) ( $8.95 \times 10^3 \text{ M}^{-1}\text{s}^{-1}$ ) and tetraamino CoPc ( $2.20 \times 10^5 \text{ M}^{-1}\text{s}^{-1}$ ) modified electrodes [49-51].

### 5.3.7 Rotating Disk Electrode Studies

Rotating disk electrode (RDE) studies were conducted to investigate the hydrodynamic kinetics of the electro-oxidation of *L*-cysteine on the CMEs. Figs. 5.33 and 5.34 show the linear sweep voltammograms (LSVs) at different rotational speeds for 3-GCE and 5-GCE, respectively. In the event that the oxidation of *L*-cysteine at the CMEs is purely mass transfer-controlled, the relationship between the limiting current and the rotational speed should obey the Levich equation [52]:

$$I_L = 0.62nFAD^{2/3}\nu^{-1/6}\omega^{1/2}C$$

where  $D$  is the diffusion coefficient,  $\nu$  is the kinematic viscosity,  $\omega$  is the rotational speed,  $C$  is the bulk concentration of the solution,  $I_L$  is the limiting current and all other parameters have their usual meanings. Linear plots indicating convection-controlled mass transport were obtained from plots of  $I_L$  versus  $\omega^{1/2}$  (see Figs. 5.33 and 5.34). The kinetic rate constants were determined from Koutecky-Levich plots of  $I_L^{-1}$  vs  $\omega^{-1/2}$  (Figs. 5.35A, 5.36A) using the equation [53]:

$$\frac{1}{I_L} = \frac{1}{nFAkC} + \frac{1}{0.62nFAD^{2/3}\nu^{-1/6}\omega^{1/2}C}$$

From the intercepts of the plots,  $k$  was calculated to be  $8.25 \times 10^{-3} \text{ cms}^{-1}$  and  $2.25 \times 10^{-3} \text{ cms}^{-1}$  for 3-GCE and 5-GCE, respectively.

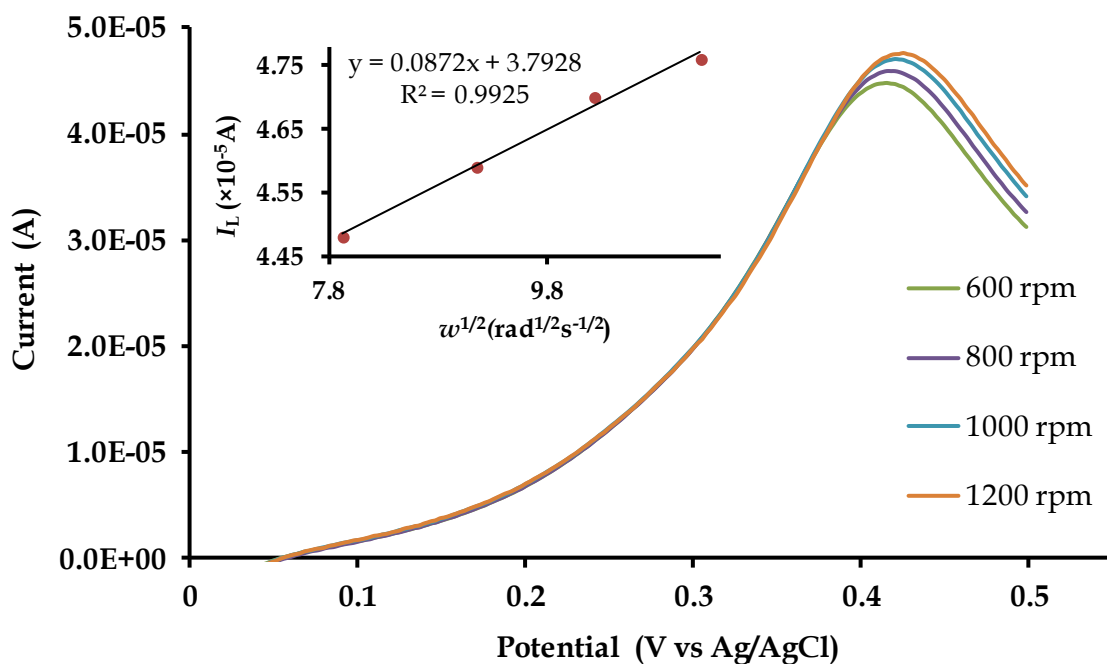


**Figure 5.33:** Comparative RDE voltammograms for 3-GCE at different rotational speeds.  
Inset: Levich Plot.

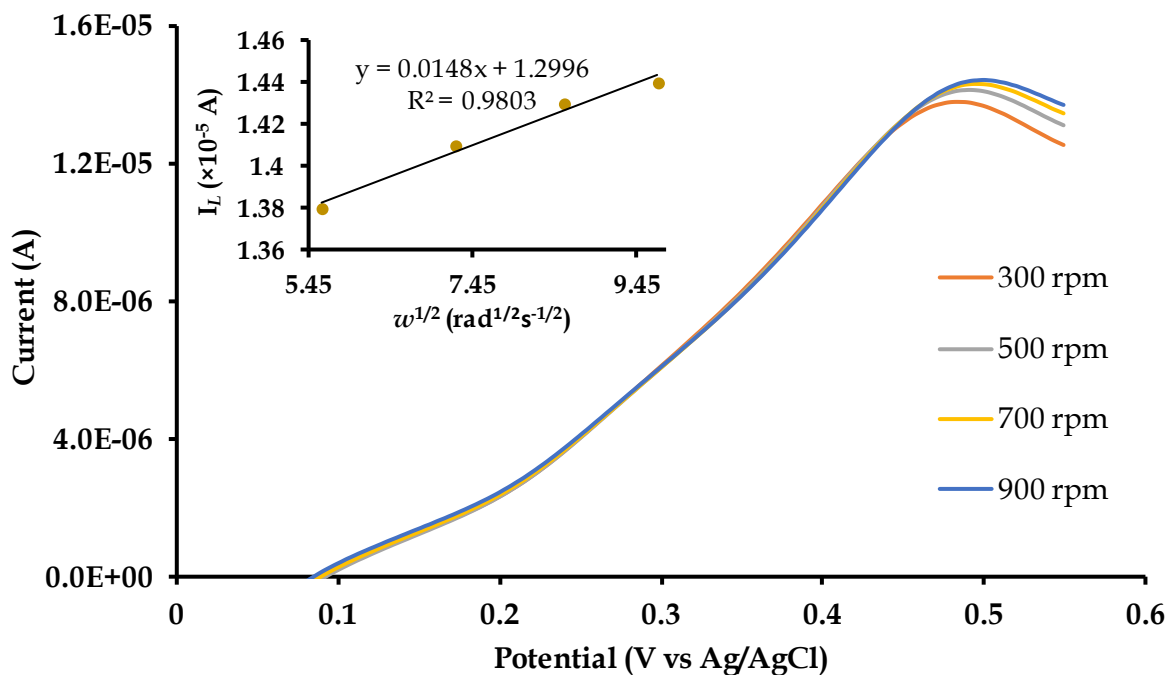


**Figure 5.34:** Comparative RDE voltammograms for 5-GCE at different rotational speeds.  
Inset: Levich Plot.

Plots of  $I^{-1}$  vs  $w^{-1/2}$  (Figs. 5.35B, 5.36B), where current was taken from the rising part of the LSVs, resulted in nearly parallel straight lines, implying a first order reaction with respect to *L*-cysteine electro-oxidation [54].

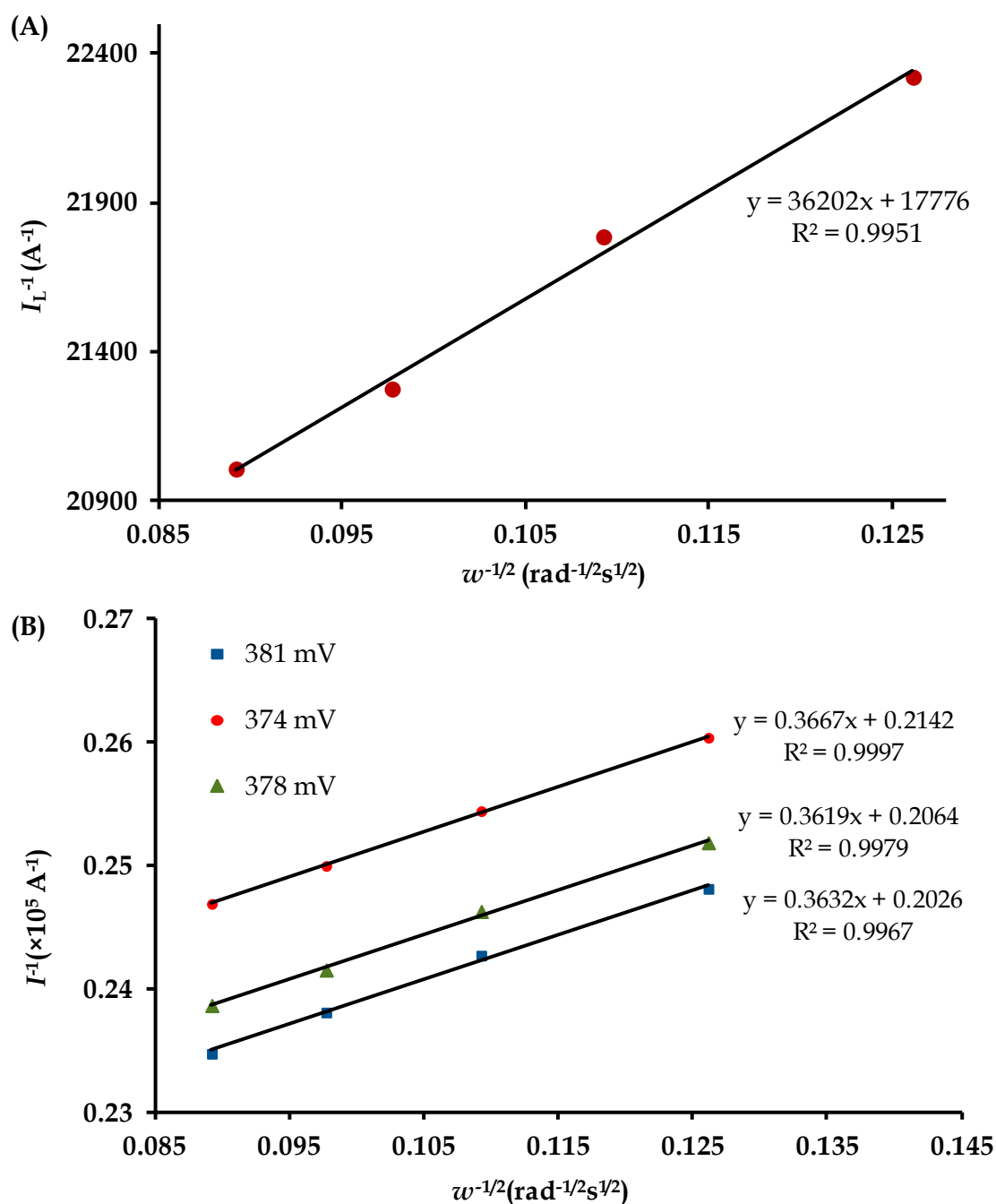


**Figure 5.35:** (A) Koutecky-Levich plot of 3-GCE. (B) Plot of  $I^{-1}$  vs  $w^{-1/2}$  for 3-GCE at different rotational speeds at the indicated potentials.

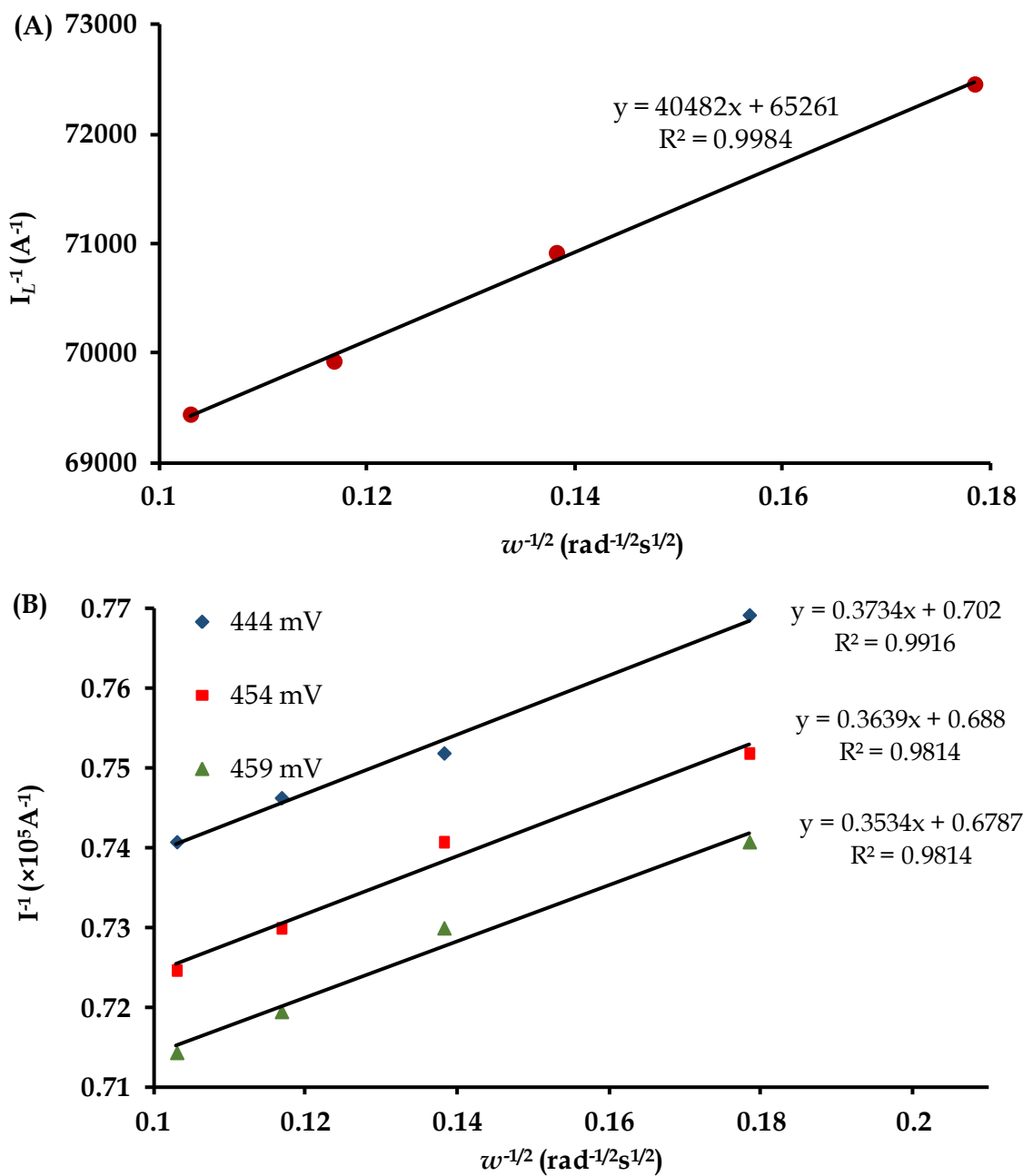


**Figure 5.36:** (A) Koutecky-Levich plot of 5-GCE. (B) Plot of  $I^{-1}$  vs  $\omega^{-1/2}$  for 3-GCE at different rotational speeds at the indicated potentials.

## 5.4 Conclusion

CoPcs bearing tetrahydropyran and furan substituents were synthesized and spectroscopically characterized. Both CoPcs exhibited similar voltammetric behaviour. The UV-Vis spectral changes accompanying each redox couple confirmed the respective voltammetric assignments and were comparable to those reported for similar tetra-substituted mononuclear CoPcs. Chemically modified GCEs were prepared using CoPc-thp and the previously reported CoPc-cou (chapter three) *via* the drop-dry method. Both fabricated GCEs were found to electrocatalytically enhance the detection of *L*-cysteine.

**Table 5.1** *Crystal data and structure refinement data.*

Chemical formula	C <sub>13</sub> H <sub>8</sub> N <sub>2</sub> OS
Formula weight	240.27
Temperature (K)	100
Crystal system	Monoclinic
Space group	P2 <sub>1</sub> /n
Unit cell dimensions (Å, °)	$a = 12.8790$ (11) $b = 4.6086$ (4) $c = 20.0734$ (18) $\alpha = 90$ $\beta = 106.563$ (5) $\gamma = 90$
Crystal size (mm)	0.21 × 0.18 × 0.12
V(Å <sup>3</sup> )	1142.00 (17)
Z	4
Density (calc.) (Mg/m <sup>3</sup> )	1.397
Absorption coefficient (mm <sup>-1</sup> )	0.27
F(000)	496
$\theta$ range for data collection (deg)	1.69; 26.05
Reflections measured	9156
Observed reflections [ $I > 2\sigma(I)$ ]	2079
Independent reflections	2257
Data/Restraints/parameters	2257/0 /154
Goodness of fit on $F^2$	1.080
Observed $R$ , $wR^2$	0.029, 0.076
$R_{int}$	0.021

**Table 5.2:** Selected bond lengths [ $\text{\AA}$ ] and bond angles [ $^\circ$ ] for **2**.

C6-C13	1.405(2)
C10-C12	1.394(2)
C9-N1	1.150(2)
C1-O	1.372(2)
C1-C2	1.339(2)
C2-C3	1.432(2)
C6-S	1.755(2)
C5-S-C6	103.66(6)
C1-O-C4	106.09(1)

#### 5.4 References

- [1] I. Ohtsu, N. Wiriyathanawudhiwong, S. Morigasaki, T. Nakatani, H. Kadokura, H. Takagi, *J. Biol. Chem.*, 2010, **285**, 17479.
- [2] N. Maleki, A. Safavi, F. Sedaghati, F. Tajabadi, *Anal. Biochem.*, 2007, **369**, 149.
- [3] R. Devasenathipathy, V. Mani, S.-M. Chen, K. Kohilarani, S. Ramaraj, *Int. J. Electrochem. Sci.*, 2015, **10**, 682.
- [4] X. Wang, L. Zhang, L. Miao, M. Kan, L. Kong, H. Zhang, *Sci. Chi. Chem.*, 2011, **54**, 521.
- [5] Z.-X. Zheng, Q.-L. Feng, J. Li, C.-M. Wang, *Sens. Actuators, B*, 2015, <http://dx.doi.org/10.1016/j.snb.2015.07.069>.

- [6] F. de Assis dos Santos Silva, M.G.A. da Silva, P.R. Lima, M.R. Meneghetti, L.T. Kubota, M.O.F. Goulart, *Biosens. Bioelectron.*, 2013, **50**, 202.
- [7] P.C. Pandey, A.K. Pandey, D.S. Chauhan, *Electrochim. Acta*, 2012, **74**, 23.
- [8] Z. Liu, H. Zhang, S. Hou, H. Ma, *Microchim. Acta*, 2012, **177**, 427.
- [9] J. Obirai, T. Nyokong, *Electrochim. Acta.*, 2005, **50**, 5427.
- [10] M.K. Halbert, R.P. Baldwin, *Anal. Chem.*, 1985, **57**, 591.
- [11] A.T. Bilgicli, A. Gonsel, M. Kandaz, A. Altindal, H. Comert, *J. Organomet. Chem.*, 2015, **785**, 112.
- [12] K.I. Ozoemena, T. Nyokong, *Electrochim. Acta*, 2006, **51**, 2669.
- [13] S.L. Vilakazi, T. Nyokong, *J. Electroanal. Chem.*, 2001, **512**, 56.
- [14] S.B.A. Barrosa, A. Rahim, A.A. Tanaka, L.T. Arenas, R. Landers, Y. Gushikem, *Electrochim. Acta*, 2013, **87**, 140.
- [15] T. Nyokong, *N<sub>4</sub>-Macrocyclic Metal Complexes*, ed. J.H. Zagal, F. Bedioui, J.-P. Dodelet, Springer Science + Business Media, LLC, New York, 2006, ch. 7, pp. 315-361.
- [16] J.H. Zagal, S. Griveau, J.F. Silva, T. Nyokong, F. Bedioui, *Coord. Chem. Rev.*, 2010, **254**, 2755.
- [17] A.P. Gutierrez, S. Griveau, C. Richard, A. Pailleret, S. Granados, F. Bedioui, *Electroanalysis*, 2009, **21**, 2303.
- [18] Y. Acikbas, M. Evyapan, T. Ceyhan, R. Capan, O. Bekaroglu, *Sens. Actuators, B*, 2007, **123**, 1017.
- [19] K. Wang, L. Dai, Q. Liu, H. Li, C. Ju, J. Wu, H. Li, *Analyst*, 2011, **136**, 4344.
- [20] F. Mirkhalaf, J.E. Graves, *Chemical Papers*, 2012, **66**, 472.

- [21] G. Ozgul, A. Tastemel, A.R. Ozkaya, M.Bulut, *Polyhedron*, 2015, **85**,181.
- [22] M. Camur, A.A. Esenpinar, A.R. Ozkaya, M. Bulut, *J. Organomet. Chem.*, 2011, **696**, 1868.
- [23] M.B. Kılıçaslan, H. Kantekin, A. Koca, *Dyes and Pigments*, 2014, **103**, 95.
- [24] J.C. Obirai, T. Nyokong, *J. Electroanal. Chem.*, 2007, **600**, 251.
- [25] V. Mani, R. Devasenathipathy, S.-M. Chen, S.-T Huang, V.S. Vasantha, *Enzyme Microb. Technol.*, 2014, **66**, 60.
- [26] K. Manna, Y.K. Agrawal, *Bioorg. Med. Chem.*, 2009, **19**, 2688.
- [27] L. Ignatovich, V. Romanov, J. Spura, J. Popelis, I. Domracheva, I. Shestakova, *Chem. Heterocycl. Compd.*, 2012, **47**, 1502.
- [28] J.V. Kosaric, D.M. Cvetkovic, M.N. Zivanovic, M.G. Curcic, D.S. Seklic, Z.M. Bugarcic, S.D. Markovic, *JBUON*, 2014, **19**, 283.
- [29] K. Akiyama, S. Yamauchi, M. Maruyama, T. Sugahara, T. Kishida, Y. Koba, *Biosci. Biotechnol. Biochem.*, 2009, **73**, 129.
- [30] S. Chohan, I.N. Booyesen, A. Mambanda, M.P. Akerman, *J. Coord. Chem.*, 2015, **68**, 1829.
- [31] R.P. Hernandez, J.D. Roderiguez, H.N. de Armas, A. Toscano, *Bol. Soc. Chil. Quim.*, 1996, **41**, 257.
- [32] A. Hori, Y. Inoue, H. Yuge, *Acta Cryst.*, 2011, **C67**, o154.
- [33] M. Dinçer, A. Agar, N. Akdemir, E. Agar, N. Özdemir, *Acta Cryst.*, 2004, **E60**, o79.
- [34] N. Sehlotho, M. Durmus, V. Ahsen, T. Nyokong, *Inorg. Chem. Commun.*, 2008, **11**, 479.

- [35] S. Altun, A.R. Özkaya, M. Bulut, *Polyhedron*, 2012, **48**, 31.
- [36] B. Koksoy, O. Soyer, E.B. Orman, A.R. Ozkaya, M. Bulut, *Dyes and Pigments*, 2015, **118**, 166.
- [37] M. Sevim, M.N. Yaras, A. Koca, M. Kandaz, *Dyes and Pigments*, 2014, **111**, 190.
- [38] Z. Odabaş, H. Kara, A.R. Özkaya, M. Bulut, *Polyhedron*, 2012, **39**, 38.
- [39] I.A. Akinbulu, T. Nyokong, *Polyhedron*, 2009, **28**, 2831.
- [40] V. Cakir, H. Kantekin, Z. Biyiklioglu, A. Koca, *Polyhedron*, 2014, **81**, 525.
- [41] I.A. Akinbulu, T. Nyokong, *Polyhedron*, 2010, **29**, 1257.
- [42] A. Maringa, E. Antunes, T. Nyokong, *Electrochim. Acta*, 2014, **121**, 93.
- [43] F. Matemadombo, T. Nyokong, *Electrochim. Acta*, 2007, **52**, 6856.
- [44] F. Bedioui, S. Griveau, T. Nyokong, A.J. Appleby, C.A. Caro, M. Gulppi, G. Ochoa, J.H. Zagal, *Phys. Chem. Chem. Phys.*, 2007, **9**, 3383.
- [45] N. Sehlotho, T. Nyokong, *Electrochim. Acta*, 2006, **51**, 4463.
- [46] T. Mugadza, T. Nyokong, *Electrochim. Acta*, 2011, **56**, 1995.
- [47] J.B. Raof, R. Ojani, H. Beitollahi, *Int. J. Electrochem. Sci.*, 2007, **2**, 534.
- [48] M.H. Pournaghi-Azar, R. Sabzi, *J. Electroanal. Chem.*, 2003, **543**, 115.
- [49] M. Mazloum-Ardakani, H. Rajabi, H. Bietollahi, *J. Argent. Chem. Soc.*, 2009, **97**, 106.
- [50] C.C. Correa, S.A.V. Jannuzzi, M. Santhiago, R.A. Timm, A.L.B. Formiga, L.T. Kubota, *Electrochim. Acta*, 2013, **113**, 332.
- [51] S. Nyoni, T. Mugadza, T. Nyokong, *Electrochim. Acta*, 2014, **128**, 32.
- [52] T. Mugadza, T. Nyokong, *Synth. Met.*, 2010, **160**, 2089.
- [53] I.A. Akinbulu, S. Khene, T. Nyokong, *Thin Solid Films*, 2010, **519**, 911.

[54] S. Nyoni, T. Nyokong, *Polyhedron*, 2015, **98**, 47.

---

---

# CHAPTER SIX

## Conclusion and Future Work

The design, synthesis and characterization of novel cobalt- and iron phthalocyanines (Pcs) bearing chromone (chr), coumarin (cou), flavone (flav), benzoxazole (bo), tetrahydropyran (thp) or furan (fur) biological moieties were successfully achieved. The metallophthalocyanines (MPcs) were found to be redox active as was distinctly implied by the presence of both metal and Pc redox processes in their respective voltammograms which were corroborated by UV-Vis spectroelectrochemistry. The formulated compounds were used in the fabrication of chemically modified electrodes (CMEs). With the exception of CoPc-fur (refer to chapter five), all the macrocyclic metal complexes were found to be electrocatalytically active towards the analyte in question: nitrite (refer to chapter three), dopamine (refer to chapter four) and *L*-cysteine (refer to chapter five). The preparation of electrodes modified with multiwalled carbon nanotubes (MWCNTs) in conjunction with CoPcs (refer to chapter four) produced superior electrocatalytic behaviour than CMEs fabricated with only MPcs. The kinetic rate constants (refer to chapters four and five) compared well with values found in literature.

The scope of this research will be expanded to include the formulation of new tetraimino substituted metallophthalocyanines containing uracil or benzothiazole moieties (see **Fig. 6.1**). The choice of these biologically relevant moieties is

rationalized by the fact that uracil is a major oxidation product of the DNA nucleotide base thymine [1] while benzothiazoles have shown to exhibit a wide range of biological activities including anti-inflammatory, antitubercular, antiviral and anticonvulsant activities [2]. Furthermore, these analytes typically show specific *in vivo* biodistribution patterns (e.g. the heavy metal pollutant, mercury selectively targets thymine moieties); hence, the presence of these biologically relevant moieties (*viz.* uracil or benzothiazole) may increase the selectivity of the MPc CMEs [3-5]. In addition, we hypothesize that stable CMEs will be fabricated through the formation of self-assembled monolayers on Au electrodes (using the tetrasubstituted benzothiazole MPcs) and electropolymerized nanofilms on glassy carbon electrodes (using the tetrasubstituted uracil MPcs).

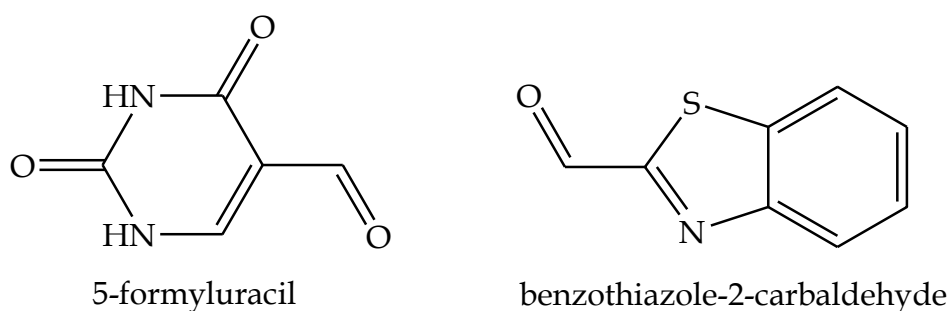


**Figure 6.1:** Structures of the biologically relevant uracil and benzothiazole ligand precursors.

## References

- [1] S. Bjelland, H. Anensen, I. Knaevelsrud, E. Seeberg, *Mutat. Res.-DNA Repair*, 2001, **486**, 147.
- [2] R. Ali, N. Siddiqui, *J. Chem.*, 2013, <http://dx.doi.org/10.1155/2013/345198>.
- [3] N. Zhou, H. Chen, J. Li, L. Chen, *Microchim. Acta*, 2013, **180**, 493.
- [4] X. Liu, C. Sun, H. Wu, Y. Zhang, J. Jiang, G. Shen, R. Yu, *Electroanalysis*, 2010, **22**, 2110.
- [5] J. Wan, G. Yin, X. Ma, L. Xing, X. Luo, *Electroanalysis*, 2014, **26**, 823.